UNIVERSITY OF SOUTHAMPTON

FACULTY OF ENGINEERING AND THE ENVIRONMENT

Electro-Mechanical Engineering Group

Design and Optimisation of Constrained Electromagnetic Energy Harvesting Devices

by

Mehdi Hendijanizadeh

Thesis for the degree of Doctor of Philosophy

March_2014

UNIVERSITY OF SOUTHAMPTON

ABSTRACT

FACULTY OF ENGINEERING AND THE ENVIRONMENT

Electro-Mechanical Engineering Group

Doctor of Philosophy

Design and Optimisation of Constrained Electromagnetic Energy Harvesting Devices

By Mehdi Hendijanizadeh

This thesis investigates the design and optimisation of constrained electromagnetic energy harvesters. It provides optimal design guidelines for constrained electromagnetic energy harvesters under harmonic and random vibrations. To find the characteristics of the vibration source, for instance vertical motion of a boat, the spectrum of the excitation amplitude should be obtained. Two Kalman filter based methods are proposed to overcome the difficulties of calculating displacement from measured acceleration. Analytical models describing the dynamics of linear and rotational electromagnetic energy harvesters are developed. These models are used to formulate a set of design rules for constrained linear and rotational energy harvesters subjected to a given sinusoidal excitation. For the sake of comparison and based on the electromechanical coupling coefficient of the systems, the maximum output power and the corresponding efficiency of linear and rotational harvesters are derived in a unified form. It is shown that under certain condition, rotational systems have greater capabilities in transferring energy to the load resistance and hence obtaining higher efficiency than linear systems. Also, the performance of a designed rotational harvester in response to broadband and band-limited random vibrations is evaluated and an optimum design process is presented for maximizing the output power under these conditions. It is furthermore shown that the profile of the spectral density of the measured acceleration signal of a typical boat can be approximated by a Cauchy distribution which is used to calculate the extracted power extracted by the proposed energy harvester in real conditions. In order to increase the operational bandwidth of rotational energy harvesters, subjected to time-varying frequency vibrations, a variable moment of inertia mechanism is proposed to adaptively tune the resonance frequency of harvester to match the excitation frequency. Also, the effects of combining the variable moment of inertia mechanism and adjusting the load resistance to increase the operational bandwidth of the system for constrained and unconstrained applications are studied. Finally, a ball screw based prototype is manufactured and the experimental results of its testing are presented which confirm the validity of the design and the derived dynamic equations of the system.

Remember that all models are wrong;

the practical question is how wrong do they have to be to not be useful.

George E. P. Box (statistician)

To my beloved parents

Table of Contents

List of tables

List of figures

Declaration of authorship

I, **Mehdi Hendijanizadeh** declare that this thesis and the work presented in it are my own and has been generated by me as the result of my own original research.

Design and Optimisation of Constrained Electromagnetic Energy Harvesting Devices

I confirm that:

1. This work was done wholly or mainly while in candidature for a research degree at this University;
2. Where any part of this thesis has previously been submitted for a degree or any other qualification at this University or any other institution, this has been clearly stated;
3. Where I have consulted the published work of others, this is always clearly attributed;
4. Where I have quoted from the work of others, the source is always given. With the exception of such quotations, this thesis is entirely my own work;
5. I have acknowledged all main sources of help;
6. Where the thesis is based on work done by myself jointly with others, I have made clear exactly what was done by others and what I have contributed myself;
7. Parts of this work have been published as:

   M. Hendijanizadeh, M. Moshrefi-Torbati, S. M. Sharkh, Constrained Design Optimisation of Vibration Energy Harvesting Devices, *Journal of Vibration and Acoustics*, 2013, vol. 136 (2), doi:10.1115/1.4025877.

   M. Hendijanizadeh, S. M. Sharkh, S. J. Elliott, M. Moshrefi-Torbati, Output power and efficiency of electromagnetic energy harvesting systems with constrained range of motion, *Smart Material and Structures*, 2013, vol. 22 (11), doi:10.1088/0964-1726/22/12/125009.

   S. M. Sharkh, M. Hendijanizadeh, M. Moshrefi-Torbati, and M. Russell, An inertial coupled marine power generator for small boats, IEEE International Conference on Clean Electrical Power (ICCEP), 14-16 Jun 2011. 4pp, Ischia, Italy.

Signed: M. Hendijanizadeh

Date: 16/01/2014

Acknowledgements

First and foremost I would like to express my deepest gratitude to my supervisors, Dr. Suleiman Sharkh and Dr. Mohamed Moshrefi-Torbati, for their guidance, support, and encouragement throughout my studies. Without their kindness and willingness to give me a chance to pursue my goals, it would have been impossible for me to come this far. They are always willing to share their experience and I have learned innumerable lessons and insights on research and other academic issues from them.

I feel deeply grateful to Mr Mike Russell for financially supporting the project, for his indispensable assistance for collecting boat motion and for his patience to pass his invaluable knowledge and experience through several meetings.

I am especially indebted to Professor Steve Elliott for his great support and funding the manufacturing and testing the prototype through the Engineering Non-linearity Grant.

My special thanks go to Mike Street at EDMC workshop for his help in designing of the energy harvester. Also, I would like to express my thanks to Tim Hartley, Peter Russell, Weidong Gong and other technicians at Electromechanical and Human Factor Research Laboratories for helping me to manufacture and testing the prototype.

I would like to express my appreciation to Dr. Jamil Renno for facilitating the high-frequency vibration experiment and Mr L. Auboin for his help with collecting boat motion data and conducting simulated boat motion Lab experiments.

I want to thanks all students and staff at Electromecanical engineering group who have contributed with their friendship and support to complete this journey.

Finally, this work would not be possible without the vital support and constant encouragement of my beloved parents, my sister Shima and my brother Mohamed for which I am deeply grateful.

Symbols

A_w	Cross-sectional area of the wire
a	Acceleration
B	Magnetic flux density
C_l	Load capacitance
c_{bg}	includes the mechanical viscous damping of the combined ball screw connections and generator
c_e	Electrical damping coefficient
c_m	Mechanical damping coefficient
c_{mb}	Mechanical damping of ball screw
c_{mg}	Mechanical damping of generator
D	Ball bearing centre-to-centre diameter
d	Ball screw shaft minor diameter
E_b	Efficiency of rotational energy harvester
E_l	Efficiency of linear energy harvester
E_l	Effectiveness of energy harvester
f_d	Coulomb friction
$i(t)$	Electrical current
F_{EM}	Electromotive force
J, J_t	Total moment of inertia
J_b	Ball screw moment of inertia
J_g	Generator moment of inertia
J_{mi}	Moment of inertia due to rotational mass
J_r	Moment of inertia of rotational rod
K_t	Emf constant, force constant
k	Spring stiffness
L	Length of perpendicular rotational shaft

L_i	Coil inductance
l	Ball screw lead
l_b	Distance between two mounting distance
m	Inertial mass
m_r	Movable mass
$P_l(t)$	Instantaneous power
P_{l-ave}	Average of output power transferred to the load resistance
P_{l-peak}	Peak value of output power
Q	Process noise covariance
R	Measurement noise covariance
R_i	Generator internal resistance
R_l	Load resistance
T_i	Emf constant, torque constant
T_s	Constant time interval
V_C	Volume of coil
V_{emf}	Induced voltage
$v(k)$	Velocity
$\mathbf{w}(k)$	Process noise
X	Amplitude of mass displacement
x	Mass displacement
$\dot{x}$	Mass velocity
$\ddot{x}$	Mass acceleration
Y	Amplitude of base displacement
y	Base displacement
$\dot{y}$	Base velocity
$\ddot{y}$	Base acceleration
$y(k)$	Displacement
Z	Amplitude of relative displacement

Z_0	Maximum allowable relative displacement
Z_n	Amplitude of relative displacement when harvester excited at natural frequency
$Z_{resonance}$	Relative displacement at resonance frequency
z	Relative displacement
$\dot{z}$	Relative velocity
$\ddot{z}$	Relative acceleration
$z(k)$	Integral of displacement
ξ	Damping ratio
Λ_{em}	Electromechanical co/upling coefficient
τ_G	Generator electrical torque
τ_v	Time constant
$\mathbf{v}$	Measurement noise
$\upsilon(t)$	Rotational speed
ω	Frequency of excitation
ω_n	Natural frequency of harvester
$\omega_{resonance}$	Resonance frequency of harvester

Chapter 1: Introduction

1.1 Energy harvesting

Energy harvesting is defined as the process of capturing and converting energy from an ambient energy source into electrical energy for powering electrical equipment. The interest in energy harvesting from ambient sources arises partly from its potential to increase the operational lifecycle of autonomous or standalone applications by reducing their reliance on finite power sources, e.g. batteries or super-capacitors. This advantage reduces the maintenance cost and increases the reliability of utilizing the off-grid electrical components and extends the exploitation of ambient sources of energy in a wide range of applications such as medical implants [1, 2], wireless sensor networks [3, 4] and applications in remote areas and harsh environments [5]. In addition, in large-scale applications, the ambient sources of energy are considered as clean and renewable alternative sources for fossil fuels to power electrical grids [6, 7].

There are different types of energy sources in the environment and technologies have been developed over the years to harvest energy from these resources. Photovoltaic is the most commonly utilised source of energy. Solar radiation and indoor illumination provide sufficient energy to power a range of electrical equipment from a small refrigerator mounted on a camel's back [8] to wristwatches and calculators [9]. Electromagnetic radiation from sources like radio and microwave communications is another source of energy available in the environment, which can be exploited in some applications such as passive radio frequency (RF) tags for automatic identification and surveillance [10]. Thermal energy harvesters rely on a thermal gradient to generate energy, for instance utilising the temperature difference between earth layers [11] or between human body and the ambient environment [12]. Kinetic energy is presented in any moving object including fluids such as air and water [13, 14, 15]. If the moving object performs a reciprocating motion, the source of energy can be viewed as a "vibration energy source". With this definition, a wide range of energy sources such as ocean waves, human body motion and civil structures movement can be categorized under vibration energy sources and hence, vibration energy is regarded as one of the most ubiquitous sources of energy which offers a great potential for ambient energy harvesting.

1.2 Vibration energy harvesting

Harvesting energy from ambient vibration and moving structures has been the subject of significant research in the last decade, which has resulted in a numerous publications, including a number of review articles [16, 17, 18]. These articles report vibration energy harvesting in a wide range of devices and applications. The majority of research is related to applications with a vibration frequency of 10 Hz to 20 kHz and the power generation in the range of 10μW to 100 mW. This level of energy is enough to power wireless sensors and low-power electronics. However, in some situations the vibration can be very large, for example the vibration of tall buildings [19], vehicle systems [20], ocean waves [21] and human motion [22]. In these applications, usually the frequency of vibration is less than 10 Hz but due to the large amplitude of vibrations, the potential for harvesting energy from 1 W to 100 kW or more exists. Recently, with the elevated concerns on the global energy and environmental issues, harvesting energy from large-scale vibrations is more attractive and hence it has become one of the important research areas [16].

Regardless of the device size, a typical vibration energy harvester comprises a mechanical system with external excitation, a transducer that converts the vibration energy into electrical form and mechanisms for motion magnification and transmission. In addition, power electronics and control systems are employed to maximize and manage the power flow to loads and energy storage devices. Traditionally, vibration energy is dissipated as wasted heat by the damping elements of the systems. However, transducers in vibration energy harvesting systems can convert mechanical energy into electricity. The common means of converting vibration energy into electricity are piezoelectric, electrostatic and electromagnetic conversion mechanisms.

1.2.1 Electrostatic energy harvesters

Electrostatic generators are comprised of two conductive plates that are electrically separated by air or a dielectric, which move relative to each other. The principle of operation is based on the change of capacitance between the parallel plates. When the plates move relative to each other due to vibrations, the capacitance between the conductors varies that in turn boosts the energy stored in the harvester [18]. There are two modes of operations for such systems, the charge-constrained mode and the

voltage-constrained mode [23]. In the charge-constrained mode of operation, the charge on the capacitor is kept constant and when the capacitance reduces, due to the gap increase between the plates or the overlap reduction, the voltage between the plates increases. In the voltage constrained-mode, the voltage between the plates remains constant; therefore, the charge on the plates increases when either the gap between the plates is reduced or the plates overlap area is increased. In the former mode of operation, one voltage source would be required for the initial charging of the electrostatic based harvester. Whereas, for the latter mode of operation, two voltage sources would be required, one for initial charging and the second one for keeping the voltage constant during operation [23, 24].

One advantage of electrostatic harvesters is their compatibility with microelectromechanical systems (MEMS) fabrication processes that enable the manufacture of miniaturized electrostatic energy harvesters for micro devices [25]. In addition, electrostatic based harvesters are capable of producing one to several volts and hence ordinary rectifying circuits can be used for AC to DC conversion. However, they exhibit high output impedances that result in low levels of output current. The major concerns in utilizing electrostatic energy harvesters are the necessity of a pre-charge voltage and the requirement of a switching circuit for their operation. Another disadvantage is that, for many configurations, a mechanical stop must be employed to ensure that the capacitor electrodes do not come into contact and short the electrical circuit [23, 26].

1.2.2 Piezoelectric energy harvesters

The piezoelectric materials used in these harvesters consist of polarized domains, which are oriented randomly under unloaded condition. However, when the piezoelectric material is subjected to mechanical strain or deformation, the dipole domains orient themselves and create a charge separation across the material, resulting in a potential difference. Polycrystalline ceramics and piezoelectric polymers are some of the most commonly used piezoelectric materials [27]. Piezoelectric polymers are widely used due to their low cost and high flexibility, however, their piezoelectric coefficient is much smaller than that of piezoelectric ceramics.

A cantilever beam is one of the most common structures in piezoelectric energy harvesters [17]. Thin layers of piezoelectric materials are deployed on a micro-fabricated cantilever beam, and a proof mass attached to the beam is used to tune the frequency of the harvester, which is related to the weight and position of the mass. Energy harvesters with only one layer of piezo-material on the cantilever beam are referred to as unimorph piezoelectric harvesters [28, 29]. The harvesters that utilize two layers of piezoelectric materials on either sides of the cantilever beam architecture are known as bimorph piezoelectric harvesters [30]. Also, in some applications, an array of coated piezoelectric cantilever beam is employed to broaden the harvester's bandwidth [31].

It is commonly assumed that piezoelectric devices produce voltage in the order of one to several volts [17]. This ability is important as it provides the possibility of utilizing an ordinary rectifying system in the electrical circuit for AC to DC conversion. However, the high output impedance of these devices causes low level of current. In general, the voltage and current levels mainly depend on the design and electrical load circuit of the energy harvester. Therefore, an advantage of piezoelectric energy harvesters is the possibility of designing a harvester that produces appropriate ranges of voltage and current for directing power to an electrical load such as wireless sensors. Also, in contrast with electrostatic based harvesters, no separate voltage source is required to initiate the transducer. In addition, no mechanical stoppers are needed and therefore an energy harvester can be designed that will exhibit very little mechanical damping [32]. In addition, piezoelectric harvesters are a neat choice for direct force generator in wearable devices as they do not have a noticeable effect on the user's gait [18]. In general, they are a reliable choice for applications where space or weight is a concern [33]. However, the use of piezoelectric based harvesters remains limited to harvesting energy from small amplitude vibrations due to geometry constraints and deformation of piezoelectric materials.

1.2.3 Electromagnetic energy harvester

According to Faraday's law of induction, when a wire is moved relative to a magnetic field, or vice versa, an electromotive force is produced. If the wire is connected to an electrical load, current flows and thus electrical power is generated.

Utilizing the principle of Faraday's law, an electromagnetic energy harvester produces power due to the relative movement of a coil and a magnet, which induces voltage across the coil terminals. A typical electromagnetic energy harvester, in its simplest form, comprises a magnet, a coil, a mechanical spring and a frame. The spring supports either the magnet or the coil and allows the relative movement in the device. There will be mechanical damping arises from air resistance and surface friction and the electrical damping appears due to current flow in the coil.

In comparison with electrostatic and piezoelectric energy harvesters, the output voltage of electromagnetic based systems is in the order of few μV to several mV. However, due to their low output impedances, they produce relatively higher current levels [17]. Also, electromagnetic based harvesters are preferred in situations where vibration has large velocity or amplitude. Therefore, electromagnetic generators are the transducers of choice in large-scale energy harvesting applications. Energy recovery from vehicle suspensions [22], building vibration dampers [34] and ocean waves [35] are some examples of large-scale electromagnetic energy harvesters.

1.3 Electromagnetic harvesting of vibration energy in marine environment

Due to the availability of wide sources of energy in the marine environment, different energy harvesting mechanisms have been identified. Solar energy can be converted to a useful form by using photovoltaic systems [36] or thermal panels [37]. An osmotic process is utilized to produce energy form salinity gradient [38]. More recently, ocean thermal energy conversion techniques (OTEC) have been developed [39] and several versions of wind turbines have been installed in offshore wind farms [40, 41].

Vibration energy in the form of wave energy is another conventional source of energy in marine environment. This type of renewable energy has attracted investment and research funding due to its great potential following the oil crises in 1973 [42]. Surface buoyancy energy generation is a well-known method of harvesting energy from wave. These systems are composed of either a floating buoy driving a generator or several floating rafts that move relative to one another [43].

The other well-known and commercial method for harvesting energy from wave is overtopping. This relies on a ramp enabling water to be trapped into a reservoir. The reservoir border is located at a certain height above the average water level. The wave potential energy is thus absorbed and a turbine driven generator is activated as water goes back to the ocean level. A large-scale example of this architecture is the Wave Dragon which has been produced by Ocean Power Delivery Ltd [42].

Another type of electromagnetic energy harvester in marine environment is based on an inertia mass being placed in a host vessel either similar to a pendulum or a gyroscope. A large-scale example of the inertial pendulum harvesting mechanism is Searev [44] and an example of the gyroscope type is the Gyro-gen [45].

Another method of harvesting energy from waves is an oscillating water column which consists of a partially submerged hollow structure. The waves compress and decompress the trapped air column, which is thus forced to cross a Wells turbine. This type of turbine rotates regardless of the direction of the airflow. These types of systems have a disadvantage in that their efficiency decreases because of the air compressibility. An example of this type of mechanism is Limpet [42]. Many electromagnetic energy harvesting systems in a marine environment rely on a proof mass coupled to an electric generator whose relative movement is, directly or indirectly, caused by the waves. However, in these applications the frequency of vibration and hence the relative speed of the proof mass is low. Therefore, a direct drive generator can be quite large and expensive relative to the amount of power it produces, i.e. the power density of the generator will be very low. This is due to the fact that the size of an electric generator is proportional to its torque (or force in a linear generator) and accordingly the power density is proportional to its speed. Compared to a linear generator, a brushless rotary generator is dimensionally smaller and more cost-effective. Therefore, in some energy harvesting systems, an intermediate mechanism is utilised to convert a linear low frequency motion to a high frequency rotational motion to reduce the size and cost of the device. Rome *et al.* [46] developed a backpack driven energy harvesting system based on a rack-and-pinion mechanism. This mechanism converts the linear movement to a rotary motion to drive a rotary generator. This energy harvesting device produces an average power of 5.6 W from a normal human walk. The idea of utilising a rack-and-pinion mechanism has also been used in some electromagnetic dampers [20, 47].

However, due to friction and backlash, the use of a rack-and-pinion mechanism has usually resulted in a low efficiency system.

Matsouka et al. [48] propose a fixed type and a floating type wave energy conversion system using a ball screw type turbine. A ball screw is a high efficiency alternative gearing mechanism, which is employed in some energy harvesting systems [48, 49, 50]. The fixed type is composed of a pressure plate and a ball screw settled in a caisson, and the floating type is composed of a floating body and a wave power buoy with a ball screw connected to a generator. The ball screw is useful in transforming slow linear motion into fast rotary motion with a high efficiency of more than 90%. The ball screw rotates by the wave force that directly hits the pressure plate and the wave power is efficiently converted into electric power by a generator that is connected to the ball screw.

Agamloh et al. [49] study a medium scale system where a ball screw is employed to convert the linear displacement of a moored buoy to rotational motion for driving a permanent magnet generator. They have reported that commonly proposed ocean energy extraction techniques based on hydraulic or pneumatic intermediaries are prone to failure with high maintenance costs. One way of eliminating the intermediate systems is to use direct-drive techniques to convert the slow linear motion, produced by the waves, to rotary or linear motion by means of an efficient and simple system. To harvest energy from the movement of a buoy, they suggested a contact-less force transmission system (CFTS), which employs magnetic fields for contact-less mechanical thrust transmission. This system has enhanced the design of a new direct-drive ocean wave energy converter (OWEC) using a ball screw to act as a mechanical gear system for fast speed and torque transmission. The system comprises an outer float inside which is a ferromagnetic cylinder which slides against an inner module. As the outer float slides, it pulls the piston of the inner module along with the help of the CFTS. The inner module is completely sealed. The buoyancy force on the outer cylinder is transmitted through the wall of the inner module to the ball nut by the magnetic fields of the piston.

However, reviewing the studies on ball screw based electromagnetic energy harvesters in marine environment indicates that most are generally related to fixed, large-scale, land-based or tethered power generation systems whereas for a boat, a medium-scale system needs to be considered. Furthermore, in those applications the maximum displacement of the oscillating mass has not been considered as a constraint

while in practice the range of motion of the mass is limited. In addition, in most of the aforementioned systems the floating parts are directly driven by the wave (i.e., there is no spring component in the system) whilst for boats, a portable base excited energy harvesting mechanism should be employed which requires a spring element.

1.4 Thesis motivation and objectives

In some energy harvesting applications, the maximum displacement of the seismic mass is constrained and by following the conventional design and optimization rules only sub-optimal performances are obtained. This limitation is specially highlighted in those applications where due to the availability of large amount of input power, the design process involves restricting the motion of the seismic mass. Also, the nonlinear behaviour of springs, when over-extended and limited size of the energy harvesting device are other parameters which necessitate the considering of the maximum allowable mass displacement as a constraint in the design process. On the other hand, due to limitations on geometry and finite permissible deformation of other transducers, the electromagnetic induction method is the more appropriate choice for large-scale applications.

One of the large-scale applications of vibration energy harvesting can be found in the marine environment where harvesting energy from the movement of a boat is of interest. In general, cruising and racing yachts are increasingly reliant on electrical power for lighting, navigation equipment and for automatic steering systems, in the case of single-handed sailing. Power requirement is typically in the range of 10 to 50 watts for which a 12-volt lead acid storage battery is commonly used. For most short range cruising conditions the battery is kept charged by the main engine. However, this is not allowed during racing and many cruising yachtsman would prefer to avoid using the main engine solely for battery charging. For these applications, utilizing the renewable sources of energy available in the marine environment is an attractive option that must be considered.

Despite the diversity of the energy sources in marine environment [51], when harvesting energy for a boat is of interest, only few of the available methods are applicable. Wind generators, towed impeller generators and solar cells are the most commonly used alternative power sources on boats but they all have their own

limitations. On relatively large racing yachts, the wind and towed impeller devices tend to interfere with rigging, and solar panels do not always provide enough power particularly in northern European waters. However, the almost perpetual boat vertical motion can be considered as an auxiliary source of energy for extracting power. The objectives of this research can be summarised as:

1. Studying the characteristics, including amplitude, main frequency and the frequency range, of the vertical excitation of a typical boat in marine environment.

2. Studying the analytical model of linear and rotational electromagnetic energy harvesters for constrained applications.

3. Providing a set of design criteria for designing linear and rotational energy harvester for constrained applications.

4. Designing a rotational energy harvester for harvesting energy from vertical movement of a boat as an example of a constrained application.

5. Evaluating the performance of the designed rotational system under broadband and band-limited excitations.

6. Studying a novel strategy for broadening the operational frequency range of rotational energy harvesting devices.

7. Constructing and testing a prototype of a rotational energy harvester to validate the analytical model of the system.

1.5 Thesis contributions and chapters summary

Motivated by the above discussion, this thesis studies the design and constrained optimisation of electromagnetic energy harvesting devices. Designing a device for harvesting energy from a boat's vertical motion is presented as a typical application of a constrained electromagnetic energy harvester. Therefore, in course of addressing the above mentioned objectives, the thesis consists of the following chapters:

The first step of designing an energy harvester is to investigate the vibration characteristics of the environment. Therefore, chapter 2 studies the frequency and displacement of the vertical motion of a boat obtained from the measured acceleration signal in real environment. The main frequency of oscillations is obtained from the

spectrum of the recorded acceleration signal. However, it is shown that using direct numerical integration to calculate velocity and displacement from the acceleration signal suffers from low frequency noise amplification and integration wind-up. In this chapter, two Kalman based methods are proposed to eliminate integration wind-up which are validated by conducting experiments. The methods are developed based on the fact that in many vibrating structures, the average of velocity and displacement amplitudes remain constant.

Chapter 3 investigates the conditions for obtaining maximum output power and the corresponding efficiencies of two types of electromagnetic energy harvesting systems (i.e. linear and rotational) with constraints on their range of motions. This chapter introduces a set of design rules for optimum design of linear and rotational electromagnetic harvesters in constrained applications. In addition, in this chapter the equations for power and corresponding efficiency of both systems are derived in unified forms so that a comparison between them can be made. The comparison reveals that in the case of a linear system, the maximum amount of transferrable power to the load is half the mechanical power transferred by the harvester and hence the efficiency of the system is always less than 50%. However, a rotational system can be designed to have an efficiency greater than 50%. The criterion that guarantees the efficiency of a rotational system is more than 50% is presented. Furthermore, this chapter conducts a study on the effect of scaling the size of the electromagnetic generator component of an energy harvesting system on the output power and efficiency. It is shown that by increasing the size of the energy harvesting system the efficiency is increased for both constrained linear and rotational systems.

Chapter 4 proposes a ball screw based device for harvesting energy from the vertical motion of small boats and yachts. The device is comprised of a sprung mass coupled to an electrical generator using a ball screw. The mathematical equations describing the dynamics of the system are derived and used as a basis for determining the optimum device parameters, namely its mass, spring stiffness, ball screw lead and load resistance. In this chapter to extract maximum energy from the vertical motion of a boat, the harvester's parameters are selected based on a constrained optimization process. Here, a design process flowchart is developed that provides guidelines for optimum selection of the system parameters. The proposed technique considers

practical limiting factors involved in the design of a constraint ball screw system including the maximum allowable displacement of the oscillating mass. It is shown that, unlike unconstrained energy harvesting systems, for such energy harvester where the maximum displacement is constrained, selecting the optimum load resistance should be considered at early stages of the design process (i.e., not a posteriori step). The suggested system with a mass of 8 kg is estimated to produce more than 30 watts for a typical boat motion that oscillates with average amplitude of 1 m at 0.5 Hz. This amount of energy is sufficient to supply a typical boat's internal power usage demand.

Chapter 5 evaluates the performance of the proposed ball screw based device for harvesting energy under broadband and band-limited random vibrations. In this chapter, based on dynamic equations of the system, its frequency response function is obtained by utilizing the theory of random vibration and the mean power acquired from the harvester when it is subjected to broadband and band-limited stationary Gaussian white noise. The power expressions are derived in dimensional form to provide an insightful understanding of the effect of the physical parameters of the system on output power. Also, an expression for the optimum load resistance to harvest maximum power under random excitation is derived and validated by conducting Monte-Carlo simulation. The discussion presented in this chapter provides a guideline for designers to maximize the expected harvested power from a system under broadband and band-limited random excitations. In addition, in this chapter it is shown that the profile of the spectral density of the measured acceleration of a typical boat represents a Cauchy distribution. Therefore, the power spectral density of the real environmental vibration is estimated with an analytical expression which leads to calculating the expected power generated by the designed rotational harvester for realistic conditions.

In chapter 6, a new strategy is proposed for broadening the frequency range of the ball screw based harvester. It is shown that by changing the moment of inertia of the harvester in combination with tuning the load resistance at its optimum value, the output power of the system under time varying frequency condition is significantly improved.

In Chapter 7, a prototype of the proposed ball screw based energy harvester is constructed and tested to verify its feasibility. The device characteristics such as the actual mechanical damping, frequency response of the system and the optimum load resistance to harvest the maximum power are investigated. The results of this chapter

are used to validate the dynamic equations of the designed energy harvester that are derived in chapter 3.

Chapter 2: Boat's vertical displacement

2.1 Introduction

The first step in designing an energy-harvesting device to capture energy from ambient vibration is to study the vibration characteristics of the target environment. Therefore, where the harvesting energy from the vertical movement of a boat is of interest, information such as the frequency range of vibrations, the dominant resonant frequency and typical displacement amplitude of the boat are absolutely necessary.

A review of different studies has shown that the vertical movement of typical sailing boats is inherently random with the dominant frequency of vibration being less than 1 Hz [52]. This was confirmed by the authors' own boat acceleration measurement obtained while sailing in the English Channel, as shown in figure 2-1. The boat was a double hull catamaran, 34 feet long, 14 feet wide with a total weight of approximately 3.5 tones. To measure the acceleration of the vertical movement of the boat, a micro-machined silicon static accelerometer was positioned about 1 m from the bow. The power spectral density of the recorded acceleration shown in figure 2-2, indicates a strong response at the frequency of 0.5 Hz. In general, spectral analysis of the recorded data confirms that significant response also occurred at frequencies below 1 Hz, mainly between 0.4 Hz to 0.6 Hz.

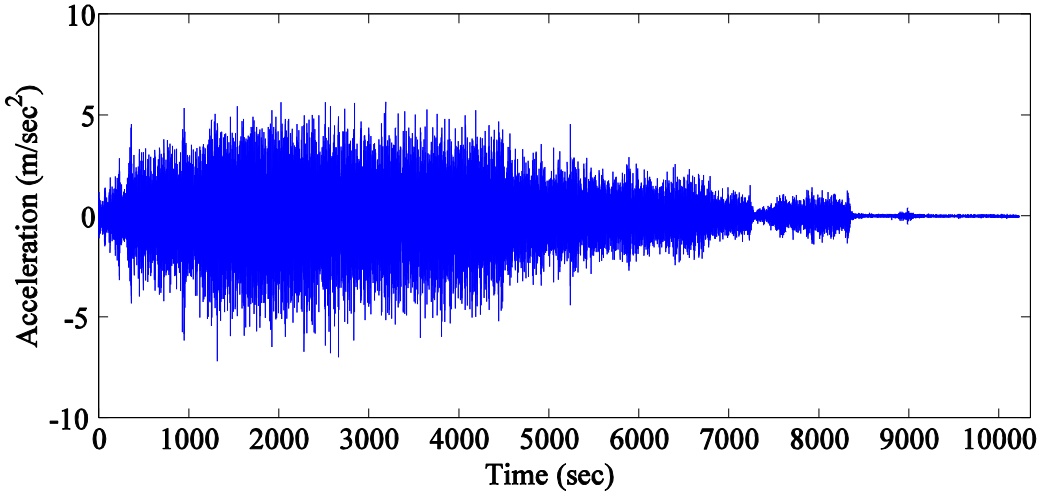

Figure 2-1 Typical boat bow vertical acceleration measured while sailing in the English Channel.

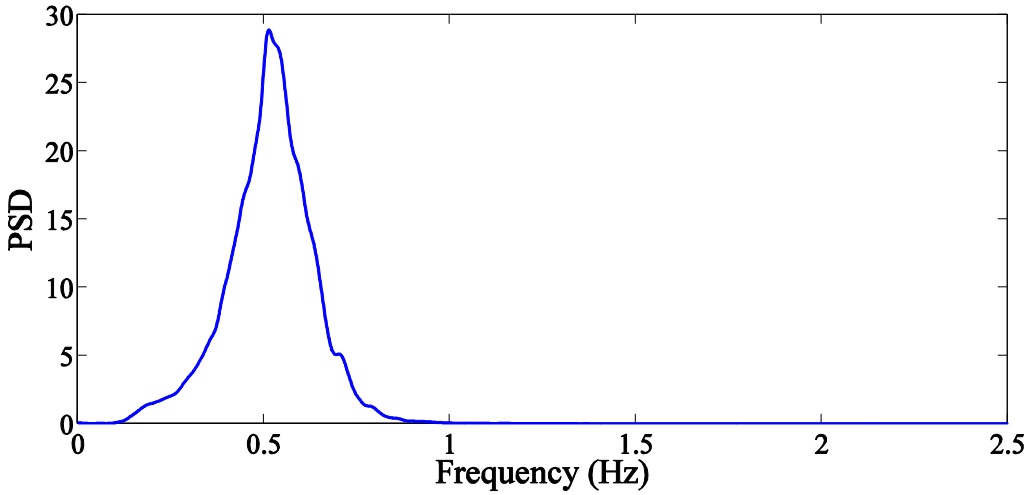

(a)

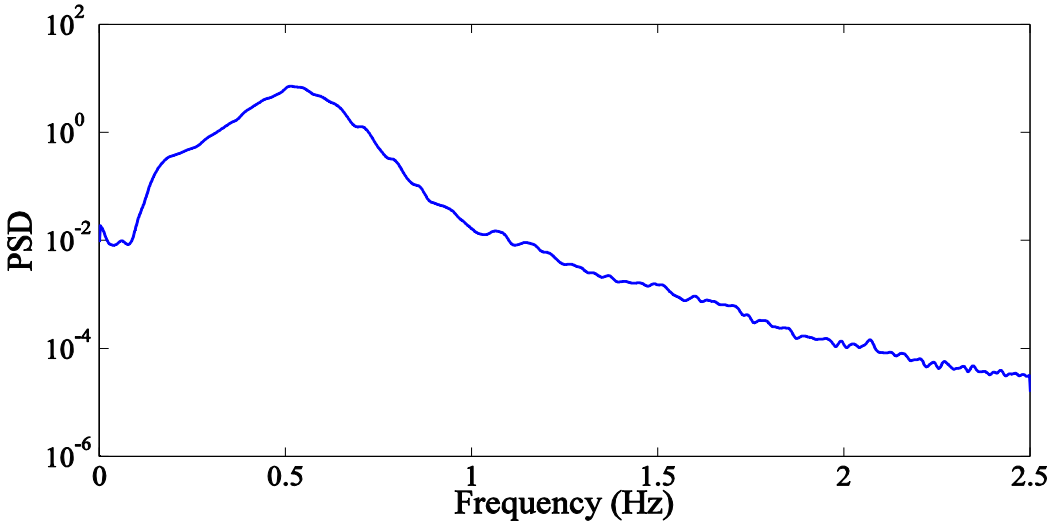

(b)

Figure 2-2 Power spectral density of the measured acceleration shown in normal and semi-log.

However, whilst in general it is straightforward to extract information on the frequency components, the reconstruction of the velocity and displacement time histories of the boat movement in response to sea waves is not an easy task and applying direct double integration results in unacceptable result. To understand the reasons for this issue and the suggested approaches to solve this problem, the relevant literature will be reviewed next.

2.2 Background

Direct measurement of displacement and velocity are not always feasible, as they require a sensor to be fixed to an inertial frame of reference, which may not be readily available. The measurement may simply be impractical, e.g., when measuring the displacement of a high bridge or a ship. For this reason, accelerometers are often used and the signal is then integrated to obtain velocity and displacement. Accelerometers have the additional advantages of lower cost, smaller size and higher bandwidth than electromagnetic velocity and displacement sensors. However, direct integration of an acceleration signal poses two main difficulties. The first arises from the presence of low frequency noise and dc drift, which are amplified by the integration process leading to integral wind-ups. The second arises from not knowing the values of the initial velocity and displacement, which are often non-zero. This could also cause integral wind-up. Further errors are caused by digital sampling, particularly if the sampling rate and the ADC resolution are poor [53].

To overcome these problems, various methods have been investigated in the literature in the context of different engineering applications. There are two main basic methods using either numerical integration of the time domain signal (direct integration method) or integrating its Fourier series equivalent (frequency domain method). The frequency domain method suffers from the problem of spectral leakage, especially when the signal is random and irregular. The spectral leakage problem is usually overcome by zero padding, i.e., setting the false frequency components caused by leakage to zero [54] .

Taira *et al.* [55] utilize the frequency method to estimate the vertical displacement of a ship. They apply a Fast Fourier Transform (FFT) algorithm to the measured acceleration signal. However, since the motion of a ship is inherently random and irregular, the FFT method causes errors in the estimation of displacement, which is referred to as leakage error. The maximum leakage error caused by all frequencies components that compose the signal is investigated and the frequency corresponding to the maximum amount of leakage error is found. After double integration of the Fourier series of the acceleration signal, the displacement amplitude for all frequencies below the maximum leakage error frequency are assumed to be zero. Although, the frequency domain method suffers from the problem of spectral leakage, especially when the signal

is random and irregular, this method is demonstrated to be effective in accurately calculating the vertical displacement of a ship from acceleration measurements. The estimated ship displacement is used to correct the wave gauge measurements and accordingly estimate the waves' heights. However, it is not possible to apply this approach in real time.

To achieve good accuracy with direct integration techniques, the sampling rate needs to be much higher than the highest frequency in the signal [54, 56]. It needs to be more than 12 times the highest frequency component of the signal to reduce the integration error to less than 1% when the trapezoidal rule is used to perform the integration [54]. Several techniques have been proposed by different authors to overcome the integral wind-up problem. Gavin *et al.* [53] proposed using an integrator with a loop feeding back the average of the integrated signal obtained using a low pass filter. They demonstrated the technique using both analogue and hybrid analogue-digital circuits. The analogue circuit performed well in terms of linearity and hysteresis when integrating random wide-band signals, but less so when integrating long-period signals. The hybrid circuit had excellent accuracy when integrating long-period signals, but produced phase and bias errors when integrating wide-band signals.

The method proposed by Park *et al.* [57] basically repeats the direct integration for a range of initial velocity conditions, to find a suitable value for which integrator wind-up is eliminated. However, this method cannot be used in real time and the authors have found that in practice it is necessary to segment the signal and apply the method to each segment individually.

Zhou *et al.* [58] suggest a multi-step scheme to correct the drift produced when calculating the displacement of soil from measured acceleration during a shaking table laboratory test. These steps include applying baseline correction before each integration step and then applying a high pass filter to remove long-period oscillations from the displacement signal. Yang *et al.* [59] also use a direct integration and base line correction method, assuming the acceleration base line to be parabolic; In this work, they calculate the mathematical formulae for the velocity and displacement base line correction. The coefficients of the trend line polynomials are calculated using least square curve fitting. A high-pass filter is finally used to remove long-period oscillations from the displacement signal.

To reconstruct the dynamic displacement induced by structural vibration from a measured acceleration signal, Hong *et al.* [60] propose two types of finite impulse response filter to suppress the low frequency noise components in the measured acceleration. They use a frequency domain integration approach. However, instead of using the actual transfer function of an integrator to calculate displacement, a transfer function relating the acceleration and displacement of a beam on an elastic foundation is suggested. The two methods are investigated using simulation and field experiment.

Smyth *et al.* [61] overcome the integral wind-up and amplification of low frequency noise problem by using a multi-rate Kalman filter based method to fuse information obtained from both low sampling displacement sensors and high sampling rate acceleration sensors. By combining the two signals they overcome the problems of low frequency noise amplification of integration of acceleration signals and high frequency noise caused by differentiation. The method is also beneficial in applications where non-linear behaviour and permanent deformation are present. Obviously, this method requires the use of two sensors that will be more costly.

In this chapter two Kalman filter based methods are suggested and validated to calculate the displacement and velocity from an acceleration signal. The methods are based on the fact that in many vibrating structures, the average of velocity and displacement remain constant. These can be utilised in the Kalman filter as additional measurements to overcome the integration difficulties of low frequency noise amplification and integral wind-up. These proposed methods are used to calculate the displacement time history of the boat from acceleration signal.

2.3 Kalman Filter with post filtering step

The Kalman filter, as a recursive least-square observer, has been applied in areas as diverse as aerospace, marine navigation, nuclear power plant instrumentation, demographic modeling and manufacturing. It uses a state-space model of the system together with actual measurements to optimally estimate the state variables of the system [62].

2.3.1 Equations

The calculation of displacement from acceleration can be formulated in state-space

form as follows. Assuming that the acceleration signal *a* is sampled at constant time intervals of T_s, the velocity can be calculated by using the following discrete equation:

$$v(k) = v(k-1) + a_{k-1}T_s \tag{2.1}$$

where k is the sample number. The displacement y can be calculated by integrating (2.1), resulting in:

$$y(k) = y(k-1) + v(k-1)T_s + \frac{1}{2}a_{k-1}T_s^2 \tag{2.2}$$

In addition to the measured acceleration, in many applications the average value of the displacement of the system is constant (normaly assumed to be zero), if non-linear behaviour and permanent deformation can be neglected. Calculating the average value, by integrating over one period, requires the frequency of the signal to be known which is not always possible. Alternatively, a low pass filter with a tranfer function of $1/(s+\omega_o)$ may be used to extract the average value. However, to accurately integrate the low frequency components of the signal, the cut-off frequency ω_o needs to be small, and in the limit when $\omega_o \to 0$ the transfer function of the filter becomes that of an integrator. As a first approximation it is therefore reasonable to assume that average displacement could be approximated to be the integral of the displacement $z = \int y\,dt$ whose measured value is zero. In discrete form,

$$z(k) = z(k-1) + y(k-1)T_s + \frac{1}{2}v(k-1)T_s^2 + \frac{1}{6}a_{k-1}T_s^3 \tag{2.3}$$

Considering z to be the output of the system and *a* the input then equations (2.1), (2.2) and (2.3) can be expressed in the following state space form allowing for the process noise $\mathbf{w}(k)$:

$$\mathbf{x}(k) = \mathbf{A}\mathbf{x}(k-1) + \mathbf{B}(\mathbf{u}(k) + \mathbf{w}(k)), \tag{2.4}$$

where:

$$\mathbf{A}=\begin{pmatrix} 1 & 0 & 0 \\ T_s & 1 & 0 \\ \frac{1}{2}T_s^{\,2} & T_s & 1 \end{pmatrix}, \quad \mathbf{B}=\begin{pmatrix} T_s \\ \frac{1}{2}T_s^{\,2} \\ \frac{1}{6}T_s^{\,3} \end{pmatrix} \tag{2.5}$$

$$\mathbf{x}=\begin{pmatrix} x_1 \\ x_2 \\ x_3 \end{pmatrix}=\begin{pmatrix} v \\ y \\ z \end{pmatrix}, \quad \mathbf{u}=\begin{pmatrix} a \end{pmatrix} \tag{2.6}$$

In matrix form, the output equation is written as:

$$\mathbf{Y}=\mathbf{C}\mathbf{x}+\boldsymbol{\nu} \tag{2.7}$$

where $\mathbf{C}=\begin{pmatrix} 0 & 0 & 1 \end{pmatrix}$ and $\boldsymbol{\nu}$ is measurement noise of the output **Y**. The algorithm for the Kalman filter [63] assumes that the noise terms $\mathbf{w}$ and $\boldsymbol{\nu}$ have a normal probability distribution with zero mean and covariances of *Q* and *R*, respectively:

$$\begin{aligned} p(\mathbf{w}) &\sim N(0,Q) \\ p(\boldsymbol{\nu}) &\sim N(0,R) \end{aligned} \tag{2.8}$$

In some applications, the process noise covariance *Q* and the measurment noise covariance *R* matrices might change with each time step or measurement, however, in this work they are assumed to be constant. The Kalman filter is a predictor-corrector algorithm. The prediction step contains the time update equations which are utilized to obtain the current state and error covariance estimations. The correction step equations, based on the measurement, provide a feedback to improve the estimated value:

Prediction Step:

$$\hat{\mathbf{x}}^{-}(k)=\mathbf{A}\hat{\mathbf{x}}(k-1)+\mathbf{B}u(k) \tag{2.9}$$

$$\mathbf{P}^{-}(k)=\mathbf{A}\mathbf{P}(k-1)\mathbf{A}^{\mathbf{T}}+\mathbf{B}Q\mathbf{B}^{\mathbf{T}} \tag{2.10}$$

Correction Step:

$$\mathbf{K}(k) = \mathbf{P}^{-}(k)\mathbf{C}^{\mathrm{T}}\left(\mathbf{C}\mathbf{P}^{-}(k)\mathbf{C}^{\mathrm{T}} + R\right)^{-1} \tag{2.11}$$

$$\hat{\mathbf{x}}(k) = \hat{\mathbf{x}}^{-}(k) + \mathbf{K}(k)\left(\mathbf{Y}(k) - \mathbf{C}\hat{\mathbf{x}}^{-}(k)\right) \tag{2.12}$$

$$\mathbf{P}(k) = \left(\mathbf{I} - \mathbf{K}(k)\mathbf{C}\right)\mathbf{P}^{-}(k) \tag{2.13}$$

Matrix **P** is the covariance of the error, given by:

$$\mathbf{P} = E\left\{\left(\mathbf{x} - \hat{\mathbf{x}}\right)\left(\mathbf{x} - \hat{\mathbf{x}}\right)^{T}\right\} \tag{2.14}$$

As will be shown later, the assumption of $z = 0$ in the Kalman filter is effective in eleminating dc drift as well as overcoming the unknown initial value problem. However, there remains a low frequency trend component, which needs to be removed using a high-pass filter. A complete diagram of the operation of the Kalman filter is shown in figure 2.3.

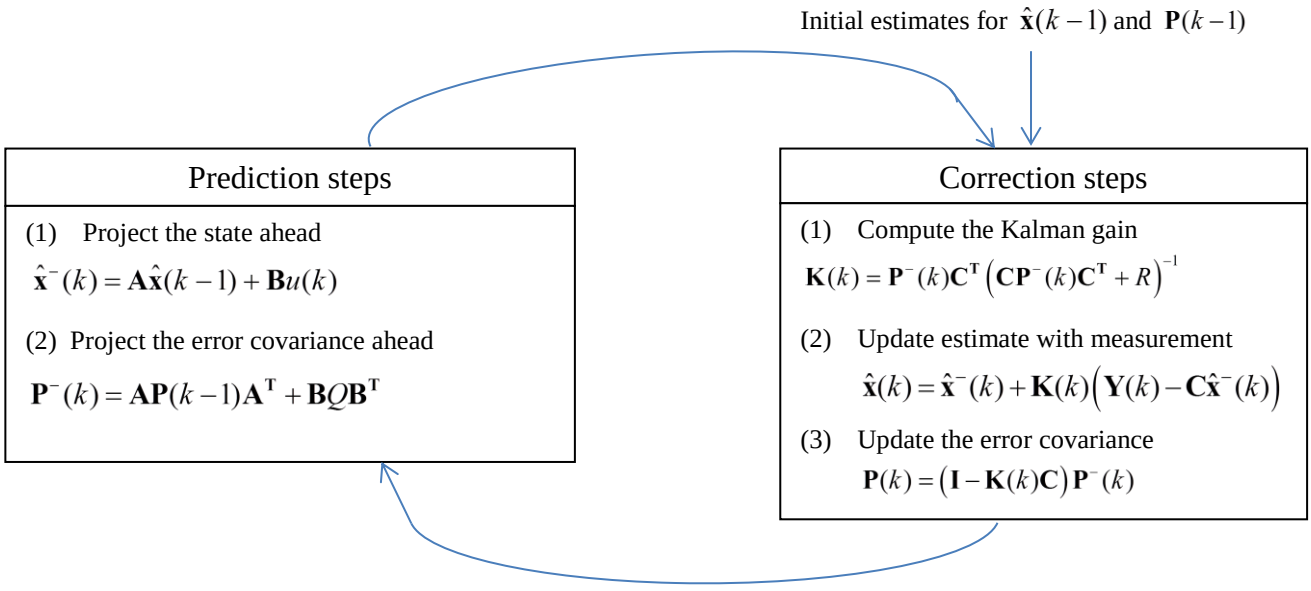

Figure 2-3 Diagram of operation of Kalman filter

2.3.2 Experimental Methods and Results

2.3.2.1 Displacement of a shaker

The validity of the proposed method is demonstrated through two laboratory investigations on systems with different specifications in terms of amplitude, frequency and sampling rate. The apparatus used in the first experiment is shown in figure 2-4. A piezoelectric accelerometer was used to measure the acceleration of a shaker. This accelerometer, which was attached to the shaft of the shaker, is manufactured by the PCB Company Pty Ltd. It has a maximum range of ±500 g (g is the gravitational acceleration), a sensitivity of 9.54 mv/g, a frequency range of 1 Hz-10 kHz and a 10 bit resolution (approximately 1 g). A Keyence laser sensor installed on top of the shaker was used to measure displacement. The sensor has a range of ±40 mm with a resolution of 10 µm. In this experiment, the acceleration and displacement signals were recorded simultaneously.

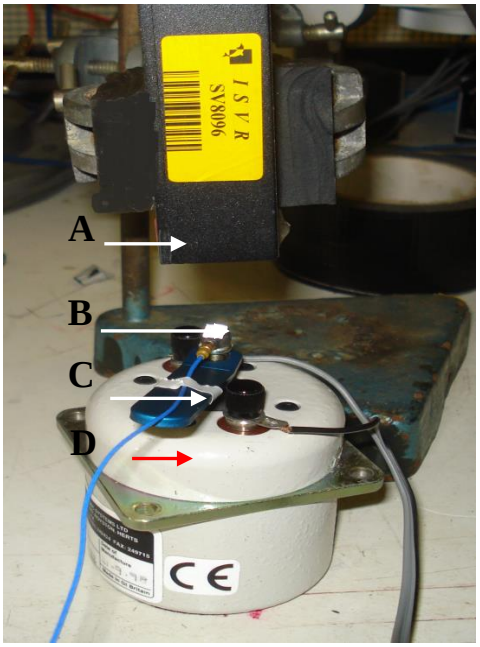

Figure 2-4 Lab apparatus used to measure acceleration and displacement of a shaker A) laser sensor, B) Accelerometer, C) Support, D) Shaker

Figure 2-5 shows a portion of the acceleration and displacement waveforms of the shaker, measured when the shaker oscillated with a single frequency of 20 Hz sampled at a frequency of 1 kHz. The result of double integration (using the trapezoidal rule) of

the acceleration signal is shown in figure 2-6, which illustrates the integral wind-up problem.

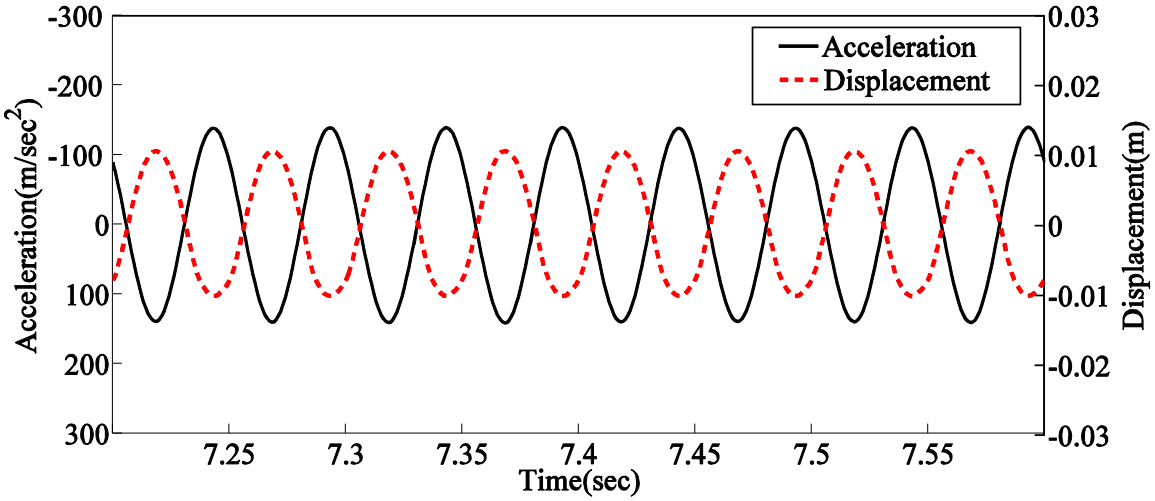

Figure 2-5 Measured 20 Hz acceleration and displacement signals.

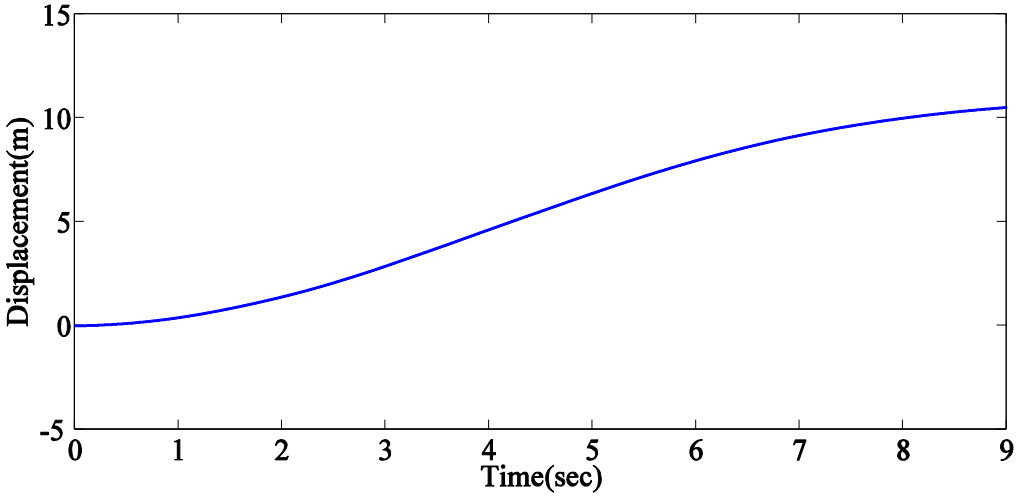

Figure 2-6 Calculated displacement using double integration of the acceleration signal in the previous figure.

Figure 2-7 shows the displacement calculated using the proposed Kalman filter method, before the trend removal filter was used; the values of the covariances Q and R were selected to minimise the Normalised RMS Error percentage (*NRE*%) as discussed below. Figure 2-8 shows the results after a fifth order Butterworth high pass filter with a 3 Hz cut-off frequency is applied. Good agreement is observed between the measured and estimated waveforms.

The Normalized RMS Error percentage (*NRE*%) was calculated for a range of values of Q and R using the following equation [64] :

$$NRE\% = 100\frac{rms[y(t)-\tilde{y}(t)]}{4rms[\tilde{y}(t)]} \quad \textbf{(2.15)}$$

where *y(t)* is the displacement estimated from the Kalman filter method and $\tilde{y}(t)$ is the actual displacement measured by the laser sensor. The results are shown in figure 2-9, which suggest that the *NRE%* value depends on the ratio of the Q/R rather than their absolute values. The absolute values of Q and R affect the speed of convergence of the filter; the larger the values the slower the filter response. A realistic value of Q could be estimated based on the resolution of the instrument to be g^2=96 m^2s^{-4}; this value was found to provide a satisfactory response. In fact, the process of tuning the Kalman filter is conducted by assuming Q on the basis of a realistic estimation and then selecting R to minimise the *NRE%*. Note that in many Kalman filter applications, the process noise and measurement noise are uncorrelated. However, the objective of applying the presented method in this work is minimizing the *NRE% a*nd hence calculating the real displacement more accurately. Dependence of the *NRE%* on the ratio of Q/R indicates that for applying this method Q and R cannot be selected independently or, in other words, they are correlated.

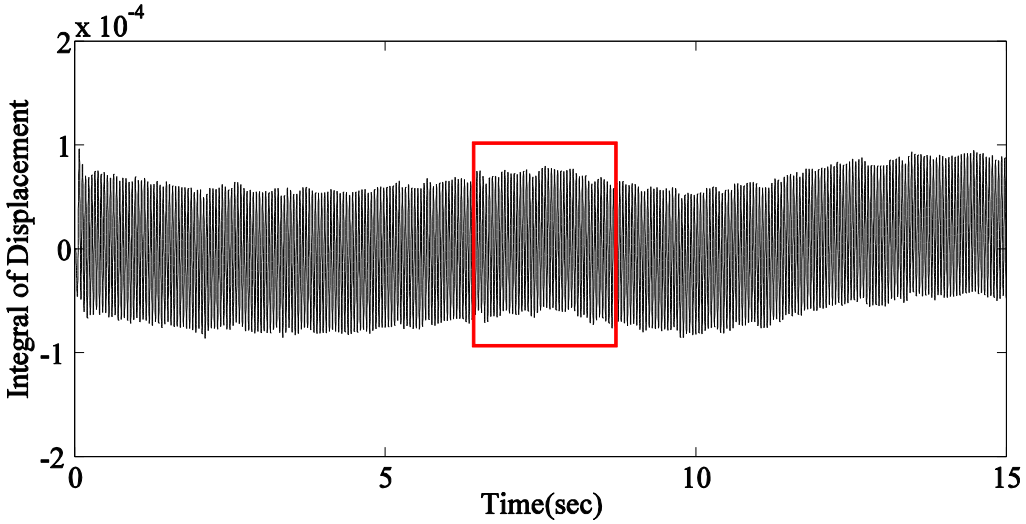

a) Full waveform

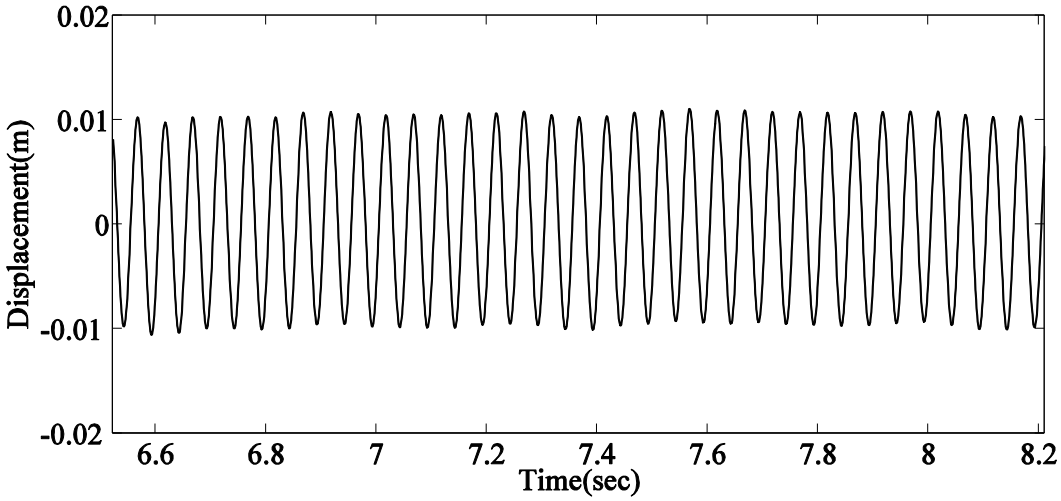

b) Magnified waveform

Figure 2-7 Calculated displacement using Kalman filter method before filtering.

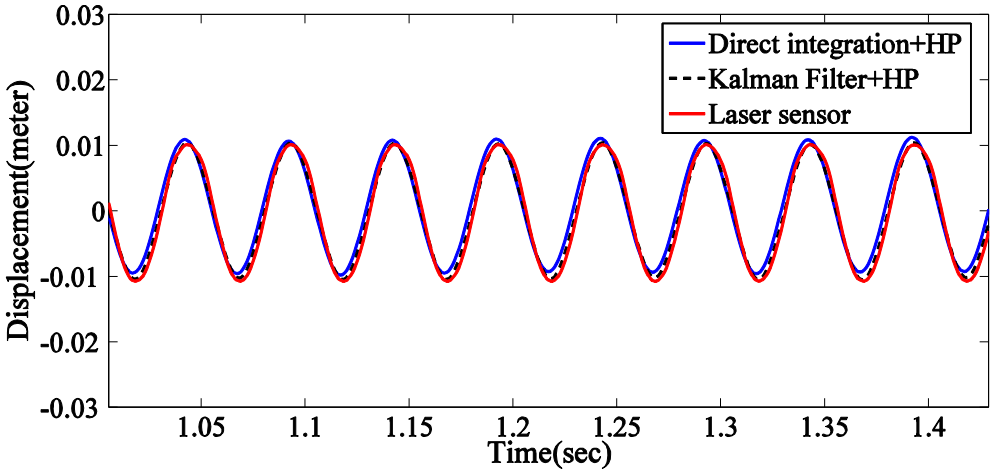

Figure 2-8 Calculated displacement using Kalman filter method after filtering using a 3 Hz high-pass filter.

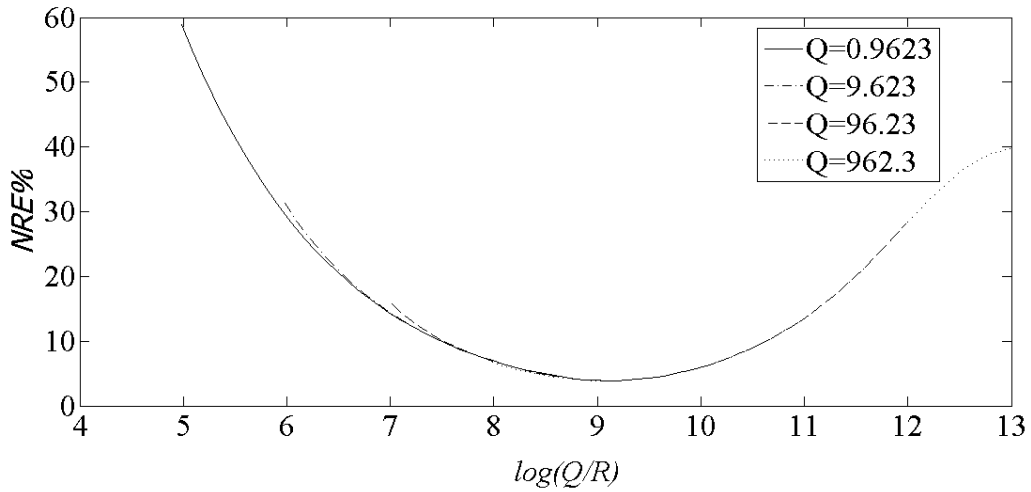

Figure 2-9 *NRE*% versus log(*Q*/ *R*).

The second scenario focused on calculating the displacement of the shaker when its motion was random. The measured acceleration in this case is sampled at a frequency of 1 KHz. Figure 2-10 shows the recorded acceleration and displacement. The power spectral density of the acceleration obtained using Welch's method, in figure 2-11, shows random excitation over the frequency range of 20-30 Hz. A good agreement is again observed in figure 2-12 between the displacement measured by the laser sensor and that estimated using the proposed Kalman filter method. However, there are noticeable differences between the estimated and actual displacements in the vicinity of peaks and troughs. The proposed method estimates the displacement with 4.8% Normalized RMS Error.

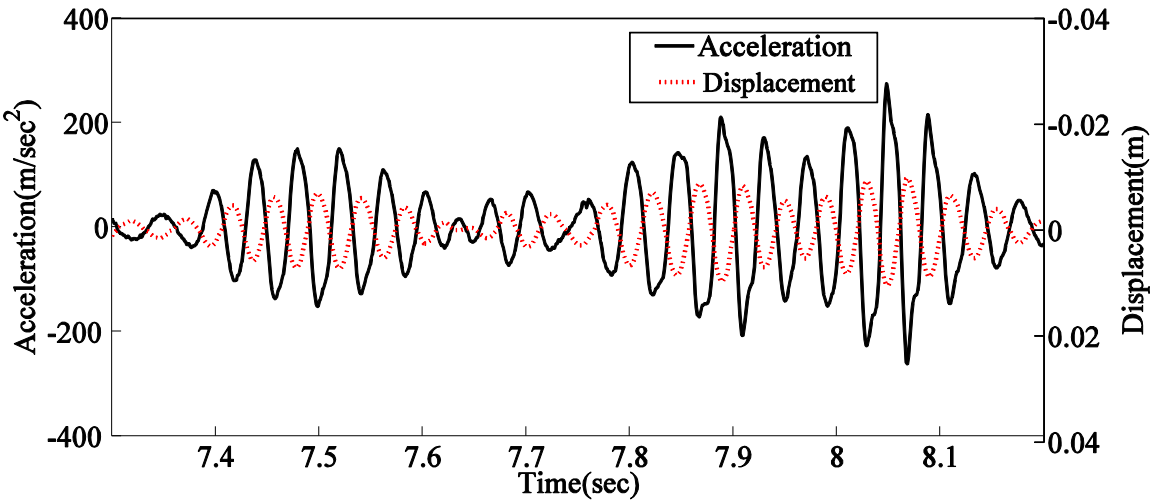

Figure 2-10 Measured acceleration and displacement when the shaker is moving randomly.

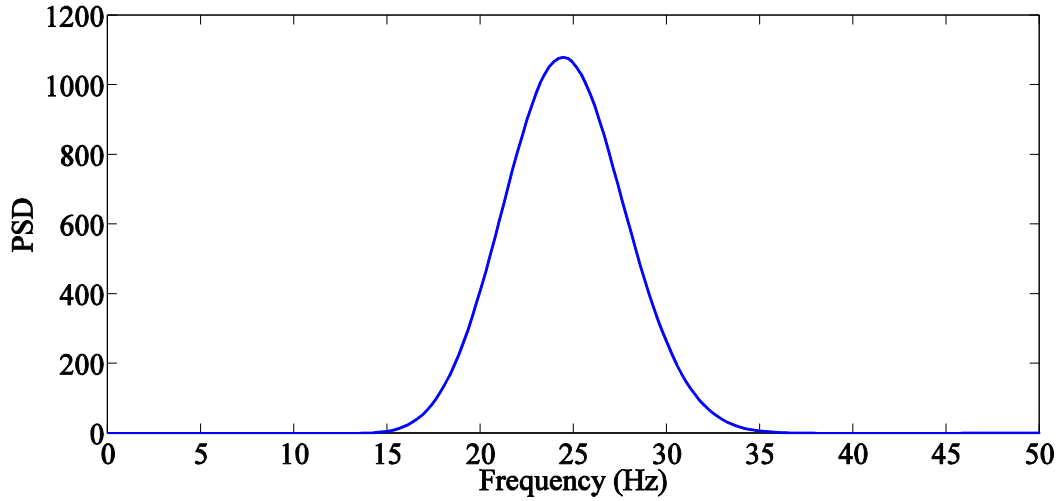

Figure 2-11 Power spectral density of the measured random acceleration of the shaker.

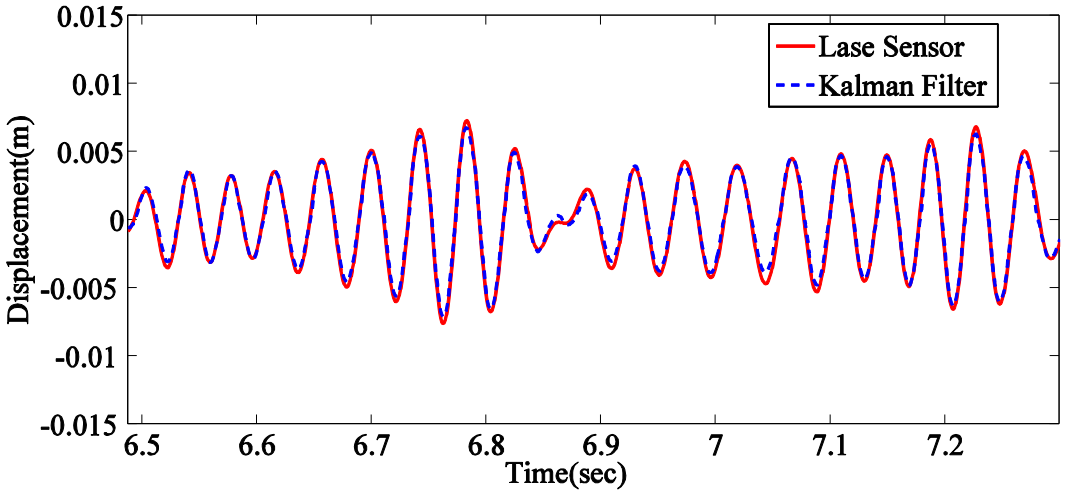

Figure 2-12 A magnified view of the calculated and measured random displacement of the shaker.

2.3.2.2 Displacement of a boat

To verify the accuracy of the proposed Kalman filter method when a low sampling rate accelerometer is used, a second experiment was devised to mimic the motion of the boat in the laboratory. An HC12 processor was used to record the acceleration of the boat at a rate of 5 Hz and a resolution of g/100 ms^{-2} or 0.0981 ms^{-2}. i.e., a relatively higher resolution but lower sampling rate than the accelerometer used in the shaker experiment described in the last section.

In this experiment, the accelerometer and associated HC12 processor and batteries were placed in a box attached to a seesaw board as shown in figure 2-13. The wooden board was swung manually and randomly at a frequency less than 1 Hz. The displacement of the accelerometer was measured from images recorded by a 25 frames per second video camera and associated image processing toolbox, which tracks the position of a black square attached to the accelerometer; the resolution is estimated to be less than 1.4 mm. Typical measured acceleration and position signals are shown in figure 2-14. The power spectral density of the acceleration waveform in figure 2-15 shows that it has a dominant frequency of 0.5 Hz, which is similar to that experienced by a boat.

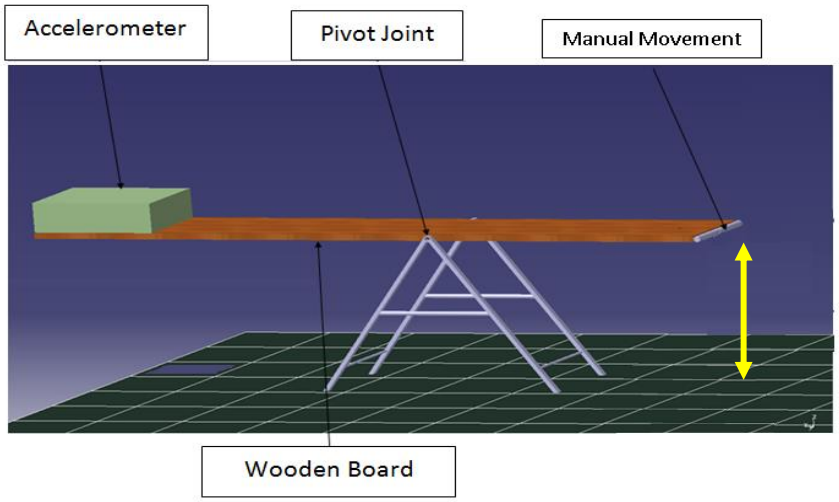

Figure 2-13 Second experimental set-up used to mimic the motion of a boat.

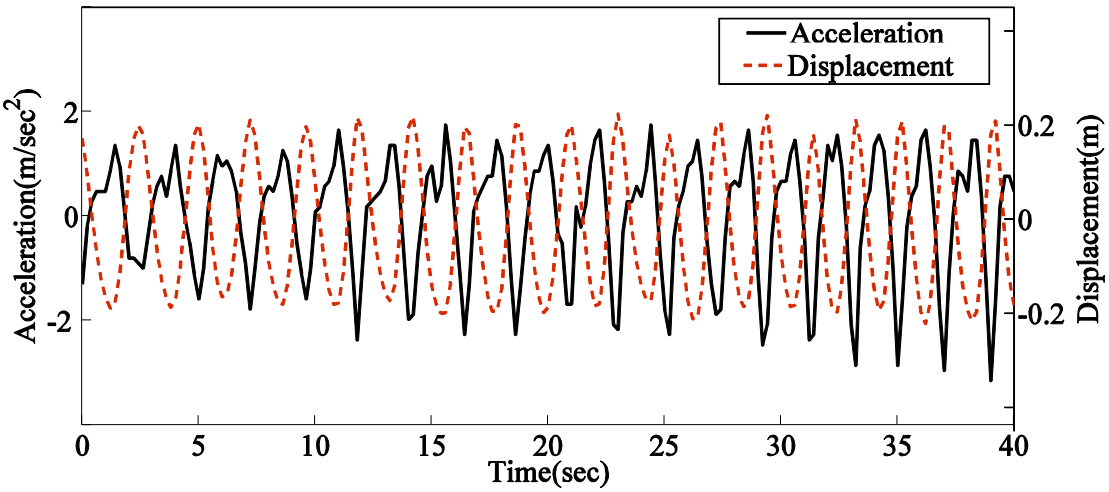

Figure 2-14 Measured acceleration and displacement of the random motion of the seesaw board.

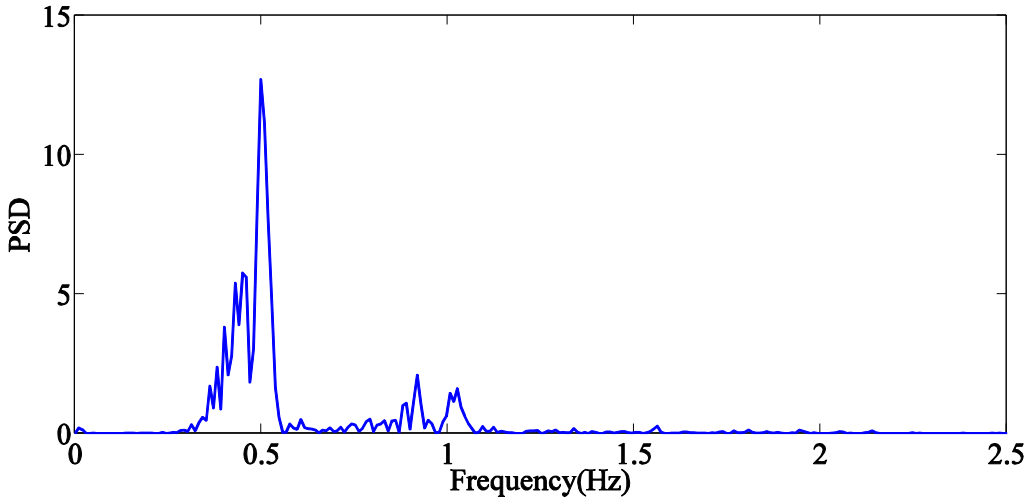

Figure 2-15 Power spectral density of the measured random acceleration of the seesaw board.

Figure 2-16 shows the result of applying the proposed Kalman filter method to calculate the displacement of the seesaw board. Although the sampling frequency of the acceleration signal is only 5-10 times more than the frequency range of the vibration, the result shows a reasonable agreement between the measured and calculated displacements curves. Our assumption on zero average displacement and also assuming white Gaussian noise can result in the appearance of a low frequency drift in the estimated displacement. Hence, a high-pass filter with a cut-off frequency of 0.01 Hz is applied to remove the very low frequency offsets. Here, the Kalman filter method estimates the displacement of the board relatively accurately with about 6.9% Normalized RMS Error after using the high pass filter. This percentage of error is greater than the error involved in the previous experiment. This is mainly due to the low sampling rate (5 Hz) of the data logger used in this experiment compared with the high sampling rate (1 K Hz) utilised in the previous experiment. However, it is worth noting that selecting the proper cut-off frequency is not a straightforward matter and, as discussed in many references such as [57], there is no general guideline for selecting an appropriate cut-off frequency of the noise-removing step and it should be investigated for each case separately. In an effort by Miles [64], when measurement of the ship motion is of interest, the optimum value for cut-off frequency is claimed to be $0.8\times f_1$ where f_1 is defined as the frequency above which 99 percentage of the energy of the encountered wave spectrum lies. In this experiment, if the cut-off frequency of the high-pass filter was to be selected based on Miles suggestion, a high-pass filter with a cut-off frequency of 0.143 Hz would've been employed.

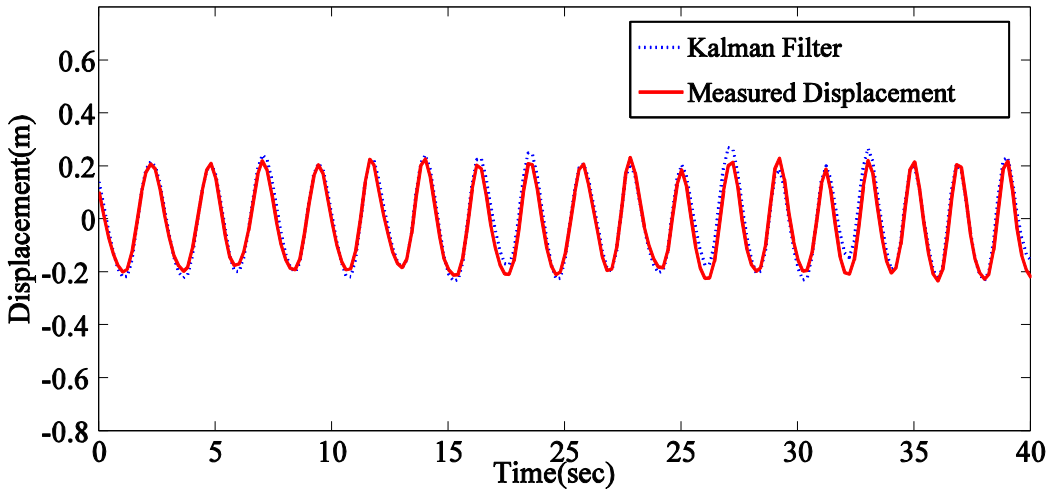

Figure 2-16 Comparison between the measured displacement with the estimated signal using the proposed Kalman filter method.

Whereas, it is shown that a reasonable agreement between calculated and real displacement is obtained by using a high-pass filter with a cut-off frequency of 0.01 Hz. Therefore, here the probability of eliminating part of the real displacement is reduced dramatically. In addition, it is worth mentioning that when acceleration is being recorded, the user usually can observe the platform that helps in applying the presented method with more confidence. For example, in this experiment, when we use a high-pass filter with cut–off frequency of 0.01 Hz it is known that the period of oscillation of the board is of the order of a few seconds and it does not have a displacement contribution with a long period of say 100 seconds that is to be eliminated by applying the high-pass filter.

Figure 2-17 shows the estimated displacement of the real boat (whose acceleration is shown in figure 2-1), using the Kalman filter method including a high-pass filter with a cut-off frequency of 0.01 Hz. The figure 2-17 shows a maximum displacement of 1.25m, which agrees with the observed behaviour of the boat (the actual boat displacement measurement was not possible). Using direct integration results in a growing displacement curve approaching hundreds of meters due to integral wind-up.

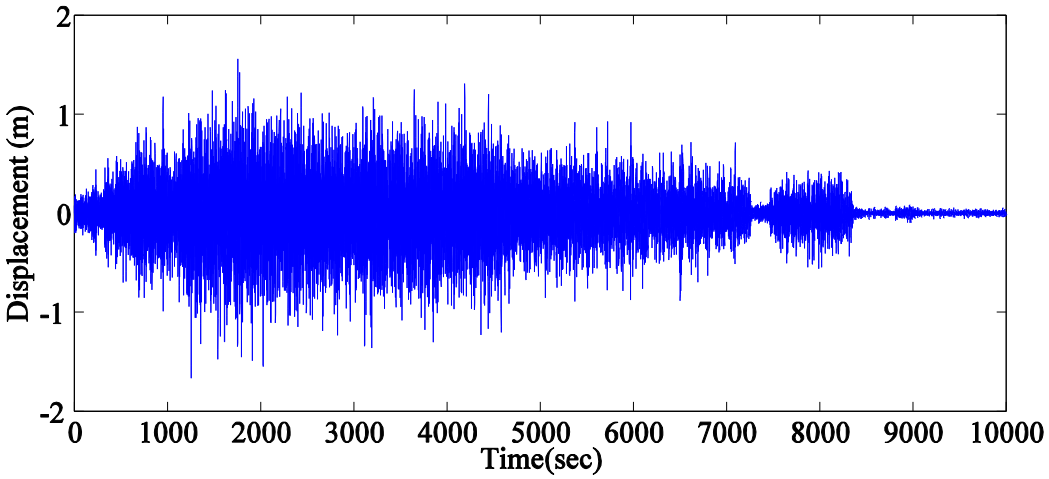

Figure 2-17 Calculated displacement of a bow vertical displacement of a boat whose acceleration is shown in figure 2-1.

2.4 Kalman Filter with integrated high-pass filter

In this section, another method based on the Kalman filter approach is introduced to calculate the displacement from a measured acceleration signal. This method is based on the fact that in many vibrational structures, the average of displacement and velocity remains constant. The transfer function of a first order low-pass filter in the Laplace domain (continuous) can be written as

$$H_v(s) = \frac{1}{1+s\tau_v}, \tag{2.16}$$

where τ_v is the time constant of the low-pass filter. To accurately integrate the low frequency components of the signal, the cut of frequency $f_v = 1/2\pi\tau_v$ needs to be very small. Therefore, the average of velocity is given by

$$\bar{V}(s) = \frac{1}{1+s\tau_v} V(s), \tag{2.17}$$

To utilize the continuous equation in designing the Kalman filter, it should be converted into it's the discrete time equivalent in the Z-space, e.g., using the Bilinear Transform (Tustin's method) [65]. Based on Tustin's method, the discrete formulation of $H_v(s)$ is derived if *s* is replaced by

$$s \approx \frac{2}{T_s}\frac{z-1}{z+1} \tag{2.18}$$

where T_s is the sampling time. Now, the low-pass filter transfer function in the Z-domain can be written as follow

$$H_v(z) = \frac{1+z^{-1}}{A_v + z^{-1}B_v}, \tag{2.19}$$

where

$$A_v = 1 + \frac{2\tau_v}{T_s} \tag{2.20}$$

$$B_v = 1 - \frac{2\tau_v}{T_s} \tag{2.21}$$

Hence, the average of velocity in Z-domain is written as

$$\bar{V}(z) = \frac{1+z^{-1}}{A_v + z^{-1}B_v} V(z). \tag{2.22}$$

If τ_d is assumed to be the time constant of the low-pass filter in the Z-domain, then the average displacement in the Z-domain can be obtained from

$$\bar{Y}(z) = \frac{1+z^{-1}}{A_d + z^{-1}B_d} Y(z), \tag{2.23}$$

Where

$$A_d = 1 + \frac{2\tau_d}{T_s}, \tag{2.24}$$

$$B_d = 1 - \frac{2\tau_d}{T_s}. \tag{2.25}$$

From (2.22) and (2.23), the discrete formulation of the average velocity and displacement can respectively be derived as follows

$$\bar{v}(k) = \frac{-B_v}{A_v}\bar{v}(k-1) + \frac{1}{A_v}v(k-1) + \frac{1}{A_v}v(k), \tag{2.26}$$

$$\bar{y}(k) = \frac{-B_d}{A_d}\bar{y}(k-1) + \frac{1}{A_d}y(k-1) + \frac{1}{A_d}y(k). \tag{2.27}$$

If we replace $v(k)$ and $y(k)$ from (2.1) and (2.2) into (2.26) and (2.27), we get

$$\bar{v}(k) = \frac{-B_v}{A_v}\bar{v}(k-1) + \frac{2}{A_v}v(k-1) + \frac{a}{A_v}T_s, \tag{2.28}$$

$$\bar{y}(k) = \frac{-B_d}{A_d}\bar{y}(k-1) + \frac{2}{A_d}y(k-1) + \frac{1}{A_d}v(k-1)T_s + \frac{1}{2A_d}aT_s^2. \tag{2.29}$$

Considering $\bar{v}(k)$ and $\bar{y}(k)$ to be the outputs of the system and *a* the input then equations (2.1), (3.2), (3.26) and (2.27) can be expressed from (2.4) as

$$\mathbf{A} = \begin{pmatrix} 1 & 0 & 0 & 0 \\ \frac{2}{A_v} & \frac{-B_v}{A_v} & 0 & 0 \\ T_s & 0 & 1 & 0 \\ \frac{T_s}{A_d} & 0 & \frac{2}{A_d} & \frac{-B_d}{A_d} \end{pmatrix}, \mathbf{B} = \begin{pmatrix} T_s \\ \frac{T_s}{A_v} \\ \frac{T_s^2}{2} \\ \frac{T_s^2}{2A_d} \end{pmatrix}, \tag{2.30}$$

$$\mathbf{x} = \begin{pmatrix} x_1 \\ x_2 \\ x_3 \\ x_4 \end{pmatrix} = \begin{pmatrix} v \\ \bar{v} \\ y \\ \bar{y} \end{pmatrix}, \mathbf{B} = \begin{pmatrix} T_s \\ \frac{T_s}{A_v} \\ \frac{T_s^2}{2} \\ \frac{T_s^2}{2A_d} \end{pmatrix}. \tag{2.31}$$

Also ,in matrix form, the output equation can be otained from (2.7) where

$$\mathbf{C} = \begin{pmatrix} 0 & 1 & 0 & 0 \\ 0 & 0 & 0 & 1 \end{pmatrix}. \tag{2.32}$$

Note, that here Q and R are defined as

$$Q = w^2, \tag{2.33}$$

$$R = \begin{pmatrix} v^2 & 0 \\ 0 & v^2 \end{pmatrix}. \tag{2.34}$$

2.4.1 Experimental result

Figure 2-18 shows the comparision between the measured results of the seesaw board and those calculated by applying the proposed Kalman filter method. As it is seen, there is a good agreement between the calculated and measured displacements. Here, the Kalman filter method estimates the displacement of the board relatively accurately with about 8.6% Normalized RMS Error. This results has been obtained for $\tau_d = 50\,\text{sec}, \tau_v = 100\,\text{sec}$ and the ratio of $\log(w/v)$ being 2.1.

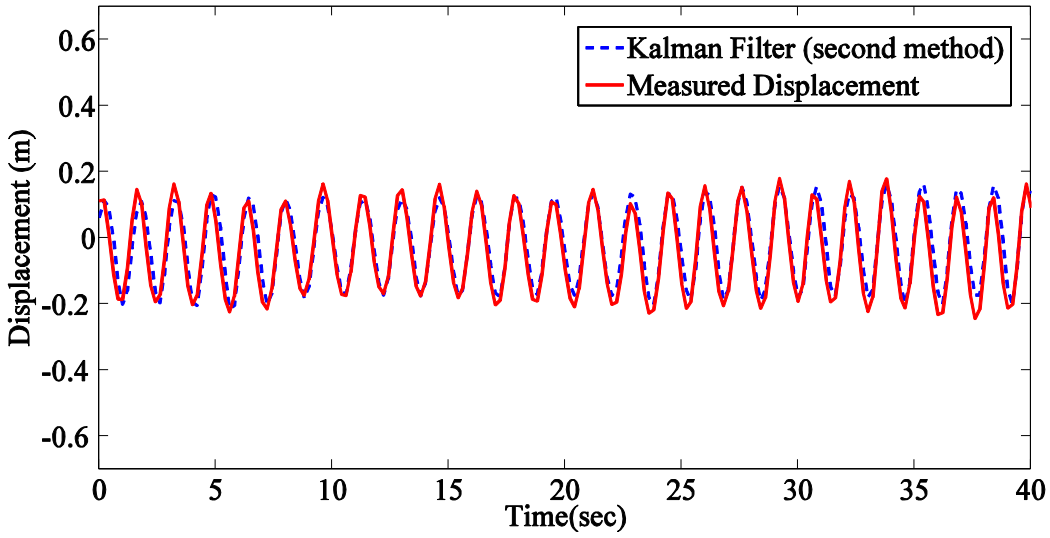

Figure 2-18 Comparison between the measured displacement and that estimated using the second proposed Kalman filter method.

Figure 2-19 shows the calculated displacement of the collected acceleration signal of the sea, shown in figure 2-1, after applying the second proposed Kalman filter method. It is seen that the result is close to the displacement calculated from the first method where a high pass filter was utilised to remove the low frequency noises from the estimated displacement.

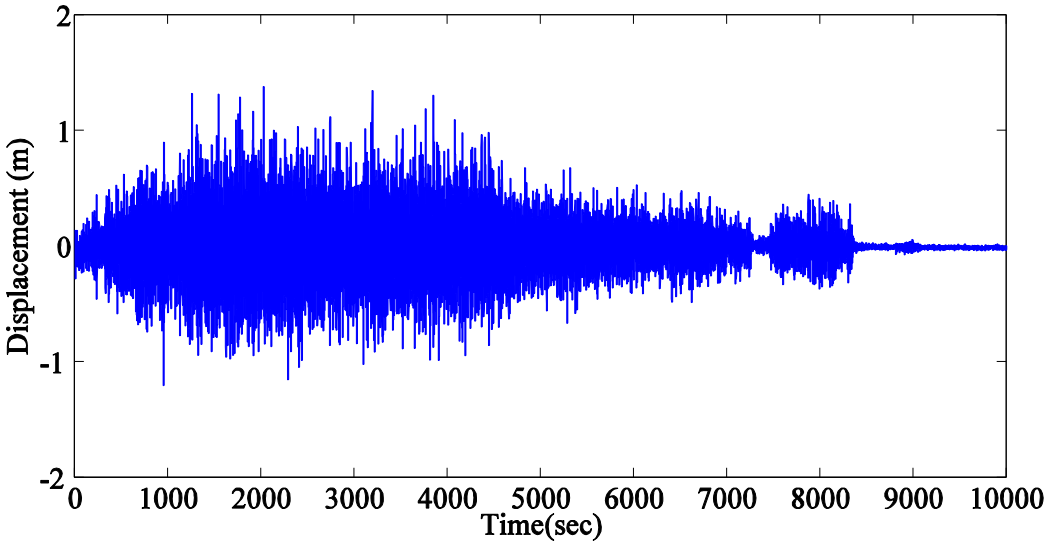

Figure 2-19 Calculated displacement of the vertical displacement of a boat whose acceleration is shown in figure 2-1 obtained from applying the second proposed Kalman filter method.

2.5 Conclusions

Accelerometers are used in many applications, e.g., ship motion, machine condition monitoring, monitoring of civil and mechanical structure and seismology, to measure velocity and displacement. However, using direct numerical integration to calculate velocity and displacement from the acceleration signal is known to suffer from low frequency noise amplification and integration wind-up. In this chapter, two Kalman filter based methods are proposed for calculating displacement from measured acceleration. In the first method, integration wind-up is eliminated by incorporating an additional state variable, namely the integral of the displacement whose "measured" value is assumed to be equal to the known average value of the displacement. This, in many applications, can be assumed constant, usually conveniently assigned to be zero, if non-linear behaviour and permanent deformations are negligible. A high-pass filter is used to remove the trend component following the Kalman filter calculations. In the second method, the average of velocity and displacement signals are estimated by incorporating two low pass filters to provide two additional state variables, namely the integral of the velocity and displacement signals that are assumed to be constant. The second Kalman filter method eliminates the necessity of applying a high pass filter to remove the dc offset from the Kalman filter output. The effectiveness and accuracy of both techniques are demonstrated experimentally. In the next chapter, the design of a

device for harvesting energy from a boat's vertical oscillation of 1 m at a dominant frequency of 0.5 Hz is of interest. The result of this chapter has given us confidence in obtaining realistic output power curves in response to the displacement curves that are obtained through our Kalman filtering methods.

Chapter 3: Constrained electromagnetic devices for harvesting vibration energy

3.1 Introduction

As discussed in chapter 1, electromagnetic generators are the more suitable options for large-scale applications [16]. Movement of a backpack carried by a human during walking [46], all-terrain-vehicle vibration [22]and vertical movement of a sailing boat [66] are some examples of relatively large-scale vibration resource. However, in addition to determining the configuration of the energy conversion device, maximizing the output power and efficiency are the main concerns in the process of design and optimization of vibration energy harvesters. Efficiency is a fundamental parameter used to compare all kinds of energy harvesters with various sizes and designs [67, 68]. Usually the main goal of an energy harvesting system is to extract the maximum power from the environment. In this chapter, the efficiency of such systems when achieving maximum power is studied. To achieve the maximum power condition, the parameters of the system need to be selected carefully. Changing the system's parameters, namely its mass and spring stiffness to resonate at the frequency of the vibrating source [69, 70], are reported to have improved energy capture. Williams et al. [71] advise that the inertial mass should be as large as possible (within the physical dimension of the device), unwanted internal damping should be minimized, and spring stiffness should be selected so that the resonance frequency of the device matches the excitation frequency.

Furthermore, tuning the load resistance to its optimum value to ascertain impedance matching in electromagnetic energy harvesters is reported in many research works to have improved energy capture [72, 73, 74]. However, none of these works consider the maximum allowable displacement of the oscillating mass as a constraint in the design process of calculating the optimum load resistance. More specifically, the optimum load resistance for harvesting maximum amount of energy is generally calculated regardless of its effect on the relative displacement of the oscillating mass. However, it is known that the load resistance can influence overall system damping and hence the relative displacement of the mass. In many transducers that are used in large size applications, due to size limitations, the oscillating mass only moves within a

specified range. Now, if the load resistance of the transducer is selected without considering the maximum permissible range of the seismic mass, there is a risk that the amplitude of the oscillating mass may exceed the physical dimensions of the transducer thus affecting the performance of the device. Therefore, for these cases, at the design stage, the physical parameters such as load resistance should be selected with regard to the constraints on the oscillating mass.

In this chapter, the maximum output power and the corresponding efficiency of two types of electromagnetic energy harvesting systems (i.e. linear and rotational) with constraints on their range of motion are studied. In a linear electromagnetic energy harvesting system (henceforth referred to as linear system) such as those studied in [22, 75, 76, 77] a linear generator is employed. However, in a rotational energy harvesting system (henceforth referred to as rotational system), an intermediate mechanism, such as rack and pinion [20, 46, 47] or a ball screw [48, 49, 50], is utilized to convert the linear motion of the mass to a rotational one to drive a rotary generator.

This chapter is distinguished by four main contributions. First, it investigates the optimum load resistance for both constrained linear and rotational systems to address the maximum output power condition. It is shown that for constrained systems the optimal load resistance is different from that of unconstrained energy harvesting systems reported in the literature [72]. Then, the efficiency of both systems corresponding to their maximum output powers is obtained. For each system, an expression for the load resistance corresponding to maximum efficiency is derived. It is shown that for linear systems it is not possible to achieve maximum efficiency when maximum power is extracted from the transducer. However, for rotational systems, maximum efficiency occurs at the maximum output power point. The second contribution is in introducing a set of design rules for optimum design of linear and rotational electromagnetic harvesters for constrained applications. The third contribution is the derivation of equations for power and corresponding efficiency of both systems in unified forms so that proper comparison between them can be made. These unified forms are developed based on the non-dimensional electromechanical coupling coefficient of systems introduced by Elliott and Zilletti [78]. The comparison reveals that in the case of a linear system, the maximum amount of power that can be transferred to the load is half the mechanical power transferred by the harvester and the efficiency of system is always less than 50%. However, a rotational system can be

designed to have an efficiency greater than 50%. The criterion that guarantees the efficiency of a rotational system being more than 50% is derived. The fourth contribution is a study of the effect of scaling the size of the electromagnetic generator component of the energy harvesting system on the output power and efficiency. It is shown that by increasing the size of the energy harvesting system the efficiency is increased for both constrained linear and rotational systems.

In the analysis of an energy harvesting device, it is common to study a non-dimensional model of the system. However, as the goal of this chapter is to study the optimal selection of the physical parameters of the system, a dimensional model of the dynamics of system is derived.

3.2 Linear electromagnetic energy harvesting systems

A free body diagram of a linear energy harvesting system using an electromagnetic generator is shown in figure 3-1. In this diagram, m is the seismic mass, k is the spring stiffness, c_m represents the mechanical viscous damping coefficient, and c_e is the electrical damping coefficient corresponding to the combined power dissipated in the generator's internal resistance and the power delivered to the load.

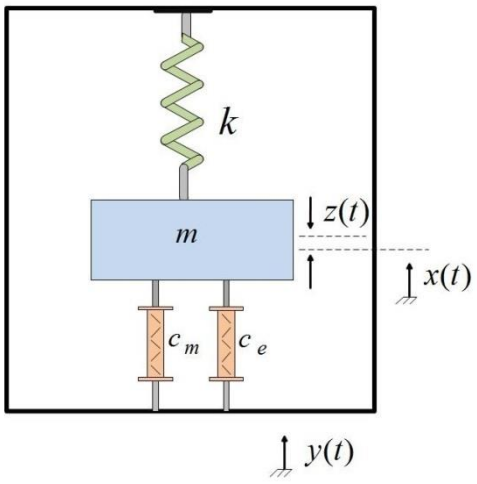

Figure 3-1 Free body diagram of a linear energy harvesting.

The governing differential equation of motion for the system shown in figure 3-1, with respect to the relative displacement of the seismic mass $z = x - y$, is

$$m\ddot{z}+\left(c_e+c_m\right)\dot{z}+k\,z=-m\,\ddot{y}. \tag{3.1}$$

For a harmonic base excitation $y=Y\sin\left(\omega t+\varphi_y\right)$, when the driving motion is assumed to be independent of the mechanical loading due to the harvester, the amplitude of the relative displacement Z, can be shown to be

$$\left|\frac{Z}{Y}\right|=\frac{m\omega^2}{\sqrt{\left(k-m\omega^2\right)^2+\left(\left(c_e+c_m\right)\omega\right)^2}}. \tag{3.2}$$

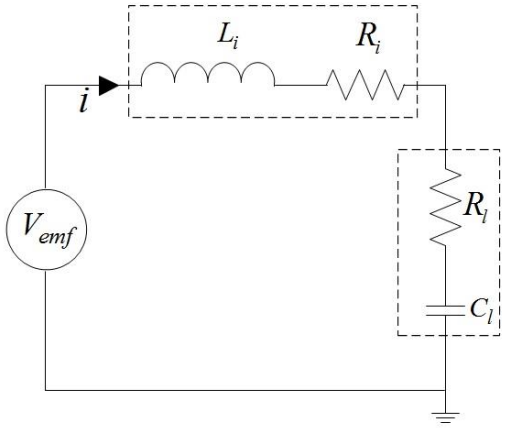

Figure 3-2 Equivalent circuit of an electromagnetic generator connected to a resistive.

In many papers on generating energy from vibrations, the effect of the generator's internal inductance is ignored. Cammarano *et al.* [73] show that even in cases where the effect of internal inductance cannot be ignored, due to a high oscillation frequency, the undesirable effect of the internal inductance can be compensated by adding a capacitor in series with the circuit. The equivalent electrical circuit of the energy harvesting device is shown in figure 3-2, in which a capacitor is added in series with the load reactance to cancel the effect of the generator's inductance. Assuming that an electrical generator with an emf (electromagnetic force) constant K_t, is directly coupled to the seismic mass, then the generated emf voltage is given by

$$V_{emf}=K_t\,\dot{z}. \tag{3.3}$$

Also, the electrical damping coefficient (c_e), corresponding to the power dissipated in the generator's internal resistance and transferred to the electrical load, is

$$c_e = \frac{K_t^2}{|Z_l + Z_i|}, \tag{3.4}$$

where

$$Z_i = R_i + \chi_i, \tag{3.5}$$

and

$$Z_l = R_l + \chi_l, \tag{3.6}$$

where $\chi_i = jL_i\omega$ and $\chi_l = 1/jC_l\omega$. In [73] it is shown that to deliver the maximum power to the load R_l, the effect of internal inductance should be compensated by tuning the capacitor such that $\chi_l = -\chi_i$.

For a spring stiffness of *k*, the natural frequency of system is equal to the base excitation frequency when $k = m\omega^2$ at which the corresponding relative displacement Z_r can be derived from (3.2) for $\omega = \omega_n$. Then $z = Z_n \sin(\omega_n t + \varphi_z)$ and $\dot{z} = Z_n \omega_n \cos(\omega_n t + \varphi_z)$, by substituting the electrical damping coefficients from (3.4) and considering $C_l = 1/L_i\omega_n^2$, the amplitude of the relative displacement is

$$\frac{Z_n}{Y} = \frac{m\omega_n}{c_m + \dfrac{K_t^2}{R_i + R_l}}. \tag{3.7}$$

The power delivered to the load resistance is

$$P_l = \frac{1}{2}R_l i^2 = \frac{1}{2}R_l\left(\frac{V_{emf}}{R_l + R_i}\right)^2 = \frac{1}{2}R_l\left(\frac{K_t\dot{z}}{R_l + R_i}\right)^2. \tag{3.8}$$

Substituting the maximum value for $\dot{z}$, which is $Z_r\omega_n$ in (3.8), the power supplied to the load is given by

$$P_{l-ave} = \frac{1}{2}\frac{R_l}{\left(R_l + R_i\right)^2}\omega_n^2 K_t^2 {Z_n}^2. \tag{3.9}$$

Equation (3.9) shows the relationship between the relative displacement, excitation frequency, load resistance and the harvested power from a given generator. Stephen [72] has shown that maximum electrical power from a resonant system, without a constraint

on the maximum displacement of the mass, is obtained when the load resistance is set to be equal to

$$R_l = R_i + \frac{K_t^2}{c_m}. \tag{3.10}$$

The parameter K_t^2 / c_m is the electrical analogue of the mechanical damping coefficient. However, in many practical devices the maximum allowable displacement of the mass (Z_0), is limited, so that $Z_n \le Z_0$. The optimum value for load resistance can be obtained by solving the following system of equations

$$\begin{cases} \max\left(P_{l-peak} = \dfrac{R_l}{\left(R_l + R_i\right)^2} \omega^2 K_t^2 Z_n^{\,2} \right) \\ subject\ to: Z_0 - Z_n \ge 0 \end{cases} \tag{3.11}$$

Therefore, we design an optimum energy harvesting system to extract maximum energy from a given vibration source with known amplitude and frequency of oscillation. This design will be accomplished based on the parameters of a given generator that has given K_t and R_i values. It is also assumed that, due to the transducer size limits, the maximum displacement of the oscillating mass is specified. Therefore, the aim of the design is the optimal selection of system parameters including k, R_l and m to harvest the maximum power from the given generator within the specified range of motion. To this end, considering Z_0 as the maximum allowable relative displacement of mass (*i.e.*, $Z_n = Z_0$ is constant), the maximum value of (3.9) is obtained when the load resistance is equal to the internal resistance of the generator in which the output power is $\omega_n^2 K_t^2 Z_n^2 / 8R_i$. The mass can then be selected from (3.7) to limit its maximum displacement to $Z_n = Z_0$,

$$m = \frac{Z_0}{Y\omega_n}\left(c_m + \frac{K_t^2}{2R_i} \right). \tag{3.12}$$

The natural frequency of system is equal to the excitation frequency when $k = m\omega^2$, considering $\omega = \omega_n$ in this condition the spring stiffness is given by

$$k = \omega_n \frac{Z_0}{Y}\left(c_m + \frac{K_t^2}{2R_i} \right). \tag{3.13}$$

To verify this approach, (3.11) was solved numerically to determine the optimum value of mass and load resistance for a system whose parameters are listed in table 3-1.

Table 3-1 First scenario system parameters.

Parameter	Value
c_m	20 N s m^{-1}
f_n	0.5 Hz
K_t	100 V s m^{-1}
R_i	40 Ω
Y	1 m
Z_0	0.30 m

In this case, the aim is to determine the optimum values of the mass and spring stiffness for a given generator while the maximum allowable mass movement (Z_0) is maintained at 0.3 m. The frequency and amplitude of the oscillations are 0.5 Hz and 1 m, respectively. Figure 3-3 shows the displacement for different values of mass and load resistance. It is seen that by increasing the load resistance, the displacement of a given mass relative to the moving base is increased. This occurs due to reduction in electrical damping. This graph also shows that, for the same amount of damping, a larger value of mass leads to a larger relative displacement.

The corresponding profile of the generated electrical power, calculated using (3.9), is shown in figure 3-4. Here, it can be seen that the maximum harvested power for a given mass occurs when the load resistance is 540 Ω. This value is in agreement with that calculated using (3.10) for optimum load resistance as derived by Stephen [72]. However, the corresponding relative displacement, from figure 3-2, violates the 0.3 m constraint considerably.

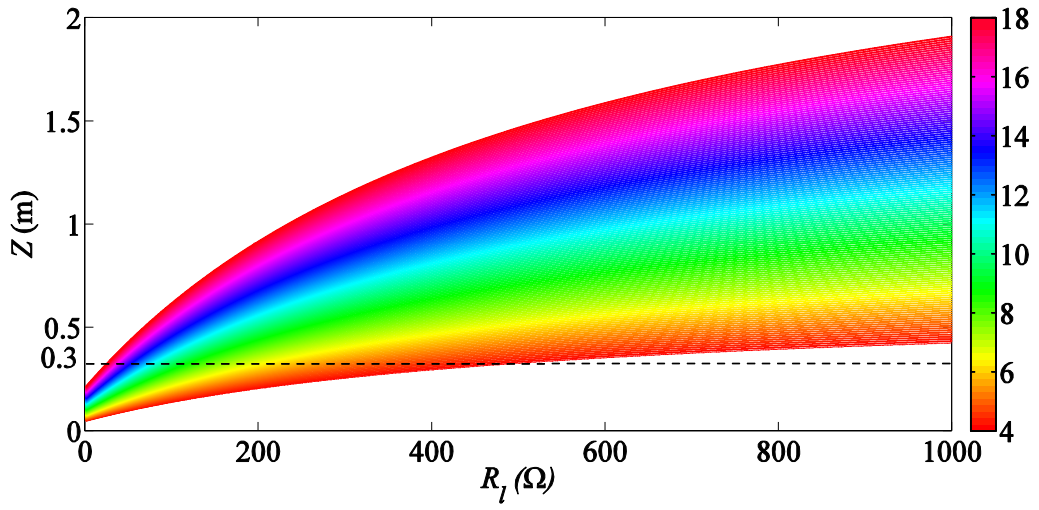

Figure 3-3Relative displacements for different values of mass and load resistance.

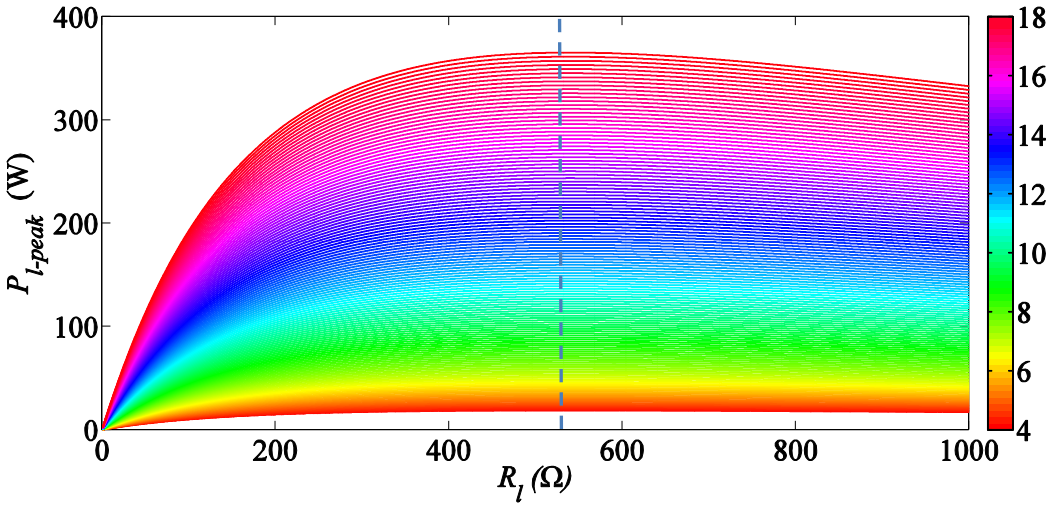

Figure 3-4 Output electrical power for different values of mass and load resistance.

Figure 3-5 shows a magnified portion of figure 3-4, with the points corresponding to a relative displacement of 0.3 m identified as the black dotted line. For instance, for a 5 kg mass, the relative displacement is 0.3 m when the load resistance is 269 Ω, resulting in an output power of 25 W. However, to have a maximum relative displacement of 0.3 m for a 16 kg mass, a load resistance of 27.8 Ω is required which would produce 53.7 W of output power. As it can be seen, there are an infinite number of mass and load resistance combinations that can satisfy the constraint of the system (i.e., $Z_n \leq 0.3\,\text{m}$). However, as shown in figure 3-5, maximum power is attained when the selected mass satisfies the constraint for the load resistance to be equal to the internal resistance of the generator (which is 40 Ω in this example). The black curve in

figure 3-5 shows that the optimum mass value is 13.84 kg which is in agreement with the value derived from (3.12). The corresponding generated power is 55.5 W. Note that the captured power decreases if the mass increases beyond 13.84 kg. Hence the guideline of using the largest mass possible, proposed in [71] for systems without displacement constraints, is no longer valid when the maximum displacement is constrained.

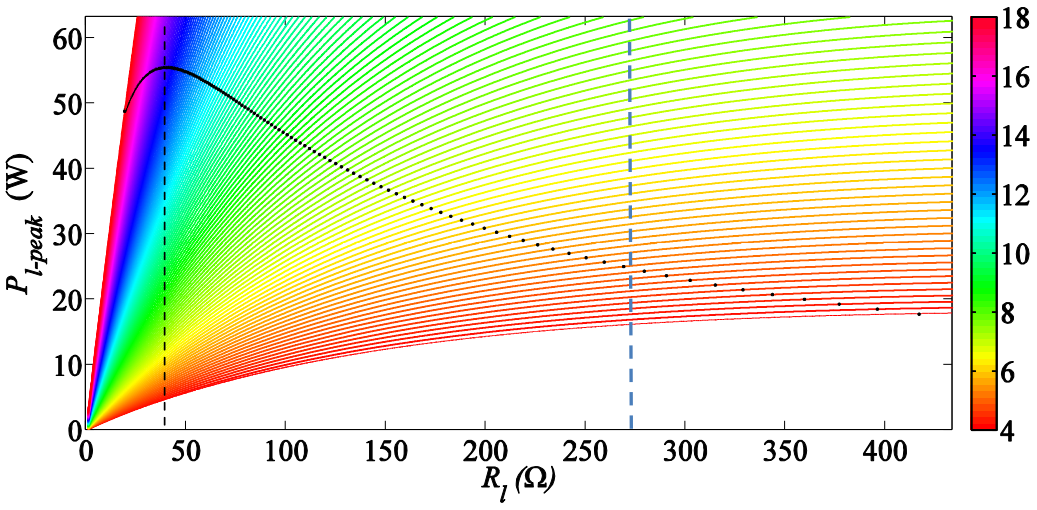

Figure 3-5 Output electrical power versus load resistance for different values of mass with dots corresponding to a relative displacement of 0.3 m.

From this study a set of design rules for optimum linear energy harvesting systems can be formulated as follow:

(i) Tune the load resistance equal to the internal resistance of the linear generator

(ii) Make the mechanical damping as small as possible

(iii) Select the mass from (3.12). It is worth emphasizing that in constrained systems making the inertial mass as large as possible does not necessarily leads to a more optimized design.

(iv) Select the spring stiffness so that the undamped natural frequency of device is equal to the frequency of the source of vibration

3.3 Rotational electromagnetic energy harvesting

Although linear electromagnetic generators can be integrated into most vibration energy harvesting devices without the need for any extra transmission mechanism, in

some applications the low frequency of vibrations and hence the slow vibration velocity and the large force would require a prohibitively large linear generator. To overcome this problem, rotating electromagnetic generators and suitable motion transmission systems are employed to convert low frequency linear motion to high frequency rotational one. A rotational energy harvesting system comprising a sprung mass coupled to an electrical generator through a motion transmission system. Ball screw is a conventional mechanism to convert linear motion to the rotational one. A free body diagram of this type of system is shown in figure 3-6. In this device, the base movement causes the mass to vibrate. The ball screw then converts the low frequency linear motion of the seismic mass to high-speed rotation.

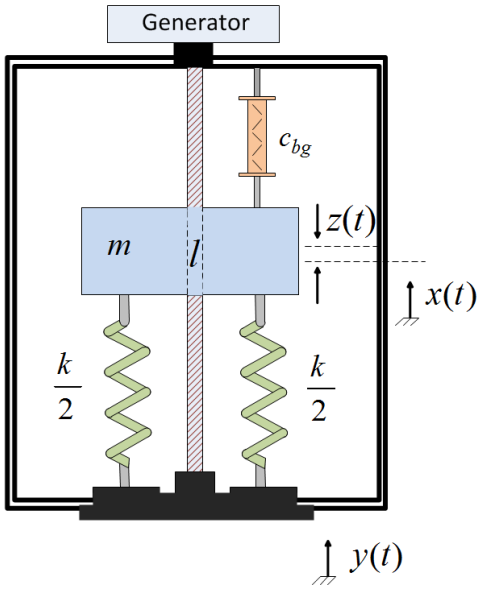

Figure 3-6 Free body diagram of an energy harvesting system consisting of a sprung mass coupled to a generator through a ball screw.

Considering l as the ball screw lead, the equivalent reflected moment of inertia of the ball screw and the generator is given by $J\left(2\pi/l\right)^2$, where J refers to the total moment of inertia of the system including the moment inertia of the ball screw J_b and generator J_g and is defined as

$$J = J_g + J_b. \tag{3.14}$$

Also c_{bg} includes the mechanical viscous damping of the combined ball screw connections c_{mb} and generator c_{mg}, *i.e.*,

$$c_{bg} = c_{mb} + c_{mg}. \tag{3.15}$$

The governing differential equation of motion, having an ideal ball screw, in figure 3-6 is written as

$$\left(m + J\left(\frac{2\pi}{l}\right)^2\right)\frac{d^2x(t)}{dt^2} + c_{bg}\left(\frac{2\pi}{l}\right)^2\frac{dx(t)}{dt} + kx(t) = J\left(\frac{2\pi}{l}\right)^2\frac{d^2y(t)}{dt^2} + c_{bg}\left(\frac{2\pi}{l}\right)^2\frac{dy(t)}{dt} + ky(t) + F_{EM} \tag{3.16}$$

and F_{EM} is defined as

$$F_{EM} = \frac{2\pi}{l}\tau_G, \tag{3.17}$$

where τ_G is the electrical torque due to the generation of an opposing magnetic field by the current flowing through the generator coil which is

$$\tau_G = -T_i\, i(t), \tag{3.18}$$

Here T_i is the generator torque constant and $i(t)$ is the current flowing through its coil. Ignoring the coil inductance, as it can be compensated by adding a capacitor in series with the generator, and defining R_i and R_l as the internal resistance of the rotational generator and the load resistance, the current flow based on the equivalent circuit of the generator, shown in figure 3-2, is related to the voltage produced across the idealized voltage source and is obtained from

$$i(t) = \frac{V_{emf}(t)}{R_l + R_i} = \frac{T_i\,\upsilon(t)}{R_l + R_i}, \tag{3.19}$$

where $\upsilon(t)$ is the rotational speed of the ball screw coupled to the generator and is given by

$$\upsilon(t) = \frac{2\pi}{l}\left(\frac{d\left(x(t) - y(t)\right)}{dt}\right), \tag{3.20}$$

and by replacing (3.17) and (3.18) in (3.16), it can be rearranged as

$$\left(m+J\left(\frac{2\pi}{l}\right)^2\right)\frac{d^2x(t)}{dt^2}+c_{bg}\left(\frac{2\pi}{l}\right)^2\frac{dx(t)}{dt}+kx(t)=J\left(\frac{2\pi}{l}\right)^2\frac{d^2y(t)}{dt^2}+ c_{bg}\left(\frac{2\pi}{l}\right)^2\frac{dy(t)}{dt}+ky(t)-T_i\left(\frac{2\pi}{l}\right)i(t). \quad \textbf{(3.21)}$$

Let the relative displacement of the system $z(t)=x(t)-y(t)$. If the base displacement is assumed to be sinusoidal $y(t)=Y_0\sin\omega t$, then $z(t)=Z\sin(\omega t+\phi)$ where Z is the amplitude of the relative displacement of mass and ϕ is the phase angle between $y(t)$ and $z(t)$. It is more convenient to analyse the system in the frequency domain. Applying the Fourier transform to (3.21) and assuming zero initial conditions, yields

$$Z(\omega)\left(\left(k-\left(m+J\left(\frac{2\pi}{l}\right)^2\right)\omega^2\right)+\mathrm{j}c_{bg}\left(\frac{2\pi}{l}\right)^2\omega\right)=m\omega^2Y(\omega)-T_i\left(\frac{2\pi}{l}\right)I(\omega), \quad \textbf{(3.22)}$$

and substituting (3.19) in (3.20) and applying the Fourier transform yields (assuming zero initial relative displacement)

$$I(\omega)=\mathrm{j}\frac{\omega\left(\frac{2\pi}{l}\right)T_i}{R_l+R_i}Z(\omega). \quad \textbf{(3.23)}$$

Substituting (3.23) into (3.22) and rearranging it results in

$$Z(\omega)\left(\left(k-\left(m+J\left(\frac{2\pi}{l}\right)^2\right)\omega^2\right)+\mathrm{j}\left(\frac{2\pi}{l}\right)^2\left(c_{bg}+\frac{T_i^2}{R_l+R_i}\right)\omega\right)=m\omega^2Y(\omega), \quad \textbf{(3.24)}$$

and the magnitude of Z is therefore given by

$$Z=\frac{m\omega^2Y_0}{\sqrt{\left(k-\left(m+J\left(\frac{2\pi}{l}\right)^2\right)\omega^2\right)^2+\left(\left(c_{bg}+\frac{T_i^2}{R_l+R_i}\right)\left(\frac{2\pi}{l}\right)^2\omega\right)^2}}. \quad \textbf{(3.25)}$$

The power supplied to the load is related to the relative displacement and is derived as follows:

$$P_l(t) = R_l\left(\frac{V_{emf}(t)}{R_l + R_i}\right)^2 = \frac{R_L}{\left(R_l + R_i\right)^2} T_i^2 \left(\frac{2\pi}{l}\right)^2 \omega^2 Z^2 \cos^2\left(\omega t + \phi\right), \tag{3.26}$$

Hence, by replacing (3.25) in (3.26), the average harvested power is given by

$$P_{l-ave} = \frac{1}{2}\frac{R_l}{\left(R_l + R_i\right)^2} T_i^2 \left(\frac{2\pi}{l}\right)^2 \omega^2 Y^2 \times \left(\frac{\left(m\omega^2\right)^2}{\left(k - \left(m + J\left(\frac{2\pi}{l}\right)^2\right)\omega^2\right)^2 + \left(\left(c_{bg} + \frac{T_i^2}{R_l + R_i}\right)\left(\frac{2\pi}{l}\right)^2 \omega\right)^2} \right). \tag{3.27}$$

From the design point of view and from (3.27), maximum power is transferred to the load when the undamped natural frequency of system matches the oscillation frequency, i.e. $\omega = \omega_n$ where ω_n is given by

$$\omega_n = \sqrt{\frac{k}{m + J\left(\frac{2\pi}{l}\right)^2}}. \tag{3.28}$$

Therefore, designing the transducer such that its natural frequency matches the excitation frequency is the first criterion in the design process. The relative displacement of the mass at this condition from (3.25) is given by

$$Z_n = \frac{mY_0\omega_n}{\left(\frac{2\pi}{l}\right)^2\left(c_{bg} + \frac{T_i^2}{R_i + R_l}\right)}. \tag{3.29}$$

For this harvester, the amplitude of the mass oscillation with respect to the base should not exceed a defined height. Let Z_0 be the maximum allowable displacement of mass, then (3.29) can be rearranged as

$$\left(\frac{2\pi}{l}\right)^2 = \frac{mY\omega_n}{Z_{n_0}\left(c_{bg} + \dfrac{T_i^2}{R_i + R_l}\right)}. \tag{3.30}$$

By substituting (3.30) into (3.27), when $\omega = \omega_n$, the average output power for the constrained system, which is independent of the ball screw lead, is obtained as

$$P_{l-ave} = \frac{1}{2}\frac{R_l}{\left(R_l + R_i\right)^2} T_i^2 \frac{mY_0\omega_n^3}{\left(c_{bg} + \dfrac{T_i^2}{R_i + R_l}\right)} Z_{n_0}. \tag{3.31}$$

The optimum value of the load resistance can be obtained from $d / d R_l \left(P_{l-ave}\right) = 0$ which leads to the following expression

$$R_{l,rotational,P_{\max}} = \sqrt{R_i^2 + R_i \frac{T_i^2}{c_{bg}}}. \tag{3.32}$$

It is worth noting here that in deriving the above expression for R_l, in effect, the ratio of P_{l-ave} / Z_n for when $Z_n = Z_0$ is maximized. By replacing the load resistance from (3.32) into (3.30), the optimum ball screw lead is then given as

$$l = 2\pi \sqrt{\frac{Z_0}{mY_0\omega_n}\left(c_{bg} + \frac{T_i^2}{R_i + \left[R_i^2 + R_i \dfrac{T_i^2}{c_{bg}}\right]^{\frac{1}{2}}}\right)}. \tag{3.33}$$

The following example demonstrates the validity of this method for designing an optimum energy harvesting device that is subject to a displacement constraint. The system parameters are shown in table 3-2. The given mass, in this example is 8 kg and its relative displacement should not exceed 0.3 m for the defined base vibration ($Y = 1\text{m}$ and $f_n = 0.5\text{Hz}$). For this device, the problem is to find the optimal ball screw lead for harvesting maximum power with respect to the defined constraint ($Z_0 = 0.3\text{m}$).

Table 3-2 System parameters for the second scenario.

Parameter	Value
c_m	0.003 N m s rad^{-2}
f_n	0.5 Hz
T_i	0.0764 V s rad^{-1}
m	8 kg
R_i	16 Ω
Y	1 m
Z_0	0.30 m

Based on (3.32) and the parameters given in table 3-2, the theoretical optimum load resistance for the system is 177.16 Ω. Now, by selecting such a load resistance and applying (3.33), the corresponding ball screw lead to satisfy the maximum allowable relative displacement ($Z_0 = 0.3\text{m}$) is calculated to be 4 mm.

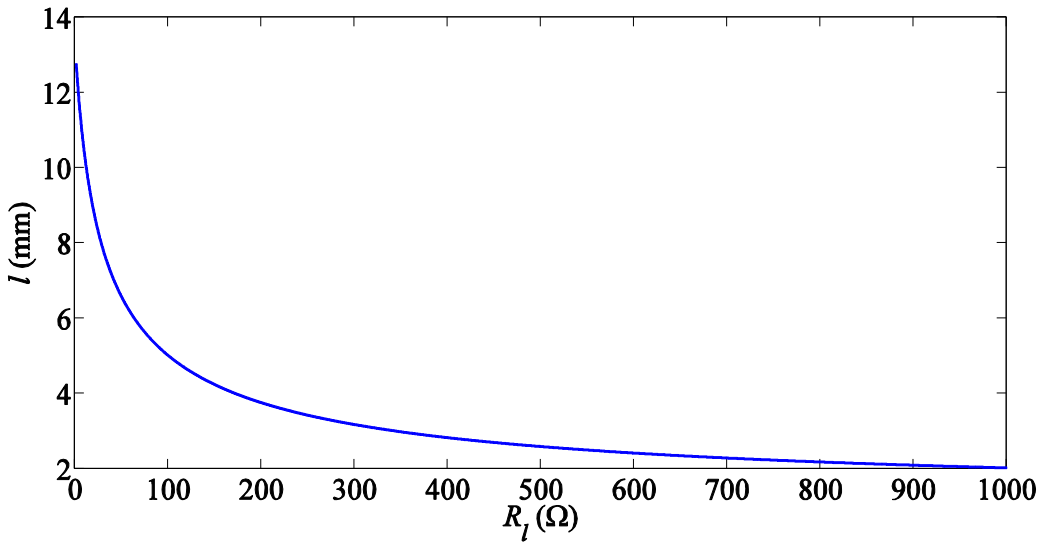

Figure 3-7 Ball screw lead and corresponding load resistance to satisfy the constraint condition.

This value of the ball screw lead was verified by carrying out numerical simulations. Figure 3-7 shows the relationship between the ball screw lead and the load resistance so that the seismic mass movement does not exceed the allowable relative displacement.

As shown, an infinite combination of ball screw lead and load resistance can satisfy the constraint; however, plotting the output power for different ball screw lead values under this condition shows that the maximum power occurs when the ball screw lead is 4 mm (see figure 3-8), which is in agreement with the value obtained from (3.33).

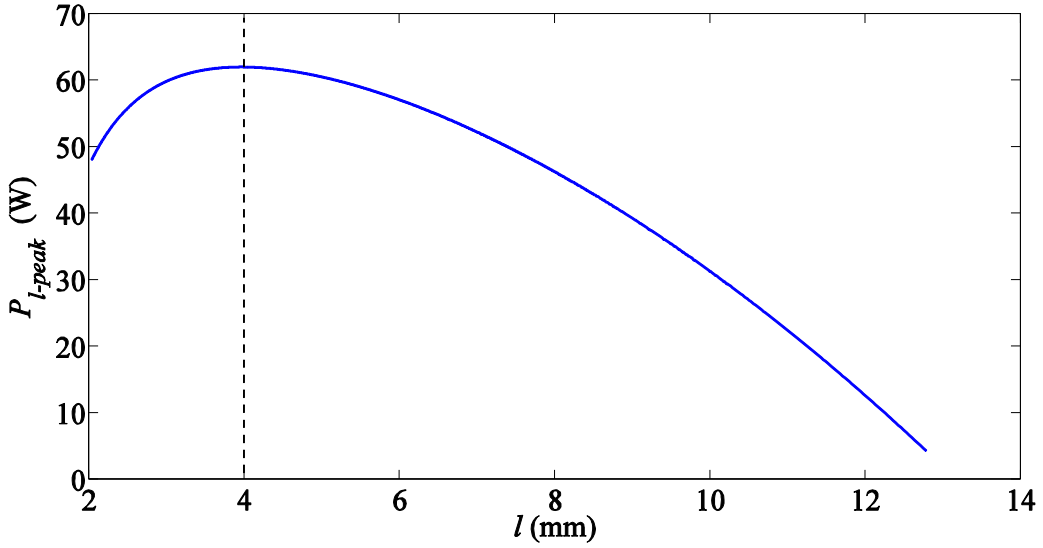

Figure 3-8 Generated power vs ball screw lead, with load resistance adjusted to restrict the displacement to 0.3 m.

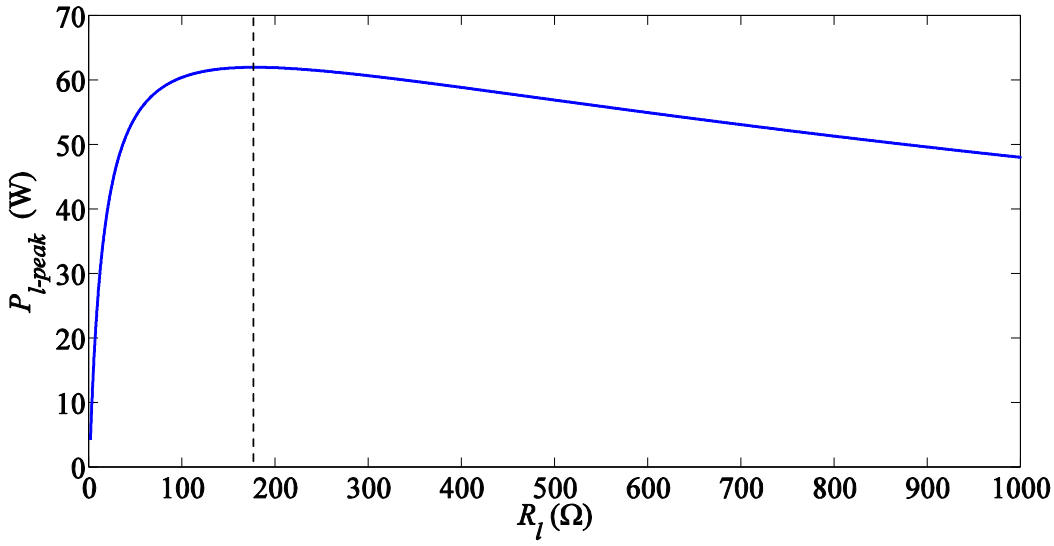

Figure 3-9 Generated power vs load resistance with screw lead adjusted to restrict the relative displacement.

Similarly, figure 3-9 shows that if one changes the load resistance and selects the corresponding ball screw lead for each load case with respect to the constraint, then maximum power occurs when the load resistance is 177.16 Ω, which is in agreement with the expected value of the optimum load resistance.

From this analysis the steps that need to be followed in order to design an optimum rotational energy harvesting system can be formulated as:

(i) Tune the load resistance equal to the value obtained from (3.32).

(ii) Make the mechanical damping as small as possible

(iii) Select the optimum size of the transfer mechanism ratio, i.e. $2\pi / l$ in this work, from (3.33)

(iv) Select the spring stiffness, k, equal to $\omega_n^2 \left(m + J \left(2\pi / l \right)^2 \right)$ to make the undamped natural frequency of the device equal to the frequency of the source of vibration.

3.4 Power and efficiency comparison between linear and rotational systems

Efficiency is a fundamental term that has been studied for different energy harvesting systems. Relying solely on the assessment of the output power of energy harvesters does not reflect their quality of performance and their capability to harvest the maximum amount of power. However, in the context of vibration harvesting systems, the concept of efficiency has received less attention in the literature than that of maximizing the output power. Traditionally, efficiency is defined as the ratio of the electrical power output to the mechanical input power; whilst, in a vibration-based energy harvester, the input mechanical power itself is related to the device characteristics. Also, the efficiency cannot be defined in terms of the potential mechanical power available from the source as, in some applications, the loading by the harvester does not influence the dynamics of the source of vibration. Hence, the potential mechanical power available from the source is effectively limitless [18].

3.4.1 Power and efficiency of an electromagnetic constrained transducer

To compare the power output of various transducers various metrics has been introduced. Power density is defined as the amount of output power over the volume of the energy harvester. Power density is usually important for end use, however, it only provide a meaningful comparison for fixed source of vibration. A dimensionless figure of merit, called *effectiveness e*, is introduced by Roundy [79] which is defined as

$$e = \kappa^2 Q^2 \frac{\rho}{\rho_0} \frac{\lambda}{\lambda_{\max}}, \tag{3.34}$$

where, Q is the quality factor and is related to the damping ratio of the system, κ is the coupling coefficient of the transduction mechanism, ρ is the actual density of the device, ρ_0 is a baseline density, λ is the actual transmission coefficient and $\lambda_{\max}$ is the maximum transmission coefficient. However, in the "*effectiveness*" index, Q is related to the damping ratio of the system and does not have a fundamental limit. Hence, this metric comparison does not reveal how well the device is optimized [74]. To investigate how close a device is to its optimum performance and distinguish between different proof mass densities and geometries, Mitcheson *et al.* [18] introduce a "*volume figure of merit"*, defined as

$$FoM_V = \frac{P_{out}}{\frac{1}{16} Y_0 \rho_{Au} V_0^{\frac{4}{3}} \omega^3}. \tag{3.35}$$

This dimensionless ratio compares the performance of the device with that of an ideal device. The device has the same total package volume but with a proof mass equal to the density of gold (ρ_{Au}), occupying half of this volume (V_0). The proof mass oscillates in the other half of this package. The power output harvested by this hypothetical device is considered as the maximum possible output for the based vibration with amplitude of Y_0 at frequency of ω. The power output of the transducer is compared with the maximum possible output to evaluate the performance of a device as a function of its overall size. Although the "*volume figure of merit"* facilitates the comparison of a harvesting device performance with a reference ideal energy harvesting system, it does not enable the calculation of input power absorbed by the system to produce a certain amount of output power.

Elliott and Zilletti [78] conducted research into scaling of linear electromagnetic transducers for power harvesting and shunt damping. In this study the efficiency is defined as the ratio of output power to the sum of the mechanical dissipated power, electrical power loss and electrical output power. This definition is closer to the original definition of efficiency. This study shows that the efficiency of a linear electromagnetic transducer depends on a non-dimensional electromechanical coupling coefficient which will be discussed later in this work. The coupling coefficient scales with the transducer's size. However, this research does not consider the constraint on the displacement of the proof mass. The mechanical input power absorbed by the energy harvesting structure is given by

$$P_{l-in} = \frac{1}{2}\left(c_m + \frac{K_t^2}{R_l + R_i} \right) \omega_n^2 Z_n^2. \tag{3.36}$$

Here, we define the efficiency of a linear system, E_l, as the ratio of the electrical power harvested from (3.9) to the supplied mechanical power from (3.36), which is

$$E_l = \frac{P_{l-out}}{P_{l-in}} = \frac{R_l K_t^2}{c_m \left(R_l + R_i \right)^2 + K_t^2 \left(R_l + R_i \right)}. \tag{3.37}$$

The load resistance corresponding to the maximum efficiency of the system, as opposed to the maximum power output, can be obtained from $\partial E_l / \partial R_l = 0$, *i.e.*, differentiation of (3.37), which results in

$$R_{l,\,linear,\,E_{\max}} = \sqrt{R_i^2 + R_i \frac{K_t^2}{c_m}}. \tag{3.38}$$

By comparing the optimum load resistance for maximum output power $\left(R_{l,linear,P_{\max}} = R_i \right)$, and the load resistance corresponding to the maximum achievable system efficiency derived in (3.38), it is realized that the latter is always greater than the former. Therefore, in a practical linear system it is not possible to achieve maximum efficiency at the maximum output power point.

The mechanical input power absorbed by the rotational system can be calculated as

$$P_{b-in} = \frac{1}{2}\left(c_{bg} + \frac{T_i^2}{R_i + R_l} \right)\left(\frac{2\pi}{l} \right)^2 \omega_n^2 Z_n^2 . \tag{3.39}$$

The harvesting efficiency, E_b, is defined as

$$E_b = \frac{P_{b-out}}{P_{b-in}} = \frac{R_l T_i^2}{\left(R_i + R_l\right)^2 c_{bg} + T_i^2 \left(R_i + R_l\right)}. \tag{3.40}$$

Also, from (3.40), the load resistance corresponding to the maximum efficiency of the system can be obtained from $\partial E_b / \partial R_l = 0$, which is

$$R_{l,rotational,E_{\max}} = \sqrt{R_i^2 + \frac{R_i T_i^2}{c_{bg}}}. \tag{3.41}$$

Comparison of (3.32) and (3.40) reveals that in the rotational system, the optimum load resistance to obtain the maximum efficiency is the same as the load resistance corresponding to the maximum power. In the other words, for a constrained rotational system the maximum efficiency occurs at the maximum output power.

3.4.2 Comparison of output power and efficiency of systems

By replacing (3.7) in (3.9) for $Z_r = Z_{r_0}$ the load power of a constrained linear energy harvesting system for the load resistance corresponding to the maximum output power ($R_{l,linear,P_{\max}} = R_i$), is

$$P_{l-out,P_{\max}} = \frac{\Lambda_{em}}{8\left(1 + \frac{\Lambda_{em}}{2}\right)} m\omega_n^3 Y Z_n, \tag{3.42}$$

where Λ_{em} is a non-dimensional electromechanical coupling coefficient of an energy harvesting system and is defined as [78]

$$\Lambda_{em} = \frac{K_t^2}{c_m R_i}, \tag{3.43}$$

for linear systems and

$$\Lambda_{em} = \frac{T_i^2}{c_{bg} R_i}, \tag{3.44}$$

for rotational systems. By increasing this coefficient (*i.e.*, $\Lambda_{em} \to \infty$) the maximum output power, given by (3.42), approaches the following expression

$$\lim_{\Lambda_{em} \to \infty} P_{l-out,P_{\max}} = \frac{1}{4} m\omega_n^3 Y Z_n. \tag{3.45}$$

This shows that the maximum theoretical power is determined by the environmental vibration characteristics (ω_n, Y) and also the system's mass and the maximum allowable displacement. Note that ω_n is a characteristic of the transducer, but here the system is designed such that the undamped natural frequency of the device is equal to the frequency of excitation. Considering (3.37), the efficiency of a constrained linear system for the load resistance corresponding to the maximum output power ($R_{l,linear,P_{\max}} = R_i$), can readily be shown to be [78]

$$E_{l,P_{\max}} = \frac{\Lambda_{em}}{4 + 2\Lambda_{em}}. \tag{3.46}$$

For weak linear coupled systems, the efficiency is low. By increasing Λ_{em} the efficiency increases until it reaches a maximum value of 50%, *i.e.*

$$\lim_{\Lambda_{em} \to \infty} E_{l,P_{\max}} = \frac{1}{2}. \tag{3.47}$$

However, considering the optimum load resistance for rotational systems from (3.31), the output power of such systems from (3.30) can be written as

$$P_{b-out,P_{\max}} = \frac{1}{2} \frac{\Lambda_{em}\left(\sqrt{1+\Lambda_{em}}\right)}{\left(1+\sqrt{1+\Lambda_{em}}\right)^2 + \Lambda_{em}\left(1+\sqrt{1+\Lambda_{em}}\right)} m\omega_n^3 Y Z_n, \tag{3.48}$$

and for the case when $\Lambda_{em} \to \infty$, the power is

$$\lim_{\Lambda_{em} \to \infty} P_{b-out,P_{\max}} = \frac{1}{2} m\omega_n^3 Y Z_n. \tag{3.49}$$

Also, the efficiency of rotational systems corresponding to the maximum output power can be obtained by replacing (3.32) in (3.39) and using (3.33), (3.43) and (3.44), which results in

$$E_{b,\,P_{\max}} = \frac{\Lambda_{em}\left(\sqrt{1+\Lambda_{em}}\right)}{\left(1+\sqrt{1+\Lambda_{em}}\right)^2 + \Lambda_{em}\left(1+\sqrt{1+\Lambda_{em}}\right)}, \tag{3.50}$$

Equation (3.50) indicates that in the case of a rotational system, it is possible to achieve an efficiency of more than 50%. To achieve such favourable design, the condition below must be met

$$2\left(1+\sqrt{1+\Lambda_{em}}\right) \le \Lambda_{em}. \tag{3.51}$$

This condition is satisfied if $\Lambda_{em} \ge 8$. Selecting the parameters according to this condition can lead to a system with an efficiency above 50%. For the case when $\Lambda_{em} \to \infty$, the efficiency of the rotational system is

$$\lim_{\Lambda_{em}\to\infty} E_{b,P_{\max}} = 1. \tag{3.52}$$

In the case that the a linear and a rotational system have same seismic mass, by replacing (3.7) in (3.36) and (3.29) in (3.39), for $Z_r = Z_{r_0}$, it can be shown that the mechanical input power for both systems is $1/2 m\omega_n^3 Y Z_{r_0}$, however, the linear system in the optimum condition can only transfer less than half of this power to the load, while, the rotational system under certain condition, *i.e.* $\Lambda_{em} \ge 8$, can harvest more power.

3.4.3 Effect of the Scaling of constrained electromagnetic harvesters on the output power and efficiency

It was shown earlier that by increasing Λ_{em}, the efficiency of a typical energy harvesting transducer is improved. A question that arises here is "how do the output power and efficiency of a system change by increasing the size of the generator?". Elliott and Zilletti [78] studied the relation between Λ_{em} and the characteristic length of a transducer [L]. In this study, assuming that A_w is the cross-sectional area of the wire used for the coil of the electromagnetic transducer and μ_w is its resistivity, the resistance of the coil is given by

$$R_i = \mu_w \frac{h_l}{A_w}. \tag{3.53}$$

Here h_l is the coil's wire length, which is approximately given by

$$h = \frac{V_C}{A_w}, \tag{3.54}$$

where V_C is the volume of the coil. For a well-designed transducer with saturated magnetic flux density B, the emf-constant (K_t for linear systems and T_i for rotational systems) is proportional to the magnetic flux density times the length of the wire in the coil (*i.e.*, K_t or $T_i = Bh$). Therefore, the electromechanical coefficient of the transducer can be re-written as

$$\Lambda_{em} = \frac{(Bh)^2}{\mu_w \frac{h}{A_w} c_m} = \frac{B^2 V_C}{\mu_w c_m}. \tag{3.55}$$

The magnetic flux density (B) and wire resistivity (μ_w) of the transducer depend on their material properties, but not on the transducer dimensions. In general, the scale of the volume of the coil (V_C) is [L^3], whereas the mechanical damping coefficient c_m for linear systems and c_{bg} for rotational systems) is related to the structure and the detailed mechanism of the transducer, but generally scales as [L] [80]. Therefore, the electromechanical coefficient shown in (3.43) and (3.44) is proportional to the square of the characteristic length of the transducer [L^2]. Hence, an option in increasing the coupling coefficient of a transducer is to increase its overall size. From (3.45) and (3.49) it is evident that, for both systems, by increasing the size of device the electromagnetic coefficient and consequently the output power of the system is increased.

In the case of a rotational system, considering the combined ball screw, mass, spring and the rotary generator as the transducer assembly, the coupling coefficient related to the generator part of the transducer can be defined as

$$\Lambda_{emg} = \frac{T_i^2}{c_{mg} R_i}, \tag{3.56}$$

where c_{mg} is the mechanical damping associated with the rotary generator. According to the discussion presented above, it is expected that Λ_{emg} will scale with the square of the characteristic length of the generator [Λ_{emg}]. This assumption will be examined in the next section by studying the specifications of a set of commercial generators. For the rotational transducer assembly, the coupling coefficient defined in (3.44) can be rewritten as

$$\Lambda_{em} = \frac{T_i^2}{\left(c_{mg} + c_{mb}\right) R_i}, \tag{3.57}$$

where c_{mb} is the mechanical damping due to the presence of other transducer's mechanical components such as ball screw, bearings and coupling shafts. Here, by increasing the size of the rotary generator, the quantity T_i^2 / R_i scales as [L^3], but c_{mg} scales as [L], while, c_{mb} does not scale up. Hence, it can be understood that by increasing the generator size, the coupling coefficient of the overall transducer assembly is increased but due to constant c_{mb}, the rate of scaling is higher than [L^2]. For instance if two rotational systems are designed based on two different rotary generators with electromechanical coefficients Λ_{emg_1} and Λ_{emg_2}, the ratio of the non-dimensional electromechanical coefficient for these generators scales as [L^2], *i.e.*,

$$\frac{\Lambda_{emg_2}}{\Lambda_{emg_1}} = \frac{\dfrac{T_{i_2}^2}{c_{mg_2} R_{i_2}}}{\dfrac{T_{i_1}^2}{c_{mg_1} R_{i_1}}} \propto \left[L^2 \right], \tag{3.58}$$

and from (3.57) the ratio of the overall electromechanical coefficient of the designed transducers is

$$\frac{\Lambda_{em_2}}{\Lambda_{em_1}} = \frac{\dfrac{T_{i_2}^2}{\left(c_{mg_2}+c_{mb}\right)R_{i_2}}}{\dfrac{T_{i_1}^2}{\left(c_{mg_1}+c_{mb}\right)R_{i_1}}} = \frac{\Lambda_{emg_2}}{\Lambda_{emg_1}} \times \frac{1+\dfrac{c_{mb}}{c_{mg_1}}}{1+\dfrac{c_{mb}}{c_{mg_2}}}. \qquad \textbf{(3.59)}$$

Therefore, if c_{mb}/c_{mg_1} is greater than c_{mb}/c_{mg_2}, then in comparison with Λ_{em_1}, Λ_{em_2} scales with a ratio greater than $[L^2]$.

3.5 Numerical study

3.5.1 Linear system examples

This section investigates the relation between size and efficiency of energy harvesting devices under constrained condition brought about by the employed commercial generator. It is assumed that a source of vibration (for example a vertical movement of a boat) with a frequency of 0.5 Hz ($\omega = \pi$ rad/sec) and amplitude of 1 m ($Y = 1\,\text{m}$) is available. We are required to design an energy harvesting device such that the maximum displacement of the seismic mass does not exceed 0.3 m.

First case is dedicated to the design of a linear energy harvesting structure based on figure 3-1. Table 3-3 lists the parameters of a variety of linear electromagnetic actuators presented in [78] that are sorted in the order of small to large scales. The last system represents a hypothetical case in which the size of the actuator is much larger than model ASP400 (~8 times). For each presented linear actuator type, the proof mass is calculated such that the oscillation at excitation frequency ($\omega = \pi$ rad/sec) occurs within the given constraint (*i.e.*, $Z_0 = 0.3$ m). For each inertial generator Λ_{em} and the seismic mass are calculated from (3.43) and (3.12), respectively. Then, at optimum load resistance ($R_{l,linear,P_{\max}} = R_i$), the output power is obtained from (3.9). As table 3-3 shows, by increasing the transducer dimensions, Λ_{em} is increased in agreement with the result presented in section 3.4. Also, by increasing the size of the linear actuator, the overall damping of the system gets larger, thus requiring a bigger mass to reach the same displacement (*i.e.*, $Z_0 = 0.3$).

Table 3-3 Parameters of a number of linear electromagnetic inertial actuator models [78].

Type	K_t (N/A)	R_i (Ω)	c_m (Ns/m)	Λ_{em}	m (kg)	$P_{l-out,P_{\max}}$ (W)
Trust headphone actuator	0.74	8	0.38	0.18	0.03	0.007
Micromega(IA-01)	1.6	3.0	1.4	0.61	0.17	0.09
Aura	7	4.4	9	1.23	1.39	1.23
Motran (IFX 30-100)	10	1.6	44	1.42	7.18	6.93
Micromega (ADD-45N)	20	4	35	2.86	8.11	11.10
ASP 400	21	1.6	30	9.19	16.02	30.60
Hypothetical case	42	0.8	60	36.75	111.01	224.8

In addition, it is seen that by increasing the size of the linear actuator, the output power increases. However, as in this case, mass is the design variable (and for hence the absorbed mechanical power is different for each design), system efficiency would therefore be a more appropriate criterion to be used in order to compare the different harvesters. Figure 3-10 shows the efficiency of the designed system corresponding to their maximum output power calculated from (3.37). It is seen that by increasing Λ_{em} due to the increase of the transducer size, the efficiency of the energy conversion system is improved. However, even in the case of a hypothetical system where the size has been increased dramatically, the efficiency of the system does not exceed 50% which is in agreement with the result obtained from (3.47).

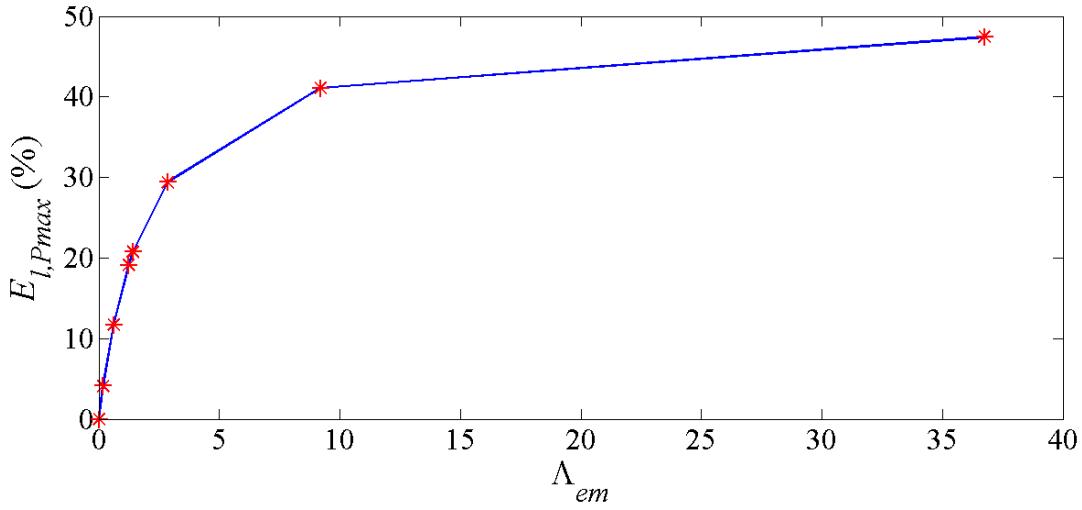

Figure 3-10 Efficiency of linear electromagnetic energy harvesting systems versus Λ_{em} for the linear actuator shown in table 3-3.

3.5.2 Rotational system examples

Table 3-4 presents the size and specifications of a number of commercial PM (permanent magnet) generators where *h* and *r*, respectively, are the length and the diameter of the rotary generator coupled to the ball screw as presented in figure 3-6. Here, for each generator, Λ_{emg} is calculated from (3.56), see table 3-4. Figure 3-11 shows the variation of the coupling coefficients of the generators in comparison with the size of the reference generator (Model a). A reasonable fit to Λ_{emg} shows that it is linearly proportional to $(V_i / V_1)^{\frac{2}{3}}$, where V_1 is the volume of generator model a, and V_i is the volume of the selected generator. This result validates the statement made in section 3.4 that the electromechanical coupling coefficient of a generator scales up with the square of the characteristic length of the device [L^2]. Also in each case Λ_{em} which represents the electromechanical coefficient of the transducer assembly is calculated from (3.57). Note that c_{mb} is not a function of the generator size and is assumed to be 3.0E-3 (mN.m.s.rad^{-1}) for all the designed transducers. A comparison of Λ_{em} and Λ_{emg} reveals that the Λ_{em} scales with a ratio higher than that of Λ_{emg}. This agrees with the discussion presented in section 3.4.

Table 3-4 The parameters of PM motors from Faulhaber [81].

Model	r (mm)	h (mm)	T_i (mNm/A)	R_i (Ω)	c_{mg} (mN.m.s.rad^{-1})	Λ_{emg}	Λ_{em}	l (mm)	$P_{b-out,P_{\max}}$ (W)
a	6	20	1.13	9.1	6E-5	2.33	0.05	1.2	0.4
b	12	26	2.77	2.3	4.2E-4	6.78	0.95	1.5	6.2
c	16	28	3.86	4.3	4.8E-4	7.22	0.99	1.6	6.4
d	20	36	6.34	3.4	1.3E-3	9.20	2.75	2	12.0
e	30	56	12.74	1.6	6E-3	16.20	10.80	3.8	20.6
f	35	64	14.52	0.6	1.4E-2	24.40	20.20	6.1	24.2
g	44	90	23.83	0.23	6E-2	39.94	38.4	13.5	27.3

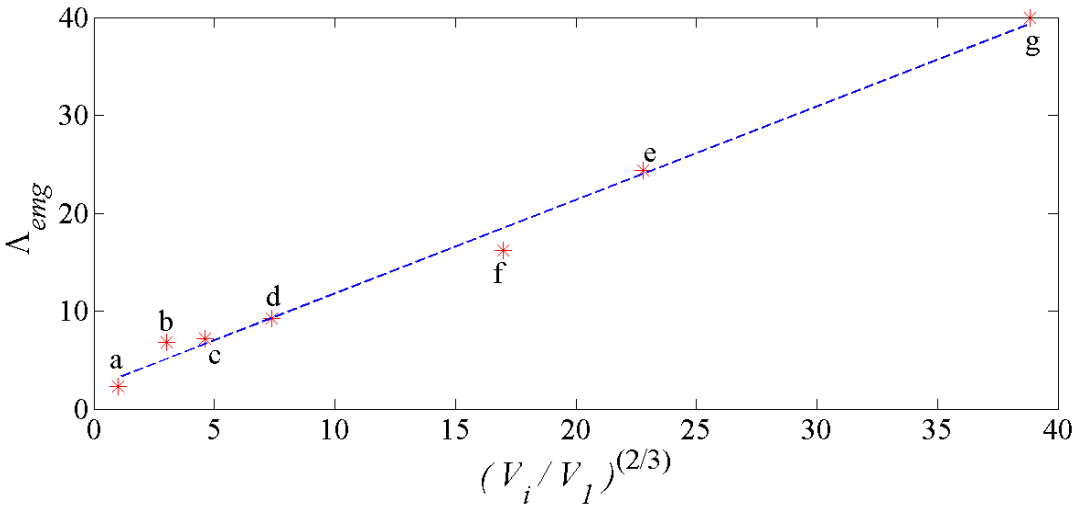

Figure 3-11 The coupling coefficient of rotary generators presented in table 3-4 versus ratio of their sizes to the reference generator in power of two over 3.

Now, it is assumed that the environmental vibration condition and the constraint on the maximum allowable displacement of the seismic mass are the same as the values considered in the first case ($Y_0 = 1\text{m}, \omega = \pi$). In this case, based on each of the PM (permanent magnet) generators presented in table 3-4, a rotational harvesting system is designed. It is assumed that the energy harvester has a mass of 8.1 kg, and the design

variables are l and R_l. The optimum load resistance for each case is obtained from (3.32), and then the optimum lead size for the ball screw is calculated from (3.33). Table 3-4 presents the ball screw lead values and the generated power of each system corresponding to the relevant selected PM generator in each case. It is seen that by increasing the size of the generator, Λ_{em} and consequently the output power of the system is increased which is in agreement with (3.44). Figure 3-12 shows the efficiency of the designed rotational systems versus Λ_{em}. It is seen that by increasing the size of PM generators, the efficiency of the system increases. Here, in contrast with linear systems, an efficiency above 50% is achievable. This occurs for those systems whose Λ_{em} meet the criterion presented in (3.51), *i.e.*, systems designed based on generators e, f and g. However, if Λ_{em} does not satisfy the condition presented in (3.51), *i.e.*, $\Lambda_{em} \geq 8$, designing a rotational energy harvesting system may result in a sub-optimum energy harvesting device in comparison with the linear system. For instance comparison of the designed systems based on the generators a, b and c with the linear system designed based on Micromega (ADD-45N), reveals that although the rotational systems utilize the same mass, they produce less power compared with the linear system. Therefore, for constrained applications, in the design process of the energy harvesting systems, a rotary generator should be selected carefully to allow the designer to take advantage of the superiority of the rotational systems over the linear systems.

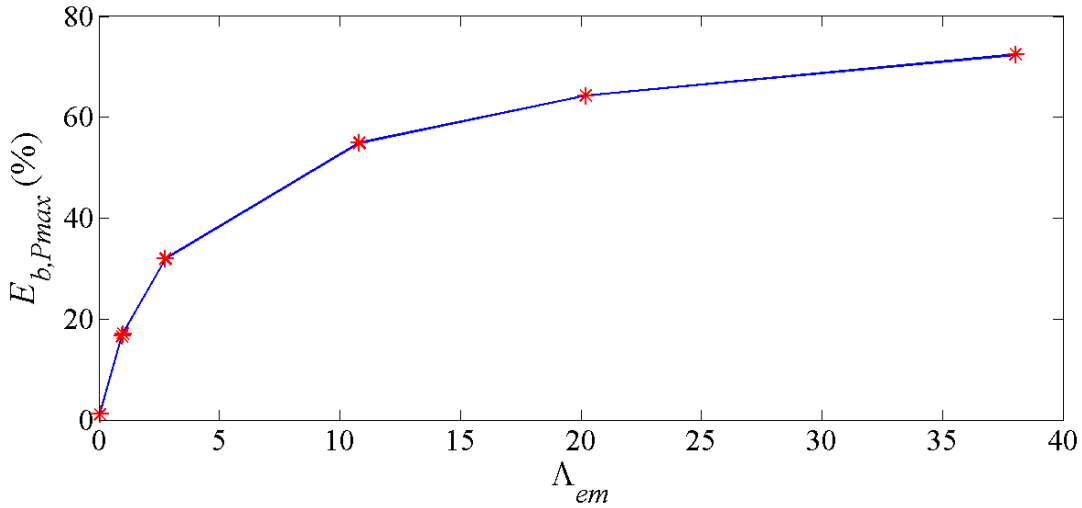

Figure 3-12 Efficiency of rotational electromagnetic energy harvesting systems versus Λ_{em} for the rotary generators shown in table 3-4.

3.6 Conclusion

In some energy harvesting systems, the maximum displacement of the oscillating mass will be limited due to the physical constraints of the device. In systems where this limitation does not exist, choosing the optimum load resistance with the goal of maximizing the energy harvested from the environment is a process that takes place after the machine design. This is why, in these cases, the phrase "tuning" is used to refer to the selection of the resistance load. However, in systems where the maximum displacement of the mass is limited (constrained systems), choosing the optimum load resistance is part of the actual design process and cannot be done independently of choosing other parameters.

In this chapter, the maximum power condition and the corresponding efficiency for constrained vibration based linear and rotational energy harvesting devices are presented. For convenience, and for enabling the comparison of different systems, the definition for the coupling coefficient of an energy harvesting device given by (3.43) and (3.44) are employed.

In a linear system, electromechanical coupling coefficient (Λ_{em}) is shown to increase with the size of the transducer according to its characteristic length squared. However, in the case of a rotational system, although Λ_{emg} of the rotational generator, itself, increases as [L^2], the value of Λ_{em} for the whole transducer assembly (including the ball screw) scales by a ratio greater than [L^2].

It is shown that in a system with linear motion and constrained throw, even with the assumption of negligible mechanical losses, the maximum harvestable power (at optimum condition, *i.e.*, $R_{l,linear,P_{\max}} = R_i$) is half of the mechanical power that can be absorbed by the transducer.

In addition, it is shown that the output power and efficiency of linear systems increase by increasing the size of the structure. However, the maximum efficiency for such devices cannot be more than 50%.

In contrast, rotational systems with a constrained throw show greater capability in transferring energy to the resistance load. In these systems, the ratio of the optimum

load resistance and the internal resistance of the generator can be written according to equation (3.32) and (3.44) as follows:

$$\frac{R_{l,\,rotational,\,P_{\max}}}{R_i} = \sqrt{1+\Lambda_{em}}. \tag{3.60}$$

Therefore, by increasing Λ_{em}, that be achieved by enlarging the rotary generator size, the ratio of the generator internal resistance to the load resistance increases. A comparison between the efficiency of linear and rotational energy harvesting systems presented in this chapter is shown in figure 3-13.

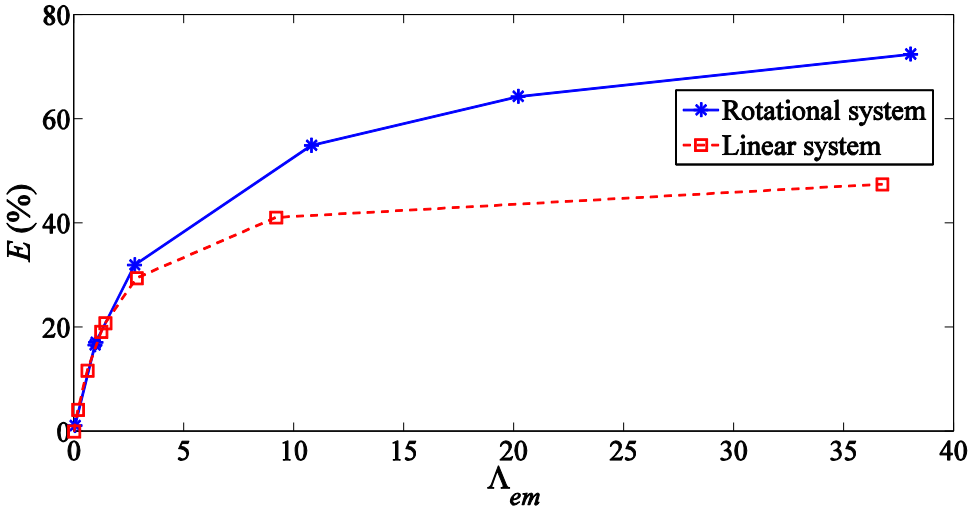

Figure 3-13 Comparison the efficiency of linear and rotational electromagnetic energy harvesting systems presented in this chapter.

Figure 3-14 shows the logarithmic plot of Λ_{em} against the generator volumes over reference volume to the power of two over three for both linear and rotational transducers, respectively presented in tables 3.3 and 3.4.

Due to the fact that the mass of a linear actuator over the mass of a reference generator is proportional to the ratio of their volumes, for the comparison shown in figure 3-14, the equivalent mass of the generator model (a), has been selected as the reference mass for linear actuators. The mass of linear actuators have been obtained from [78]. It is seen that Λ_{em} for rotational systems scales with a greater ratio in comparison with the linear systems. Hence, scaling the generator part in a rotational system can be more beneficial in terms of improvement of the system's efficiency and output power.

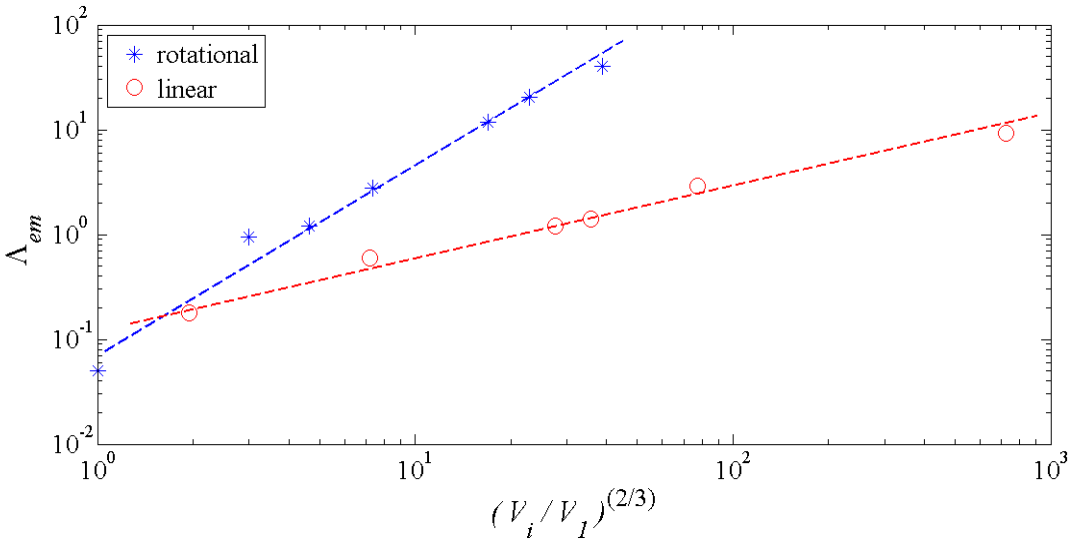

Figure 3-14 Log-log plot of Λ_{em} versus volume over the reference volume to the power of two over three for linear and rotational systems presented in tables 3.3 and 3.4.

It is demonstrated that these transducers can be designed to operate with efficiencies above 50%. The criterion that guarantees this superior efficiency is derived in (3.51) which can be used in the design process. This superiority of rotational systems over linear systems is due to the presence of an intermediate mechanism viz ball screw that can provide an extra design variable, thus enabling us to optimize the power output of the system subject to displacement constraint more desirably. For a defined environmental condition and a given proof mass with constrained maximum allowable displacement, the amount of power delivered to the electrical load by a rotational system can be as high as twice the amount delivered by a linear system.

Chapter 4: Design procedure for a rotational energy harvester

4.1 Introduction

In this chapter, the procedure for designing a ball screw based device, shown in figure 4-1, for harvesting energy from the vertical motion of a boat is presented. This device may also be used for small-scale wave energy harvesting purposes. The proposed system is a base excited mass-spring system in which the relative motion of the mass is caused by the vertical oscillation of a boat or a buoyant.

This chapter proposes the design process guidelines for the optimum selection of the system parameters. Note that in many electromagnetic energy harvesting systems presented in the literature, choosing the optimum load resistance with the goal of maximizing the energy harvested from the environment, is a process that is carried out after the design stage. This is why, in these cases, the phrase "tuning" is used to refer to the selection of the resistance load. However, in some applications such as the one presented in this chapter where the maximum displacement of the mass is limited, choosing the optimum load resistance is an integral part of the design process and cannot be done independently of choosing other parameters.

4.2 System description

Figure 4-1 shows a drawing of the proposed device. It comprises a sprung mass coupled to an electrical generator via a ball screw. The boat's vertical motion causes the mass to vibrate relative the boat which in turn drives a generator through the ball screw coupling. The free body diagram of the presented device is similar to that shown in figure 3-6. The governing equations of the motion of mass and the output power were derived in chapter 3.

Form (3.25) the maximum value of the relative displacement occurs when $\partial Z / \partial \omega = 0$ which gives the following expression for the resonance frequency:

$$\omega_{resonance} = \frac{2k}{\sqrt{4k\left(m + J\left(\frac{2\pi}{l}\right)^2\right) - 2\left(\left(c_m + \frac{T_i^2}{R_l + R_i}\right)\left(\frac{2\pi}{l}\right)^2\right)^2}}, \quad \textbf{(4.1)}$$

The maximum relative displacement is then given by

$$Z_{resonance} = \frac{2mk^2 Y_0}{\sqrt{4k^3\left(\left(c_{bg} + \frac{T_i^2}{R_l + R_i}\right)\left(\frac{2\pi}{l}\right)^2\right)^2\left(m + J\left(\frac{2\pi}{l}\right)^2\right) - k^2\left(\left(c_{bg} + \frac{T_i^2}{R_l + R_i}\right)\left(\frac{2\pi}{l}\right)^2\right)^4}}. \quad \textbf{(4.2)}$$

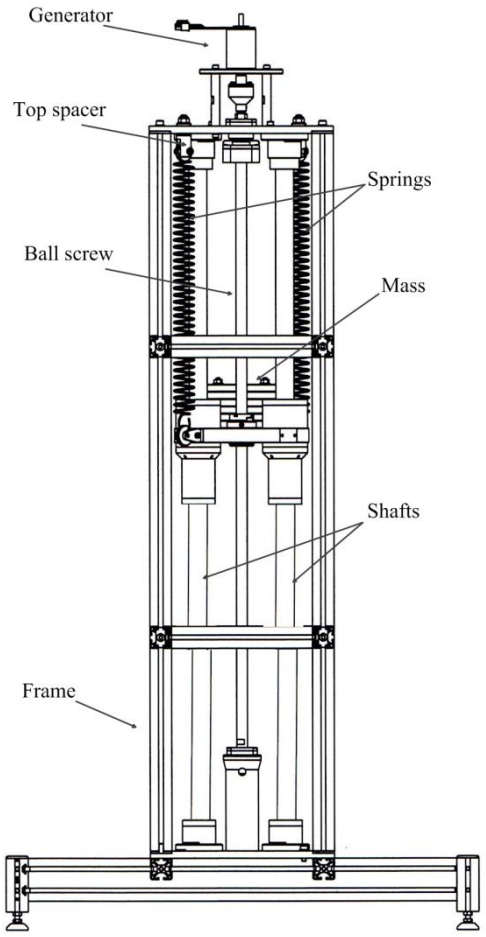

Figure 4-1 The proposed design for harvesting energy from boat's vertical movement.

4.3 Design optimization

In this section, the process of optimal selection of physical parameters of the proposed energy harvesting device is studied. The optimal design of such a device strongly depends on the combination of mass, spring, rotational generator, ball screw and load resistance parameters. Figure 4-2 shows the design process for the energy harvesting system.

The first step in designing an energy harvesting device is to establish the characteristics of the vibration environment. In the case of a boat's vertical movement, as the source of excitation, obtaining the main frequency and amplitude of the vertical movement of the boat is indispensable. Hence, the design process begins with the study of the characteristics of the boat's vertical oscillation.

4.3.1 Environmental vibration conditions

In general, the amplitude and frequency of a boat's vertical motion is related to the parameters such as weather condition, sea depth, boat speed, boat size, etc. A review of different studies shows that the vertical movement of typical sailing boats is inherently random with the dominant frequency of vibration being less than 1 Hz [82]. Based on the discussion presented in chapter 2, to investigate the dominant vibration frequency of a typical boat, measurements were conducted on a sailing boat in the English Channel. The boat was a double hull catamaran, 34 feet long, 14 feet wide with a total weight of approximately 3.5 tonnes. To acquire the oscillation data, a micro-machined silicon static accelerometer was positioned three feet from the bow of the boat.

The results of this research confirmed that significant boat vertical motion occurs at the frequency of 0.5 Hz and the main amplitude of the boat movement is about 1 m. Therefore, the initial scope of this work is to design the energy harvesting device for the condition where its base is subjected to a 0.5 Hz vibration with amplitude of 1 m ($Y_0 = 1$ m , $\omega = \pi$ rad/sec).

4.3.2 Selection of mass and its maximum stroke

Equation (3.49) shows that the maximum theoretical output power is not only determined by the environmental vibration characteristics (ω , Y_0) but also the relative

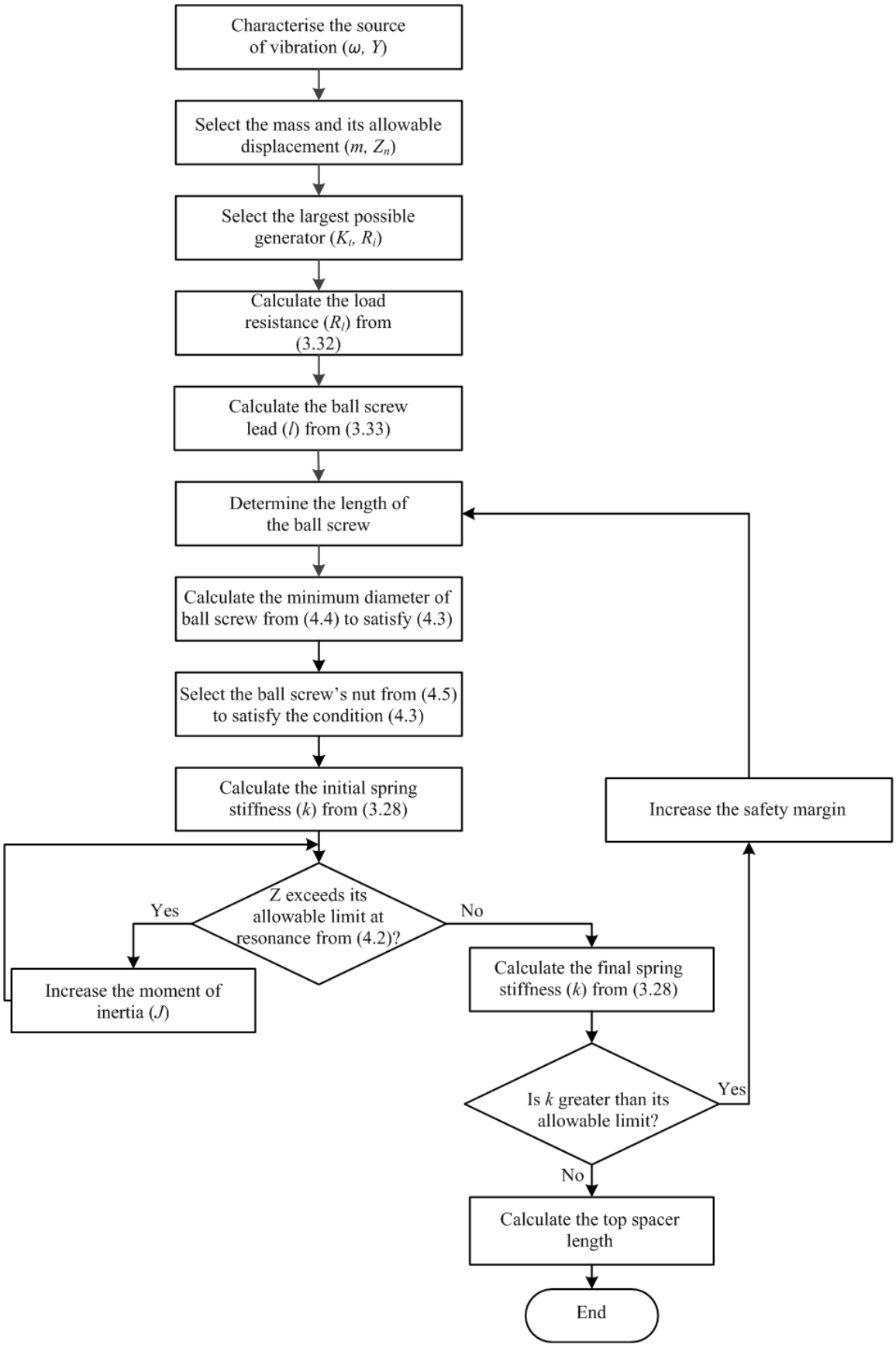

Figure 4-2 Process of designing the energy harvesting system parameters.

displacement of the mass. The mass and its maximum allowable displacement (Z_{n_0}) should ideally be as large as possible. However, it is known that in practice, the mass and its relative displacement are limited by the actual size and weight of the device. In this work, the proof mass is assumed to be 8 kg ($m =$ 8 kg) and the maximum displacement from equilibrium position is ±300 mm ($Z_{n_0} = 300$ mm). In the following sections, the physical parameters of the system are selected so that the output power is maximised.

4.3.3 Generator selection

In an ideal generator, for energy harvesting purposes, the internal resistance should be as small as possible. Also, the mechanical damping associated with the generator should be minimum. Generally, PM generators are suitable choices for these types of applications as for a comparable power rating they possess lower mechanical damping and smaller coil resistance than other types of rotary generators. In addition, with no winding on their rotors, they tend to have a small rotor moment of inertia which reduces the mechanical time constant of the generator. From (3.49) it is evident that by increasing the electromagnetic coefficient of a transducer (Λ_{em}), the amount of harvested power is increased. In chapter 3, it was shown that the electromagnetic coefficient of a transducer is proportional to its size. It was also found that by increasing the size of the generator in an energy harvesting transducer, the electromagnetic coefficient of the generator and consequently the overall electromagnetic coefficient of the transducer are increased. Therefore, the generator should be selected to be as large as possible. After choosing the generator, the load resistance can be calculated from (3.32). However, in selecting the ball screw, some practical constraint should be considered, as discussed in the following section.

4.3.4 Ball screw selection

The size of ball screw lead can be calculated form (3.33) and its length from the sum of the overall traveling distance of the mass ($2Z_{n_0}$ = 600 mm) plus a margin of 100 mm for safety purposes and an extra length (240 mm in our case) to accommodate the bearings and coupling shaft. Hence, the total length of the ball screw here is 940 mm.

The next parameter of the ball screw that needs to be determined is its diameter. However, before that we need to find the maximum rotational speed of the ball screw (υ). This speed should be lower than the maximum permissible rotational speed of the ball screw, where

$$\upsilon = \omega_n Z_{n_0} \left(\frac{2\pi}{l} \right) \leq \text{smaller value of } N_1 \text{ and } N_2. \quad \textbf{(4.3)}$$

The maximum permissible rotational speed of a ball screw is the lower value of the critical speed (N_1) and ball bearing maximum permissible speed (N_2). Critical screw speed is related to the natural frequency of the screw shaft. Exceeding this value may result in excessive vibration. The critical speed (N_1) can be found by using the following equation [83]

$$N_1 = \lambda \frac{d}{l_b^2}, \quad \textbf{(4.4)}$$

where λ is called the mounting factor and is determined according to the mounting configuration of the ball screw ends. The highest value of λ is achieved when both ends of the ball screw are fixed. Parameter l_b is the distance between two mounting surfaces and d is the screw shaft thread's minor diameter.

Another consideration is related to the velocity of the ball bearings rotating around the screw shaft (N_2). Exceeding this value may result in damaging the ball circulation components. This value is obtained from

$$N_2 = \frac{C_r}{D}. \quad \textbf{(4.5)}$$

where D is the ball centre-to-centre diameter and the parameter C_r depends on the manufacturing details of the ball screw and nut, and is determined by the manufacturing companies for each product. The permissible rotational speed is determined by the lower values of N_1 and N_2. Therefore, the minimum permissible diameter of the ball screw is initially determined from (4.4) so that to satisfy the condition of (4.3). The type and size of ball bearings of the ball screw nut are determined from (4.4) so that to meet the condition presented in (4.3).

Although the minimum permissible diameter of the ball screw is determined from (4.3), in practice a larger diameter may be required. The diameter of a ball screw

dominantly determines the overall moment of inertia of the system. Even though the device is designed based on the main frequency of base excitation, its functionality should not be jeopardized when subjected to higher frequencies. In other words, when the moment of inertia of the system is low (meeting the condition presented in (4.3)), the relative displacement of the moving mass at high frequencies may exceed its maximum allowable set by the physical constraints of the device. On the other hand, selecting a ball screw with an unnecessarily large diameter not only increases the cost but also the overall moment of inertia of the system. Therefore, the spring stiffness should be increased to compensate for the effect of the high-reflected inertia and maintain the natural frequency of the system being equal to the excitation frequency. However, utilizing a very stiff spring does not allow the mass to be positioned in the middle of the active length of the ball screw, which limits the maximum permissible stroke.

After selecting the ball screw with minimum permissible diameter, the initial spring stiffness can be obtained from (3.28) to ensure that the natural frequency of the system matches the excitation frequency. However, if the relative mass displacement at higher frequencies (including the resonance frequency from (4.1)) exceeds its maximum limit, i.e. the active length of the ball screw plus the additional safety margin, the system performance will be impaired. To avoid this problem, the overall moment of inertia of the system needs to be increased and that can be achieved by increasing the ball screw diameter. Therefore, the optimum size of the ball screw diameter needs to be as small as possible subject to the condition that guarantees the operation of the system at frequencies higher than natural frequency of system including the resonance frequency obtained from (4.1). In other words, if the system is supposed to be subjected to an excitation with a frequency equal to its resonance frequency, the moment inertia of the system needs to be selected so that the maximum relative displacement at resonance obtained from (4.2) is less than the safety length of the ball screw.

After selecting a suitable ball screw, based on the overall moment of inertia of the system, the final value of the spring stiffness can be calculated from (3.28). However, in the process of designing and selecting the spring, some practical issues should be considered which are discussed next.

4.3.5 Spring selection

In theory, two types of springs (compression and tension) may be selected for this apparatus. However, extending a compression spring beyond its free length will alter its free length. Therefore, in the next compressive part of the cycle, the load exerted by the spring would be higher due to the increased free length while the stiffness would remain the same. To overcome this problem, the stiffness of the spring should be such that the entire oscillation occurs within its original free length. This imposes an extra constraint on the selection of the spring as it implies here that the loaded spring should be compressed by 300 mm in the equilibrium position. Obtaining such a compression gives rise to the problem of buckling. The maximum allowable spring deflection that avoids buckling depends on the free length, coil diameter and spring ends configurations [84] (such as pivot ball or ground and square). For a spring with 800 mm free length and a deflection of 600 mm to avoid buckling, as a rule of thumb, the mean diameter of the spring's coils should be at least one quarter of its free length, i.e., the spring diameter needs to be more than 200 mm. Utilizing this size of spring (especially when a pair of springs in parallel are required) increases the device size to an unacceptable level. Buckling of the springs could be prevented by using supporting shafts, however, the friction between the spring and the shaft will degrade the performance of the system.

To avoid difficulties associated with using compression springs, tension springs are therefore proposed. Using tension springs not only reduces the size of the device but also reduces friction and power losses during the operation of the system. With a maximum allowable displacement of 600 mm, the spring stiffness should be such that the entire oscillation occurs when the spring is in extension mode where the loaded spring is extended at least 300 mm in the equilibrium position. For a mass of 8 kg, it means that the maximum allowable spring stiffness is 261.6 N/m. If the calculated spring stiffness is larger than this amount, the diameter of the ball screw should be decreased to reduce the moment of inertia of the system and consequently the spring stiffness. If reducing the moment of inertia will jeopardize the performance of the system at frequencies higher than its natural frequency, then the considered safety margin should be increased. For the spring stiffness of less than 261.6 N/m, the length of the upper spacer connection is determined so that the equilibrium position of the loaded spring is in the middle of the active length of the ball screw.

4.4 Numerical example

In this section, the performances of some energy harvesters, designed with different generators are compared. Table 4-1 presents the specifications of six PM generators that including parameters such as size, internal load resistance, torque constant and overall mechanical damping. For each generator, by considering the environmental conditions ($\omega = \pi$ rad/sec, $Y = 1$ m) , the given mass ($m = 8$ kg), and the maximum allowable displacement at the dominant frequency ($Z_0 = 0.3$ m), other parameters of the energy harvesting device are calculated according to the flowchart presented in figure 4-2. Here, an additional 50 mm of the active length of the ball screw, on each side, has been considered as a safety margin. Therefore, if the traveling length of the oscillating mass exceeds 350 mm from the equilibrium position, the operation of the system will be hindered due to the mass hitting the end stops or the tension springs exiting their extension modes.

Table 4-1 Parameters of six PM generator [81].

Model	Diameter (mm)	Length (mm)	T_i (mNm/A)	R_l (Ω)	c_m (mNm rad^{-1}s^{-1})
a	20	36	6.34	3.4	13.6E-3
b	24	44	9.83	2.1	17.6E-3
c	30	56	12.74	1.6	22.6E-3
d	35	64	14.52	0.6	22.6E-3
e	44	90	23.83	0.23	37.1E-3
f	45	144	73.9	1.01	53.6E-3

For each harvester, table 4-2 presents the calculated electromagnetic coefficient from (3.44), optimum load resistance from (3.32) and optimum size of ball screw lead from (3.33). In addition, the amount of extracted power from each transducer, designed with the generators presented in table 4-1, is calculated. It is shown that by increasing the generator's size, the electromagnetic coefficient increases and, as expected from (3.49), the amount of harvested power monotonically increases. From (3.49) the maximum harvestable power for the given condition is 37.2 W, however, as it is seen in

table 4-2 due to mechanical and electrical power losses, in all cases the transferred power to the load resistance is less than this amount. It is further seen that by increasing the generator size, the size of ball screw lead is increased which reduces υ in the left hand side of (4.3). Hence, by increasing the size of a generator the fulfilment of the condition presented in (4.3) and as a result the selection of the ball screw would be much easier. Figure 4-3 shows the efficiency of the designed systems versus their electromagnetic coefficients. It is seen that by increasing Λ_{em} the efficiency of the transducer increases.

Table 4-2 Six energy harvesting systems designed based on presented PM generators in table 4-1.

Model	l (mm)	R_l (Ω)	Λ_{em}	P_{l-ave} (W)
a	3	4.65	0.87	5.77
b	4	3.97	2.6	11.50
c	5	3.74	4.46	14.91
d	7	2.18	12.26	21.17
e	12	1.89	66.72	29.14
f	16	10.18	110.75	30.05

Designing an energy harvesting device based on the guidelines presented in figure 4-2 can guarantee harvesting the maximum amount of power when the environmental excitation frequency matches the natural frequency of the system. At this condition, the output power is not a function of the moment of inertia of the system. In a real environment, an energy harvesting system may be subjected to a wide range of frequencies including the resonance frequency, which is the frequency corresponding to the maximum relative displacement of its mass. Now, if the resonance frequency of the device is within the expected excitation frequency range, then the moment of inertia of the system should be selected so that the maximum relative displacement of the oscillating mass, obtained from (4.2), is less than its given limit, i.e., the active length of the ball screw plus the safety margin.

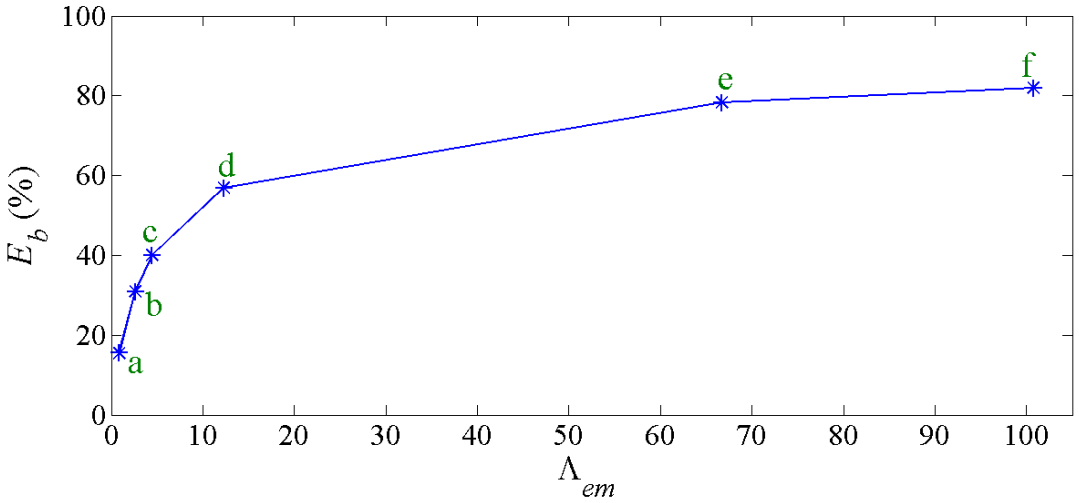

Figure 4-3 Efficiency of the designed systems versus their electromagnetic coefficients.

Figure 4-4 shows the relative displacement of the mass for four harvesters, with different total moments of inertia, that have been designed with the generator Model f in table 4-1. Here, it is assumed that the base oscillation varies over a wide range of frequencies, including resonance frequency, at the same amplitude (1 m).

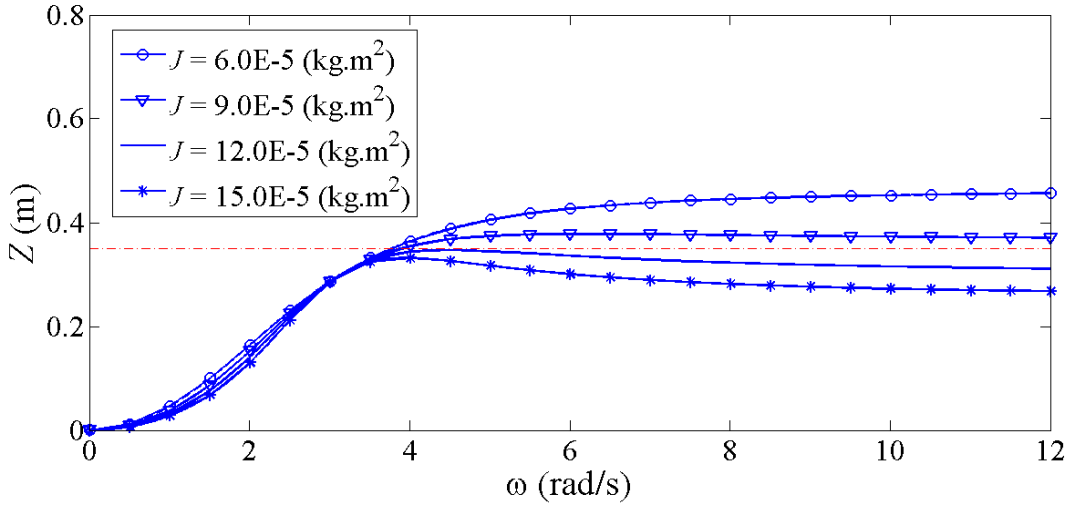

Figure 4-4 Relative displacement of the oscillating mass when the frequency of vibration varies in a wide range.

When the harvester's moment of inertia is low (e.g., small ball screw diameter), by increasing the excitation frequency, the traveling amplitude may exceed its allowable limit, which is 350 mm. Despite reducing the efficiency of the system, by increasing the moment of inertia (see figure 4-4 when J =12e-5 kg.m^2), the harvester can be designed so that its functionality over a wide range of frequencies is guaranteed because the maximum traveling distance of its oscillating mass is always less than its

permissible limit. The parameters of a suggested harvester, designed with the generator Model f, according to the guidelines presented in figure 4-2 is shown in table 4-3. As it is seen in table 4-2, this system produces a maximum power of 30.05 W when it is subjected to 1 m oscillation at the frequency of 0.5 Hz. With the optimum size of 16 mm for ball screw lead, from (3.20) the maximum rotational speed of the ball screw in this system is 370.1 rad/sec or 3524 rpm, hence, a suitable ball screw and nut should be selected to satisfy the condition presented in (4.3). The power density of the designed energy harvester is 480.8 W/m^3.

Table 4-3 Parameters of the suggested harvesters designed based n generator Model f.

Parameter	Value	Parameter	Value
m	8 kg	R_l	10.18 Ω
l	16 mm	K_t	73.9 mNm/A
k	261 N/m	R_i	1.01 Ω
J	12E-5 kg.m^2	ball screw length	0.94 m

4.5 Maplesim Simulation

To validate the derived equations and suggested parameters, the designed energy harvester is simulated using Maplesim, which is a modelling environment for creating and simulating multi-domain physical systems. It allows the user to build a components diagram that represents a physical system in a graphical form and therefore the result of simulation can validate the derived dynamic equations for the simulated system. The diagram of the suggested energy harvester is shown in figure 4-5 and the considered model of generator in Maplesim is shown in figure 4-6.

Figure 4-7 shows the base movement and the relative displacement of the harvester mass. It is seen that for a base displacement of 1 m at the frequency of 0.5 Hz, the relative mass displacement is restricted to the amplitude of 0.3 m. The output power that is shown in figure 4-8 indicates that the average harvested power is in agreement with the predicted amount of 30.05 W.

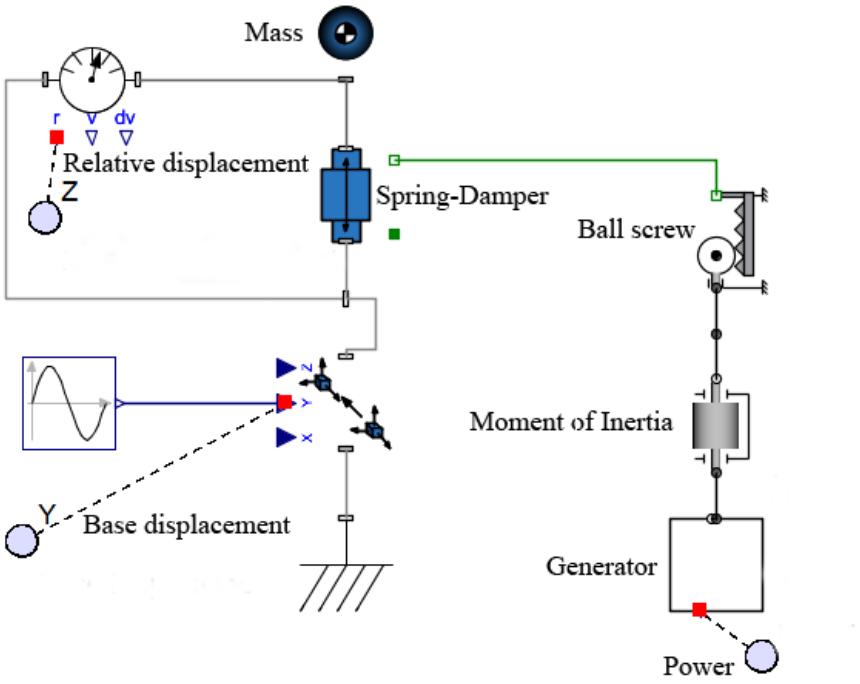

Figure 4-5 Maplesim model of the proposed energy harvester.

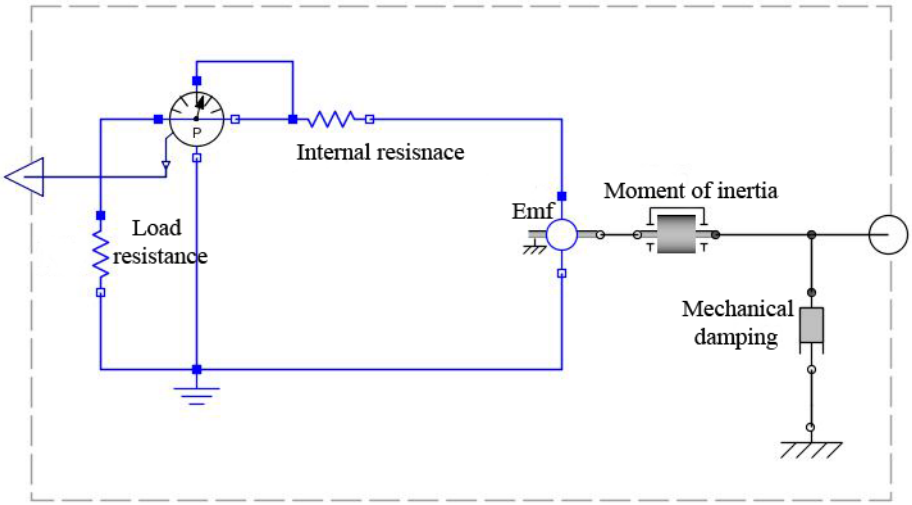

Figure 4-6 Generator model in Maplesim.

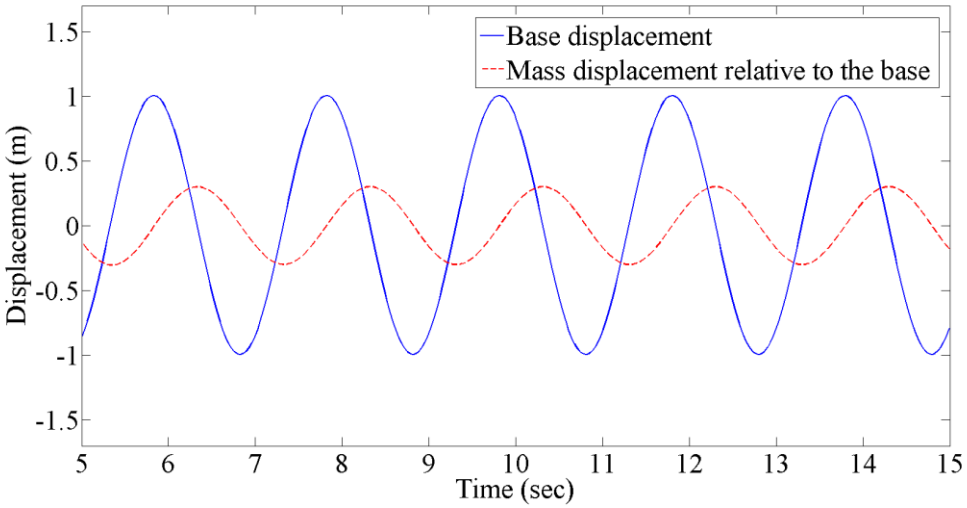

Figure 4-7 Base displacement and relative displacement of the oscillating mass in Maplesim simulation.

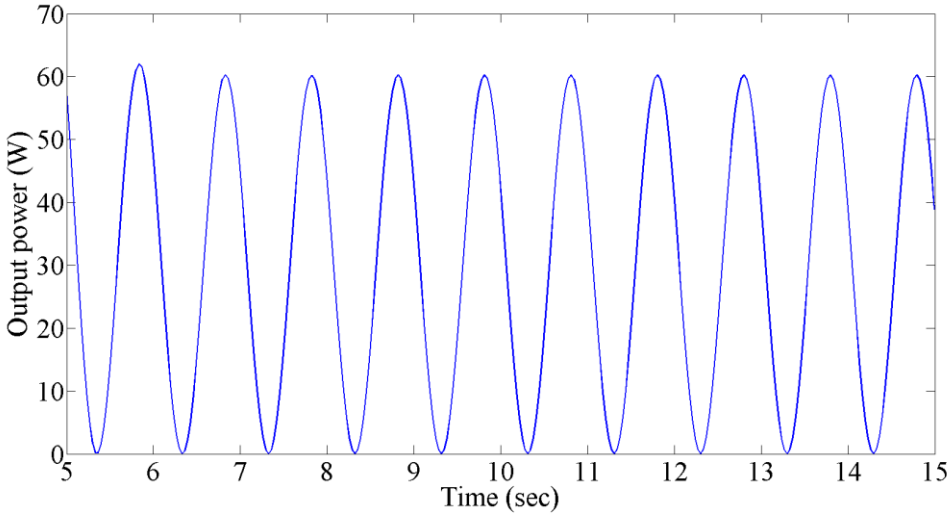

Figure 4-8 Harvested power from the proposed energy harvester when it is subjected to a sinusoidal movement with the amplitude of 1 m and frequency of 0.5 Hz, obtained by Maplesim simulation.

4.6 Time varying frequency and amplitude excitation

Although the energy harvester presented in this chapter is designed for a given environmental condition with known excitation amplitude and frequency, in practice, these may vary. Therefore, it is worth studying the performance of the designed energy harvester when it is subjected to a time-varying frequency and amplitude excitation. Figure 4-9 shows the relative mass displacement for the energy harvester with its parameters shown in table 4-3, when the frequency and amplitude of base displacement,

respectively, vary form 1.0 rad/sec to 7.0 rad/sec and 0.2 m to 1.0 m. It is seen that by increasing the amplitude of the base displacement, the relative displacement is increased. However, by increasing the excitation frequency, for the frequencies below the resonance frequency of the device, i.e 4.5 rad/sec obtained from (4.1), the relative mass displacement is increased and for the frequencies above this value it is decreased.

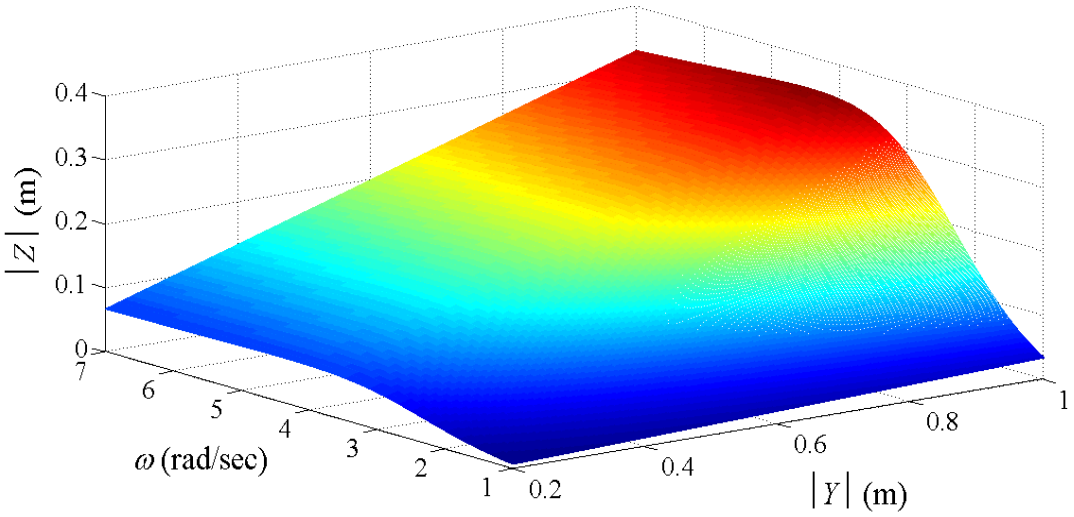

Figure 4-9 Relative displacement of mass when the amplitude and frequency of base excitation, respectively, vary from 0.2 m to 1m and from 1 rad/sec to 7 rad/sec.

Figure 4-10 shows the output power of the system when the energy harvester is subjected to time-varying excitation. It is seen that by increasing the excitation amplitude and frequency, the output power is increased whilst, based on figure 4-9, the harvester operates within the allowable, i.e Z<0.35.

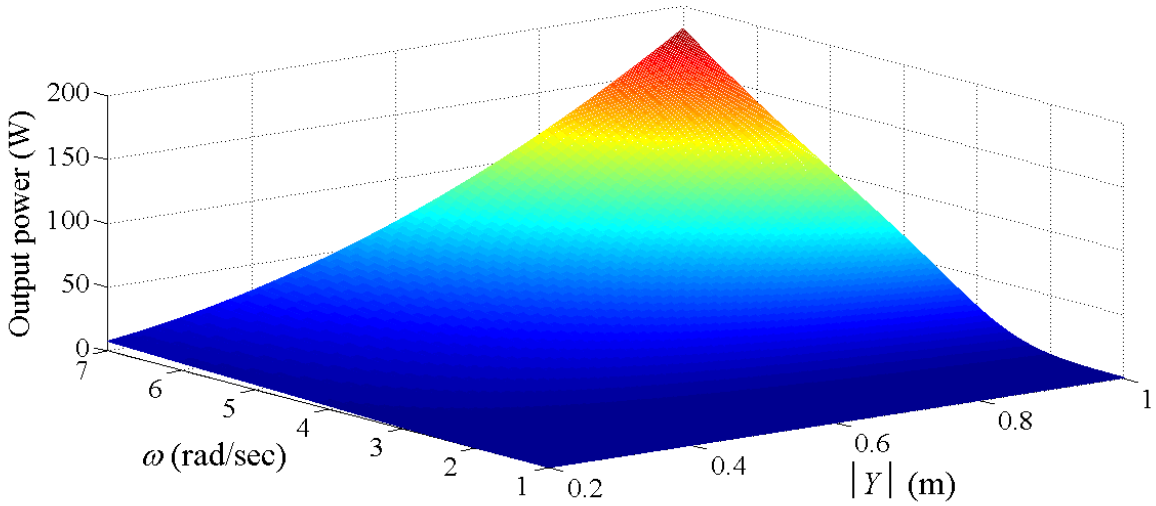

Figure 4-10 Output power when the amplitude and frequency of base excitation, respectively, vary from 0.2 m to 1m and from 1 rad/sec to 7 rad/sec.

To evaluate how optimize is the harvester in time-varying excitation condition, the effectiveness of system is studied. Here, the effectiveness is defined as [18]

$$E_H = \frac{\text{Output power}}{\text{Maximum possible oputput}} = \frac{\text{Output power}}{\frac{1}{2} mYZ\omega^3} \qquad (4.6)$$

Figure 4-11 shows the effectiveness of energy harvester when it is subjected to a time-varying frequency and amplitude excitation. It is seen that the maximum effectiveness is obtained when the excitation frequency matches the natural frequency of device, i.e. ω=πrad/sec and for the frequencies away from the natural frequency of harvester the effectiveness of system declines. In other words, the harvester with pre-tuned natural frequency is unable to achieve optimal power output for all frequency range of excitation. Hence, to improve the performance of system under time-varying frequency condition, we need to incorporate a tuning mechanism to increase its functionality. Therefore, the next step of this research, which will be presented in future chapters, is to introduce a variable moment of inertia mechanism to tune the natural frequency of system in time-varying conditions.

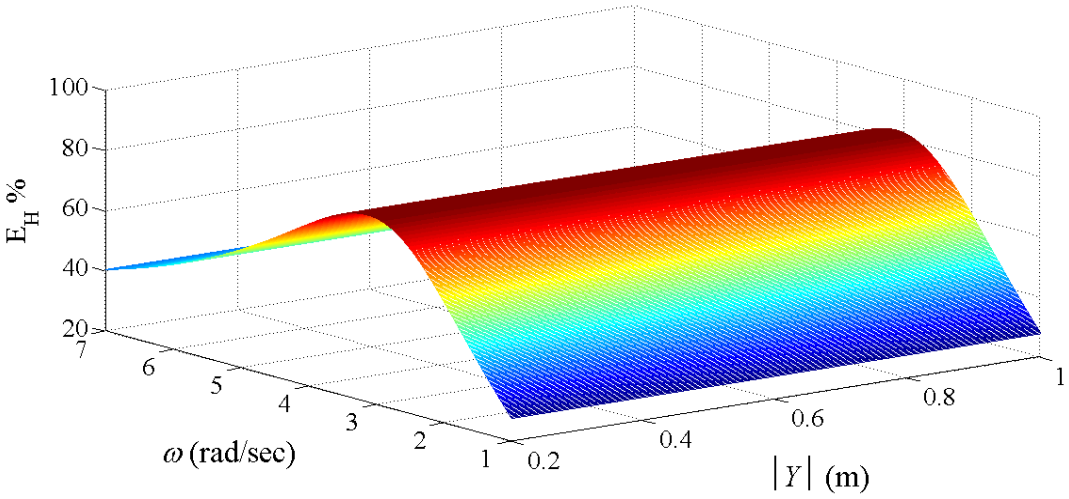

Figure 4-11 The effectiveness of energy harvester when the amplitude and frequency of base excitation, respectively, vary from 0.2 m to 1m and from 1 rad/sec to 7 rad/sec.

4.7 Conclusion

In this chapter, a constrained optimization process for a proposed ball screw based energy harvester is studied to extract maximum energy from vertical motion of a boat. In the proposed device, a ball screw converts the linear oscillatory motion of the mass to the rotational motion in order to drive a PM generator. The design process flowchart is developed to provide guidelines for the optimum selection of system parameters. The proposed technique considers practical limiting factors involved in the design of a constraint ball screw system including the maximum allowable displacement of the mass. It is shown that, unlike unconstrained energy harvesting systems, an energy harvester for which the maximum displacement is a constraint, selecting the optimum load resistance should be considered at an early stage of the design process (i.e., not a posteriori step). The suggested system with a mass of 8 kg is estimated to produce more than 30 watts for a typical boat motion which oscillates with average amplitude of 1 m at 0.5 Hz. This amount of energy is enough to supply a typical boat's internal power usage demand. In addition, it is shown that under time-varying conditions, the effectiveness of device for the frequencies away from the natural frequency of system declines. Chapter 6 will demonstrate how the performance of the harvester can be improved by employing a variable moment of inertia mechanism.

Chapter 5: Harvesting energy from random excitation

5.1 Introduction

Notwithstanding that many suggested energy harvesters in the literature have been designed, characterized and optimized by assuming that the device is under harmonic excitation [85, 86, 87], the majority of vibrations encountered in the real environment are random by their nature [88]. The vibration of vehicles due to roads irregularities, vibration of aircraft engines, trains and missiles are some examples of random excitations [89]. In the case of the proposed energy harvester in this thesis, in real conditions such as the marine environment, the device may be subjected to vibration which is distributed over a broadband of frequencies and random in nature. In these environments, the ambient vibration can be described using the theory of random process. The theory of random vibration applied to mechanical systems has been studied by a number of researchers [90, 91, 92]. Halvorsen [93] first used linear random vibration theory to obtain closed-form expression of the output power of a general energy harvester model. Adhikari et al [94] used the same approach to derive an expression for the mean normalized harvested power of a piezoelectric based energy harvester. Renaud et al. [68] derived closed-form formulas describing the power and efficiency of a piezoelectric energy harvester for sinusoidal and random vibrations. It was shown that under random excitation, the optimum generated power is directly proportional to the efficiency of the harvester.

Tang et al [95] studied the performance of single-mass and dual-mass electromagnetic energy harvesters under random force, displacement, velocity and acceleration. However, in their discussion, no distinction is made between the internal resistance and the load resistance of a generator. Therefore, the derived power formula is the total sum of the useful electrical energy and the electrical power loss. It is worth mentioning here that the current chapter focuses on power flow from the mechanical environment into the electrical domain rather than the delivery of useful power to an electrical load which is more appropriate. In addition, none of the above mentioned research works

investigate the performance of an electromagnetic energy harvesting system under band-limited excitation.

In this chapter, the analytical solutions within the theory of random vibration are extended to the proposed electromagnetic harvester that was presented in chapter 4. The closed-form expressions of output power under random broadband and band-limited excitations are derived. Also, an insightful discussion is provided to study the effect of the physical parameters of the energy harvester on the expected power to maximize its output power. In addition, in this chapter based on the spectral density of the measured acceleration, the expected harvested power by the energy harvester in real conditions is calculated.

5.2 A review of stationary random vibration

The principle characteristic of a random vibration is to simultaneously excite all the frequencies of a structure [90]. Let us assume that $Y_p(t)$ is a random function in time. The cumulative distribution function of $Y_p(t)$, $F_{Y_p}(y_p,t)$ is defined as

$$F_{Y_p}(y_p,t)=P_r\{Y_p(t)\le y_p\}, \tag{5.1}$$

that shows the probability of $Y_p(t)$ being smaller than or equal to a given value y_p. The probability density function (PDF) is defined as

$$f_{Y_p}(y_p,t)=\frac{\partial F_{Y_p}(y_p,t)}{\partial y_p}. \tag{5.2}$$

The mean value of $Y_p(t)$, $E[Y_p(t)]$ is obtained from

$$E[Y_p(t)]=\int_{-\infty}^{+\infty} y_p f_{Y_p}(y_p,t)\,dy_p. \tag{5.3}$$

$E\left[Y_p(t)\right]$ is the location of the centre of PDF function. The second statistical moment of $Y_p(t)$, $E\left[Y_p^2(t)\right]$ is

$$E\left[Y_p^2(t)\right] = \int_{-\infty}^{+\infty} y_p^2 f_{Y_p}(y_p, t)\, dy_p. \tag{5.4}$$

and is called the mean square value of the function $Y_p(t)$. The random function $Y_p(t)$ is said to be stationary when its value in $t_2 = t_1 + \tau$ depends only on the difference between the two time instants, *i.e.* τ. The autocorrelation function for a random process $Y_p(t)$ is defined as the average value of the product of $Y_p(t_1)Y_p(t_1+\tau)$ which is

$$R_{Y_p}(t_1, t_2) = E\left[Y_p(t_1).Y_p(t_1+\tau)\right] = R_{Y_p}(\tau). \tag{5.5}$$

The spectral density of a stationary random function $S_{Y_p}(\omega)$ is defined as the Fourier transform of its autocorrelation function $R_{Y_p}(\tau)$ and is obtained from

$$S_{Y_p}(\omega) = \int_{-\infty}^{+\infty} R_{Y_p}(\tau) e^{-j\omega\tau} d\tau, \tag{5.6}$$

and it can be shown that

$$R_{y_p}(\tau) = \int_{-\infty}^{+\infty} S_{Y_p}(\omega) e^{j\omega\tau} d\omega, \tag{5.7}$$

The dimension of the spectral density function is (quantity)^2/frequency. Equations (5.6) and (5.7) are called Wiener-Khintchine formula, stating that $R_{Y_p}(\tau)$ and $S_{Y_p}(\omega)$ are related through a Fourier transformation [96]. These formulations are convenient because it can be shown that

$$E\left[Y_p^2(t)\right] = \int_{-\infty}^{+\infty} S_{Y_p}(\omega) e^{j\omega\tau} d\tau. \tag{5.8}$$

Thus, the mean square of a quantity y_p is the integral of its spectral density over the frequency range. Also, for a linear system of the form $I_p(\omega) = H_p(\omega) Y_p(\omega)$, where $H_p(\omega)$ is the transfer function, it can be shown that the spectral density of I_p is related to the spectral density of Y_p by [88]

$$S_{I_p}(\omega) = \left|H_p(\omega)\right|^2 S_{Y_p}(\omega). \tag{5.9}$$

Therefore, for large *t*, we have

$$E\left[I_p^2(t)\right] = R_{I_p I_p}(0) = \int_{-\infty}^{+\infty} \left|H_p(\omega)\right|^2 S_{Y_p}(\omega) d\omega. \tag{5.10}$$

To calculate the integral presented in the right-hand side of (5.10) we can use the general solution presented in [97]. In general, the following form of the calculation of the integral

$$H_n = \int_{-\infty}^{+\infty} \frac{\Theta_n(\omega)}{\Psi_n(\omega)\Psi_n^*(\omega)} d\omega \tag{5.11}$$

where

$$\Theta_n(\omega) = \alpha_{n-1}\omega^{2n-2} + \alpha_{n-2}\omega^{2n-4} + \cdots + \alpha_0 \tag{5.12}$$

and

$$\Psi_n(i\omega) = \beta_n(i\omega)^n + \beta_{n-1}(i\omega)^{n-1} + \cdots + \beta_0 \tag{5.13}$$

is applicable if the system whose mean square response is of interest is stable and this will be satisfied if all roots of $\Psi_n(\omega)$ have negative real parts. Having satisfied this condition, the solution of (5.11) is obtained from [97]

$$H_n = \frac{\pi}{\beta_n} \frac{\det\begin{bmatrix} \alpha_{n-1} & \alpha_{n-2} & & \cdots & & & \alpha_0 \\ -\beta_n & \beta_{n-2} & -\beta_{n-4} & \beta_{n-6} & \cdots & 0 & \cdots \\ 0 & -\beta_{n-1} & \beta_{n-3} & -\beta_{n-5} & \cdots & 0 & \cdots \\ 0 & \beta_n & -\beta_{n-2} & -\beta_{n-4} & \cdots & 0 & \cdots \\ 0 & \cdots & & & \cdots & 0 & \cdots \\ 0 & 0 & & & \cdots & -\beta_2 & \beta_0 \end{bmatrix}}{\det\begin{bmatrix} \beta_{n-1} & -\beta_{n-3} & \beta_{n-5} & -\beta_{n-7} & & & \\ -\beta_n & \beta_{n-2} & -\beta_{n-4} & \beta_{n-6} & \cdots & 0 & \cdots \\ 0 & -\beta_{n-1} & \beta_{n-3} & -\beta_{n-5} & \cdots & 0 & \cdots \\ 0 & \beta_n & -\beta_{n-2} & \beta_{n-4} & \cdots & 0 & \cdots \\ 0 & \cdots & & & \cdots & 0 & \cdots \\ 0 & 0 & & & \cdots & -\beta_2 & \beta_0 \end{bmatrix}} \quad \textbf{(5.14)}$$

5.3 Harvesting energy from broadband white noise

The type and frequency range of vibration may vary from one environment to another. However, based on the central limit theorem, many random processes in nature, which play the role of excitations to vibratory systems, are at least approximately normal (Gaussian). An interpretation of this theory is that a random process will approximately be normal if each of its sample functions can be considered to have been generated by the superposition of a large number of independent random sources, without any single one of them contributing significantly [98]. In this section, the output power of the energy harvester when subjected to a broadband random process with a Gaussian distribution is calculated. A broadband vibration is a stationary random process whose mean square spectral density has a significant value over a range of frequencies which is of roughly the same order of magnitude as the centre frequency of the band. An ideal random excitation with equal power per unit bandwidth, which results in a flat power spectral density across the frequency range of interest, is called white noise excitation [90]. If the signal has a uniform density over all frequencies, it is called a broadband white noise. If the uniform density of signal is distributed over a certain range of frequencies, it is called band-limited white noise.

5.3.1 Mean value of output power from broadband random excitation

To evaluate the performance of the energy harvesting device under random vibration, first the frequency response function of the device should be derived. For figure 3-6, the relative displacement of the seismic mass can be written as:

$$Z(\omega) = I(\omega)\frac{R_l + R_i}{j\omega\left(\frac{2\pi}{l}\right)T_i}, \tag{5.15}$$

and (3.24) can be written as

$$Z(\omega)\left(\left(k - M\omega^2\right) + jc\omega\right) = m\omega^2 Y(\omega), \tag{5.16}$$

where c is the reflective damping of the system, defined as

$$c = \left(c_{bg} + \frac{T_i^2}{R_l + R_i}\right)\left(\frac{2\pi}{l}\right)^2, \tag{5.17}$$

And the reflective mass is defined as

$$M = m + J\left(\frac{2\pi}{l}\right)^2. \tag{5.18}$$

Substituting (5.15) into (5.16) and rearranging it results in

$$I(\omega)\left(k - M\omega^2 + jc\omega\right)\left(R_l + R_i\right) = j\left(\frac{2\pi}{l}\right)T_i m\omega^3 Y(\omega). \tag{5.19}$$

Now, if we assume $Y_A(\omega) = -\omega^2 Y(\omega)$ as the Fourier transform of the base acceleration signal, the transfer function between the load current and the base acceleration signal is

$$H_{IY_A}(\omega) = \frac{I(\omega)}{Y_A(\omega)} = \frac{-jm\left(\frac{2\pi}{l}\right)T_i\omega}{\left(k - M\omega^2\right)\left(R_l + R_i\right) + jc\omega\left(R_l + R_i\right)}, \tag{5.20}$$

and from (5.9), the spectral density of the load current is obtained form

$$S_I(\omega) = \left|H_{IY_A}(\omega)\right|^2 S_{Y_A}(\omega). \tag{5.21}$$

Note that $S_{Y_A}(\omega)$ is the spectral density of the base acceleration signal and is assumed to be constant with respect to frequency, i.e. $S_{Y_A}(\omega) = S_0$. The mean value of the load power is obtained from

$$E\left[P(t)\right] = E\left[R_l |I|^2\right] = R_l \int_{-\infty}^{+\infty} S_I(\omega)\, d\omega = R_l \int_{-\infty}^{+\infty} \left|H_{IY_A}(\omega)\right|^2 S_{Y_A}(\omega)\, d\omega = \frac{m^2 R_l T_i^2 S_0}{\left(R_i + R_l\right)^2}\left(\frac{2\pi}{l}\right)^2 \int_{-\infty}^{+\infty} \frac{\omega^2}{\left(k - M\omega^2\right)^2 + \left(c\omega\right)^2}\, d\omega. \tag{5.22}$$

Comparing the integral presented on the right-hand side of (5.22) with the general form of integral shown in (5.11), (5.22) can be re-written as

$$E\left[P(t)\right] = \frac{m^2 R_l T_i^2 S_0}{\left(R_i + R_l\right)^2}\left(\frac{2\pi}{l}\right)^2 \times \int_{-\infty}^{+\infty} \frac{\omega^2}{\left[k + c\left(j\omega\right) + M\left(j\omega\right)^2\right]\left[k + c\left(-j\omega\right) + M\left(-j\omega\right)^2\right]}\, d\omega, \tag{5.23}$$

where

$$\Psi_2(\omega) = k + c\left(j\omega\right) + M\left(j\omega\right)^2, \tag{5.24}$$

The roots of the characteristic equation of the system is obtained from

$$k + c\lambda + M\lambda^2 = 0, \tag{5.25}$$

Hence, the roots are

$$\lambda_{1,2} = \frac{-c \pm \sqrt{c^2 - 4Mk}}{2M}. \tag{5.26}$$

In (5.26) *c*, *k* and *M* are physical parameters and are all positive, therefore, the real parts of the roots of (5.25) are always negative and hence the system is stable. This guarantees the feasibility of applying the approach presented in (5.14). Based on the

general solution for this type of integral from (5.23) we have

$$\begin{aligned} &n=2, \quad \alpha_1=1, \quad \alpha_0=0 \\ &\beta_2=M, \ \beta_1=c, \quad \beta_0=k, \end{aligned} \tag{5.27}$$

and

$$H_2(\omega)=\frac{\pi}{M}\frac{\det\begin{bmatrix}1 & 0\\ -M & k\end{bmatrix}}{\det\begin{bmatrix}c & 0\\ M & k\end{bmatrix}}. \tag{5.28}$$

Hence, the mean value of power is

$$E[P]=\frac{S_0 m^2 R_l T_i^2}{M\left(R_i+R_l\right)^2}\left(\frac{2\pi}{l}\right)^2\frac{\pi}{c}. \tag{5.29}$$

By replacing (5.17) and (5.18) into (5.29), the mean value of output power based on the physical parameters of the energy harvester becomes

$$E[P]=\frac{\pi S_0 m^2 R_l T_i^2}{\left(c_{bg}\left(R_l+R_i\right)^2+T_i^2\left(R_l+R_i\right)\right)\left(m+J\left(\frac{2\pi}{l}\right)^2\right)}. \tag{5.30}$$

In chapter 3, it was shown that when the system is excited by a single frequency, to maximize the output power, it should be designed so that its undamped natural frequency is matched to the frequency of excitation. Therefore, in a single excitation condition, the harvested power is independent from the moment of inertia of the system. However, (5.30) indicates that the expected load power under random excitation is inversely proportional to the sum of the seismic mass and the reflected moment of inertia of the system. This implies that to harvest maximum power from a base excited rotational harvester under random excitation the moment of inertia of the system should be as small as possible.

The optimum value of the load resistance to maximize the output power can be obtained by solving $\frac{\partial}{\partial R_l}E[P]=0$, which results in

$$R_l = \sqrt{R_i^2 + \frac{T_i^2}{c_{bg}} R_i}. \tag{5.31}$$

Interestingly, comparing (5.31) with (3.32) in chapter 3, reveals that the optimum load resistance when designing a constraint energy harvesting system for a single frequency of excitation is the same as the optimum load resistance when the system is subjected to a random excitation.

To validate the analytical expression obtained for the optimum load resistance of the rotational electromagnetic energy harvesting system, a Monte-Carlo simulation is conducted. The Monte-Carlo simulation technique is a method that uses a random number sequence to evaluate the characteristics of the system based on a stochastic process [99]. Here, the expected output power is obtained for different values of the load resistance for a system whose parameters are presented in table 5-1.

Table 5-1 Parameters of the energy harvester for Monte-Carlo test.

Parameter	Value
mass (m)	8 kg
generator resistance (R_i)	1.01 Ω
mechanical damping (c_{bg})	5.36E-5 N.s/m
spring stiffness (k)	261 $N.m^{-1}$
coupling coefficient (T_i)	7.39E-3 $V.s.m^{-1}$
ball screw lead (l)	0.016 m
ball screw moment of inertia (J)	12.0E-5 $kg.m^2$

In order to simulate the input acceleration, 2000 samples of wide-band pseudo-random signals are generated, as follows

$$\sum_{i=1}^{N} \ddot{y}_i(i.\Delta t) = \sum_{i=1}^{N} \Upsilon_i \sin(\varpi_i(i.\Delta t) + \varphi_i). \tag{5.32}$$

where variables ϖ_i , Υ_i and φ_i are independent and normally distributed, respectively in [0, ϖ_{max}], [0, Υ_{max}] and [0, φ_{max}]. In addition, the maximum value of i is defined as N, which depends on the duration of the simulation τ and the time step Δt as

$$N = \frac{\tau}{\Delta t}. \tag{5.33}$$

It is known that white noise has a constant spectral value over the whole frequency range. However, in practice, for simulation purposes generating such a signal is not feasible. Here we assume that $\varpi_{\max} = 400\,\pi$ rad/sec, which is much larger than the natural frequency of the simulated system, ($\omega_n = \pi$ rad/sec), and is thus a reasonable approximation. The simulation is conducted for a period of 20 seconds, i.e. $\tau = 20$ sec, a sampling time of $\Delta t = 0.001$ sec, and $\Upsilon_{\max} = 10$ m sec^{-2}. The parameters of the Monte-Carlo simulation are shown in table 5-2.

Table 5-2 Simulation parameters of the Monte-Carlo technique.

Parameter	Value
$\varpi_{\max}$	400 π rad sec^{-1}
$\Upsilon_{\max}$	10 m sec^{-2}
$\varphi_{\max}$	π rad
τ	20 sec
Δt	0.001 sec

The histograms shown in figure 5-1 illustrate the harvested power for different values of load resistance obtained from 2000 sets of random accelerations applied to the system for 20 seconds. As it is seen, the histogram of the average amount of harvested power for the produced base acceleration results in an output power with a Gaussian distribution. Statistical results of the output power obtained from Monte-Carlo simulation are shown in table 5-3.

Table 5-3 Statistical results of Mote-Carlo simulation.

Load resistance $R_l(\Omega)$	Expected power $\mu = E[P]$ (W)	Standard deviation σ (W)
0.5	12.67	0.86
3.0	27.60	2.96
7.0	30.63	4.53
10.2	31.03	5.28
15.0	30.22	6.04
30.0	27.50	7.13
60.0	22.38	7.32
100.0	17.78	6.66

Figure 5-2 compares the statistical output of the Monte-Carlo simulation due to different load resistance values with the analytical expected power for each load resistance. As it is seen, maximum power is transferred to the load resistance for the case where $R_l = 10.2\,\Omega$ which is equal to the optimum load resistance calculated from (5.31) for the harvester parameters presented in table 5-1. The Monte-Carlo simulation confirms the calculated value for the optimum load resistance for harvesting maximum amount of power when the device is excited by a broadband random acceleration.

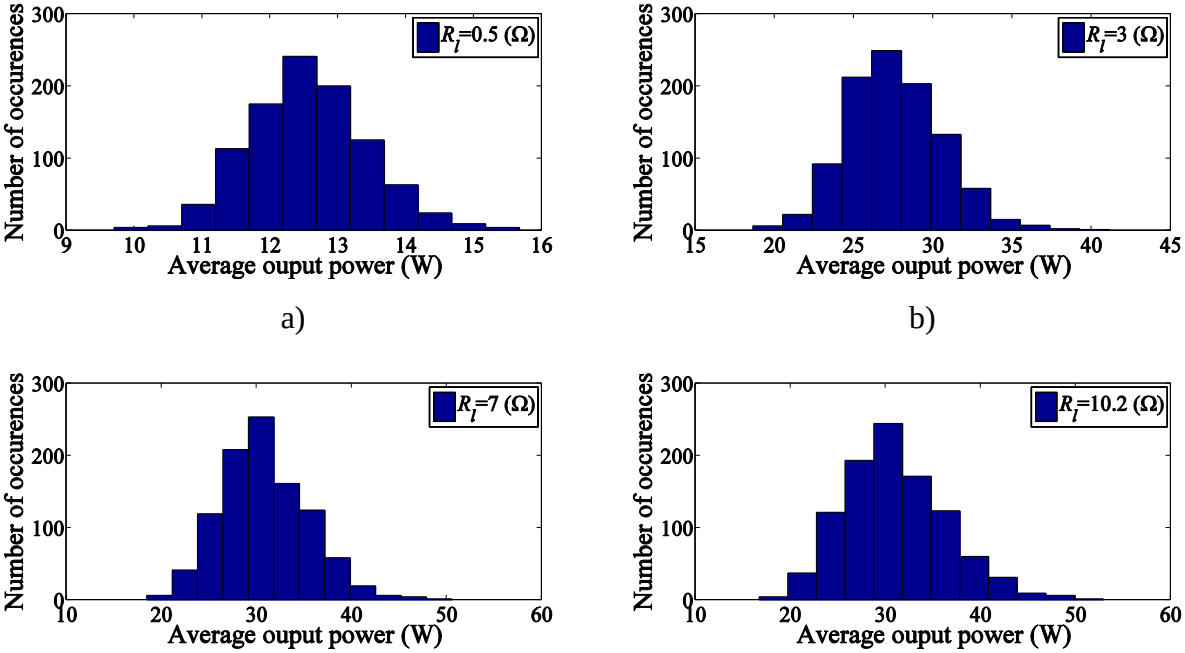

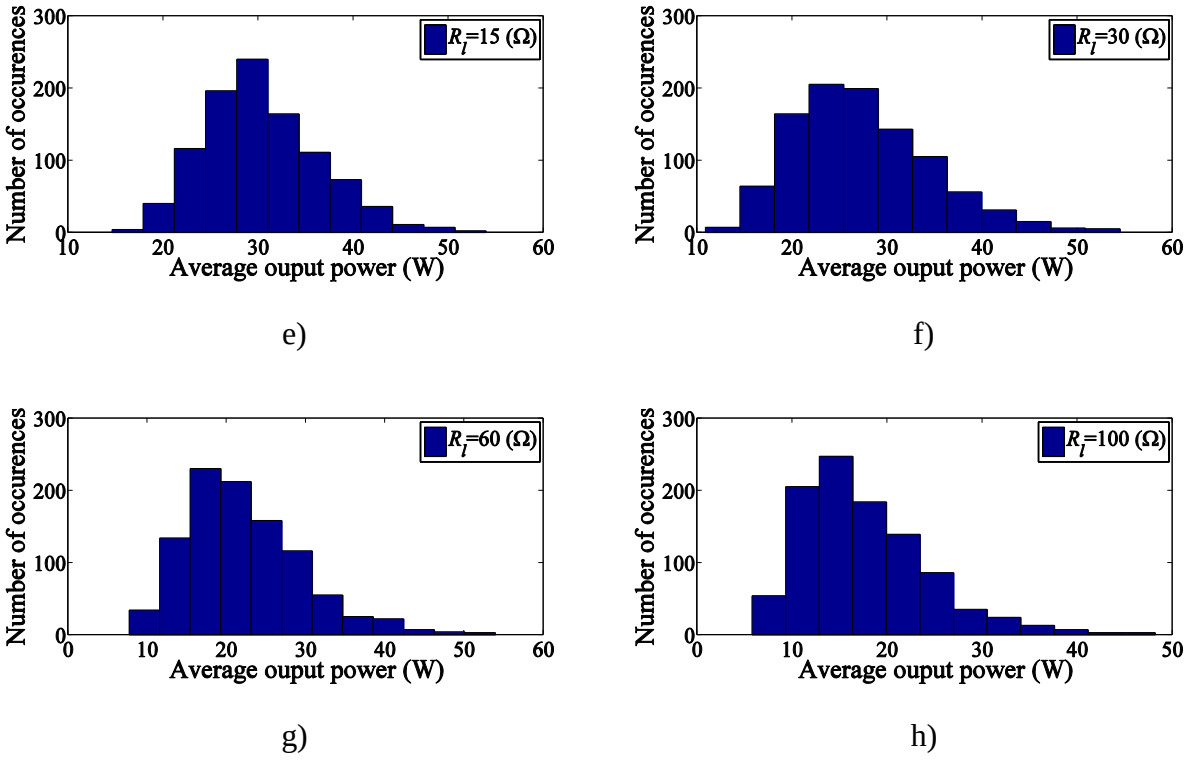

Figure 5-1 Histograms of harvested power for 2000 generated random acceleration runs.

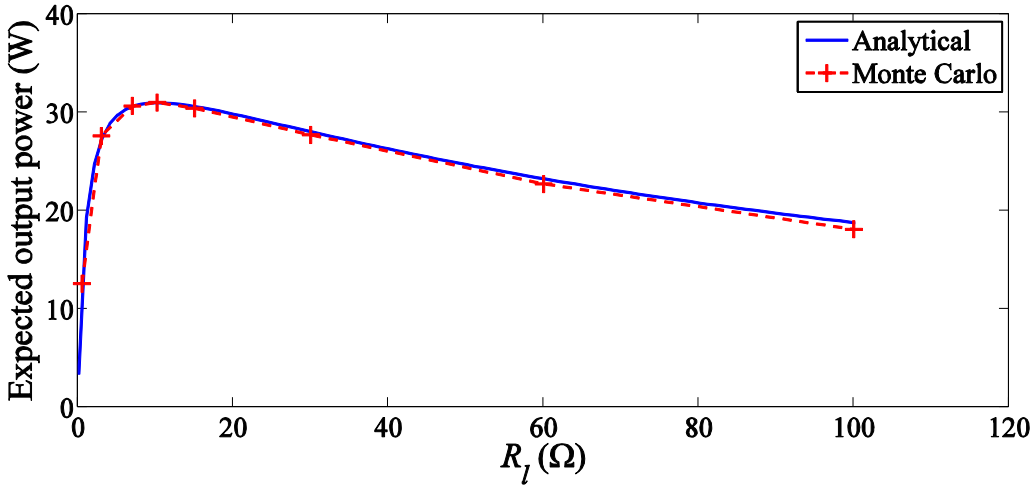

Figure 5-2 Comparison of the analytical expected power with the average harvested power in Monte-Carlo simulation for different resistances.

5.4 Harvesting energy from band-limited white noise excitation

The system is subjected to a band-limited white noise if $S_{Y_A}(\omega) = S_0, \omega_1 \le |\omega| \le \omega_2$, for which the corresponding power spectral density of the load current is

$$S_I(\omega)=\begin{Bmatrix}\dfrac{m^2\left(\dfrac{2\pi}{l}\right)^2 T_i^2\omega^2 S_0}{\left(k-M\omega^2\right)^2\left(R_l+R_i\right)^2+c^2\omega^2\left(R_l+R_i\right)^2} & \omega_1\le|\omega|\le\omega_2\\ 0 & \text{elsewhere}\end{Bmatrix}. \quad \textbf{(5.34)}$$

For this condition, the mean value of the output power is obtained from

$$E\left[P(t)\right]_{\omega_1\le|\omega|\le\omega_2}=\int_{-\omega_2}^{-\omega_1}+\int_{\omega_1}^{\omega_2}R_l S_I(\omega)\,d\omega=\int_{-\omega_2}^{-\omega_1}\frac{m^2\left(\dfrac{2\pi}{l}\right)^2 T_i^2\omega^2 R_l S_0}{\left(k-M\omega^2\right)^2\left(R_l+R_i\right)^2+c^2\omega^2\left(R_l+R_i\right)^2}d\omega$$
$$+\int_{\omega_1}^{\omega_2}\frac{m^2\left(\dfrac{2\pi}{l}\right)^2 T_i^2\omega^2 R_l S_0}{\left(k-M\omega^2\right)^2\left(R_l+R_i\right)^2+c^2\omega^2\left(R_l+R_i\right)^2}d\omega. \quad \textbf{(5.35)}$$

Equations (5.11) and (5.14) do not apply to the incomplete integrals presented in (5.35). However, these integrals can be solved by using a partial fraction expansion method that is presented in [89]. In this method, if $\Phi(\omega)$ is the spectral density of the response function of a stationary random process as

$$\Phi(\omega)=\begin{Bmatrix}\dfrac{\Phi_0}{\left(\omega_n^2-\omega^2\right)^2+4\xi^2\omega^2\omega_n^2} & \omega_1\le|\omega|\le\omega_2\\ 0 & \text{elsewhere}\end{Bmatrix}, \quad \textbf{(5.36)}$$

Then the result of the second spectral moment is

$$m_2=\int_{-\infty}^{+\infty}\omega^2\Phi(\omega)\,d\omega=\frac{\pi\Phi_0}{2\xi\omega_n}\left[\Delta\left(\frac{\omega_2}{\omega_n},\xi\right)-\Delta\left(\frac{\omega_1}{\omega_n},\xi\right)\right], \quad \textbf{(5.37)}$$

where

$$\Delta\left(\frac{\omega}{\omega_n},\xi\right)=\frac{1}{\pi}\arctan\frac{2\xi\left(\dfrac{\omega}{\omega_n}\right)}{1-\left(\dfrac{\omega}{\omega_n}\right)^2}-\frac{\xi}{2\pi\sqrt{1-\xi^2}}\ln\frac{1+\left(\dfrac{\omega}{\omega_n}\right)^2+2\left(\dfrac{\omega}{\omega_n}\right)\sqrt{1-\xi^2}}{1+\left(\dfrac{\omega}{\omega_n}\right)^2-2\left(\dfrac{\omega}{\omega_n}\right)\sqrt{1-\xi^2}}. \quad \textbf{(5.38)}$$

and $\omega_n=\sqrt{k/M}$. To calculate the definite integral of (5.35), (5.38) can be expressed as

$$\Delta\left(\frac{\omega}{\omega_n},\xi\right)=\frac{1}{\pi}\left[\frac{\pi}{2}-\operatorname{arcot}\frac{2\xi\left(\frac{\omega}{\omega_n}\right)}{1-\left(\frac{\omega}{\omega_n}\right)^2}-\frac{\xi}{2\pi\sqrt{1-\xi^2}}.\ln\frac{1+\left(\frac{\omega}{\omega_n}\right)^2+2\left(\frac{\omega}{\omega_n}\right)\sqrt{1-\xi^2}}{1+\left(\frac{\omega}{\omega_n}\right)^2-2\left(\frac{\omega}{\omega_n}\right)\sqrt{1-\xi^2}}.\right] \quad \textbf{(5.39)}$$

and hence, (5.35) can be written as

$$E\left[P(t)\right]_{\omega_1\le|\omega|\le\omega_2}=\frac{m^2\left(\frac{2\pi}{l}\right)^2K_{tr}^2R_lS_0}{M^2\left(R_l+R_i\right)^2}\left[\int_{-\omega_2}^{-\omega_1}+\int_{\omega_1}^{\omega_2}\frac{\omega^2}{\left(\omega_n^2-\omega^2\right)^2+4\xi\omega^2\omega_n^2}d\omega\right], \quad \textbf{(5.40)}$$

where ξ is the damping ratio, defined as

$$\xi=\frac{c}{2M\omega_n} \quad \textbf{(5.41)}$$

Comparing (5.40) to (5.37) shows that the mean value of the output power when the harvester is subjected to a band-limited stationary white noise is given by

$$E\left[P(t)\right]_{\omega_1\le|\omega|\le\omega_2}=\frac{m^2\left(\frac{2\pi}{l}\right)^2T_i^2R_l\pi S_0}{M\left(R_l+R_i\right)^2c}\left[\Delta\left(\frac{\omega_2}{\omega_n},\xi\right)-\Delta\left(\frac{\omega_1}{\omega_n},\xi\right)\right], \quad \textbf{(5.42)}$$

The first term in (5.42) is the mean value of the output power when the system is subjected to a broadband white noise. However, the term presented in the square bracket is the correction factor for a band-limited vibration. In other words, for broadband white noise, the term $\left[\Delta(\infty,\xi)-\Delta(0,\xi)\right]$ tends to unity. However, this term is less than unity when system is subjected to a band-limited vibration. Figure 5-3 shows the behaviour of $\Delta(\omega/\omega_n,\xi)$ for different value of ξ. It is seen that $\Delta(\omega/\omega_n,\xi)$ is a monotically increasing function of ω/ω_n with values between 0 and 1. This figure shows that for lightly damped systems most variations occur near its natural frequency. Increasing the damping ratio of the system, widens its bandwidth (defined as $2\omega_n\xi$) and reduces the sharpness of $\Delta(\omega/\omega_n,\xi)$ around its natural frequency.

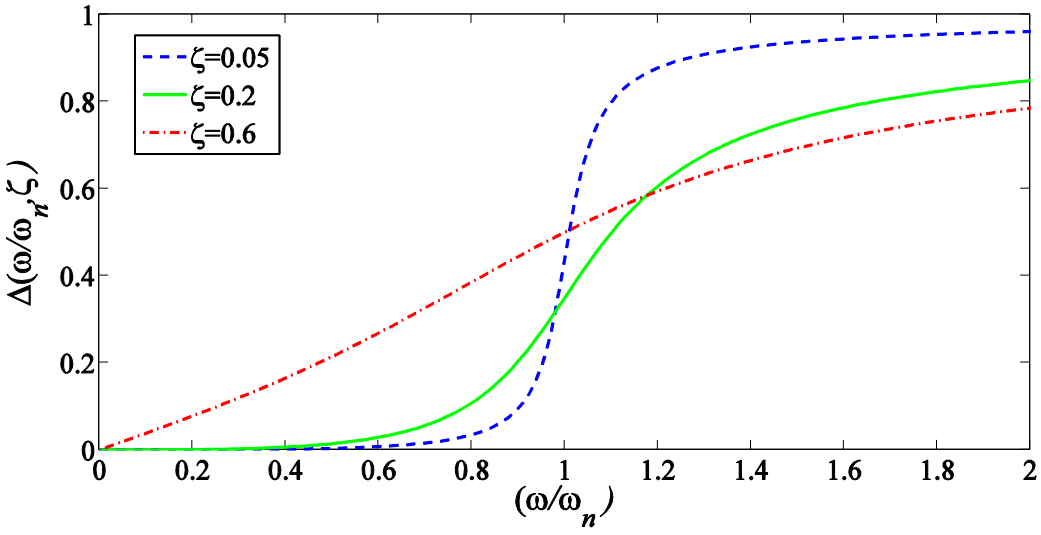

Figure 5-3 Variation of $\Delta(\omega/\omega_n,\xi)$ as a function of ω/ω_n for three different values of ξ

Figure 5-4 shows the values of the correction factor in (5.41) for the mean output power of the system under band-limited random excitation. The correction value is presented for the case of $\xi = 0.50$. This is the corresponding damping ratio of the system presented in table 5-1 for its optimum load resistance of $R_l = 10.2\Omega$. This graph illustrates that when the band-limited excitation is in the range of ω_1 to ω_2, including the resonant frequency of the system, the correction factor is slightly less than unity. However, when the natural frequency of system is outside the excitation band, i.e. when both (ω_1/ω_n) and (ω_2/ω_n) are either less than or greater than unity, the correction factor is very small which drastically reduces the mean value of the expected power. Therefore, from the design point of view, an obvious conclusion is made that in order to harvest maximum output power from band-limited random excitation, the natural frequency of the system should fall between ω_1 and ω_2.

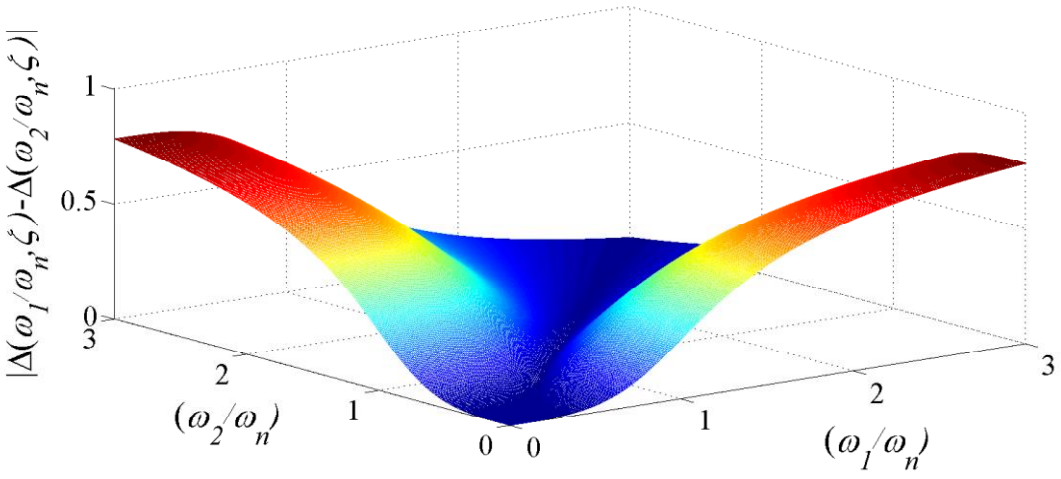

Figure 5-4 Correction factor for calculation of the expected output power of energy harvester under band-limited excitation for a device with $\xi = 0.50$.

The optimum value of ω_n can be obtained from numerical optimization of $\left[\Delta(\omega_2/\omega_n,\xi)-\Delta(\omega_1/\omega_n,\xi)\right]$ for a given ω_2, ω_1. Replacing ξ from (5.41) in (5.39) gives the correction factor as a function of ω_n. Considering the physical parameters of the harvester from table 5-1, and assuming a variable spring stiffness, the correction factor is a function of stiffness through ω_n. Figure 5-5 shows the variation of the correction factor for the case when $\omega_1 = 1$ rad/sec and $\omega_2 = 10$ rad/sec. It is seen that for this system the maximum value of the correction factor is 0.79, which is obtained when the natural frequency of the system is $\omega_n = 3.2$ rad/sec. From (5.41), the corresponding value of the optimum damping ratio for the system is $\xi = 0.49$. Hence, to harvest the maximum power under band-limited excitation conditions, the designer should ensure that the parameters of the system match its optimally obtained natural frequency. For instance, considering the physical parameters of the above simulated system from table 5-1 and the obtained optimum value of $\omega_n = 3.2$ rad/sec, the optimum spring stiffness that would maximize the power harvested from band-limited excitation is $k = 271.4$ N/m.

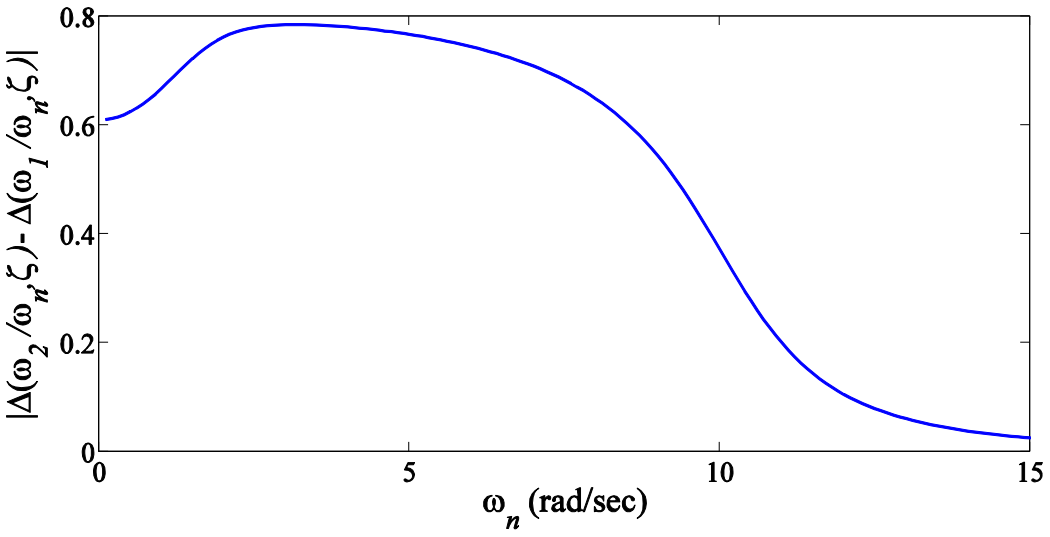

Figure 5-5 Correction factor for calculation of the expected output power of energy harvester presented in table 5-1 under band-limited excitation ($\omega_1 = 1$ rad/secand $\omega_2 = 10$ rad/sec) versus ω_n.

5.5 Harvested power in real environment

This section is dedicated to the estimation of the output power from the recorded random excitation applied to a boat in a real environment, as presented in figure 2-2. The derived expressions for the expected power in previous sections are helpful to quantify the harvested power under broadband and band-limited white noise excitations. However, the approach described in this section can be extended to find the mean value of the expected power when the power spectral density of the random excitation is not necessarily constant. For this purpose, the mathematical function corresponding to the power spectral density distribution of the random excitation should be investigated and then the expected output power can be estimated from (5.32). Note that, here $S_{Y_A}(\omega)$ is not constant and cannot be taken out of the integral term.

Comparing the recorded random excitation shown in figure 2-2 with various distributions [100] indicates that the presented spectral density is very close to a Cauchy distribution with the general form of [101, 102]

$$f(u;\alpha,\beta) = \frac{\alpha S_f}{\pi\left[\alpha^2 + (u-\beta)^2\right]} \qquad \textbf{(5.43)}$$

where α is the scale parameter, S_f is the height factor and β is the location parameter. Figure 5-6 shows Cauchy distribution for different values of α, S_f and β.

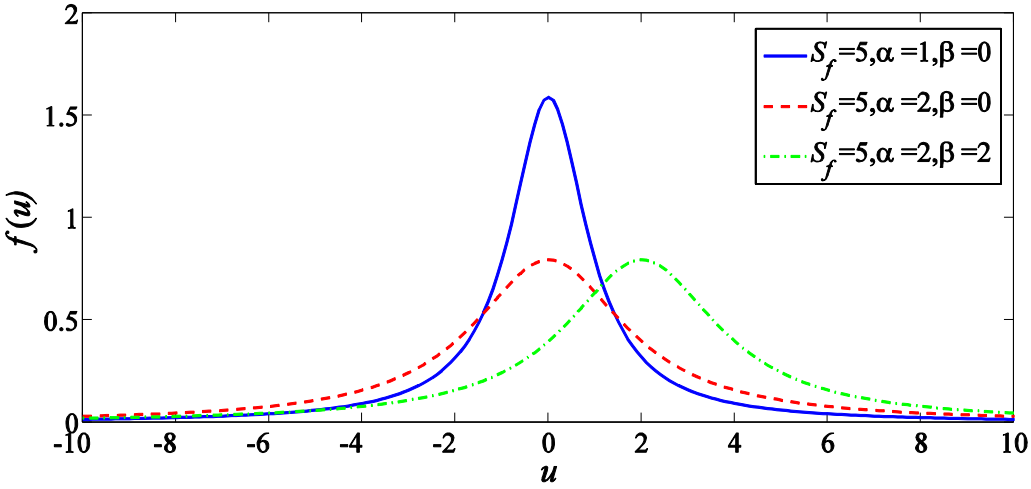

Figure 5-6 Cauchy distribution for different values of α, S_f and β.

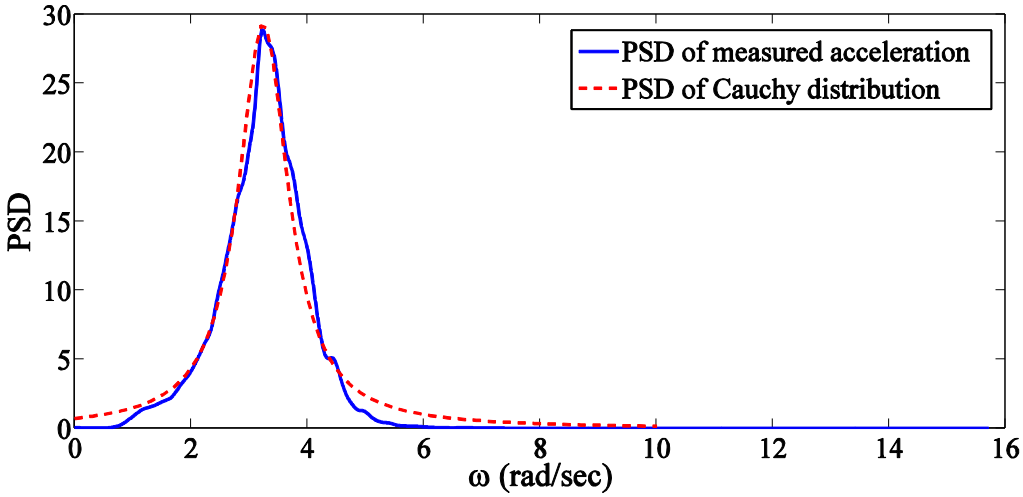

Figure 5-7 Fitting the Cauchy distribution on the measured vertical excitation of the boat

Figure 5-7 shows the PSD of the recorded acceleration from the boat motion and the mathematical estimation of the PSD plotted based on the Cauchy distribution when the parameters of distribution are $\alpha = 0.52$, $S_f = 48$ and $\beta = 3.2$. It is seen that there is good agreement between the spectral density of the recorded acceleration signal and the mathematical estimated distribution. Therefore, the spectral density of the recorded acceleration can be written as

$$S_{Y_A} = \frac{24.96}{\pi\left[0.27+\left(u-3.2\right)^2\right]}. \tag{5.44}$$

Replacing (5.44) in (5.22), the mean value of the harvested power is obtained from

$$E\left[P(t)\right] = \frac{m^2 R_l {K_{tr}}^2}{\left(R_i+R_l\right)^2}\left(\frac{2\pi}{l}\right)^2 \int_{-\infty}^{+\infty} \frac{\omega^2}{\left(k-M\omega^2\right)^2+\left(c\omega\right)^2}.\frac{24.96}{\pi\left[0.27+\left(\omega-3.2\right)^2\right]}d\omega, \tag{5.45}$$

and the expected output power can be obtained by numerical integration of (5.45) which can be shown to be 20.45 W.

5.6 Conclusion

This chapter has investigated the performance of the proposed energy harvester in this work under random vibration conditions. Specifically, analytical expressions have been derived for the non-dimensional mean harvested power due to stationary broadband and band-limited white noise excitations. In the case of harvesting energy from broadband random source, it is shown that the output power is proportional to the weight of the actual mass used in the device. However, the output power is inversely proportional to the moment of inertia of the system's rotating components. Therefore, a system with the lowest moment of inertia would be better when the harvester is subjected to a random excitation. In addition, it is shown that the output power expression is independent of the spring's stiffness. The optimum load resistance to harvest the maximum power from broadband white noise excitation was obtained and validated by Monte-Carlo simulation. The derived optimum load resistance is identical to when the constrained system is subjected to a sinusoidal excitation with a frequency equal to its natural frequency. Furthermore, the closed-form expression of the output power from band-limited random excitation showed that the output power is a function of the physical parameters of the system including the spring stiffness and moment of inertia. Therefore, from the derived power expression, the optimum natural frequency of the energy harvester that falls within the excitation band is obtained. Based on this optimum natural frequency and the corresponding mass and reflected moment of inertia,

the optimum spring stiffness of the energy harvester can be then obtained.

Also in this chapter, the profile of the spectral density of the measured acceleration signal of a typical boat is approximated by a Cauchy distribution. The distribution parameters of the spectral density of the acceleration signal are then estimated and subsequently used to calculate the expected power of the proposed energy harvester under real conditions.

Chapter 6: Adaptive tuning of the energy harvester for increasing its operational bandwidth

6.1 Introduction

Like other energy harvesters, the rotational energy harvester presented in previous chapters, was designed to generate maximum power when its resonant frequency matches the ambient vibration frequency. However, in applications where the ambient vibration frequency is spread over a wide range, an energy harvester with fixed resonance frequency would operate in sub-optimum conditions. This important matter limits the applicability of a harvester. Therefore, it is vital to design a tuning mechanism for varying the resonance frequency and hence increasing the operational bandwidth of the device. To this end, recent studies have focused on strategies for increasing the operating frequency range of vibration based energy harvesters, resulting in many publications including some review papers [103, 104].

In some studies, the resonance frequency of a single generator is tuned by continuously changing the mechanical characteristics of the harvester, namely its mass or stiffness. For instance, it is known that in a cantilever resonator, the resonance frequency is a function of the beam length and the centre of gravity of the proof mass. Wu et al. [105] present a piezoelectric cantilever energy harvester where the resonance frequency of the harvester is tuned by changing the position of a moveable proof mass. The centre of gravity of the movable proof mass is tuned by driving a screw. It is shown that by adjusting the centre of gravity of the proof mass over a range of 21 mm, the resonance frequency can be tuned between 130 Hz and 180 Hz. Gieras et al. [106] have patented an electromagnetic generator that comprises a cantilever and a set of magnets attached to its free end with its fix end being clamped to a base. In this device, a linear generator moves a slider back and forth to change the effective length of the cantilever and hence tune the resonance frequency of the generator. Eichhorn et al. [107] studied the feasibility of applying an axial load to change the stiffness and thus alter the resonance frequency of a Piezo-ceramic. The axial force is applied from a screwed spring to the free end of the cantilever beam and is proportional to the number of the

revolution of the screw. In a prototype of this device, resonance is adjustable over a range of 290-380 Hz by applying a compressive load. Applying a magnetic force is another method that is employed to alter the stiffness and thus the resonance frequency of an energy harvester. In a device, proposed by Chall et al. [108], two magnets are fixed to the free end of a cantilever beam. Two other moveable magnets are placed on top and bottom of the fixed magnets so that all magnets are vertically aligned. By varying the distance between the two sets of tuning magnets on top and bottom of the cantilever with the fixed magnets, the force applied to the cantilever and consequently the resonance frequency of the structure is changed. In this device, a maximum tuning distance of 3 cm provides tuneability over the frequency range of 22-32 Hz. Another approach to alter the resonance frequency is based on the fact that the stiffness of a piezoelectric material is a function of the attached capacitive load. The point to note in this method is that the piezoelectric transducer is employed to alter the resonance frequency while the energy generation technique could be based on electromagnetic, electrostatic or piezoelectric conversion. Wy et al. [109] utilised this method to tune the resonant frequency of an energy harvester composed of a piezoelectric bimorph cantilever. In this generator, the lower piezoelectric layer is used for energy harvesting, whereas the upper layer is employed for frequency tuning.

Besides changing the resonance frequency, widening the operational bandwidth is another strategy to improve the performance of energy harvesters in practical environments. Exploiting nonlinear springs [110], coupled oscillators [111], structures with multiple vibration modes [112] and bistable structures [113, 114] are some of the methods employed to widen the bandwidth of harvesters.

Another approach to shift the resonance frequency of an energy harvester is to change its electrical load. It is known that when a resistive load is connected to the transducer terminals, it imposes electrical damping to the system. Tuning the electrical load at its optimum value can increase the output power of the harvester. This method was first demonstrated by Cammarano et al. [73] who used discrete load resistance and reactive components to improve the output power of a linear electromagnetic energy harvester. This method was used by some other researchers to optimize the performance of harvesters when exposed to a frequency varying excitation source [86].

In this chapter, we present a new method to broaden the operation bandwidth of the proposed ball screw based harvester. In this study, the moment of inertia of the system as a mechanical parameter is tuned so that to increase the output power of the system when the device is subjected to a frequency-varying excitation. In addition, this chapter studies the effect of optimum control of the load resistance as an electrical parameter on the output power of an energy harvester. Finally, the chapter studies the combined tuning of moment of inertia and load resistance for increasing the output power under frequency-varying conditions. The studies are conducted for both constrained and unconstrained cases.

6.2 System modelling

Figure 6-1 shows the drawing of the proposed device in Chapter 4 where a rotational rod carrying two moving masses is perpendicularly attached to the coupling shaft between the generator and the ball screw.

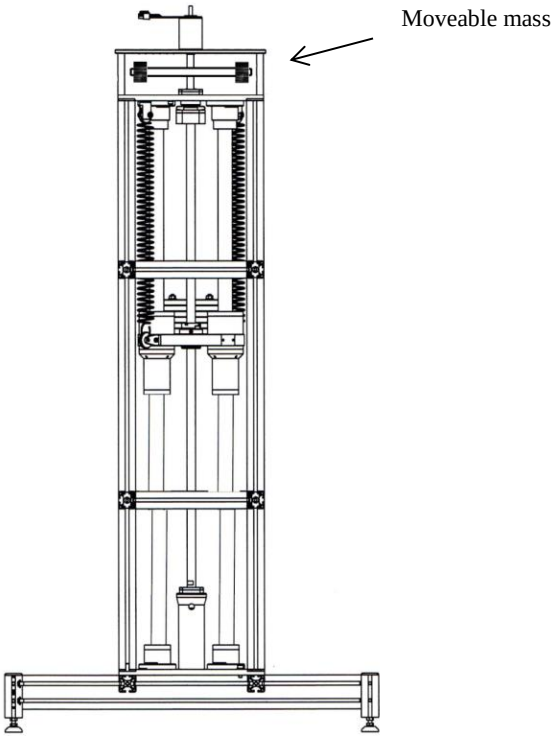

Figure 6-1 CAD drawing of the energy harvesting device an energy harvesting system consisting of a sprung mass coupled to a generator through a ball screw.

The free body diagram of the proposed harvester is shown in figure 6-2 where l, m, c_{bg} and k, respectively, represent the ball screw lead, the oscillating mass, mechanical damping and the overall spring stiffness.

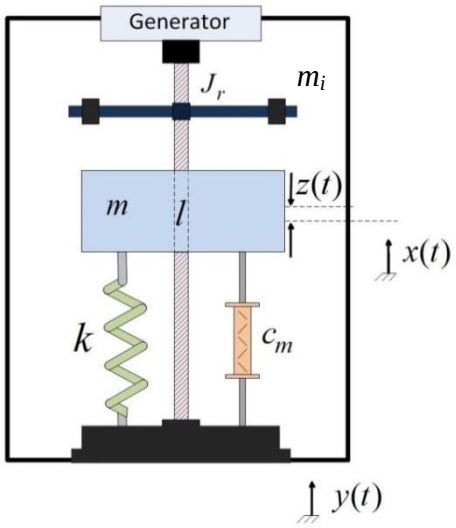

Figure 6-2 Free body diagram of the energy harvester shown in figure 6-1.

From (3.25), it can be shown that the relative displacement of mass Z is given by

$$Z = \frac{mY\omega^2}{\sqrt{\left(k - \left(m + J_t\left(\frac{2\pi}{l}\right)^2\right)\omega^2\right)^2 + \left(\left(c_{bg} + \frac{T_i^2}{R_l + R_i}\right)\left(\frac{2\pi}{l}\right)^2\omega\right)^2}}, \qquad \textbf{(6.1)}$$

where J_t refers to the total moment of inertia of the rotational components which is obtained from

$$J_t = J_{mi} + J_g + J_r + J_{bc}, \qquad \textbf{(6.2)}$$

where J_g and J_{bc} are, respectively, the moments of inertia of the generator and the total moment of inertia of the coupling shafts plus the ball screw. Also, J_r is the moment of inertia of the rotational rod and is given by

$$J_r = \frac{m_r L^2}{12}. \qquad \textbf{(6.3)}$$

Here, m_r and L are the mass and length of the rotational rod. Also, if m_i is the moveable rotational mass and r is the distance between the centre of moveable mass to the centre of the rod, i.e. rotation axis, the moment of inertia due to the rotation of the moveable mass J_{mi}, is defined as

$$J_{mi} = 2m_i r^2. \tag{6.4}$$

The natural frequency of energy harvester is given by

$$\omega_n = \sqrt{\frac{k}{m + J_t\left(\frac{2\pi}{l}\right)^2}}. \tag{6.5}$$

In addition, the maximum value of the relative displacement occurs when $\partial Z / \partial \omega = 0$ which gives the resonance frequency of

$$\omega_r = \frac{2k}{\sqrt{4k\left(m + J_t\left(\frac{2\pi}{l}\right)^2\right) - 2\left(\left(c_{bg} + \frac{T_i^2}{R_l + R_i}\right)\left(\frac{2\pi}{l}\right)^2\right)^2}}. \tag{6.6}$$

The maximum relative displacement is then given by

$$Z_{resonance} = \frac{2mk^2 Y}{\sqrt{4k^3\left(\left(c_{bg} + \frac{T_i^2}{R_l + R_i}\right)\left(\frac{2\pi}{l}\right)^2\right)^2\left(m + J_t\left(\frac{2\pi}{l}\right)^2\right) - k^2\left(\left(c_{bg} + \frac{T_i^2}{R_l + R_i}\right)\left(\frac{2\pi}{l}\right)^2\right)^4}}. \tag{6.7}$$

Also form (3.27) the amount of output power is given by

$$P_{l-out} = \frac{1}{2} I^2 R_l = \frac{1}{2} P_{l-out} = \ldots$$
$$\frac{R_l}{2\left(R_l + R_i\right)^2} T_i^2 \left(\frac{2\pi}{l}\right)^2 \frac{\left(mY\omega^3\right)^2}{\left(k - \left(m + J_t\left(\frac{2\pi}{l}\right)^2\right)\omega^2\right)^2 + \left(\left(c_{bg} + \frac{T_i^2}{R_l + R_i}\right)\left(\frac{2\pi}{l}\right)^2 \omega\right)^2}. \tag{6.8}$$

It was mentioned in the introduction that there are various methods for expanding the operational bandwidth of an energy harvesting system and thereby increasing its output power. From (6.8) it can be deduced that the output power of the system shown in figure 6-1, is a function of its load R_l and total moment of inertia J_t. This chapter investigates the optimal control of these two parameters when the excitation frequency

is variable with the aim of maximising the output power of the system. The study is carried out on two different states of the system. In the first case, which is called the unconstrained mode, the base displacement amplitude is low (Y=0.2 m) and hence, in the entire range of the frequency variations, the relative displacement amplitude of the oscillating mass is less than the maximum allowable displacement. In the second state, which is called the constrained mode, the oscillation amplitude is large (Y=1 m) and as a result, in addition to maximising the output power, the control system should be able to control the relative displacement of the mass within its allowable range.

6.3 Tuneable moment of inertia

In this section, the effect of optimal variation of the moment of inertia in order to increase the operational bandwidth and consequently the output power is investigated. The system parameters are shown in table 6-1. From (6.3), the moment of inertia of the rod supporting the moveable masses is 14.08×10^{-5} kg.m^2. Therefore, the sum of the moment inertia of the ball screw, coupling shaft, generator and rod is 18.48×10^{-5} kg.m^2. As figure 6-1 shows, the two moveable masses are placed along the same axis. From (6.4), the moment of inertia of these masses is dependent on their weights and their distances from the axis of rotation. When they move towards the centre, the resulting moment of inertia is reduced and the opposite occurs when they move out. In this study, it is assumed that the two masses move in a symmetrical fashion and hence their distances from the axis of rotation are always the same. The distance between the centre of masses and the axis of rotation varies between a minimum of 0.005 m up to a maximum of 0.125 m. Thus, the minimum and maximum moment of inertia values resulting from these distances are 5.00×10^{-5} kg.m^2 and 3125.00×10^{-5} kg.m^2, respectively.

Table 6-1System's parameters.

Parameter	Value	Parameter	Value
c_{bg}	180E-5$\left(\text{N.m.s.rad}^{-2}\right)$	L	0.26(m)
k	750$\left(\text{N.m}^{-1}\right)$	m	15.00(kg)
T_i	1.25E-1$\left(\text{N.m.A}^{-1}\right)$	m_i	1.00(kg)
J_{bc}	3.80E-5$\left(\text{kg.m}^2\right)$	m_r	0.025(kg)
J_g	0.60E-5$\left(\text{kg.m}^2\right)$	R_i	0.32(Ω)
l	0.04(m)		

6.3.1 Unconstrained system

In this section the effect of changing the moment of inertia of an unconstrained system is studied. The comparison is conducted between a harvester with the capability of changing the moment of inertia and a static system with constant moment of inertia. In both systems the load resistance is 1.70 Ω which has been obtained from the equation for the optimum load resistance derived in (3.32), and the spring stiffness is 750 N/m. The moment of inertia of the static system is 325E-5 kg.m^2 which is obtained from (6.5) corresponding to the natural frequency of the device which is equal to ω_n=2.8 rad/sec. This value of moment of inertia ensures that for the case where the amplitude of base displacement is 1m, the relative mass displacement does not exceed an allowable value which in our case is $Z_0 = 0.2\,\text{m}$. The resonance frequency is obtained from (6.6) which is ω_r=3.6 rad/sec. However, the moment of inertia of the tuneble system can be varied from 23.48E-5 kg.m^2 to 3143.48E-5 kg.m^2.

Figure 6-3 shows the relative displacement of the oscillating mass for different frequencies of vibration. It is seen that at frequencies lower and higher than 2.8 rad/sec, the displacement of the harvester mass with variable moment of inertia is larger than that of the static device. This is due to the flexibility of the moment of inertia of the tuneable harvester. In this system, the position of moveable masses is adjusted so that the natural frequency of the device matches the frequency of excitation. However, for the static device, the frequency matching occurs only at ω=2.8 rad/sec. Figure 6-4,

shows the output power of both systems. As it is seen, the harvester with moving masses produces more power for a wide range of frequencies in comparison with the static device. For instance, at frequencies of 1 rad/sec and 6 rad/sec, the tuneable energy harvester produces 0.015 W and 17.45 W, respectively; whereas the static system at the same respective frequencies does not generate more than 0.002 W and 3.68 W.

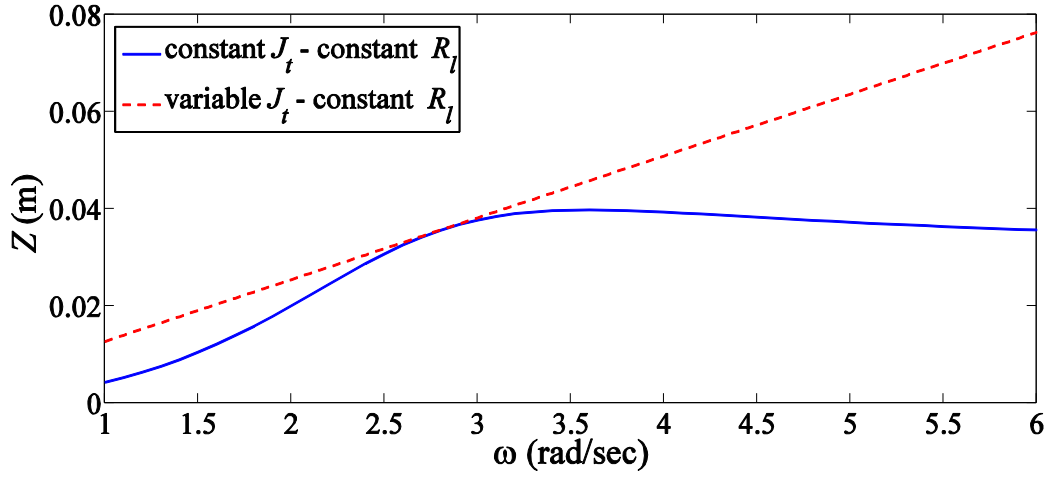

Figure 6-3 Relative displacement of mass in the static system and the system with tuneable moment of inertia for different frequencies, in the unconstrained mode.

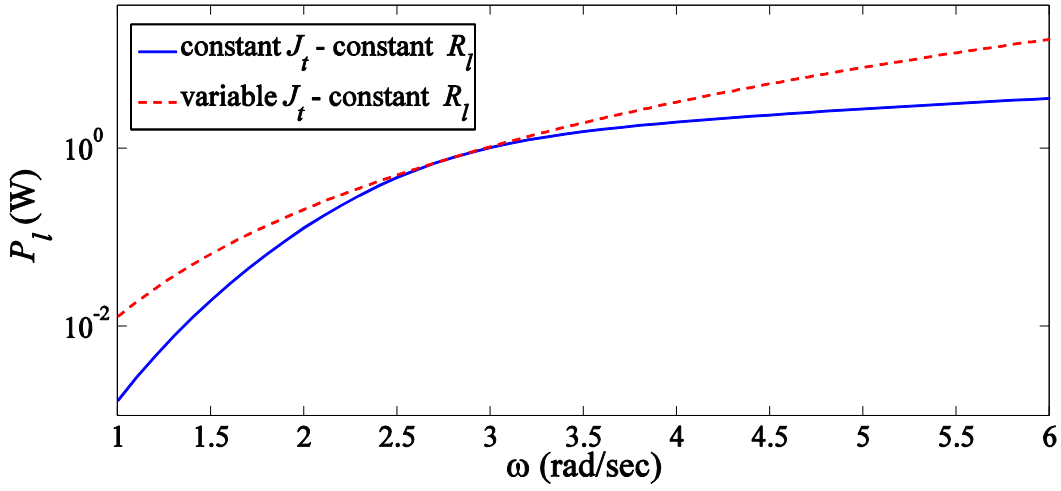

Figure 6-4 Output powers of the static system and the system with tuneable moment of inertia for different frequencies, in the unconstrained mode.

Figure 6-5, shows the total moment of inertia and the position of the moveable masses of the tuneable harvester versus the frequency of excitation. It is seen that at lower frequencies the harvester should have a large moment of inertia. The reason for

this decision can be understood from the equation of power, derived in (6.8). In fact the controller tries to minimize the term $k-\left(m+J_t\left(2\pi/l\right)^2\right)\omega^2$, presented in the denominator of (6.8). This is in agreement with the general design criterion (see Chapter 3) that the energy harvester should be designed so that its natural frequency matches the excitation frequency. When the frequency of excitation ω is small, J_t should increase to make the term $\left(m+J_t\left(2\pi/l\right)^2\right)\omega^2$ equal to the spring stiffness k. Conversely, by increasing ω, J_t should be reduced to maximize the output power. Note that there is a constraint for applying this method. As it was mentioned earlier, there is a maximum and minimum limit for varying the moment of inertia of the system. It means that if the energy harvester is excited at the frequencies above or below the defined range, then the moment of inertia of the device cannot be increased or reduced to match its natural frequency to the excitation frequency. Therefore, the length of the rod and the moveable masses should be selected carefully to provide the appropriate flexibility for the tuning system to cover the expected frequency range.

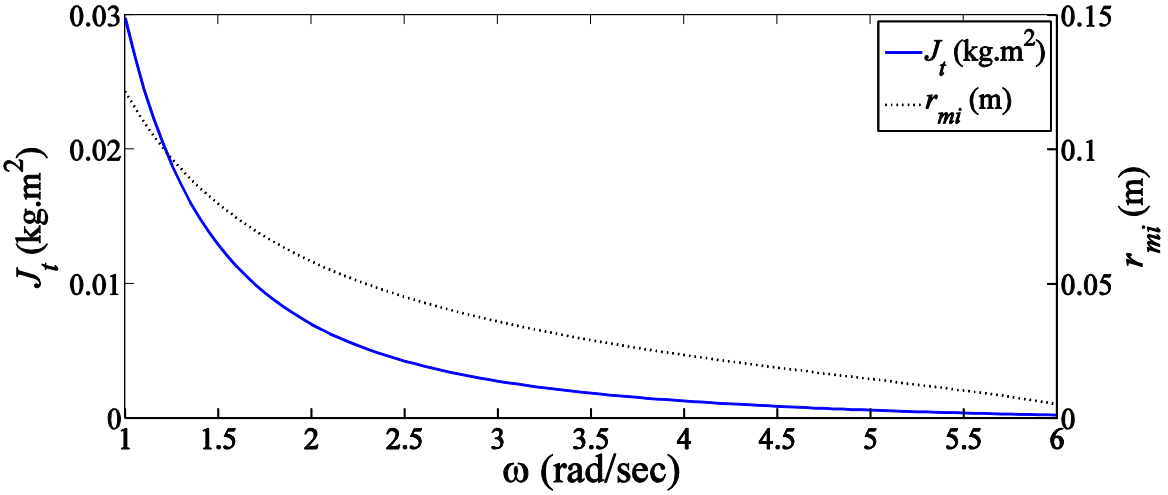

Figure 6-5 Optimal total moment of inertia and the position of variable masses of the tuneable harvester, in the unconstrained mode.

6.3.2 Constrained system

In this section, it is assumed that the amplitude of base displacement Y is 1 m. However, there is a constraint on the maximum allowable relative displacement of the mass which is $Z_0 = 0.2\,\text{m}$. As it was mentioned earlier, in the static system the moment

of inertia is designed so that for all frequencies, the maximum displacement does not exceed Z_0. However, for the system with adjustable moment of inertia, the optimum moment of inertia of the device is obtained by solving the following system of equations

$$\begin{cases} \max\left(P_{l-out}\left(J_t\right)\right) \\ subject\ to: Z_0 - Z\left(J_t\right) \geq 0. \end{cases} \quad \textbf{(6.9)}$$

Figure 6-6 shows the displacement of the oscillating mass in both static and adjustable harvesters when the frequency of excitation varies. It is seen that at low frequencies the adjustable system has a larger displacement. Also, when the excitation frequency is greater than the resonance frequency of the static system, i.e. $\omega_r = 3.61\text{rad/sec}$, the amplitude of the relative displacement of the mass in the static system declines. However, in the other harvester, the moment of inertia of the device is tuned in order to keep the mass displacement at its maximum allowable amount.

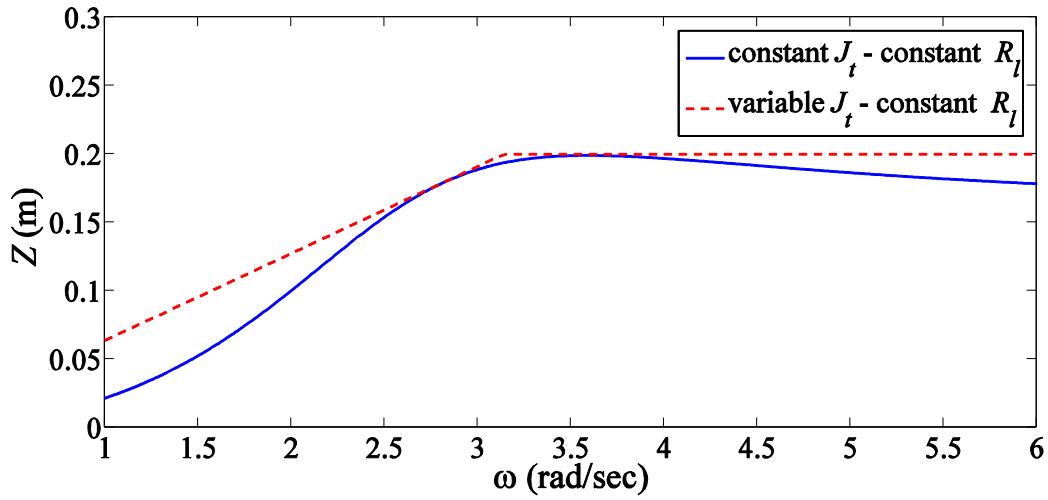

Figure 6-6 Relative mass displacements in static and tuneable harvesters versus frequency, in the constrained mode.

Figure 6-7 compares the output powers of both static and adjustable harvesters. It is seen that by controlling the optimal moment of inertia subject to the condition in (6.9), the output power of the device in both low and high frequencies is improved. This also shows that the output power of the static system at frequencies of 1 rad/sec and 6 rad/sec, respectively, is 0.04 W and 92.15 W, whereas, the adjustable harvester can produce 0.33 W and 116.75 W output power at the same frequencies. Figure 6-8 shows the optimal moment of inertia of the harvester and the position of the moveable masses

for different frequencies. It is seen that similar to the unconstrained case and as expected, at low frequencies the moment of inertia of the system must be very large. It implies that the moveable masses are at the far ends of the rod. By increasing the frequency of oscillation, the moment of inertia should be decreased which means that the two masses should be moved toward the centre of the rod. This trend is continued until the relative mass displacement is 0.2 m which occurs when the frequency of excitation is $\omega = 3.12\,\text{rad/sec}$. After this point and for a short range of excitation frequencies, i.e. up to $\omega = 3.50\,\text{rad/sec}$, the moment of inertia of the device should increase in order to keep the relative displacement of the mass constant. However, by increasing the frequency of excitation, if the controller does not reduce the moment of inertia of the harvester, the relative displacement of the mass will decline. Therefore, to keep the mass displacement at its maximum allowable distance, the moment of inertia of the device should gradually decrease.

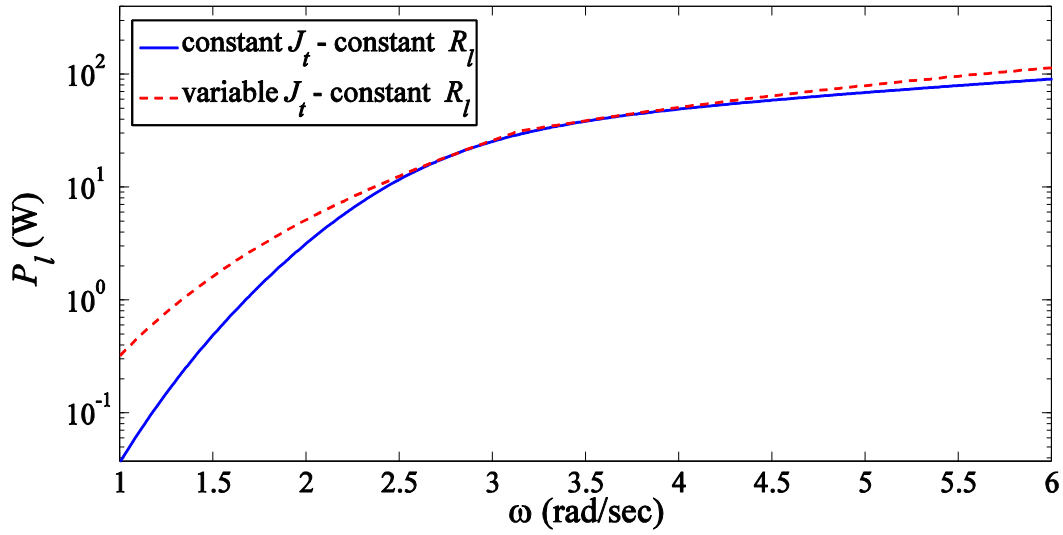

Figure 6-7 Output powers of the static and the adjustable systems for different frequencies, in the constrained mode.

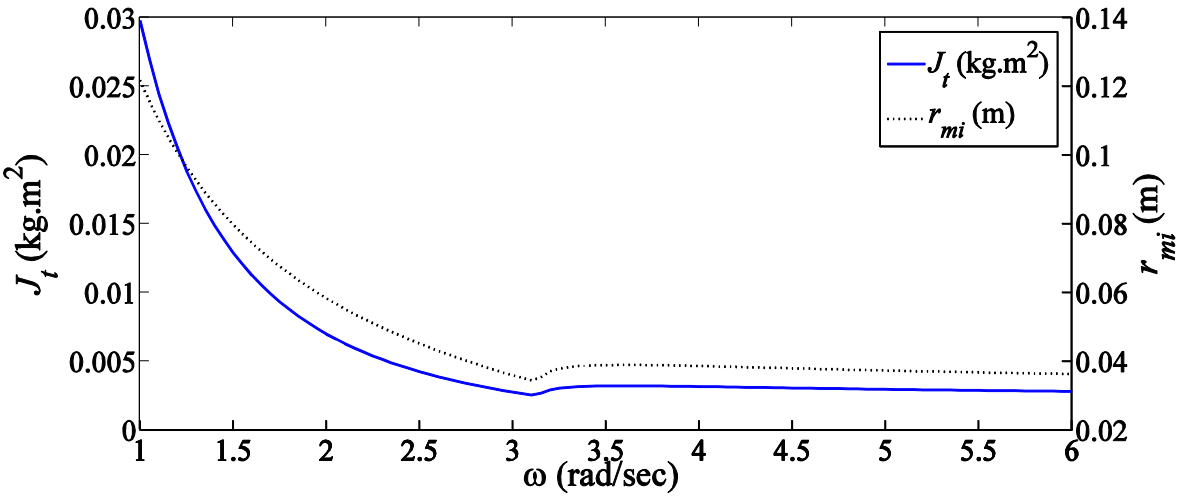

Figure 6-8 Optimal total moment of inertia and the position of variable masses of the tuneable harvester, in the constrained mode.

6.4 Variable electrical damping

In this section it is assumed that the moment of inertia of the harvester is constant but the load resistance is variable. Similar to the previous section, the comparison is conducted for both unconstrained and constrained modes.

6.4.1 Unconstrained system

The first comparison is made for the unconstrained mode. The moment of inertia of both systems is J_t=325E-5 kg.m^2. Figure 6-9 shows the relative displacement of the mass in both static and variable resistance systems for different frequencies. In the variable resistance system, the optimum load resistance is obtained from $\partial P_{l-out} / \partial R_l = 0,$ which results in

$$R_{l,\text{opt}} = \sqrt{R_i^2 + \frac{\left(\left(\frac{2\pi}{l}\right)^2 \omega K_t\right)^2 \left(2R_i c_m + K_t^2\right)}{\left(k - \left(m + J\left(\frac{2\pi}{l}\right)^2\right)\omega^2\right)^2 + \left(\left(\frac{2\pi}{l}\right)^2 c_m \omega\right)^2}} \qquad \textbf{(6.10)}$$

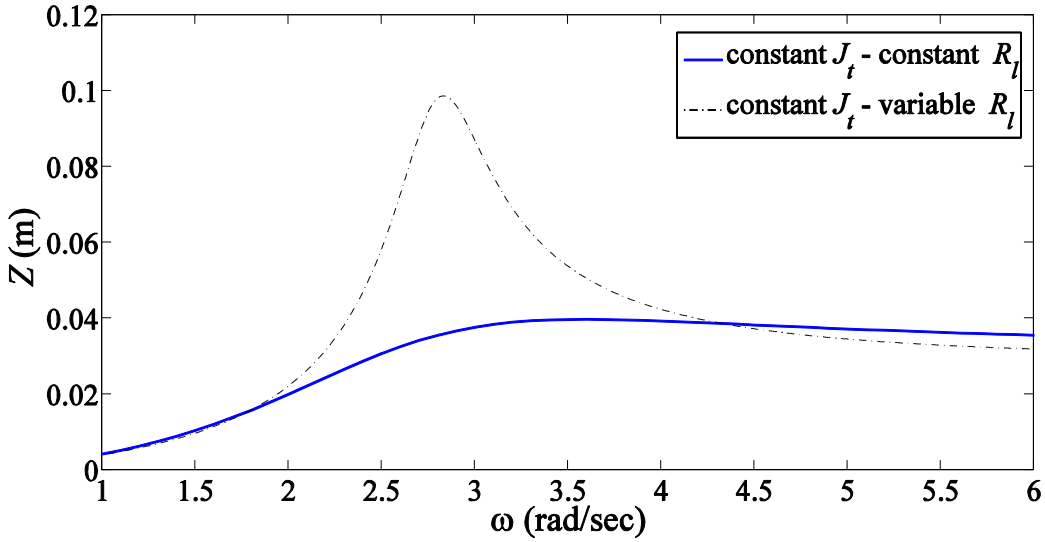

Figure 6-9 Relative mass displacement for static and tuneable resistance harvesters versus the frequency of vibration, in the unconstrained mode.

Figure 6-10 shows the output power of the static and variable load resistance systems in the unconstrained mode. As it is seen, by changing the load resistance at frequencies around the natural frequency of the device, the output power is increased significantly. For instance at 2.8 rad/sec, the harvester with variable resistance produces 1.55 W whereas, the static system produces only 0.79 W. However, in the case of simulations also indicate the superiority of the harvester with tuneable resistance over the static system is not very significant at other frequencies. For instance, at 6 rad/sec, the system with tuneable resistance produces 4.15 W, while the static system generates 3.68W. However, by increasing the excitation frequency, the advantage of having a variable resistance will be more apparent. Figure 6-11 shows the optimum load resistance obtained from (6.10) for different frequencies. The profile of the optimal load resistance indicates that the maximum load resistance is selected when the excitation frequency matches the natural frequency of the device that, for the simulated system here, is 9 Ω. This result is in agreement with the optimum load resistance of the unconstrained systems obtained in [72].

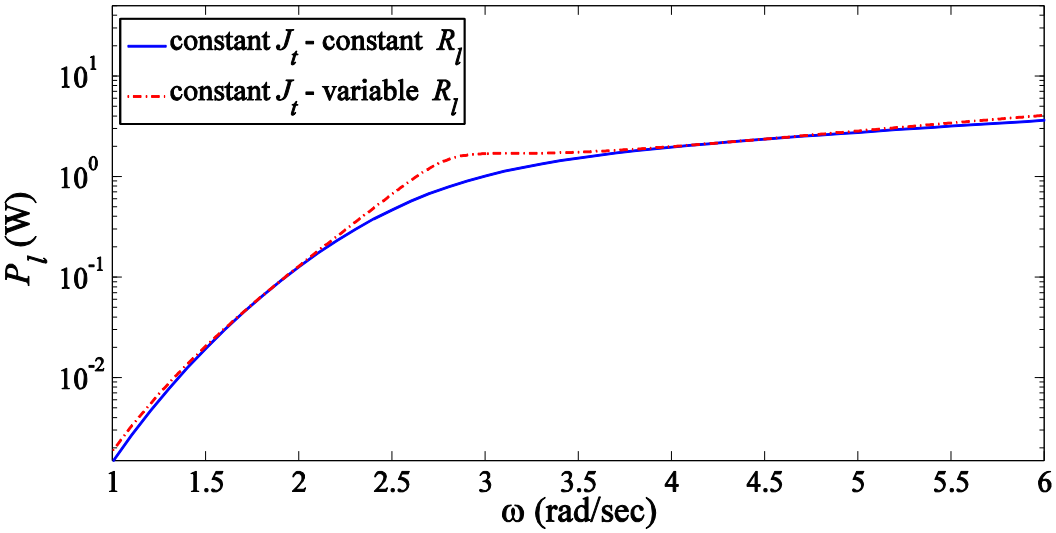

Figure 6-10 Output powers of the static and tuneable resistance harvesters versus the frequency of vibration, in the unconstrained mode.

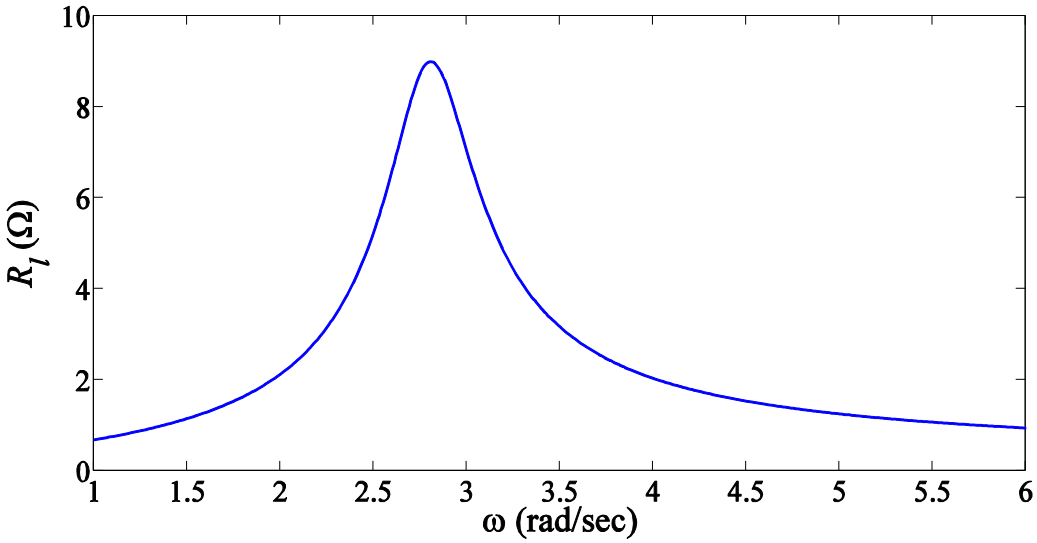

Figure 6-11 The optimal load resistance of the harvester with tuneable resistance for different frequencies, in the unconstrained mode.

6.4.2 Constrained system

In this section, the amplitude of base displacement is 1 m. For the system with the variable resistance, the optimum load resistance device is obtained by solving the following system of equations

$$\begin{cases} \max\left(P_{l-out}\left(R_l\right)\right) \\ subject\ to: Z_0 - Z\left(R_l\right) \geq 0. \end{cases} \tag{6.11}$$

Figure 6-12 shows the relative displacement of a static system and a harvester with variable load resistance in the constrained mode. The output powers of both systems are shown in figure 6-13. It is seen that the harvester with variable load resistance can produce more power and by increasing the excitation frequency, the superiority of the variable resistance harvester becomes even more significant. Figure 6-14 shows the change of load resistance for various excitation frequencies in this mode.

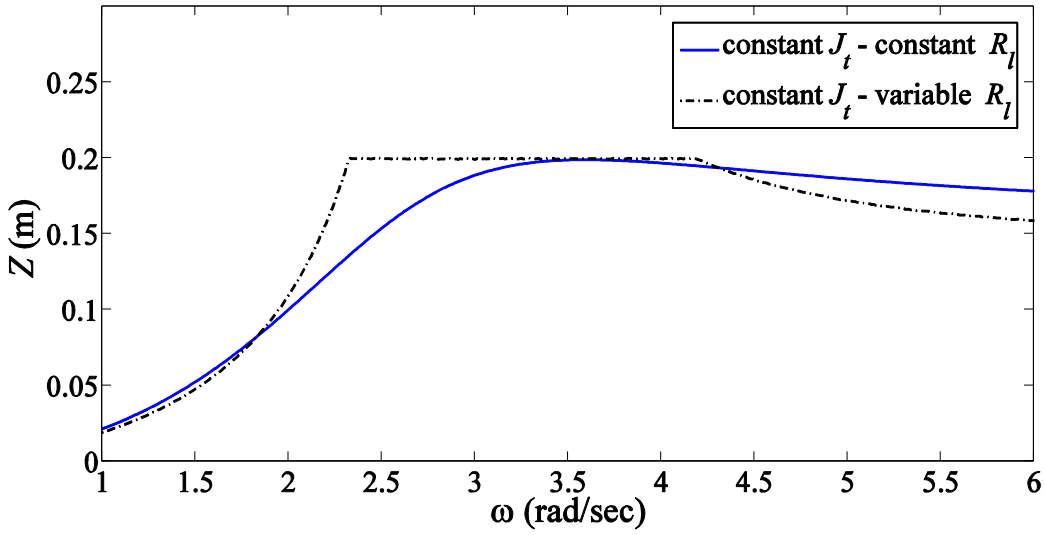

Figure 6-12 Relative mass displacement for static and tuneable resistance harvesters versus the frequency of vibration, in the constrained mode.

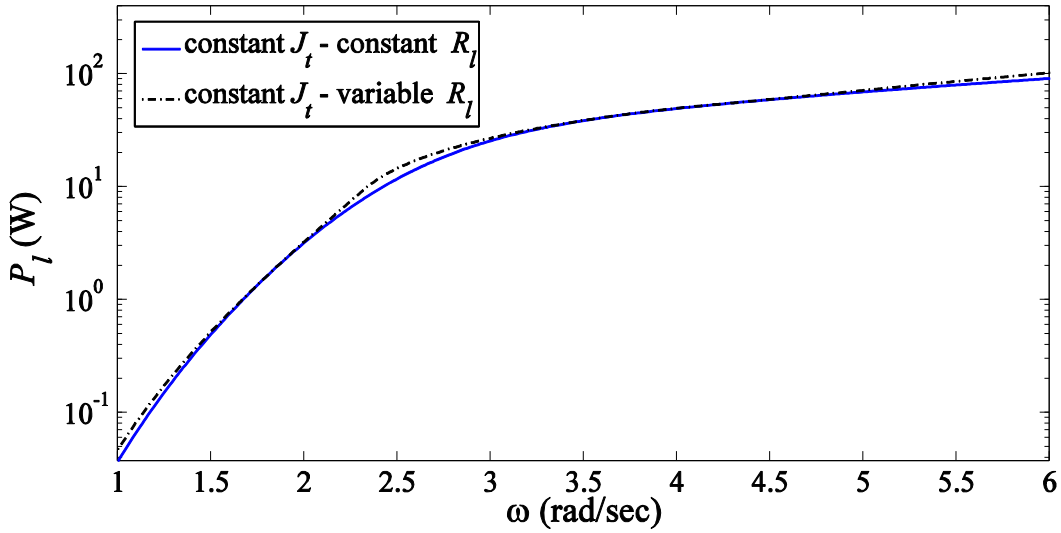

Figure 6-13 Output powers of static and tuneable resistance harvesters versus the frequency of vibration, in the constrained mode.

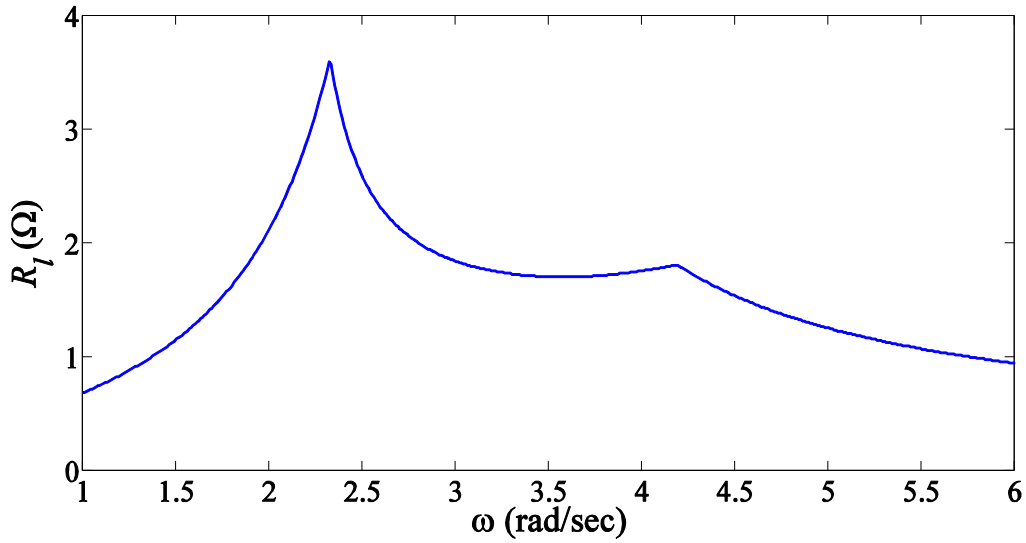

Figure 6-14 The optimal load resistance of the harvester with tuneable resistance for different frequencies, in the constrained mode.

6.5 Tuneable moment of inertia and load resistance

In this section, it is assumed that both moment of inertia and load resistance of the system are tuneable and hence, the energy harvester uses both to harvest the maximum power from a given excitation source.

6.5.1 Unconstrained system

In the unconstrained mode, the moment of inertia is varied so that the natural frequency of the energy harvester matches the excitation frequency. To have such a favourable condition the total moment of inertia of the system as a function of excitation frequency is changed based on the follow equation

$$J_{t,opt} = \left(\frac{k}{\omega^2} - m \right) \left(\frac{l}{2\pi} \right)^2 \tag{6.12}$$

Therefore, the load resistance can be obtained from (6.10) for the condition that $\omega = \omega_n$, which results in

$$R_{l,opt} = R_i + \frac{T_i^2}{c_{bg}}. \tag{6.13}$$

Figure 6-15 shows a comparison between the relative mass displacement of the static system and the harvester with tuneable moment of inertia and load resistance, in the unconstrained mode. The comparison of the output power between these two systems is shown in figure 6-16. It is seen that the amount of output power produced by the tuneable system at the frequency of 1 rad/sec is 0.025 W and at 6 rad/sec it is 31.85 W, that are significantly greater than the produced power by the static device at the same frequencies.

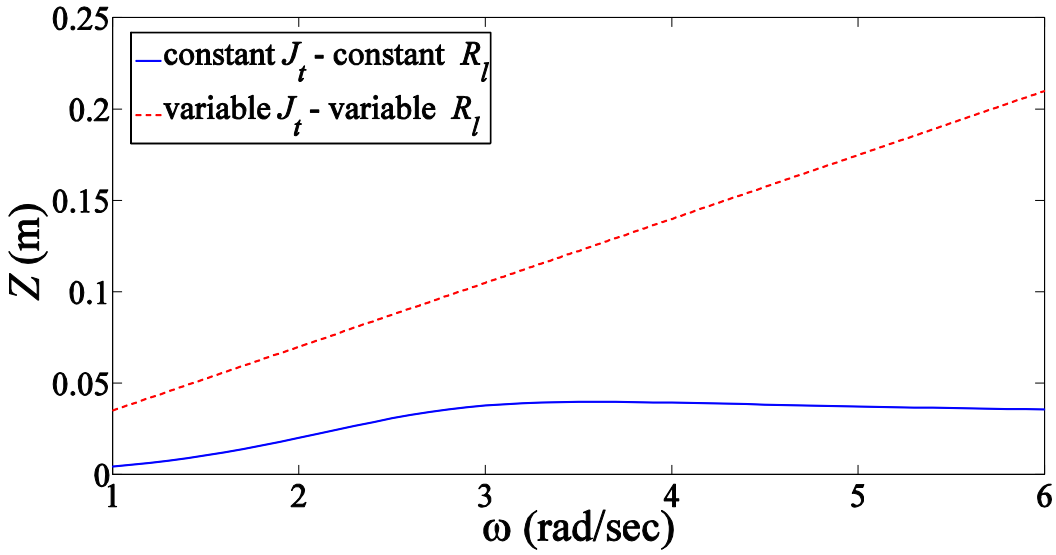

Figure 6-15 Relative mass displacement for static harvester and the device with variable moment of inertia and tuneable load resistance versus the frequency of vibration, in the unconstrained mode.

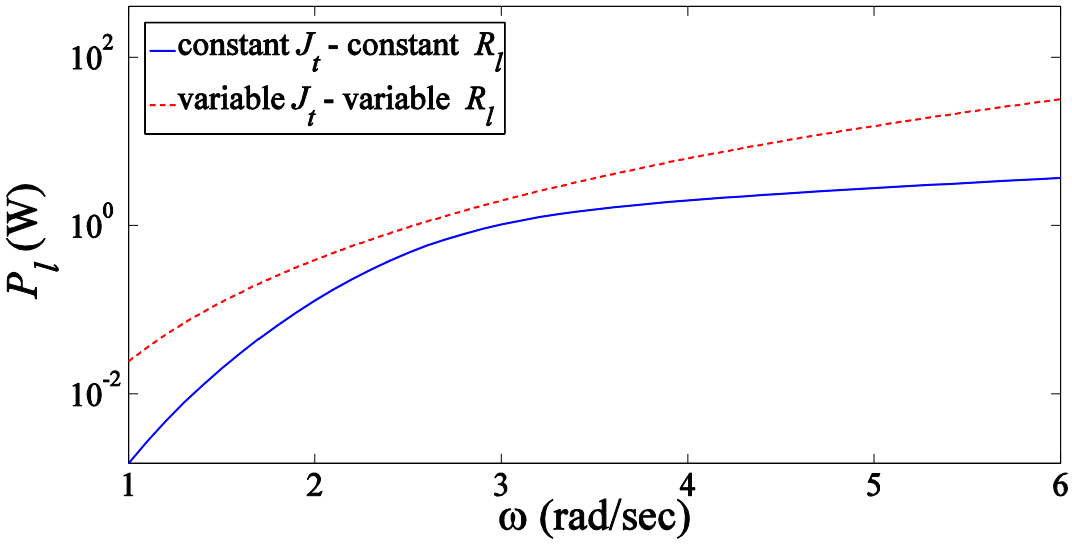

Figure 6-16 Output powers of the static harvester and the device with variable moment of inertia and tuneable load resistance versus the frequency of vibration, in the unconstrained mode.

For the case of simulated power, the moment of inertia of the system and the position of variable masses are similar to those presented in figure 6-5. The load resistance for all frequencies is calculated from (6.13) which is equal to 9 Ω.

6.5.2 Constrained system

In this section the amplitude of base displacement is again assumed to be 1 m. For the system with variable moment of inertia and variable load resistance, the optimum values are obtained by solving the following system of equations

$$\begin{cases} \max\left(P_{l-out}\left(J_t, R_l\right)\right) \\ subject\ to: Z_0 - Z\left(J_t, R_l\right) \geq 0. \end{cases} \tag{6.14}$$

The relative mass displacement is shown in figure 6.17. It is seen that, although for frequencies between 1.0 and 1.1 rad/sec, the relative mass displacement is less than 0.2 m, for all frequencies above 1.1 rad/sec, the load resistance and moment of inertia of the device can be tuned so that the mass oscillates at its maximum allowable amplitude of 0.2 m.

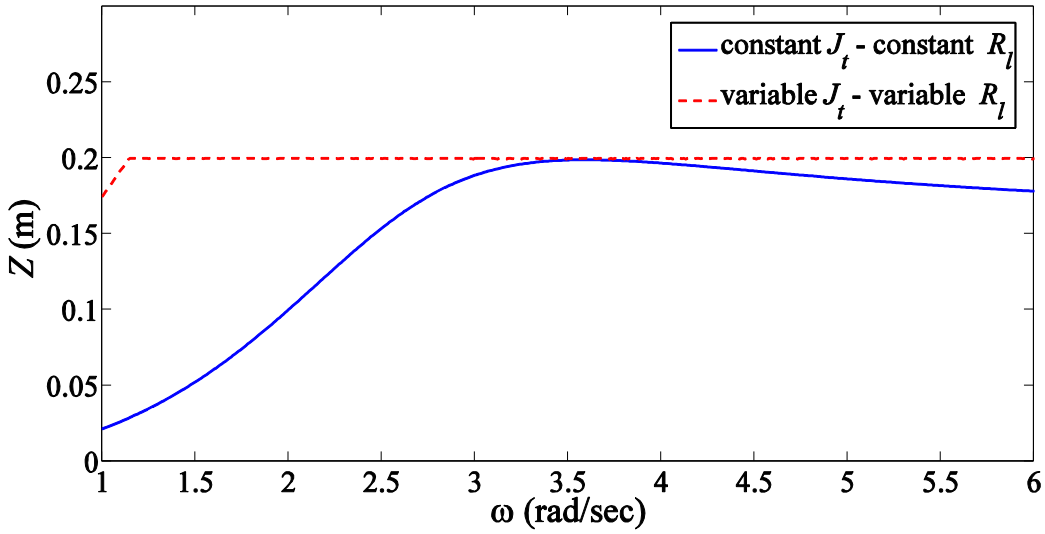

Figure 6-17 Relative mass displacement for static harvester and the device with variable moment of inertia and tuneable load resistance versus the frequency of vibration, in the constrained mode.

The output power in this mode is shown in figure 6-18. It is seen that the tuneable system can produce more power at all excitation frequencies. Furthermore, the output power of the tuneable harvester at frequencies of 1 rad/sec and 6 rad/sec, respectively, are 0.61 W and 193.5 W, which are significantly higher than the power produced by the static system.

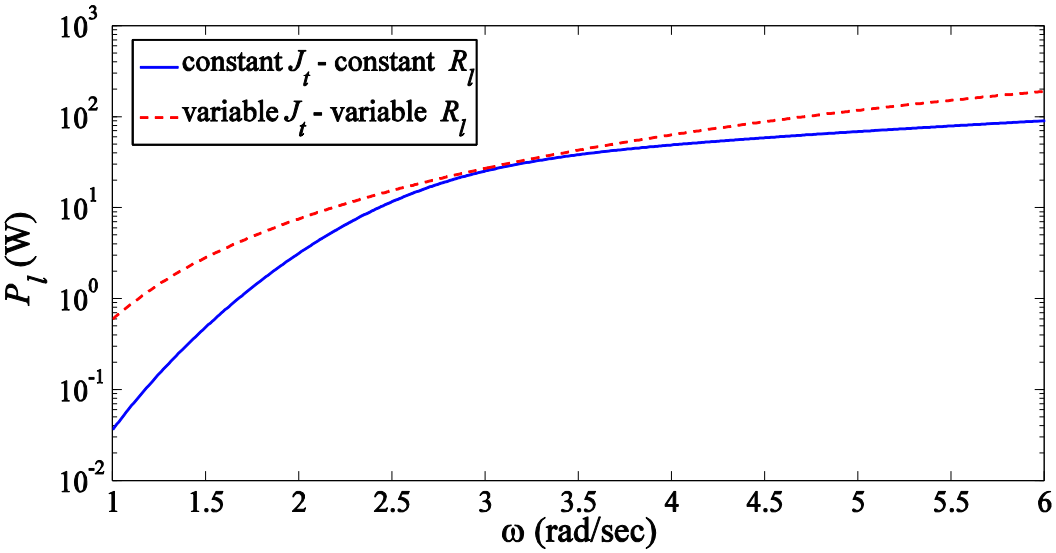

Figure 6-18 Output powers of the static harvester and the device with variable moment of inertia and tuneable load resistance versus the frequency of vibration, in the unconstrained mode.

Figures 6-19 and 6-20 respectively show the optimal values of the load resistance and the moment of inertia of the device, obtained from (6.14). On these figures, the position of the moveable masses as a function of excitation frequency is also illustrated.

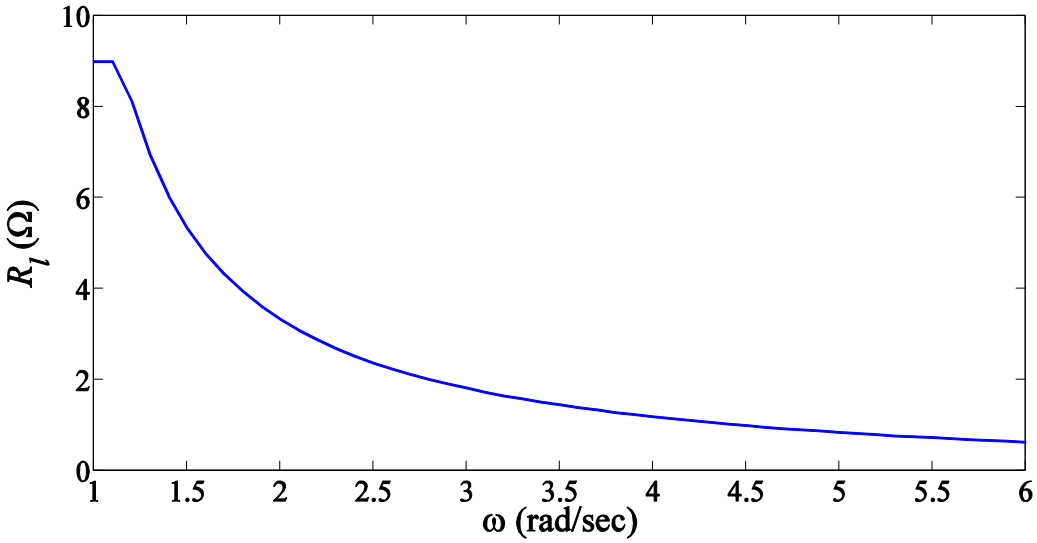

Figure 6-19 The optimal load resistance of the harvester with variable load resistance and adjustable moment of inertia for different frequencies, in the constrained mode.

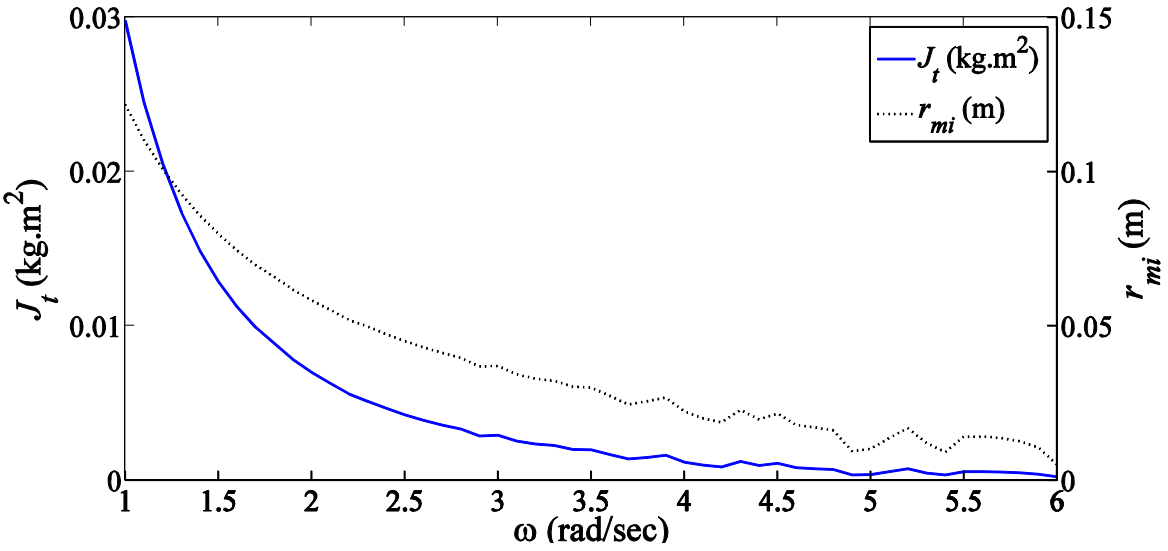

Figure 6-20 Optimal moment of inertia and the position of moveable masses for the system with variable load resistance and adjustable moment of inertia, in the constrained mode.

6.6 Discussion and Conclusion

There are a number of published approaches for increasing the output power of energy harvesters under frequency-varying conditions. Some approaches utilise the mechanical parameters of the harvester to adjust the resonant frequency of the device or to widen the bandwidth of the generator. In some earlier works, it has been shown that by tuning the electrical damping of the system the operational bandwidth of device can be increased. In this chapter, unlike other researchers that have changed the spring stiffness or mass to tune the resonance frequency, a variable moment of inertia approach to adjust the resonance frequency of the device is employed. Also, the effect of tuning the load resistance to increase the output power of harvester at different frequencies is investigated. In addition, the performance of the system when a combination of both methods, i.e. tuning moment of inertia and load resistance, is studied. The study is conducted for both constrained and unconstrained mode. In figures 6-21 and 6-22, the output powers obtained from the energy harvester with four different configurations are compared, for the unconstrained and constrained modes, respectively. It is seen that in both modes, the system with variable load resistance shows a good performance at frequencies around the natural frequency of the device. However, for frequencies away from the resonance frequencies the system with variable moment of inertia produces

more power. Also, this comparison reveals that the tuneable harvester produces significantly increased amount of harvested power.

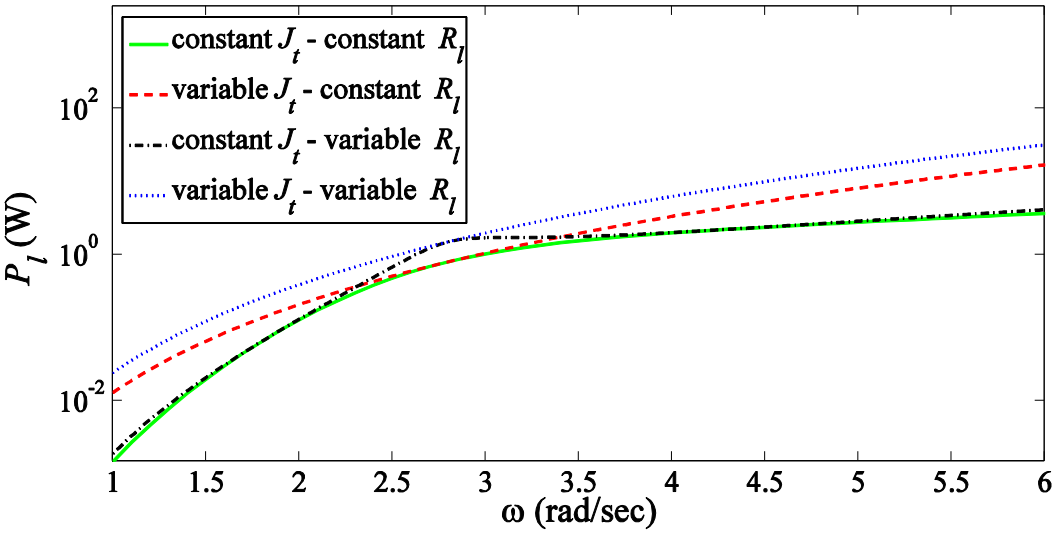

Figure 6-21 Comparison between the output power of four harvesters in unconstrained mode.

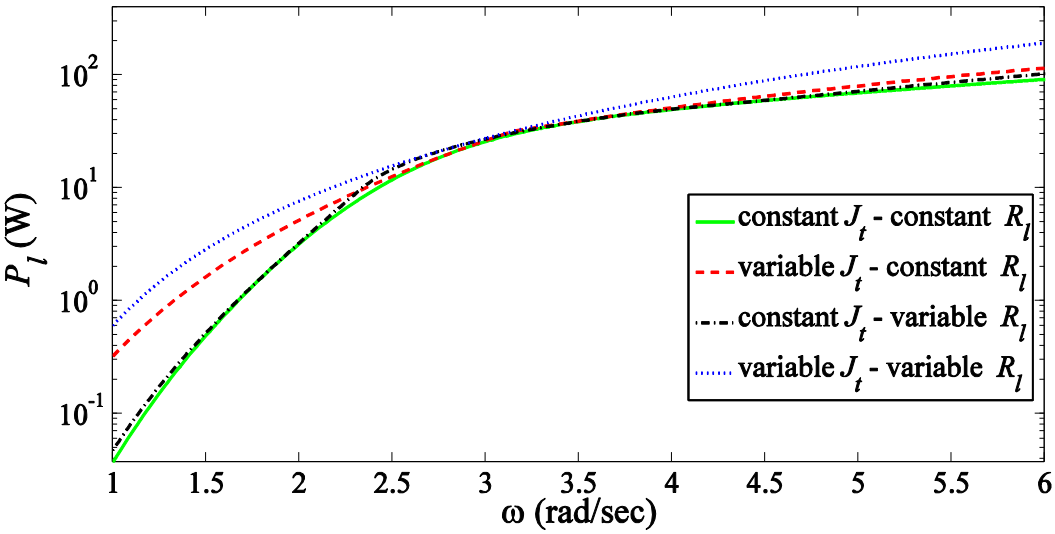

Figure 6-22 Comparison between the output power of four harvesters in the constrained mode.

In summary, it was shown here that varying the moment of inertia of the energy harvester is a promising approach for broadening its operational band-width in both constrained and unconstrained modes. It was also demonstrated that, for the presented ball screw based energy harvester, changing the load resistance to control the electrical

damping is a useful method to increase the output power of the system over a wider frequency range. Furthermore, it was shown that the combination of tuning the moment of inertia of the device and adjusting the resistance load can significantly increase the amount of harvested power. The approach described in this chapter is a first step in the direction of having an autonomous energy harvester with a wide operational bandwidth. One of the advantages of the presented method in this chapter is that, unlike some other methods [115], changing the adjustable parameters, i.e. moment of inertia and load resistance, can be conducted intermittently. In other words, this approach only consumes power during tuning operation and does not use energy once the harvester is optimally tuned. Note that, in a real environment, the frequency of vibration is mainly related to the weather condition and the boat speed and these parameters (and consequently the excitation frequency) do not often change quickly.

This research can be continued by implementing a practical variable moment of inertia mechanism. For instance one can employ two step motors as moveable masses. In this case, the amount of power needed to move the actuators and the resolution and frequency of applying the tuning operation should be determined. Also, to increase system efficiency, the energy harvester should be design so that the amount of power that is used by the controller and the moveable masses is much less than the power produced by the harvester. Designing the controller and variable load resistance circuit are outside the scope of this project and can be considered as future work.

Chapter 7: Experiments

7.1 Introduction

To validate the idea of energy harvester, a prototype of the device has been manufactured. Schematic drawing of the device is shown in Appendix B. In this section, the results of the preliminary tests on the harvester are presented. The main purpose of the initial tests is to observe the performance of the device under harmonic excitation and obtain its frequency response. In addition, experiments are conducted to characterize the friction forces and mechanical damping associated with the system. Last but not least, through the experiment, the effect of varying the load resistance on the output power is observed. The parameters of the manufactured energy harvester are shown in table 7.1.

Table 7. 1 Manufactured system parameters

Parameter	Value	Parameter	Value
m	8 kg	J_g	0.54E-5 kg.m^2
l	20 mm	R_l	0.5 Ω
k	250 N/m	K_t	23.2 mNm/A
J_b	3.66E-5 kg.m^2	R_i	0.1 Ω
J_c	0.7E-5 kg.m^2	ball screw length	0.94 m

7.2 Experimental setup

Figure 7-1 shows the schematic of the experimental setup used to test the manufactured energy harvester. In this setup the harvester is mounted on a horizontal electro-hydraulic vibrator and the generator terminals are connected to a three variable resistors with a star configuration. Two MEMS accelerometers manufactured by Silicon-Design with the sensitivity of 800 mv/g and the dynamic range of ±5g were attached to the oscillating mass and the shaker. A voltmeter sensor is used to measure the voltage across the generator terminals, i.e., the load resistance. The movement of shaker is controlled by a PC through an

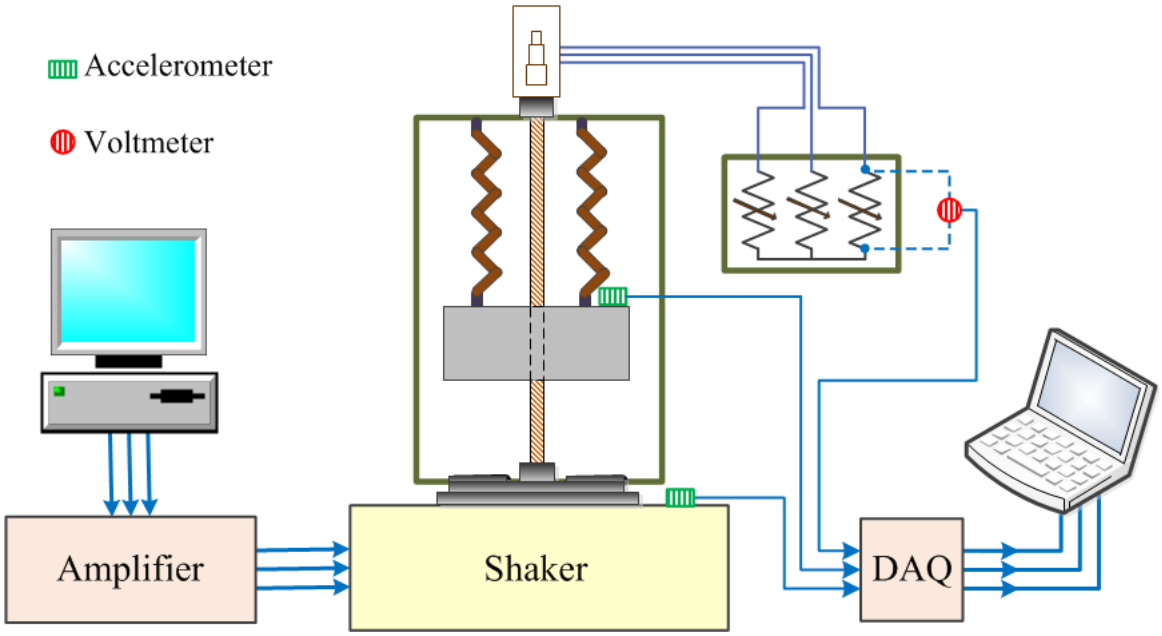

Figure 7-1 Schematic of the experimental setup

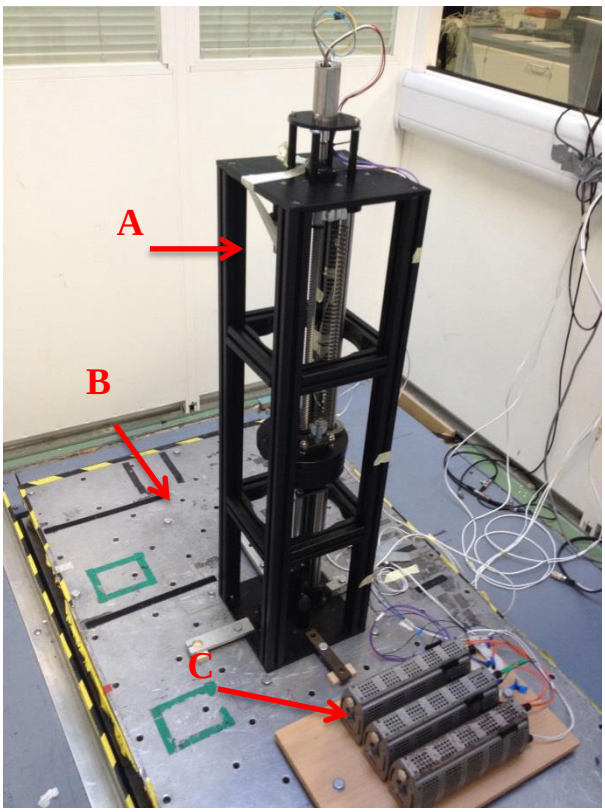

Figure 7-2 Actual implementation of energy harvester. A) Energy harvester, B) Shaker, C) Variable resistors.

amplifier model FE-376-IPF from Flyde-Signal Ltd **[116]**. The voltage output signal and the accelerations of mass and shaker are captured by a data acquisition (Daq) system from National Instrument **[117]** with a sampling rate of 256 Hz. Figure 7-2 shows the actual implementation of the test rig, including the energy harvester, shaker and variable resistors. Figure 7-3 shows the accelerometer attachment to the shaker. The acceleration of shaker is recorded by the channel 1 of the Daq system.

Figure 7-3 Accelerometer attached to the shaker

Figure 7-4 shows the attached accelerometer to the oscillating mass. The acceleration of mass is captured by the channel 2 of the Daq system. As the accelerometer is attached upside down beneath the mass, to obtain the relative acceleration of the oscillating mass to that of base, the measured acceleration signal measured by channel 2 was added to the measured acceleration by channel 1 of the Daq system. The variable resistors (rheostat), fuses and voltage sensor are shown in figure 7-5. The variable resistor consists of a coil of wire with terminals at one end and a sliding contact that moves along the coil to change the effective resistance. The resistance of the rheostats used in the experiment could be varied from 0.5 Ω to 11Ω. Also, three protective fuses were installed between the generator and load to provide an overcurrent protection of the generator.

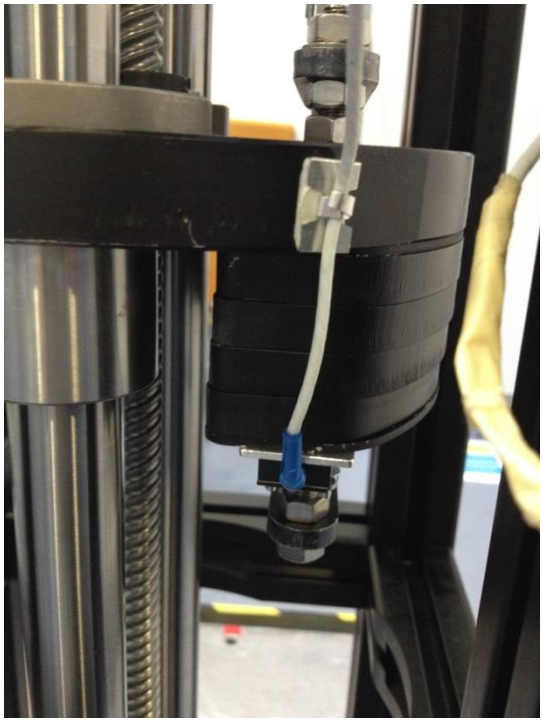

Figure 7-4 Accelerometer attached to the underneath of the oscillating mass

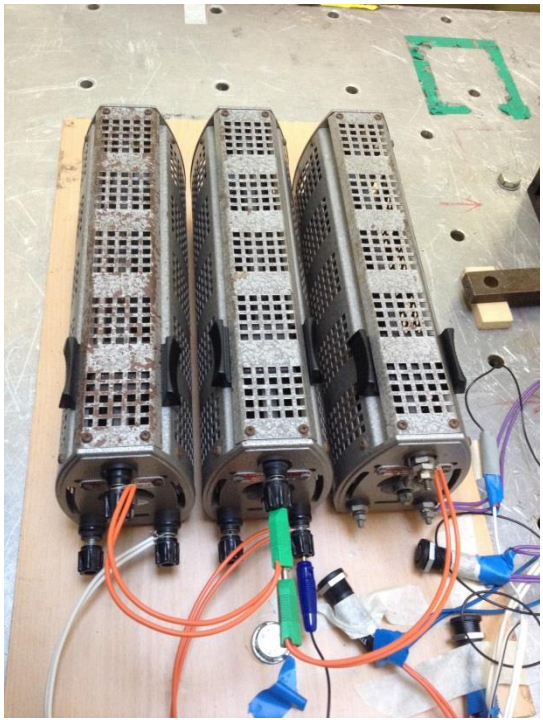

Figure 7-5 Variable resistors, protective fuses and voltage sensor

7.3 Experimental results

Despite the constraints of the shaker that does not allow us to test the energy harvester in its full stroke mode, preliminary tests are conducted to characterize the system and validate the dynamic model of the system. After constructing the test rig, it was realized that the amount of friction due to the ball screw and linear shafts is tangible. To address the presence of coulomb friction f_d, the equation of motion of the system, given by (3.16), is modified as

$$\left(m + J\left(\frac{2\pi}{l}\right)^2\right)\ddot{z}(t) + c\dot{z}(t) + f_d \operatorname{sgn}\left(\dot{z}(t)\right) + kz(t) = -m\ddot{y}(t), \tag{7.1}$$

Therefore, the experiment begun by evaluating the coulomb friction.

7.3.1.1 Coulomb's friction

To evaluate the coulomb friction of the energy harvester, the equilibrium positions of the mass in two modes were marked. In the first mode, the mass was pushed down until the springs were extended up to nearly their maximum allowable limit. Considering f_d as the coulomb friction and x_1 as the extension of springs in this mode, for equilibrium position, we have

$$mg + f_d = kx_1. \tag{7.3}$$

In the second mode, the mass is pushed up and then released. The new equilibrium position is different than that of the first mode. Considering x_2 as the extension of spring in this mode, the new equilibrium position can be written as

$$mg = kx_2 + f_d. \tag{7.4}$$

The distance between the equilibrium positions in these two modes is 6.3 cm. By subtracting (7.4) from (7.3), we have $k\left(x_2 - x_1\right) = 2f_d$, and considering $k = 250\,\text{N/m}$, f_d is 8.37 N.

7.3.2 Mechanical damping and frequency response

To obtain the frequency response of the system, the ratio of the relative displacement over the base displacement for a range of frequencies is obtained. The amplitude of acceleration in this test for all frequencies is 5 m sec^{-2}. The experiment is conducted for both open circuit condition and with the load resistances of $R_l = 0.5\ \Omega$ connected to the generator terminals with star configuration. The experimental and numerical frequency responses of the system for both these conditions are shown in figure 7-6. The numerical frequency responses are obtained by solving (7.1) using Matlab. For the open circuit condition, due to the absence of electrical damping, the coefficient *c*, presented by (7.1) is representative of the total mechanical damping of the system c_{bg}. The frequency response of the system in open circuit mode is plotted in figure 7-6 for $c_{bg} = 0.0016$ Nm $rad^{-1}s^{-1}$ which is in reasonable agreement with the experimental result. Also, figure 7-6 shows the experimental frequency response of the system for when $R_l = 0.5\ \Omega$. In this mode, the electrical damping of the system, based on the parameters shown in table 7.1 for a three phase brushless DC generator, is $3T_i^2\left(R_i + R_l\right)^{-1} = 0.0027$ Nm $rad^{-1}s^{-1}$. The theoretical frequency response of the system in this mode is shown in figure 7-6. Although there is a reasonable agreement between the theoretical and experimental results, it is seen that the theoretical frequency response is more damped that can be due to the uncertainty of the load's resistors.

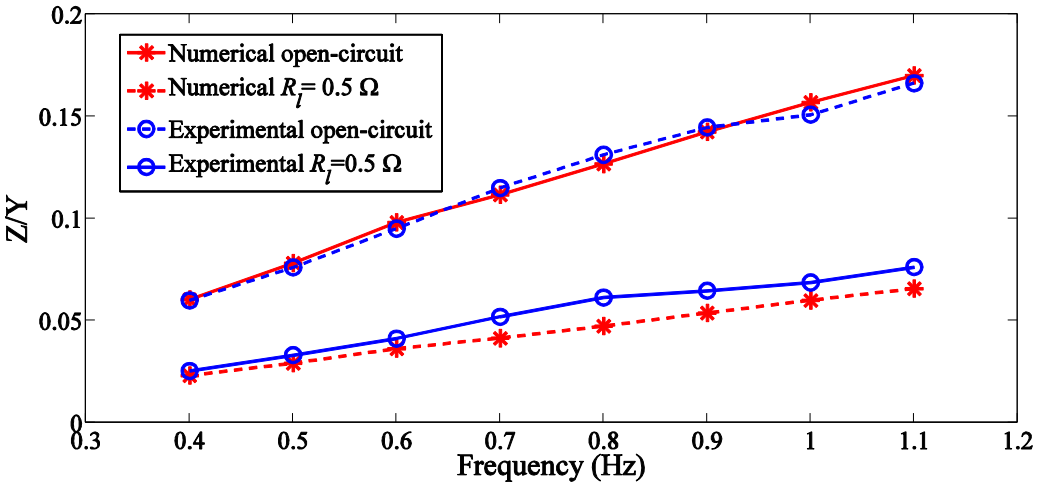

Figure 7-6 Analytical and experimental frequency response of energy harvester

The maximum electrical damping of the system occurs when the terminals of the generator are short circuited. In this condition, the electrical damping is $3T_i^2\left(R_i\right)^{-1} = 0.0161\,\text{Nm rad}^{-1}\text{s}^{-1}$. Comparing this value with the experimental mechanical damping shows that electrical damping can be up to 10 times larger than mechanical damping. This is a useful advantage for the energy harvester as it provides a desirable flexibility for tuning the electrical damping in different environmental conditions to optimize the output power.

7.3.3 Base displacement versus relative displacement

This experiment is conducted to observe the relation between the amplitude of base displacement and relative displacement at certain frequencies. The result of this test can validate the derived system's equation of motion, the mechanical damping and coulomb friction that were obtained in previous experiments. In this experiment the excitation frequency is kept constant at $f = 0.8\,\text{Hz}$ and the amplitude of base acceleration is varied from 1 m sec^{-2} to 6 m sec^{-2}. Figure 7-7 shows the measured relative displacement at different base displacement amplitudes for both cases of open circuit and with a load resistance of 0.5Ω. It is seen that there are good agreements between the results obtained from numerically solving (7.1) using Matlab and the experimental result. This validates the derived dynamic equation and the obtained value for the unknown parameters of the system including mechanical damping and coulomb friction.

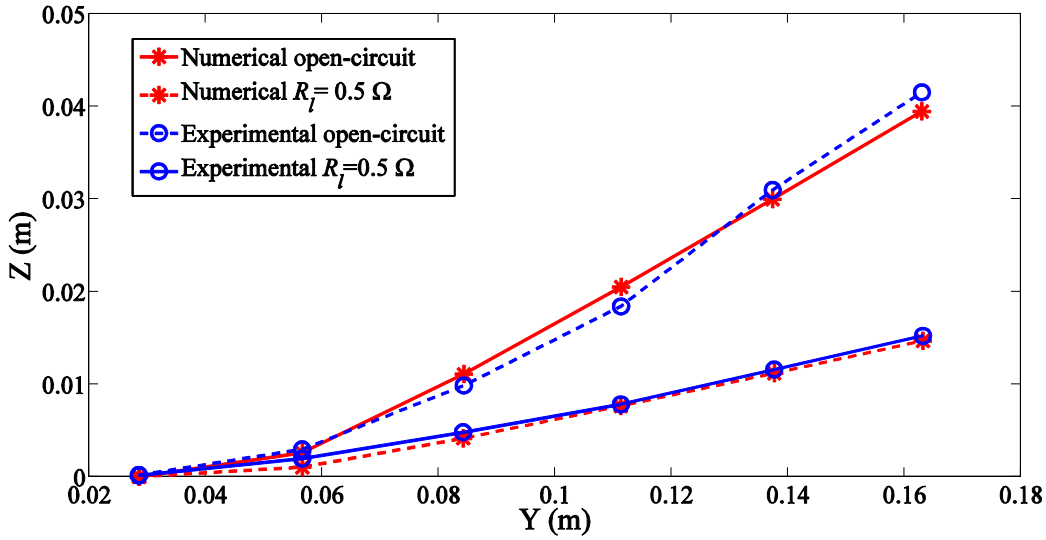

Figure 7-7 Base displacement versus relative displacement at frequency of 0.8 Hz

7.3.4 Output power versus load resistance

The purpose of this experiment is to measure the output power of the system under a given sinusoidal excitation frequency for different load resistance values. In this experiment, the amplitude of base excitation is 5 m sec^{-2} and the frequency of excitation is 0.8 Hz. A comparison between the numerical and experimental output power of the system is shown in figure 7-8 when the load resistance varies from 0.5 Ω to 11 Ω. As it is seen, the maximum power obtained from the experiment for $R_l = 1\Omega$, is very close to the maximum numerical value. However, at $R_l = 0.5\Omega$, the produced power is much less than the expected power. The load resistance corresponding to the maximum output power is derived in (6.10) when coulomb friction is ignored. Based on the parameters of the energy harvester shown in table 7.1, and for the mechanical damping value of $c_{bg} = 0.0016$ Nm $rad^{-1}s^{-1}$, when the system oscillates at 0.8 Hz, the maximum output power is obtained when the load resistance is adjusted at $1.05\,\Omega$. Therefore, in theory, the output power profile has a steep rise between the short circuit condition, i.e. $R_l = 0\Omega$, and the load resistance corresponding to the maximum output power, i.e. $R_l = 1.05\Omega$. Therefore, in this range, a slight miss-adjustment of the load resistance can change the output power dramatically which maybe the case for the $R_l = 0.5\Omega$ condition.

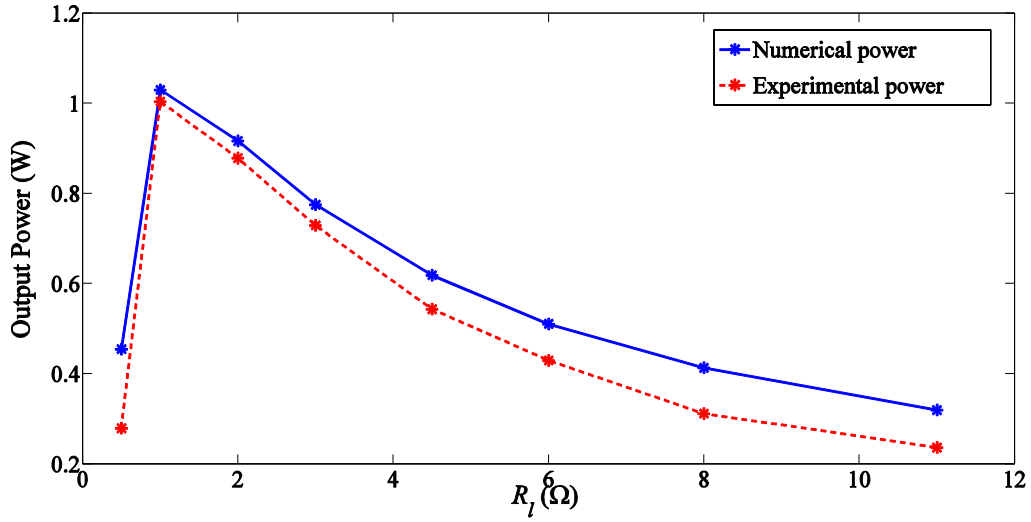

Figure 7-8 Analytical and experimental output power versus load resistance

However, in general, the power profile is in agreement with the theoretical predictions. In addition, although the maximum load resistance corresponding to the maximum power condition has been derived in (6.10) by ignoring the coulomb friction, there is still a good agreement between the theoretical and experimental values.

7.4 Conclusion

In this chapter, the experimental results of testing a ball screw based energy harvester are presented. The main purpose of conducting the experiment is to observe the performance of the system and validate the dynamic equations of the system. The experimental results that investigate the frequency response, relation between base and relative displacements and the output power profile are in reasonable agreement with the theoretical calculations. These in turn confirm the validity of the design and the derived equation of motion for the system. However, the manufactured energy harvester is found to have a mechanical damping coefficient of around $c_{bg} = 0.0016\ \text{Nm rad}^{-1}\text{s}^{-1}$ that corresponds to a damping ratio of $\xi = 1.41$. Hence, the designed energy harvester is an over-damped system which is not desirable in terms of efficiency. Therefore, the first step to improve the design of the energy harvester is to reduce its mechanical damping. To do this, the following steps may be taken:

- increase the size of the ball screw pitch,
- reduce the number of starts of the ball screw,
- reduce the ball screw diameter,
- reduce friction in the end-bearings,
- re-ball the ball screw nut to remove grease or any other contaminant, using the smaller ball-bearings in the ball screw nut.

Also, the harvester has been designed with two end-supports at the top and bottom of the ball screw. In practice and for practical purposes, the bottom support can be eliminated and the system can be tested with only one top end support. This test is helpful in measuring the mechanical damping contribution from the end supports.

Chapter 8: Conclusion and future works

8.1 Thesis summary and conclusion

This thesis has presented the study of design and optimisation of constrained electromagnetic energy harvesters. Shown here is a brief summary of the chapters from this thesis.

Chapter 2 - Boat's vertical displacement

In this chapter, having reviewed the published work in the area it is shown that using direct numerical integration to calculate velocity and displacement from an acceleration signal suffer from low frequency noise amplification and integration wind-up. Consequently, two Kalman filter based methods are proposed for calculating displacement from measured acceleration. Integration wind-up is eliminated by incorporating an additional state variable, namely the integral of the displacement whose "measured" value is assumed to be equal to the known average value of the displacement. In many applications this can be assumed to be constant, usually conveniently assigned to be zero, if non-linear behaviour and permanent deformations are negligible. In the first proposed method, a high-pass filter is used to remove the trend component following the Kalman filter calculations. In the second method, a high-pass filter is incorporated into the Kalman filter to eliminate the low frequency amplifications. The described techniques in this chapter are validated using laboratory investigations. Based on the described technique here, the displacement profile of the vertical excitation of a typical boat is established that is helpful in designing a suitable harvester.

Chapter 3 - Constrained electromagnetic devices for harvesting vibration energy

This chapter presents the study of designing electromagnetic vibration energy harvesters for constrained applications. A review of different studies shows that existing design criteria for vibration energy harvesting systems provide guidance on the appropriate selection of the seismic mass and load resistance. To harvest maximum power in resonant devices, the mass needs to be as large as possible and the load resistance needs to be equal to the sum of the internal resistance of the generator and the

mechanical damping equivalent resistance. However, it is shown in this chapter that these rules produce sub-optimum results for applications where there is a constraint on the relative displacement of the seismic mass, which is often the case. When the displacement is constrained, increasing the mass beyond a certain limit reduces the amount of harvested power. The optimum load resistance in this case is shown to be equal to the generator's internal resistance. These criteria are extended to those devices that harvest energy from a low-frequency vibration by utilizing an interface that transforms the input motion to higher frequencies. For such cases, the optimum load resistance and the corresponding transmission ratio are derived. In addition, in this chapter the maximum output power and the corresponding efficiency of linear and rotational electromagnetic energy harvesting systems with a constrained range of motion are investigated. A unified form of output power and efficiency is presented to compare the performance of constrained linear and rotational systems. It is found that rotational systems have greater capabilities in transferring energy to the load resistance than linear systems, due to the presence of an extra design variable viz. the ball screw lead. Also, in this chapter it is shown that for a defined environmental condition and a given proof mass with constrained throw, the amount of power delivered to the electrical load by a rotational system can be higher than a linear system. The criterion that guarantees this favorable design has been obtained.

Chapter 4 - Design procedure for a rotational energy harvester

This chapter studies an optimization process for a proposed ball screw based constrained energy harvester. In the proposed device, a ball screw converts the linear oscillatory motion of the mass to the rotational motion in order to drive an electrical generator. The design process flowchart is developed to provide guidelines for determining the optimum device parameters namely its mass, spring stiffness, ball screw lead and load resistance. The proposed technique considers practical limiting factors involved in the design of a constraint ball screw system including the maximum allowable displacement of the oscillating mass. It is shown that, unlike unconstrained energy harvesting systems, for such energy harvester where the maximum displacement is a constraint, selecting the optimum load resistance should be considered at early stages of the design process (i.e., not a posteriori step).

Chapter 5 - Harvesting energy from random excitation

This chapter evaluates the performance of a proposed device in chapter 4, in response to broadband and band-limited random vibrations. Based on mathematical equations describing the dynamics of the device, the frequency response function of the system is obtained by utilizing the theory of random vibration. Also, the mean power acquired from the harvester when it is subjected to broadband and band-limited stationary Gaussian white noise is derived. Power expressions are derived in dimensional form to provide an insightful understanding of the effect of physical parameters of the system on output power. In addition, an expression for the optimum load resistance to harvest maximum power under random excitation is derived and validated by conducting Monte-Carlo simulation. Interestingly, it is found that the derived optimum load resistance is identical to when the constrained system is subjected to a sinusoidal excitation with a frequency equal to its natural frequency. This chapter provides a guideline for designers to maximize the expected harvested power from a system under broadband and band-limited random excitations. Also it is shown that, the profile of the spectral density of the measured acceleration signal of a typical boat is approximated by a Cauchy distribution. The parameters of the spectral density distribution of the acceleration signal are then estimated and subsequently used to calculate the expected power of the proposed energy harvester in real conditions.

Chapter 6 -Adaptive tuning of the energy harvester for increasing its operational bandwidth

The rotational energy harvester presented in chapter 4, is designed to generate maximum power when its resonant frequency matches the ambient vibration frequency. However, in applications where this frequency is spread over a wide range, an energy harvester with fixed resonance frequency would operate in sub-optimum condition which limits its applicability. Therefore, it is vital to design a tuning mechanism for varying the resonance frequency and hence increasing the operational bandwidth of the device. It is shown that varying the moment of inertia of the energy harvester is a promising approach for broadening its operational band-width in both constrained and unconstrained modes. It is also demonstrated that for the presented ball screw based energy harvester, changing the load resistance to control the electrical damping is a useful method to increase the output power of the system over a wider frequency range.

Furthermore, it is shown that the combination of tuning the moment of inertia of the device and adjusting the resistance load can significantly increase the amount of harvested power. It is shown that changing the adjustable parameters, i.e. moment of inertia and load resistance, can be conducted intermittently. In other words, this approach only consumes power during tuning operation and does not use energy once the harvester is tuned at its optimum condition.

Chapter 7 – Experiments

In this chapter, the experimental results of testing a ball screw based energy harvester are presented. A reasonable agreement between the frequency response, the relation between base and relative displacements and output power profile of the system are obtained, which confirms the validity of the design and the derived dynamic equation of the system. However, it is shown that due to large mechanical damping associated with the ball screw, the manufactured energy harvester is over-damped, which is not desirable for an efficient energy harvester.

1.1 Future works

The research presented in this thesis has revealed a number of potential venues for further work and investigation which are discussed below:

In chapter 2, for calcutation of the displacement from acceleration by using the introduced Kalman filtering methods, it was deduced that the *NRE%* value depends on the ratio of *Q/R*. However, the optimum value of *Q/R* is obtained by trial and error which is time consuming. This research can be continued to derive by deriving the analytical expression of the optimum ratio of *Q/R* (if possible). With an analytical expression for selecting the noise and measurement covariances, not only the tuning process time is decreased but also, the presented kalman filter methods can be directly applied for real-time calculations of displacement from acceleration in different applications.

The study conducted in chapters 3 and 4 focused on designing a constraint system for a given environmental condition. However, in practice the environmental vibration may vary and hence, a fundamental challenge for such an energy harvester is its respond

to harsh weather, i.e. high amplitudes. For instance, by implementing a vibration control mechanism to ensure that high amplitudes of excitation will not pose any danger to the system.

Generator inductance has been neglected in this work. It is worth studying its effect specially when the system is subjected to high frequencies. This study can be interesting as the impedance caused by the generator inductance is related to the relative velocity of the oscillating mass, however, on the other hand the relative velocity of the mass is a function of generator impedance. Therefore, the system will have a set of recursive dynamic equations.

The current research considers the load resistance as a purely ohmic model. However, to have a more practical energy harvester an advance energy harvesting circuit and power management system should be employed. The power electronic circuits should be designed so that to achieve four main goals. Firstly, in many conditions, the electricity generated by the vibration energy harvesting system is AC, with varying frequency and amplitude which cannot power the electronic devices directly. Power electronic circuits should be used to regulate the AC harvested power to DC with a voltage level suitable for the energy storage device or load. In this regard, DC-DC converters can be used to boost or reduce the voltage to the range appropriate for the load or energy storage. Secondly, in chapter 6, it is shown that having a fixed load resistance which has been optimised for certain vibration level results in low effieicny in time-varying frequency conditions. A power electronic circuit with actively controlable parameters is a key componenet to improve the efficiency of the energy harvester in real environment. Thirdly, as it was mentioned earlier, protection of the mechanical componenets when the system is subjected to a high level of vibration is a fundumental challenge. In an energy harvester, the mechanical system and power electronic circuit are coupled and hence, the energy harvesting interface circuits have an effect on the dynamics of the mechanical system. The power electronic circuit can be used as a part of the active control process to protect the energy harvester. Fourthly, the power electronic ciruit is used to power the active control system. For instance, in the case of implimenting the variable moment of inertia mechanism presented in chapter 6, the power electronic circuit should transfer power from the storage system to moveable

masses to adjust them at the optimum position. This implies the necessity of utilising power electronic circuits with bidirectional power flow capabilities.

Some research works including [118] study the effect of employing the non-linear damping to increase the dynamic range of energy harvesters. However, these studies do not address the physical components that contribut the non-linear dampings of system. These studies can be extended to find the effect of utilizing the non-linear damping in a rotational energy harvester and also to design and implement an electrical load that presents a non-linear behaviour in the system.

In this work the idea of changing the moment of inertia has been applied to increase the operational bandwidth of a rotational energy harvester. However, the possibility of utilizing this mechanism in other applications such as inerter or vehicle suspension systems can be investigated.

In chapter 7, it was found that the manufactured harvester is over-damped and therefore some modifications, as are mentioned in chapter 7, can be conducted to reduce the mechanical damping of system. Furthermore, the dynamic equation of system presented in that chapter considers the coulomb friction associated with the mechanical components. However, the study can be continued by investigating the non-linearities of system to derive a more accurate model for the dynamic equations of system.

The current work studies the performance of system subjected to single frequency and random vibrations. The research can be continued by studying the performance of system subjected to multi-frequency vibrations. In this condition the input vibration is consisted of different single frequency vibrations. This study is more important if the non-linearities of the system are modelled and the superposition principle is not valid any more.

This research can be continued by designing a hybrid energy harvester. This system is a combination of a linear and a rotational energy harvester. If we replace the oscillating mass of the rotational energy harvester with a permanent magnet, then there is a potential to design a hybrid system. In this idea a set of coils can be located around a cylinder which its central axis is aligned with the ball screw shaft. Therefore, oscillation of the permanent magnet not only drives the ball screw but also based on the analogy of linear generator, it can induce voltage to the coils. This design provides the

possibility of applying more electrical damping to the system when it is necessary. In addition, by designing two independent power electronic circuits for each generator, we can use one of them to contribute the linear electrical damping and the other one to contribute non-linear electrical damping which makes the design of power electronic circuit much easier.

This research can be continued by adding two compression springs to the design energy harvester. Therefore, the system will have four springs which increase the design parameters of system.

The current study evaluates the performance of system under random and sinoiuidal excitations. However, in some applications the system may be subjected to impact force. Therefore, the response of system to such input power can be studied,

Appendix A

MATLAB-Simulink models

This section includes the following:

i. MATLAB simulating model of the rotational electromagnetic energy harvester for Monte-Carlo simulation.

ii. MATLAB code for Monte-Carlo simulation

i) Simulink model of energy harvester for Monte-Carlo simulation

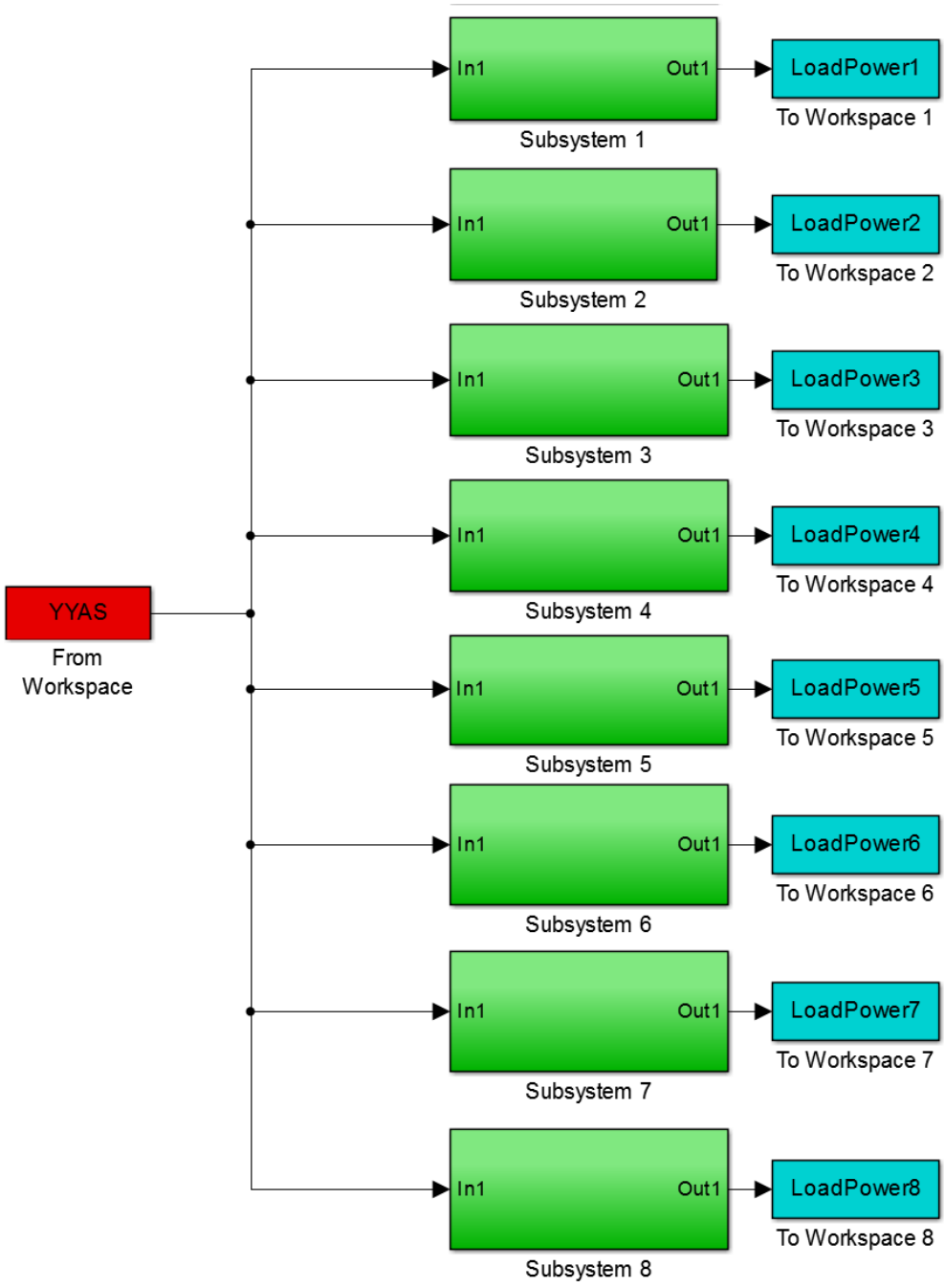

Figure A. 1 Simulink model of Monte-Carlo simulation

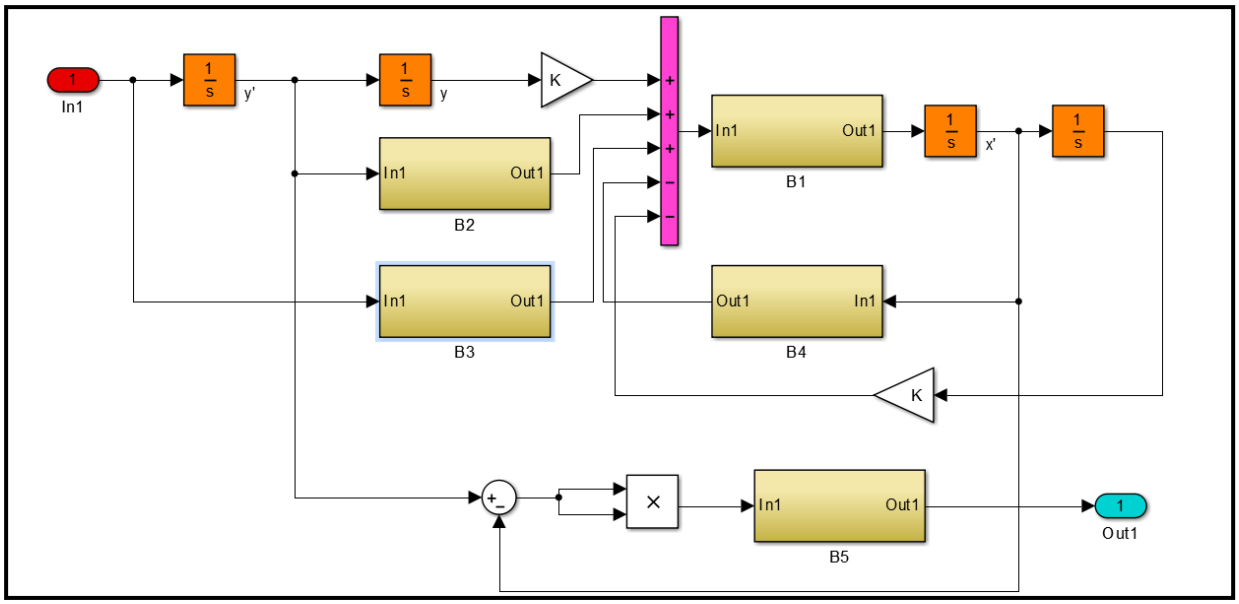

Figure A. 2 Simulink model the rotational electromagnetic energy harvesting system

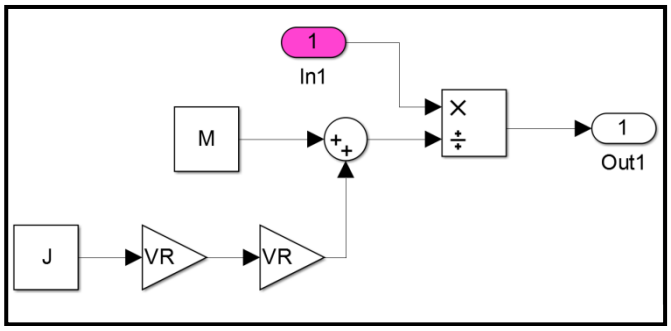

Figure A. 3 Simulink model of B1 in figure A.2

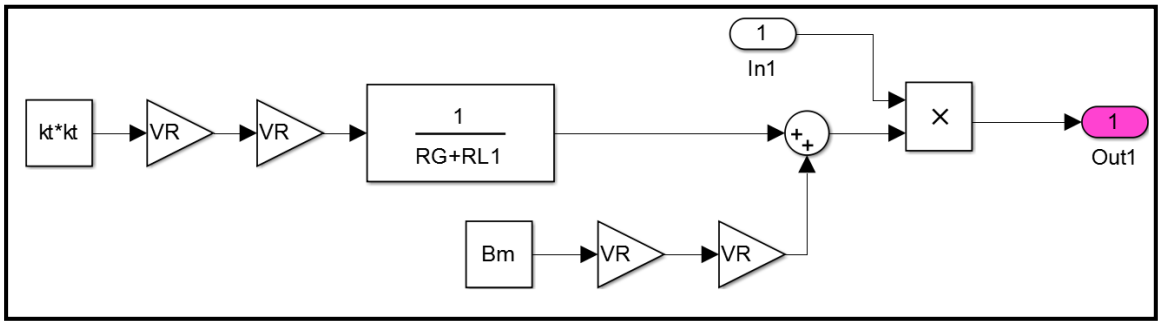

Figure A. 4 Simulink model of B2 in figure A.2

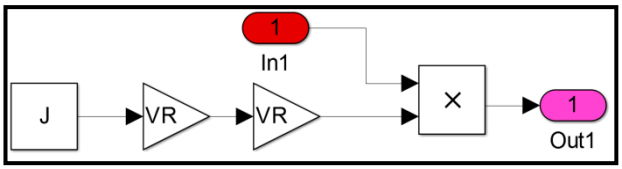

Figure A. 5 Simulink model of B3 in figure A.2

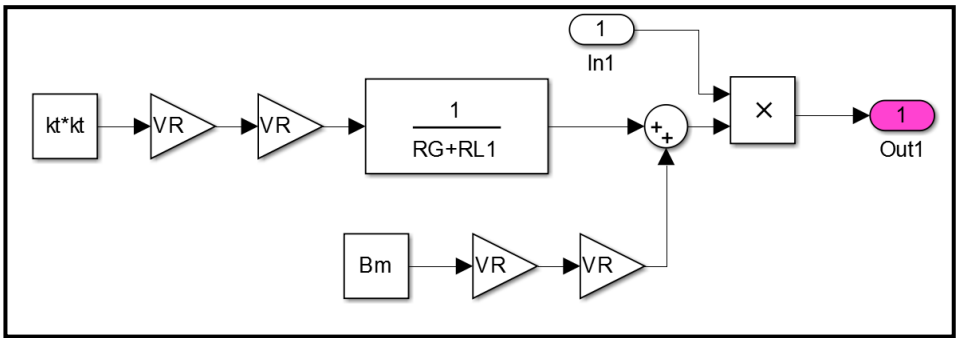

Figure A. 6 Simulink model of B4 in figure A.2

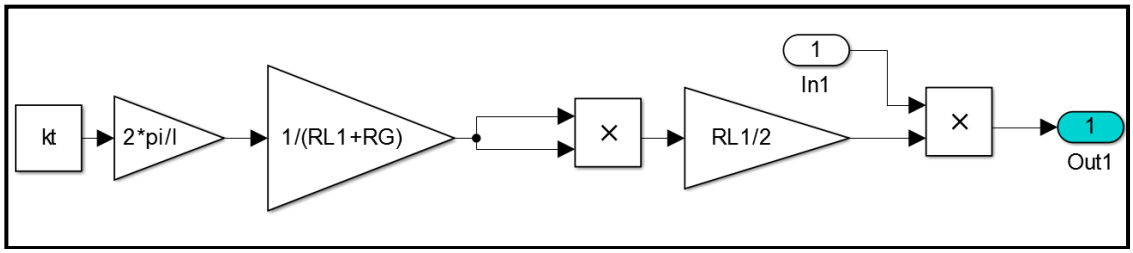

Figure A. 7 Simulink model of B5 in figure A.2

ii) MATLAB code for Monte-Carlo simulation

```
nruns=1000;
dt=.001;   % Time variable
sec=20;    % Silumation duration
nt=(1/dt)*sec;
w1=0; w2=2*200*pi;      % Frequency range
A1=0; A2=10;            % Amplitude range

%%%% Random process

for J=1:nruns
   A=A1+(A2-A1)*randn(1,nt);
   w=w1+(w2-w1)*randn(1,nt);
   phi=pi*rand(1,nt);
   i=0;
   for t=dt:dt:sec
      i=i+1;
      tt(i)=t;
      X(J,i)=A(i)*sin(abs(w(i))*t+phi(i));
   end;

end;

%% System parameters
h=0;
f=.5;
w=2*pi*f;
wd=w;
y=1;
Y0=y;
i=0;
M1=8;
Z0=0.3;
Bm=53.6e-6;
kt=0.0739;   %N.m/Amp
ke=0.0739;    %V/rad/s
Jm=1140e-7;
Js=60e-7;
J=Jm+Js;
RG=1.01;     %Ohm
RL=(RG^2+(ke*ke*RG/Bm))^.5;    % Ohm
Lm=0;%.0000000021;    %Han

B=Bm+(kt*kt/(RG+RL));
l=(Z0*4*pi*pi*B/(wd*M1*Y0))^.5;
VR=(2*pi)/l;

K=(M1+J*((2*pi/l)^2))*(w^2);

%% Runing Simulink model for different load resistance. Monte-Carlo simulation

wn=(K/M1)^.5;
RL1=0.5;  RL2=3; RL3=7;  RL4=RLopt;   RL5=15;  RL6=30;  RL7=60;      RL8=100;
TT2=.001:.001:sec;
TT(:,1)=TT2(1,:);
```

```
for i=1:nruns

    YY2=X(i,:);

    YY(:,1)=YY2(1,:);

    YYAS=[TT,YY];

    sim('RenewableEnergyJournalrandomInput8systems');

    PP1ph(i,:)=pp1(1:1000*sec);    % Output Powerrrr
    PP2ph(i,:)=pp2(1:1000*sec);
    PP3ph(i,:)=pp3(1:1000*sec);
    PP4ph(i,:)=pp4(1:1000*sec);
    PP5ph(i,:)=pp5(1:1000*sec);
    PP6ph(i,:)=pp6(1:1000*sec);
    PP7ph(i,:)=pp7(1:1000*sec);
    PP8ph(i,:)=pp8(1:1000*sec);

    clear YY;
    clear YY2;
    clear YYAS;
    clear pp1;
    clear pp2;
    clear pp3;
    clear pp4;
    clear pp5;
    clear pp6;
    clear pp7;
    clear pp8;
end;

save PP1ph;
save PP2ph;
save PP3ph;
save PP4ph;
save PP5ph;
save PP6ph;
save PP7ph;
save PP8ph;
```

Appendix B

CAD Drawing of the designed energy harvester


DO NOT SCALE
DRAWN BY
Mia Grout
DESIGNED BY
Mia Grout
DATE
21/03/2013
SCALE
A1
MATERIAL
NATURE
SURFACE FINISH
University of Southampton
Faculty of Engineering and the Environment
SUB ASSEMBLY OF INERTIA COUPLED GENERATOR
SHEET
1 of 1
No OFF
1
ASSEMBLY NUMBER
0067-000
DRAWING NUMBER
0067-001
REVISION
A
THE INFORMATION CONTAINED IN THIS DOCUMENT IS THE PROPERTY OF THE UNIVERSITY OF SOUTHAMPTON
DO NOT COPY WITHOUT WRITTEN PERMISSION.

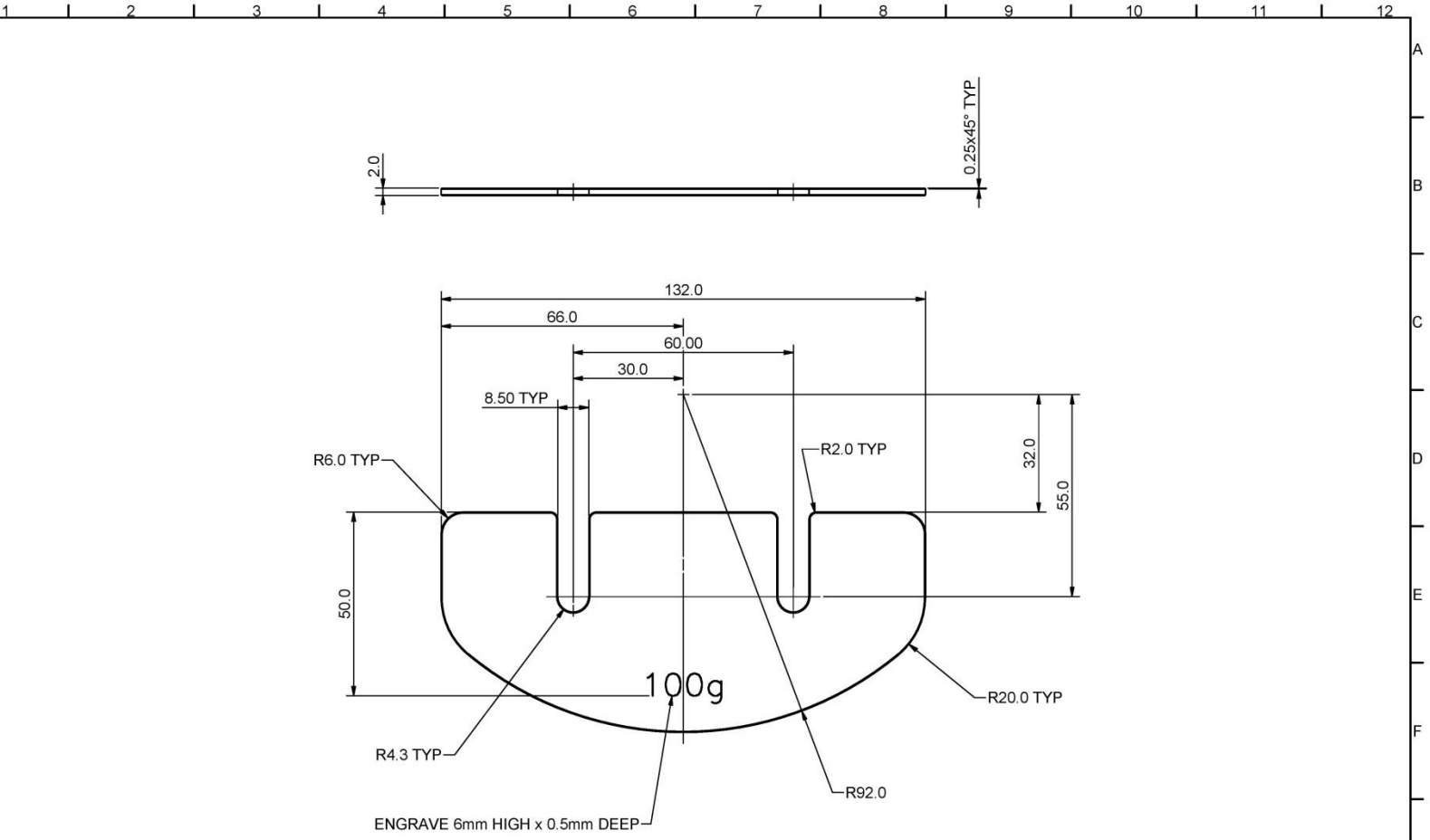

DO NOT SCALE		DRAWN BY: Mike Street		TOLERANCES UNLESS OTHERWISE STATED	UNIVERSITY OF Southampton
MASS: 0.098 kg	COST	DESIGNED BY: Mike Street		DIMS TO 1 DEC PLACE +/- 0.5mm; DIMS TO 2 DEC PLACES +/- 0.25mm; ANGULAR DIMS +/- 0.5mm	School of Engineering Sciences
A3		DATE: 21/03/2013	SCALE: 1:1	ALL DIMENSIONS IN mm UNLESS OTHERWISE STATED	TITLE: 100g VARIABLE MASS
PROJECT: INERTIA COUPLED GENERATOR	CUSTOMER: MEHDI HENDIJANIZADEH	MATERIAL: MILD STEEL	TEXTURE: SPRAY PAINT BLACK	SURFACE FINISH: ALL OVER UNLESS OTHERWISE STATED	
REMOVE ALL SHARP EDGES		THE INFORMATION CONTAINED IN THIS DOCUMENT IS THE PROPERTY OF THE UNIVERSITY OF SOUTHAMPTON DO NOT COPY WITHOUT WRITTEN PERMISSION.		SHEET: 1 of 1	No OFF: 4	ASSEMBLY NUMBER: 0067-001	DRAWING NUMBER: 0067-009	REVISION: A
IF IN DOUBT PLEASE ASK					

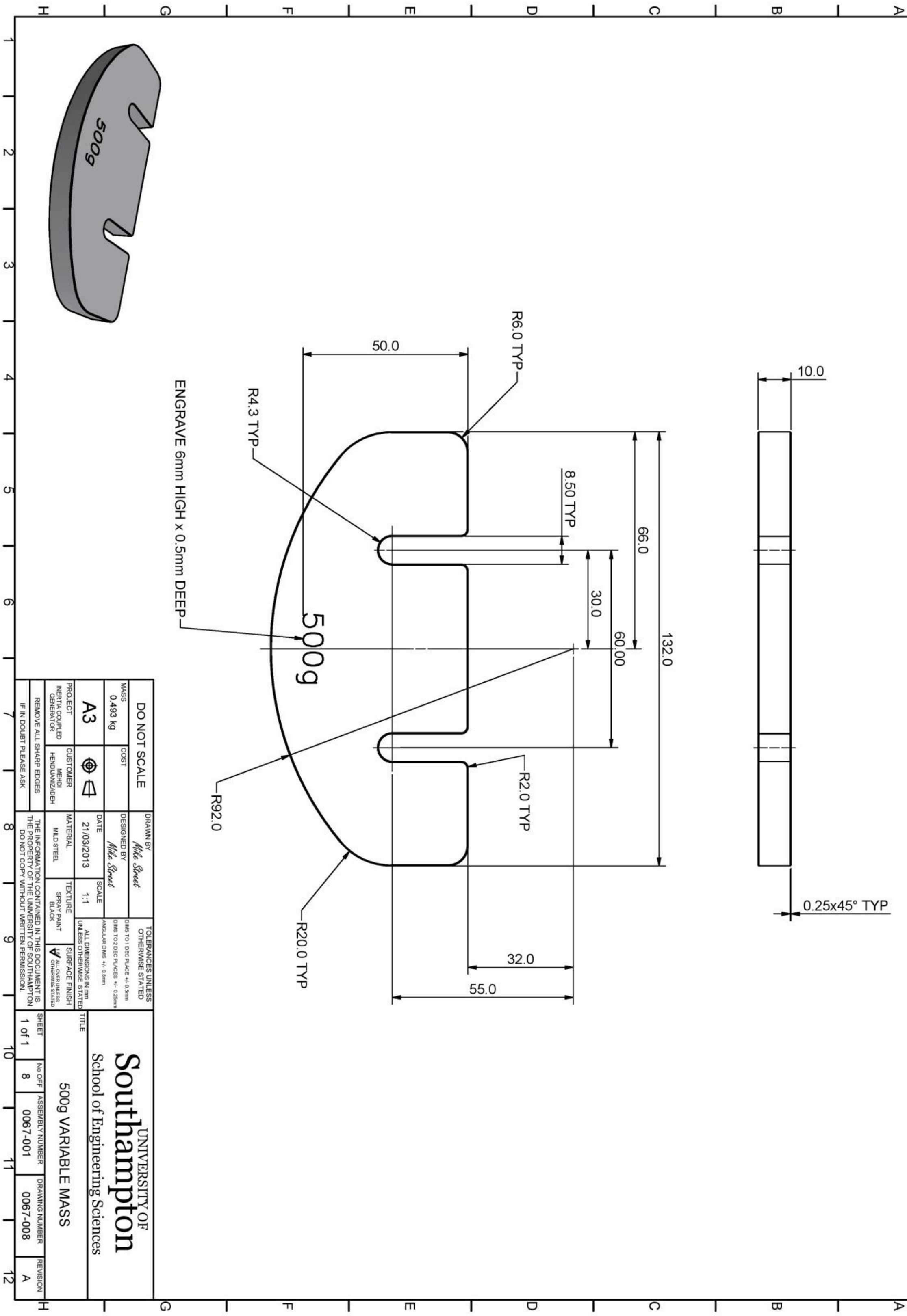
500g
50.0
R6.0 TYP
R4.3 TYP
ENGRAVE 6mm HIGH x 0.5mm DEEP
8.50 TYP
66.0
30.0
60.00
132.0
500g
R92.0
R2.0 TYP
R20.0 TYP
32.0
55.0
10.0
0.25x45° TYP
DO NOT SCALE
MASS
0.493 kg
COST
A3
PROJECT
INERTIA COUPLED GENERATOR
CUSTOMER
MEHDI HENDIJANIZADEH
REMOVE ALL SHARP EDGES
IF IN DOUBT PLEASE ASK
DRAWN BY
DESIGNED BY
DATE
21/03/2013
SCALE
1:1
MATERIAL
MILD STEEL
TEXTURE
SPRAY PAINT BLACK
TOLERANCES UNLESS OTHERWISE STATED
ALL DIMENSIONS IN mm UNLESS OTHERWISE STATED
SURFACE FINISH
THE INFORMATION CONTAINED IN THIS DOCUMENT IS THE PROPERTY OF THE UNIVERSITY OF SOUTHAMPTON DO NOT COPY WITHOUT WRITTEN PERMISSION
UNIVERSITY OF Southampton
School of Engineering Sciences
TITLE
500g VARIABLE MASS
SHEET
1 of 1
No OFF
8
ASSEMBLY NUMBER
0067-001
DRAWING NUMBER
0067-008
REVISION
A

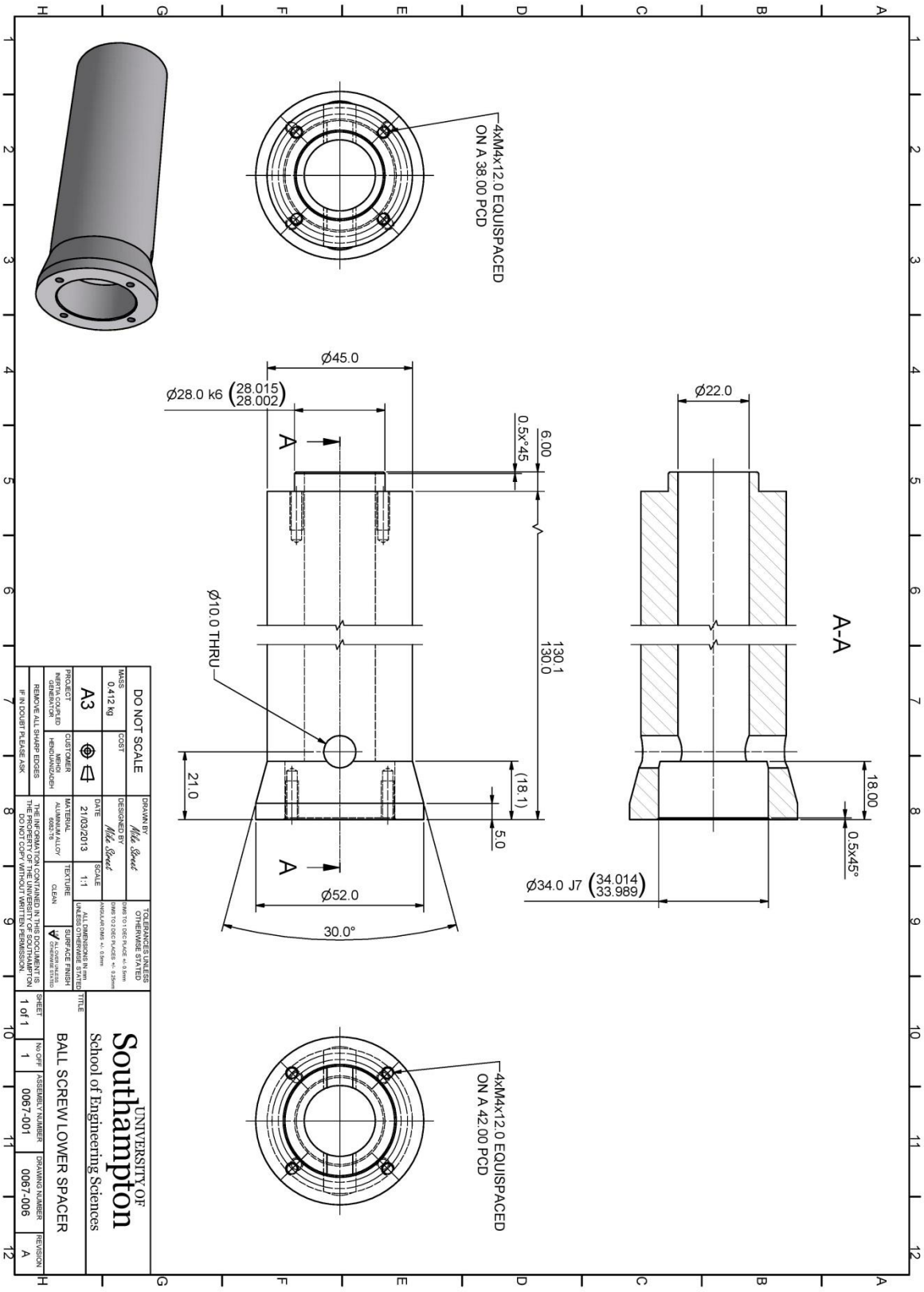
4xM4x12.0 EQUISPACED
ON A 38.00 PCD
Ø45.0
Ø28.0 k6 (28.015 28.002)
6.00
0.5x°45
Ø10.0 THRU
130.1
130.0
21.0
(18.1)
5.0
A
A
Ø52.0
30.0°
Ø22.0
A-A
18.00
0.5x45°
Ø34.0 J7 (34.014 33.989)
4xM4x12.0 EQUISPACED
ON A 42.00 PCD
DO NOT SCALE
MASS 0.412 kg
COST
A3
DATE 21/03/2013
SCALE 1:1
TEXTURE CLEAN
MATERIAL ALUMINIUM ALLOY 6082-T6
DRAWN BY Mike Sweet
DESIGNED BY Mike Sweet
TOLERANCES UNLESS OTHERWISE STATED
DIMS TO 1 DEC PLACE +/- 0.1mm
ANGULAR DIMS +/- 0.5mm
DIMS TO 2 DEC PLACES +/- 0.25mm
ALL DIMENSIONS IN mm UNLESS OTHERWISE STATED
SURFACE FINISH
ALL OVER UNLESS OTHERWISE STATED
PROJECT INERTIA COUPLED GENERATOR
CUSTOMER MEHDI HENDIJANZADEH
REMOVE ALL SHARP EDGES
IF IN DOUBT PLEASE ASK
THE INFORMATION CONTAINED IN THIS DOCUMENT IS THE PROPERTY OF THE UNIVERSITY OF SOUTHAMPTON
DO NOT COPY WITHOUT WRITTEN PERMISSION
UNIVERSITY OF Southampton
School of Engineering Sciences
TITLE
BALL SCREW LOWER SPACER
SHEET 1 of 1
No OFF 1
ASSEMBLY NUMBER 0067-001
DRAWING NUMBER 0067-006
REVISION A

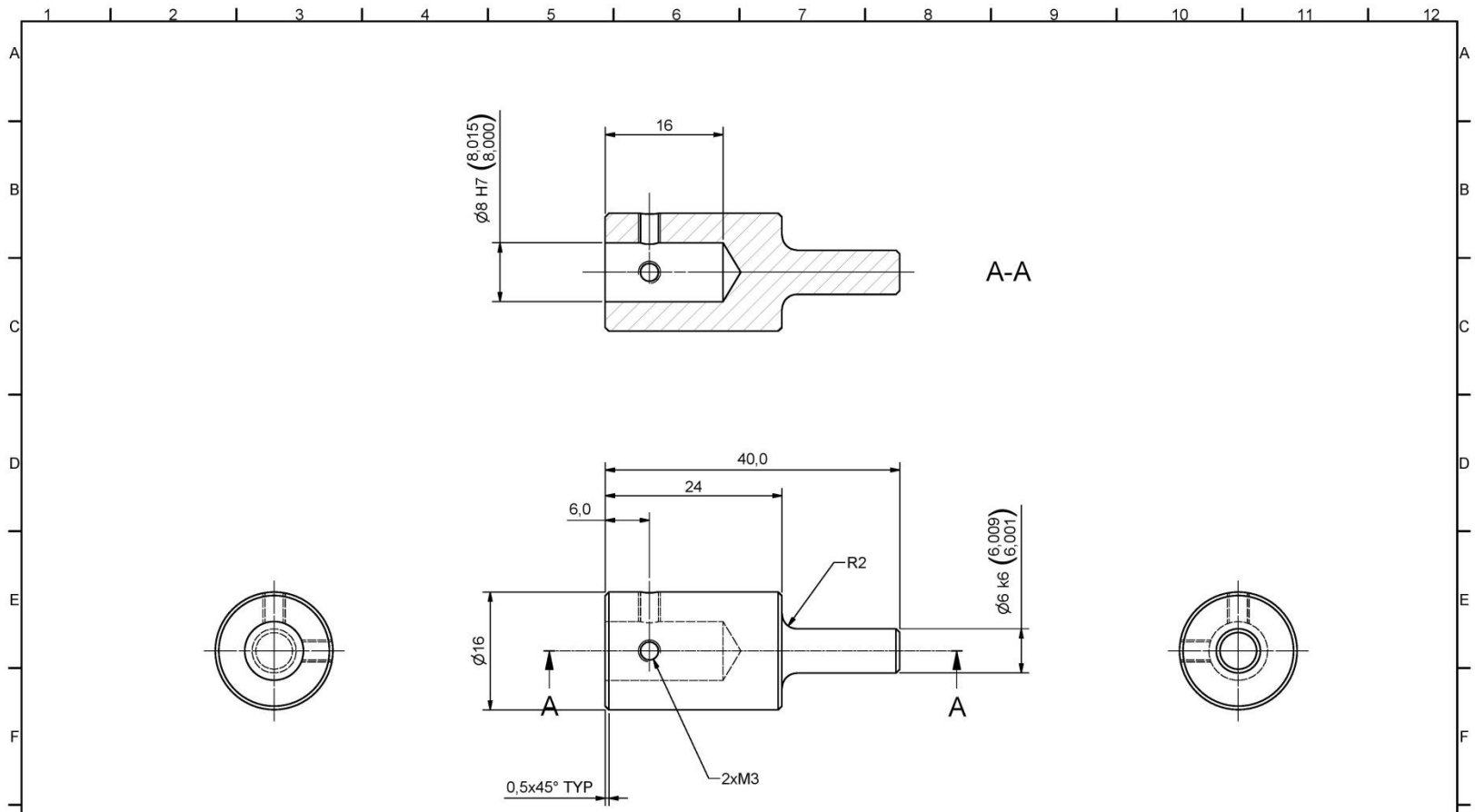

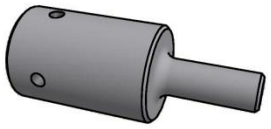

DO NOT SCALE		DRAWN BY: Mike Street	TOLERANCES UNLESS OTHERWISE STATED: LINEAR DIMENSIONS X = +/- 0.5mm, X.X = +/- 0.2mm, X.XX = +/- 0.1mm; ANGULAR DIMENSIONS X = +/- 0.5mm, XX = +/- 0.25mm; ALL DIMENSIONS IN mm UNLESS OTHERWISE STATED	UNIVERSITY OF Southampton	
MASS: N/A	COST	DESIGNED BY: Mike Street		Faculty of Engineering and the Environment	
A3		DATE: 21/03/2013	SCALE: 2:1	TITLE: BALL SCREW SHAFT ADAPTOR	
PROJECT: INERTIA COUPLED GENERATOR	CUSTOMER: MEHDI HENDIJANIZADEH	MATERIAL: MILD STEEL	TEXTURE: OILED	SURFACE FINISH: ALL OVER UNLESS OTHERWISE STATED	
REMOVE ALL SHARP EDGES		THE INFORMATION CONTAINED IN THIS DOCUMENT IS THE PROPERTY OF THE UNIVERSITY OF SOUTHAMPTON DO NOT COPY WITHOUT WRITTEN PERMISSION.			
IF IN DOUBT PLEASE ASK					

SHEET	No OFF	ASSEMBLY NUMBER	DRAWING NUMBER	REVISION
1 of 1	1	0067-001	0067-012	A

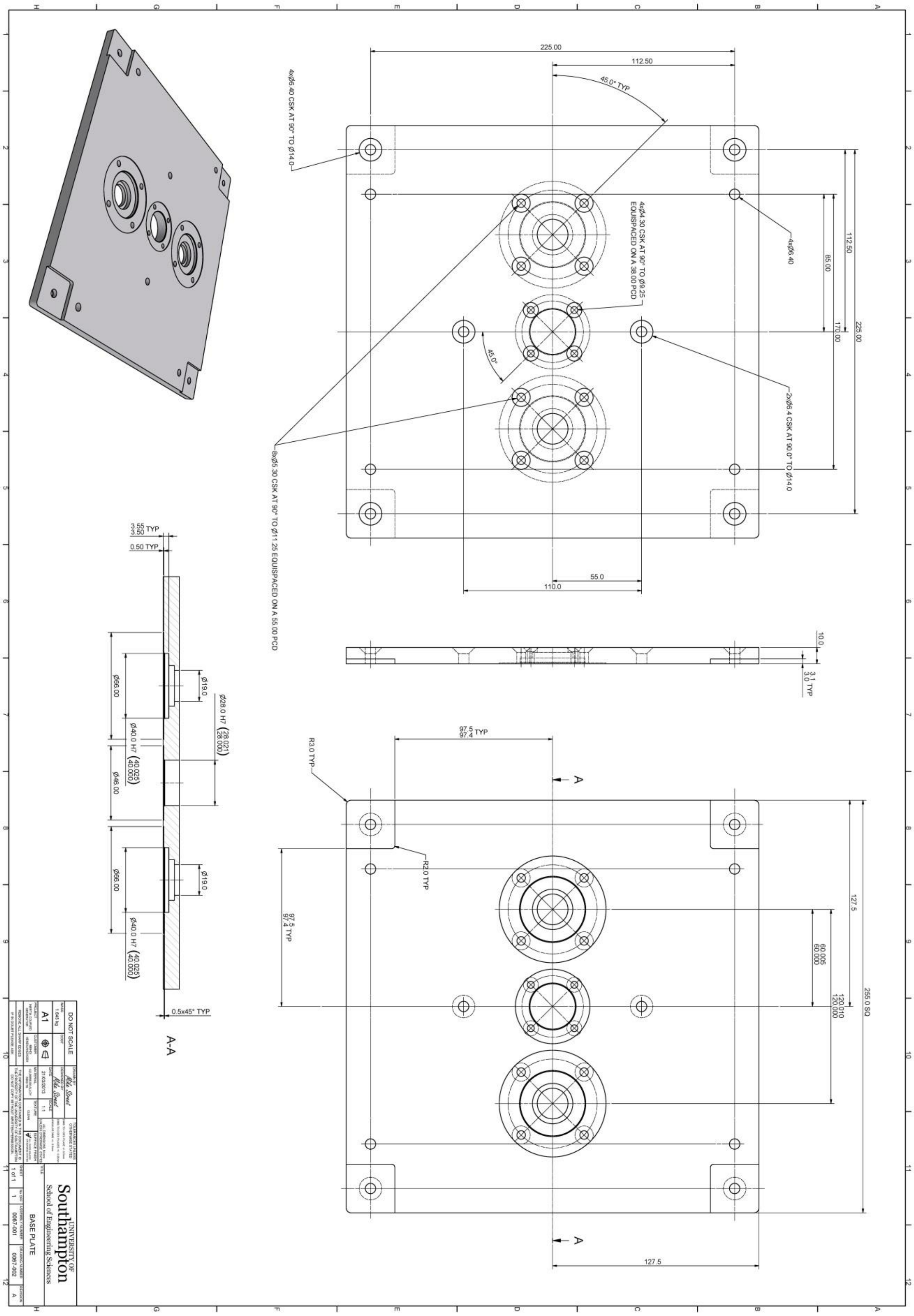
University of Southampton
School of Engineering Sciences
BASE PLATE
DO NOT SCALE
A-A

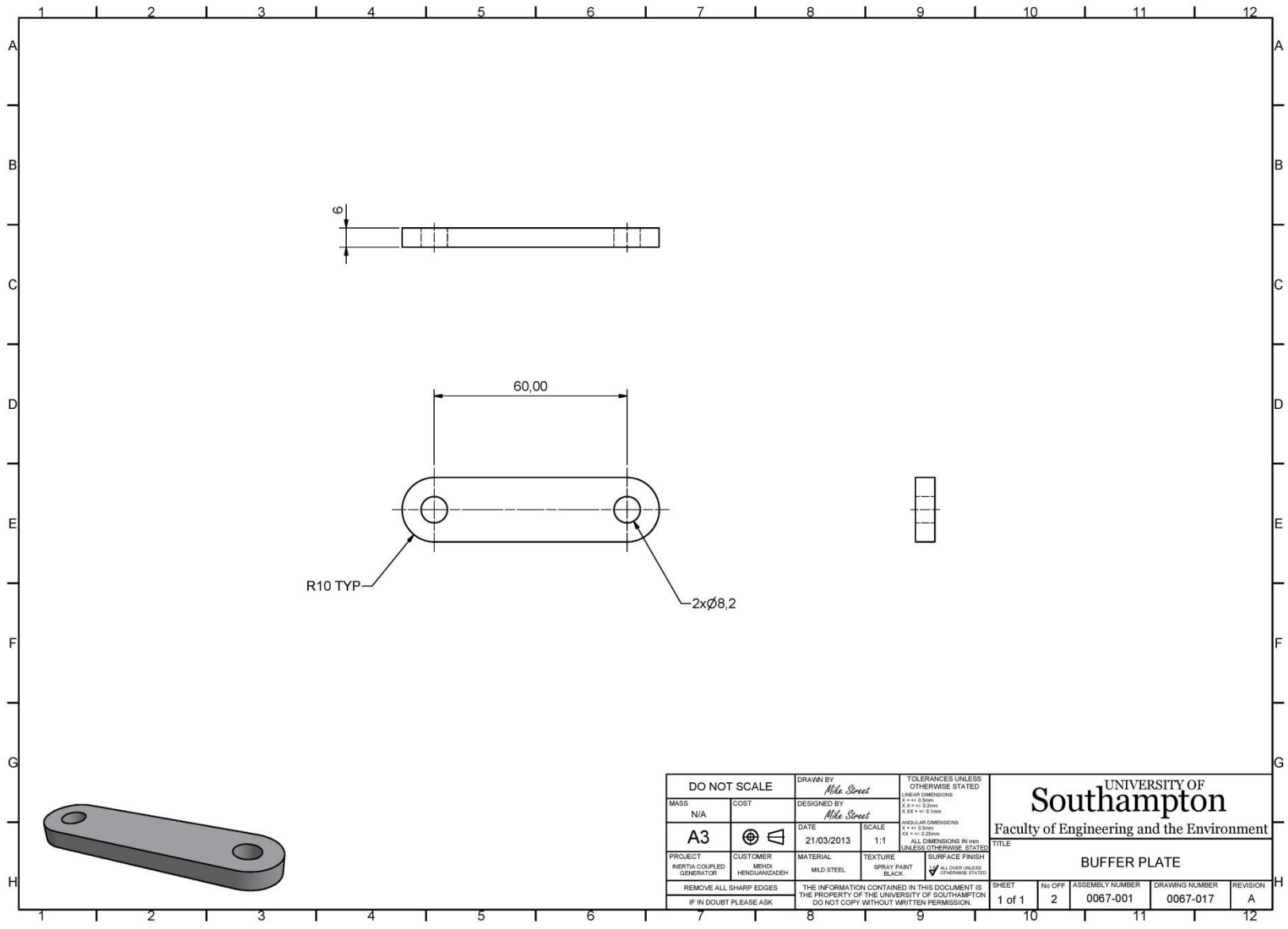

DO NOT SCALE		DRAWN BY: Mike Street		TOLERANCES UNLESS OTHERWISE STATED: LINEAR DIMENSIONS X = +/- 0.5mm, X.X = +/- 0.2mm, X.XX = +/- 0.1mm; ANGULAR DIMENSIONS X = +/- 0.5mm, XX = +/- 0.25mm; ALL DIMENSIONS IN mm UNLESS OTHERWISE STATED	UNIVERSITY OF Southampton
MASS: N/A	COST	DESIGNED BY: Mike Street			Faculty of Engineering and the Environment
A3		DATE: 21/03/2013	SCALE: 1:1		TITLE: BUFFER PLATE
PROJECT: INERTIA COUPLED GENERATOR	CUSTOMER: MEHDI HENDIJANIZADEH	MATERIAL: MILD STEEL	TEXTURE: SPRAY PAINT BLACK	SURFACE FINISH: ALL OVER UNLESS OTHERWISE STATED	
REMOVE ALL SHARP EDGES		THE INFORMATION CONTAINED IN THIS DOCUMENT IS THE PROPERTY OF THE UNIVERSITY OF SOUTHAMPTON DO NOT COPY WITHOUT WRITTEN PERMISSION.			SHEET: 1 of 1 | No OFF: 2 | ASSEMBLY NUMBER: 0067-001 | DRAWING NUMBER: 0067-017 | REVISION: A
IF IN DOUBT PLEASE ASK					

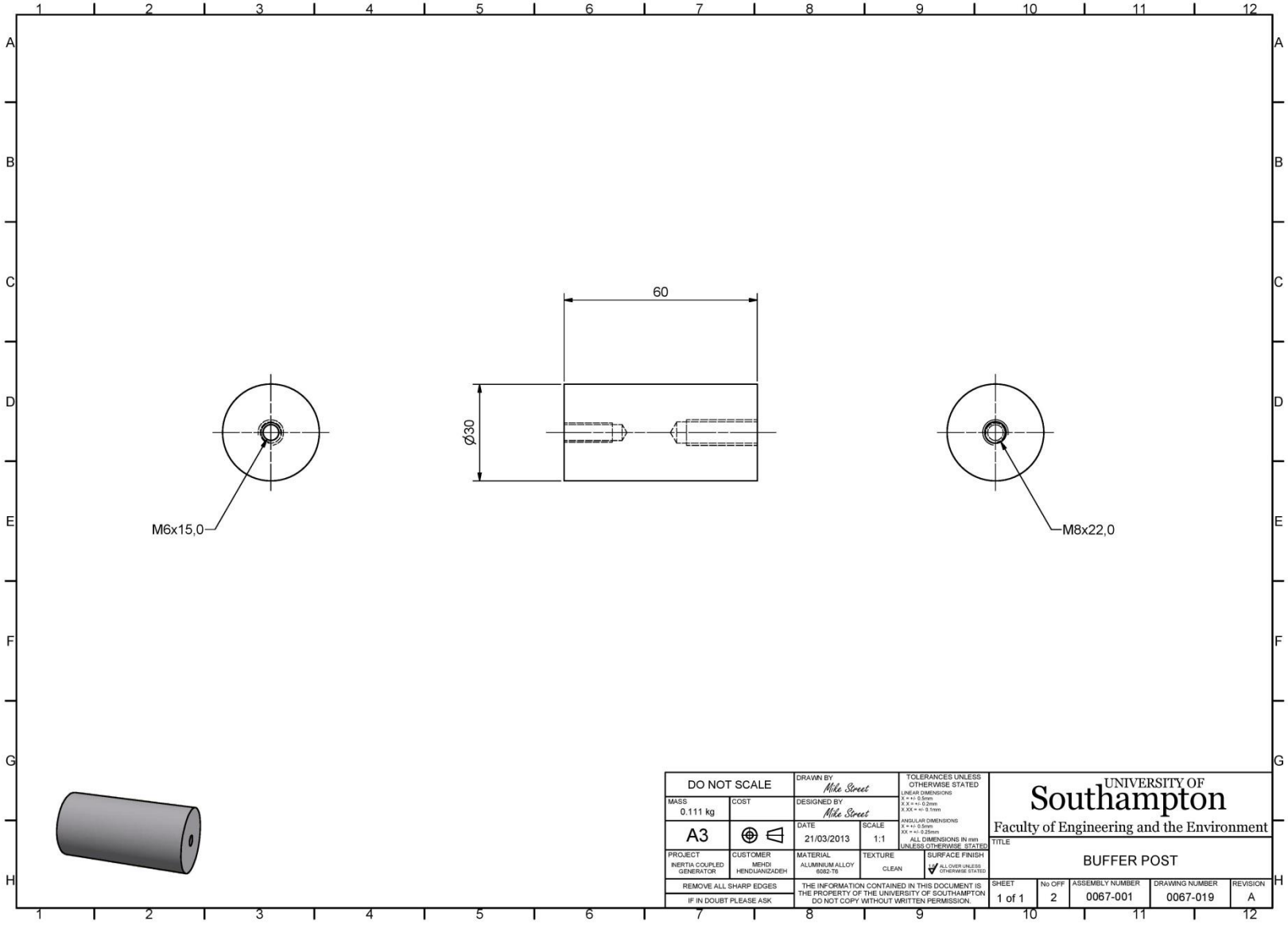

DO NOT SCALE		DRAWN BY: Mike Street		TOLERANCES UNLESS OTHERWISE STATED LINEAR DIMENSIONS X = +/- 0.5mm X.X = +/- 0.2mm X.XX = +/- 0.1mm ANGULAR DIMENSIONS X = +/- 0.5mm XX = +/- 0.25mm ALL DIMENSIONS IN mm UNLESS OTHERWISE STATED	UNIVERSITY OF Southampton Faculty of Engineering and the Environment
MASS: 0.111 kg	COST	DESIGNED BY: Mike Street			TITLE: BUFFER POST
A3		DATE: 21/03/2013	SCALE: 1:1		
PROJECT: INERTIA COUPLED GENERATOR	CUSTOMER: MEHDI HENDIJANIZADEH	MATERIAL: ALUMINIUM ALLOY 6082-T6	TEXTURE: CLEAN	SURFACE FINISH: ALL OVER UNLESS OTHERWISE STATED	
REMOVE ALL SHARP EDGES		THE INFORMATION CONTAINED IN THIS DOCUMENT IS THE PROPERTY OF THE UNIVERSITY OF SOUTHAMPTON DO NOT COPY WITHOUT WRITTEN PERMISSION.			SHEET: 1 of 1 | No OFF: 2 | ASSEMBLY NUMBER: 0067-001 | DRAWING NUMBER: 0067-019 | REVISION: A
IF IN DOUBT PLEASE ASK					

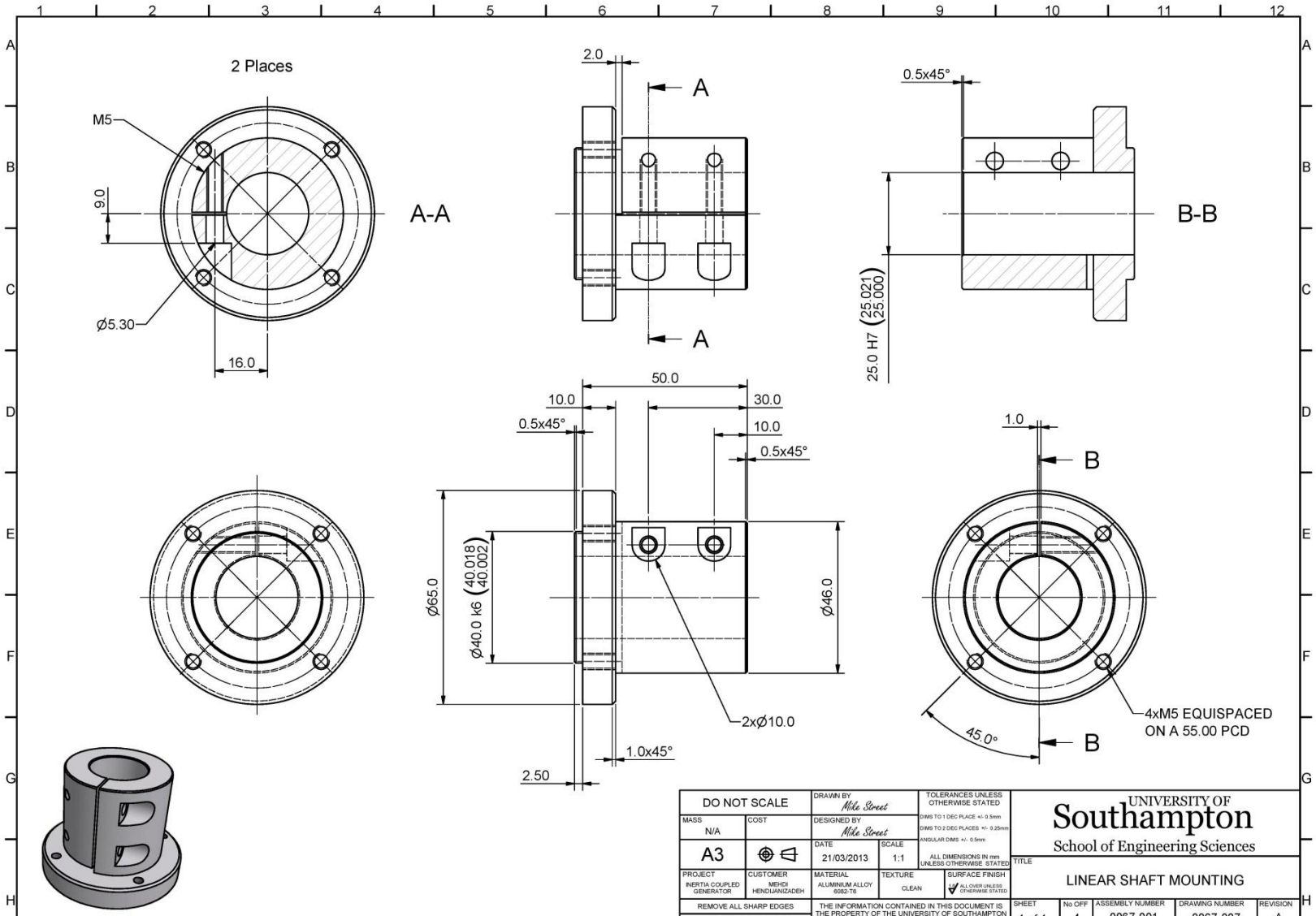
2 Places
M5
9.0
Ø5.30
16.0
A-A
2.0
A
A
0.5x45°
B-B
25.0 H7 (25.021 25.000)
50.0
10.0
30.0
10.0
0.5x45°
0.5x45°
Ø65.0
Ø40.0 k6 (40.018 40.002)
Ø46.0
2xØ10.0
1.0x45°
2.50
1.0
B
B
45.0°
4xM5 EQUISPACED
ON A 55.00 PCD
DO NOT SCALE
DRAWN BY Mike Street
TOLERANCES UNLESS OTHERWISE STATED
DIMS TO 1 DEC PLACE +/- 0.5mm
DIMS TO 2 DEC PLACES +/- 0.25mm
ANGULAR DIMS +/- 0.5mm
MASS N/A
COST
DESIGNED BY Mike Street
A3
DATE 21/03/2013
SCALE 1:1
ALL DIMENSIONS IN mm UNLESS OTHERWISE STATED
PROJECT INERTIA COUPLED GENERATOR
CUSTOMER MEHDI HENDIJANIZADEH
MATERIAL ALUMINIUM ALLOY 6082-T6
TEXTURE CLEAN
SURFACE FINISH
ALL OVER UNLESS OTHERWISE STATED
REMOVE ALL SHARP EDGES
IF IN DOUBT PLEASE ASK
THE INFORMATION CONTAINED IN THIS DOCUMENT IS THE PROPERTY OF THE UNIVERSITY OF SOUTHAMPTON DO NOT COPY WITHOUT WRITTEN PERMISSION.
UNIVERSITY OF Southampton
School of Engineering Sciences
TITLE
LINEAR SHAFT MOUNTING
SHEET 1 of 1
No OFF 4
ASSEMBLY NUMBER 0067-001
DRAWING NUMBER 0067-007
REVISION A

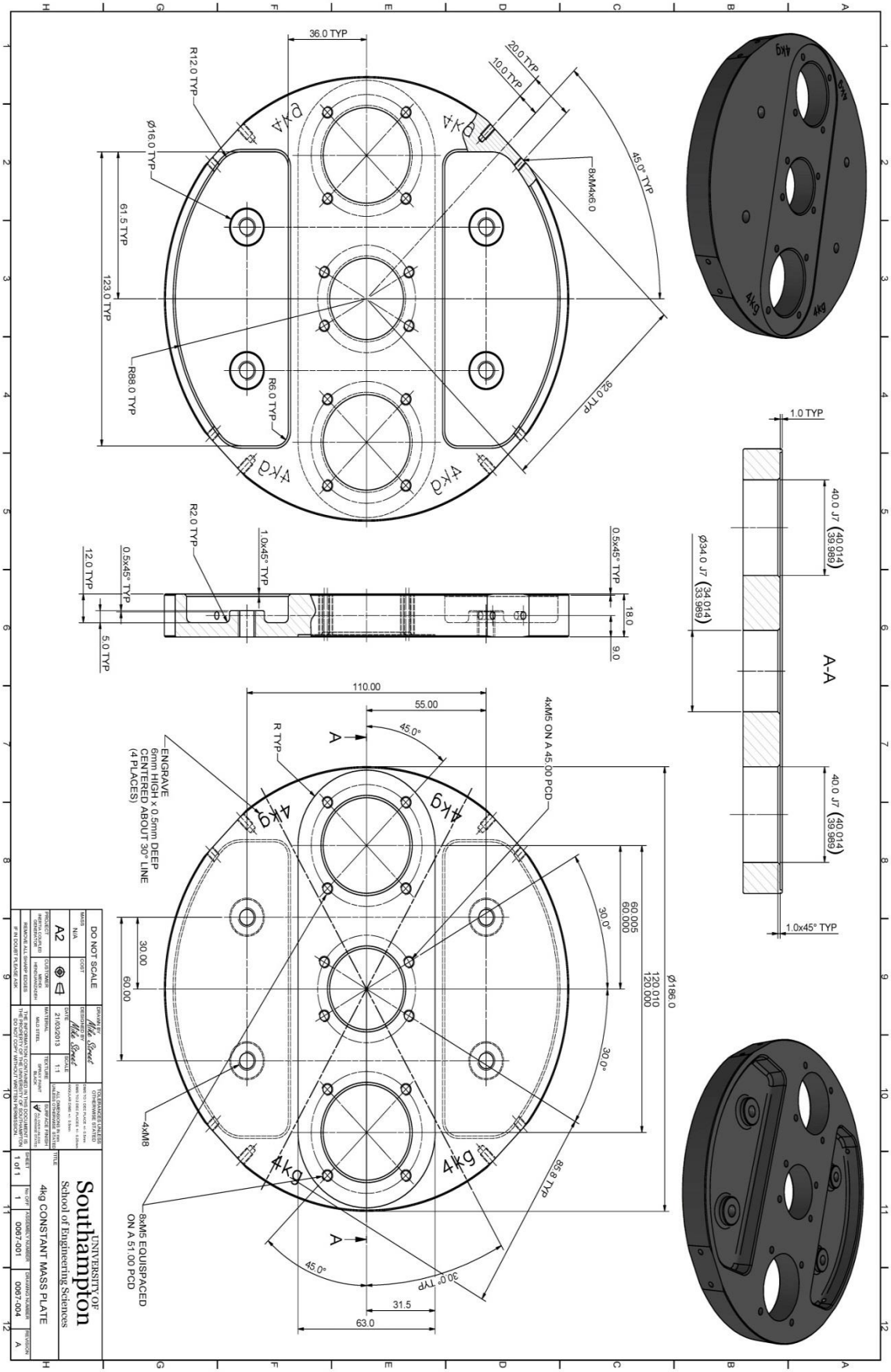
36.0 TYP
20.0 TYP
10.0 TYP
R12.0 TYP
Ø16.0 TYP
61.5 TYP
123.0 TYP
R88.0 TYP
R6.0 TYP
8xM4x6.0
45.0° TYP
82.0 TYP
4kg
1.0 TYP
40.0 J7 (40.014 39.989)
Ø34.0 J7 (34.014 33.989)
A-A
1.0x45° TYP
R2.0 TYP
0.5x45° TYP
12.0 TYP
5.0 TYP
18.0
9.0
110.00
55.00
45.0°
R TYP
ENGRAVE
6mm HIGH x 0.5mm DEEP
CENTERED ABOUT 30° LINE
(4 PLACES)
4xM5 ON A 45.00 PCD
Ø186.0
120.010
120.000
60.005
60.000
30.0°
30.00
60.00
4xM8
8xM5 EQUISPACED
ON A 51.00 PCD
85.8 TYP
30.0° TYP
31.5
63.0
DO NOT SCALE
A2
UNIVERSITY OF Southampton
School of Engineering Sciences
4kg CONSTANT MASS PLATE
0067-001
0067-004
A

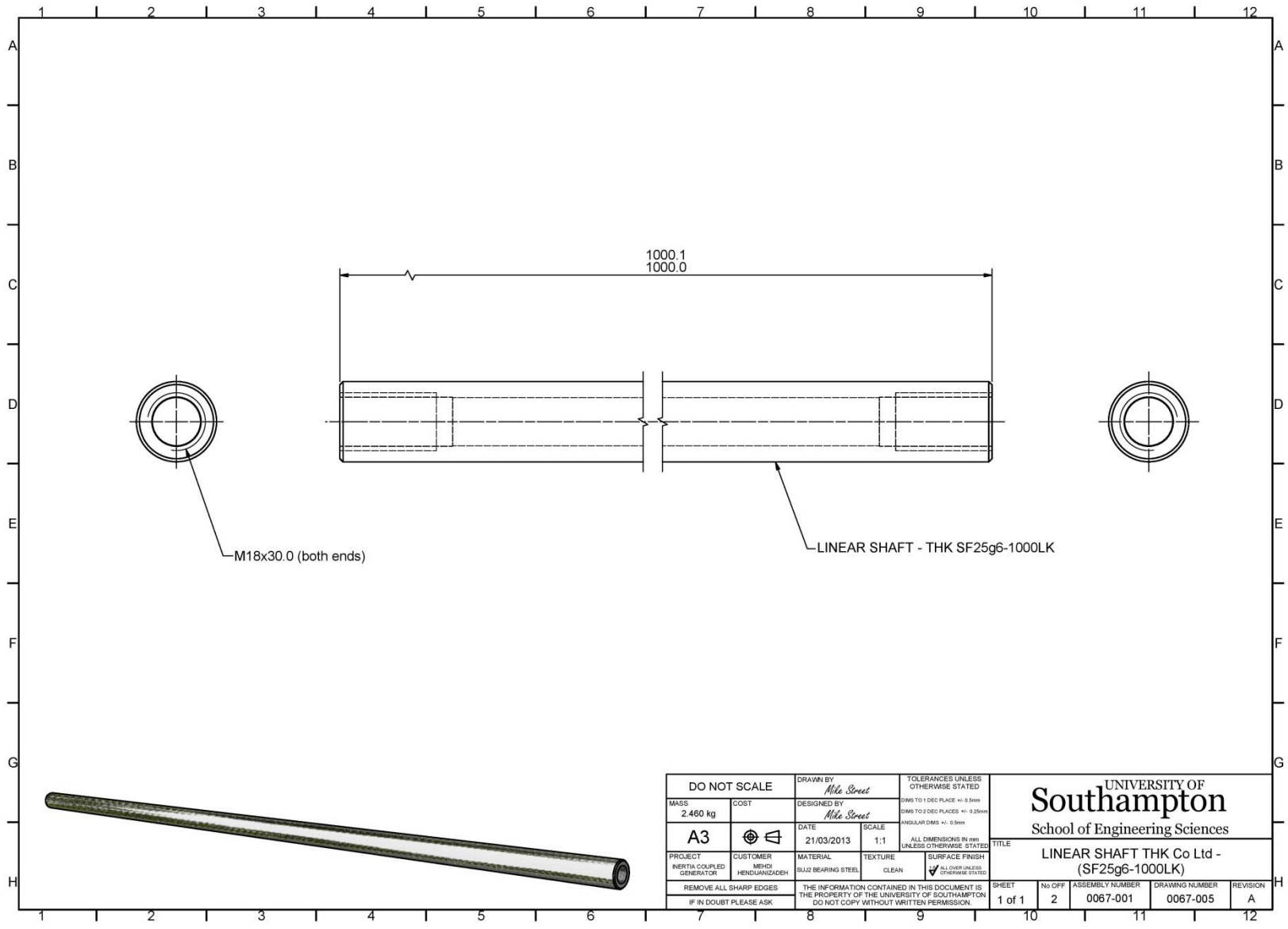

DO NOT SCALE		DRAWN BY Mike Street	TOLERANCES UNLESS OTHERWISE STATED	UNIVERSITY OF Southampton	
MASS 2.460 kg	COST	DESIGNED BY Mike Street	DIMS TO 1 DEC PLACE +/- 0.5mm; DIMS TO 2 DEC PLACES +/- 0.25mm; ANGULAR DIMS +/- 0.5mm	School of Engineering Sciences	
A3		DATE 21/03/2013	SCALE 1:1	ALL DIMENSIONS IN mm UNLESS OTHERWISE STATED	TITLE LINEAR SHAFT THK Co Ltd - (SF25g6-1000LK)
PROJECT INERTIA COUPLED GENERATOR	CUSTOMER MEHDI HENDIJANIZADEH	MATERIAL SUJ2 BEARING STEEL	TEXTURE CLEAN	SURFACE FINISH ALL OVER UNLESS OTHERWISE STATED	
REMOVE ALL SHARP EDGES		THE INFORMATION CONTAINED IN THIS DOCUMENT IS THE PROPERTY OF THE UNIVERSITY OF SOUTHAMPTON DO NOT COPY WITHOUT WRITTEN PERMISSION.		SHEET 1 of 1	No OFF 2
IF IN DOUBT PLEASE ASK				ASSEMBLY NUMBER 0067-001	DRAWING NUMBER 0067-005
					REVISION A

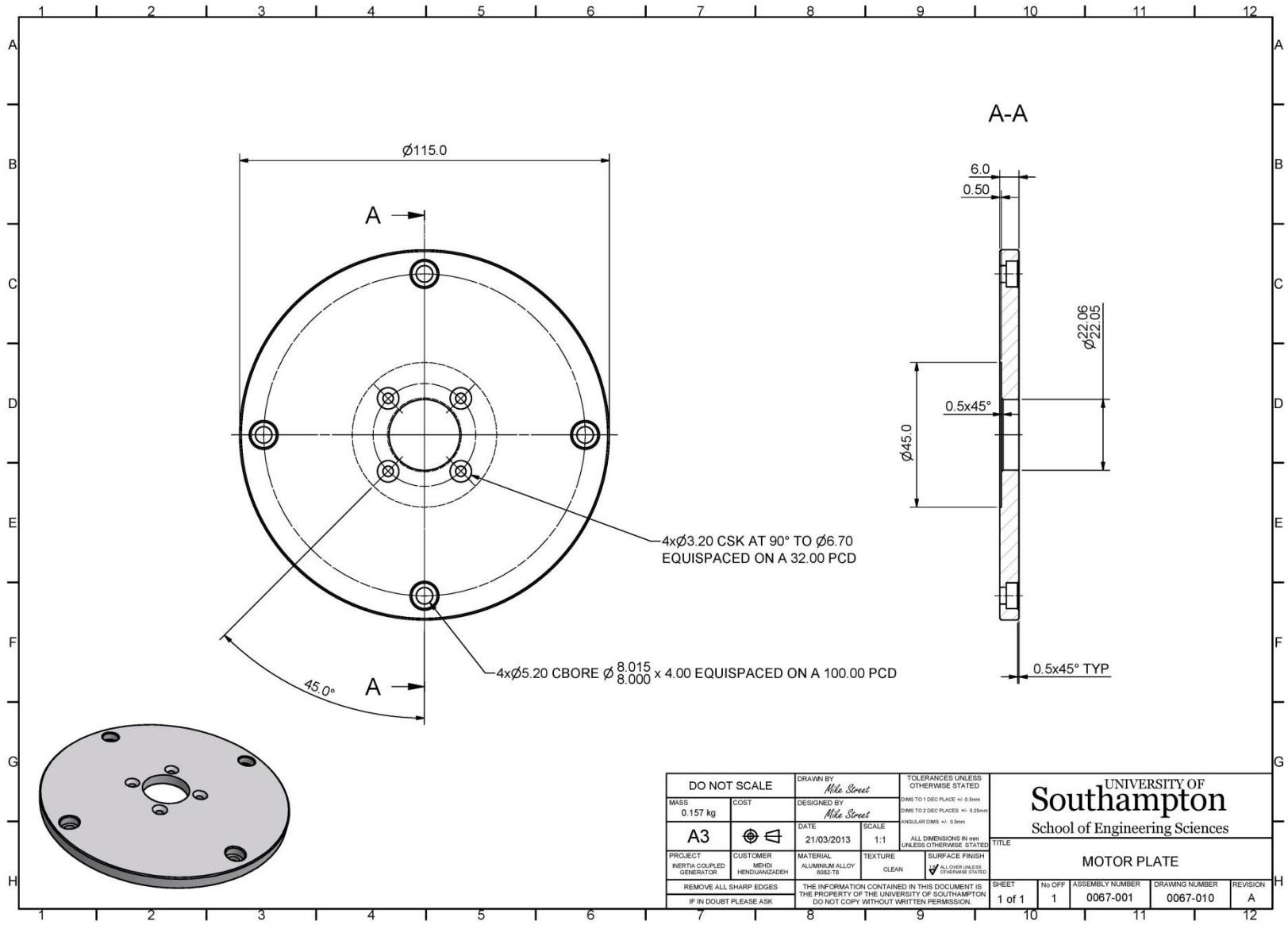

DO NOT SCALE		DRAWN BY: Mike Street		TOLERANCES UNLESS OTHERWISE STATED	UNIVERSITY OF Southampton
MASS: 0.157 kg	COST	DESIGNED BY: Mike Street		DIMS TO 1 DEC PLACE +/- 0.5mm; DIMS TO 2 DEC PLACES +/- 0.25mm; ANGULAR DIMS +/- 0.5mm	School of Engineering Sciences
A3		DATE: 21/03/2013	SCALE: 1:1	ALL DIMENSIONS IN mm UNLESS OTHERWISE STATED	TITLE: MOTOR PLATE
PROJECT: INERTIA COUPLED GENERATOR	CUSTOMER: MEHDI HENDIJANIZADEH	MATERIAL: ALUMINIUM ALLOY 6082-T6	TEXTURE: CLEAN	SURFACE FINISH: ALL OVER UNLESS OTHERWISE STATED	
REMOVE ALL SHARP EDGES		THE INFORMATION CONTAINED IN THIS DOCUMENT IS THE PROPERTY OF THE UNIVERSITY OF SOUTHAMPTON DO NOT COPY WITHOUT WRITTEN PERMISSION.		SHEET: 1 of 1	No OFF: 1
IF IN DOUBT PLEASE ASK				ASSEMBLY NUMBER: 0067-001	DRAWING NUMBER: 0067-010
					REVISION: A

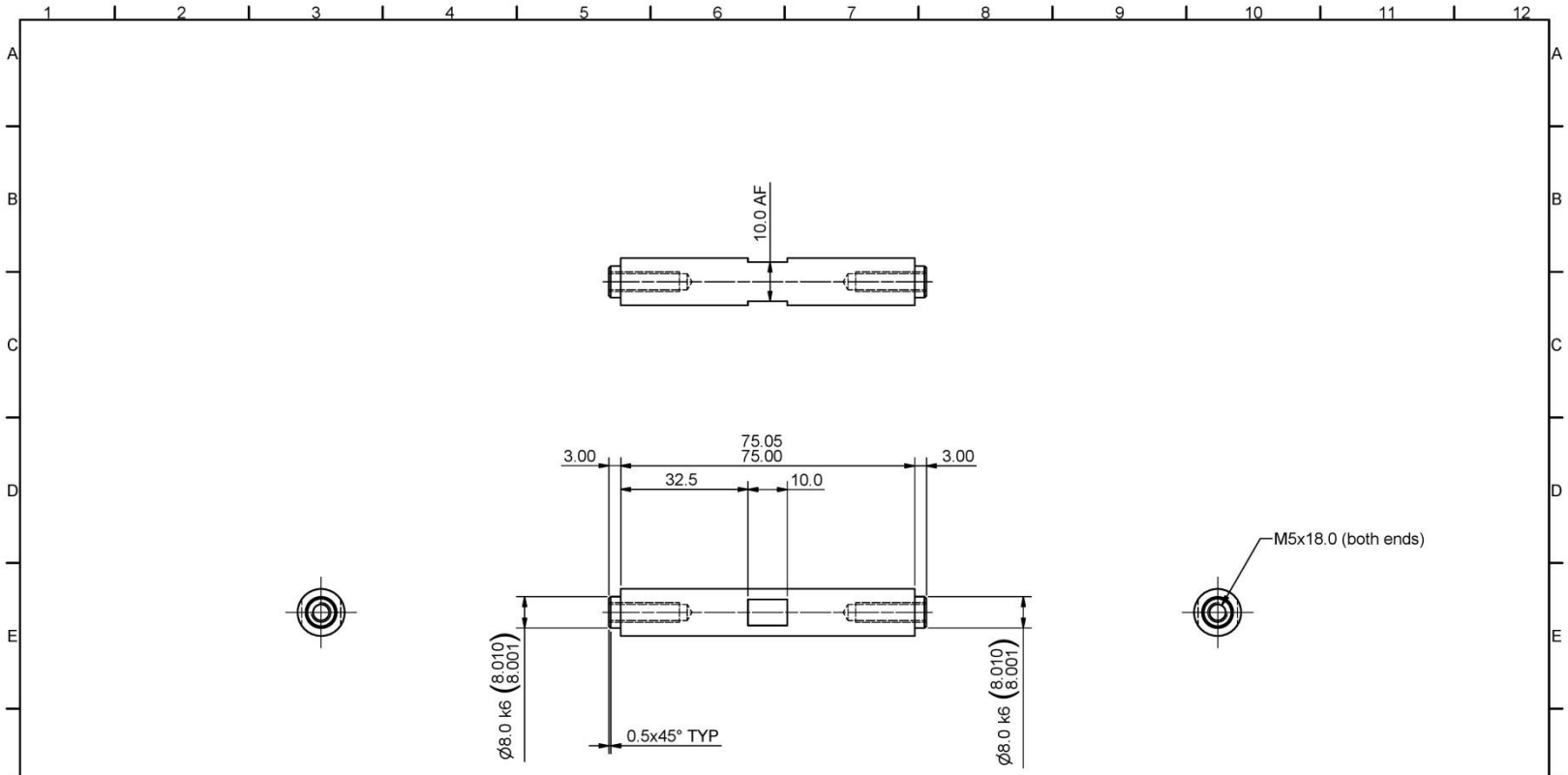

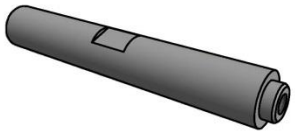

DO NOT SCALE		DRAWN BY: Mike Street	TOLERANCES UNLESS OTHERWISE STATED: DIMS TO 1 DEC PLACE +/- 0.5mm; DIMS TO 2 DEC PLACES +/- 0.25mm; ANGULAR DIMS +/- 0.5mm	UNIVERSITY OF Southampton, School of Engineering Sciences	
MASS: N/A	COST	DESIGNED BY: Mike Street			
A3		DATE: 21/03/2013	SCALE: 1:1	ALL DIMENSIONS IN mm UNLESS OTHERWISE STATED	TITLE: MOTOR POST
PROJECT: INERTIA COUPLED GENERATOR	CUSTOMER: MEHDI HENDIJANIZADEH	MATERIAL: ALUMINIUM ALLOY 6082-T6	TEXTURE: CLEAN	SURFACE FINISH: ALL OVER UNLESS OTHERWISE STATED	
REMOVE ALL SHARP EDGES		THE INFORMATION CONTAINED IN THIS DOCUMENT IS THE PROPERTY OF THE UNIVERSITY OF SOUTHAMPTON DO NOT COPY WITHOUT WRITTEN PERMISSION.			
IF IN DOUBT PLEASE ASK					

SHEET	No OFF	ASSEMBLY NUMBER	DRAWING NUMBER	REVISION
1 of 1	4	0067-001	0067-011	A

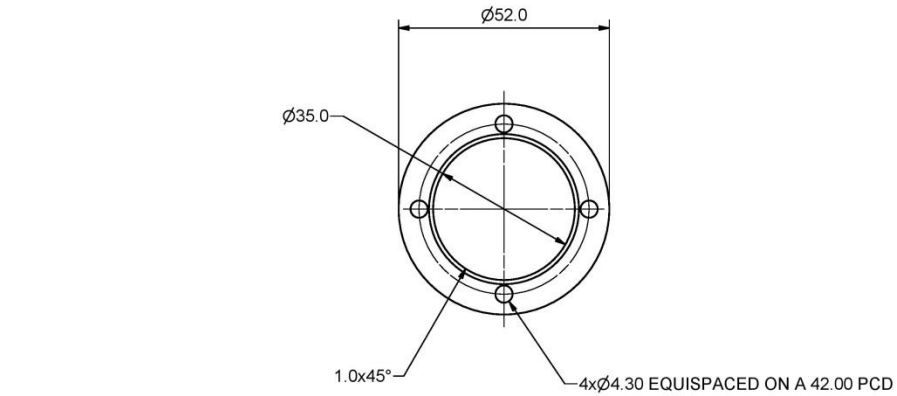

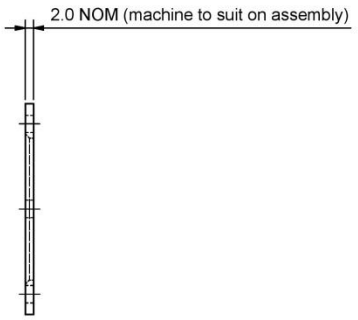

DO NOT SCALE		DRAWN BY: Mike Street		TOLERANCES UNLESS OTHERWISE STATED	UNIVERSITY OF Southampton
MASS: 0.018 kg	COST	DESIGNED BY: Mike Street		DIMS TO 1 DEC PLACE +/- 0.5mm; DIMS TO 2 DEC PLACES +/- 0.25mm; ANGULAR DIMS +/- 0.5mm	School of Engineering Sciences
A3		DATE: 21/03/2013	SCALE: 1:1	ALL DIMENSIONS IN mm UNLESS OTHERWISE STATED	TITLE: SHIM
PROJECT: INERTIA COUPLED GENERATOR	CUSTOMER: MEHDI HENDIJANIZADEH	MATERIAL: BRASS	TEXTURE: CLEAN	SURFACE FINISH: ALL OVER UNLESS OTHERWISE STATED	
REMOVE ALL SHARP EDGES		THE INFORMATION CONTAINED IN THIS DOCUMENT IS THE PROPERTY OF THE UNIVERSITY OF SOUTHAMPTON DO NOT COPY WITHOUT WRITTEN PERMISSION.		SHEET: 1 of 1	No OFF: 1
IF IN DOUBT PLEASE ASK				ASSEMBLY NUMBER: 0067-001	DRAWING NUMBER: 0067-014
					REVISION: A

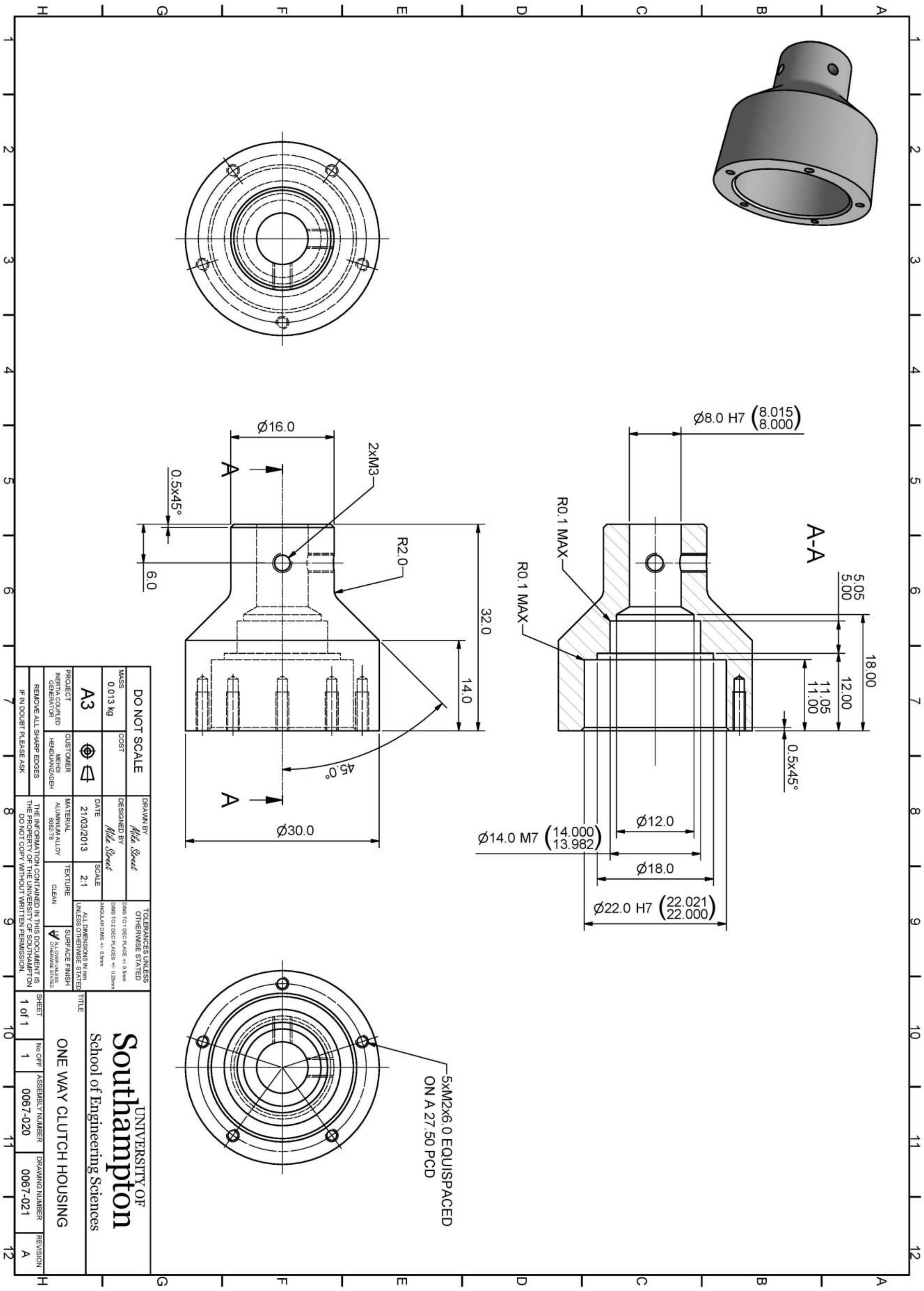

A-A
A
Ø16.0
Ø30.0
2xM3
R2.0
0.5x45°
6.0
32.0
14.0
45.0°
Ø8.0 H7 (8.015 8.000)
R0.1 MAX
5.05
5.00
18.00
12.00
11.05
11.00
0.5x45°
Ø12.0
Ø14.0 M7 (14.000 13.982)
Ø18.0
Ø22.0 H7 (22.021 22.000)
5xM2x6.0 EQUISPACED ON A 27.50 PCD
DO NOT SCALE
MASS
0.013 kg
COST
A3
PROJECT
INERTIA COUPLED GENERATOR
CUSTOMER
MEHDI HENDIJANIZADEH
REMOVE ALL SHARP EDGES
IF IN DOUBT PLEASE ASK
DRAWN BY
DESIGNED BY
DATE
21/03/2013
SCALE
2:1
MATERIAL
ALUMINIUM ALLOY 6082-T6
TEXTURE
CLEAN
THE INFORMATION CONTAINED IN THIS DOCUMENT IS THE PROPERTY OF THE UNIVERSITY OF SOUTHAMPTON DO NOT COPY WITHOUT WRITTEN PERMISSION.
TOLERANCES UNLESS OTHERWISE STATED
ALL DIMENSIONS IN mm UNLESS OTHERWISE STATED
SURFACE FINISH
UNIVERSITY OF Southampton
School of Engineering Sciences
TITLE
ONE WAY CLUTCH HOUSING
SHEET
1 of 1
No OFF
1
ASSEMBLY NUMBER
0067-020
DRAWING NUMBER
0067-021
REVISION
A

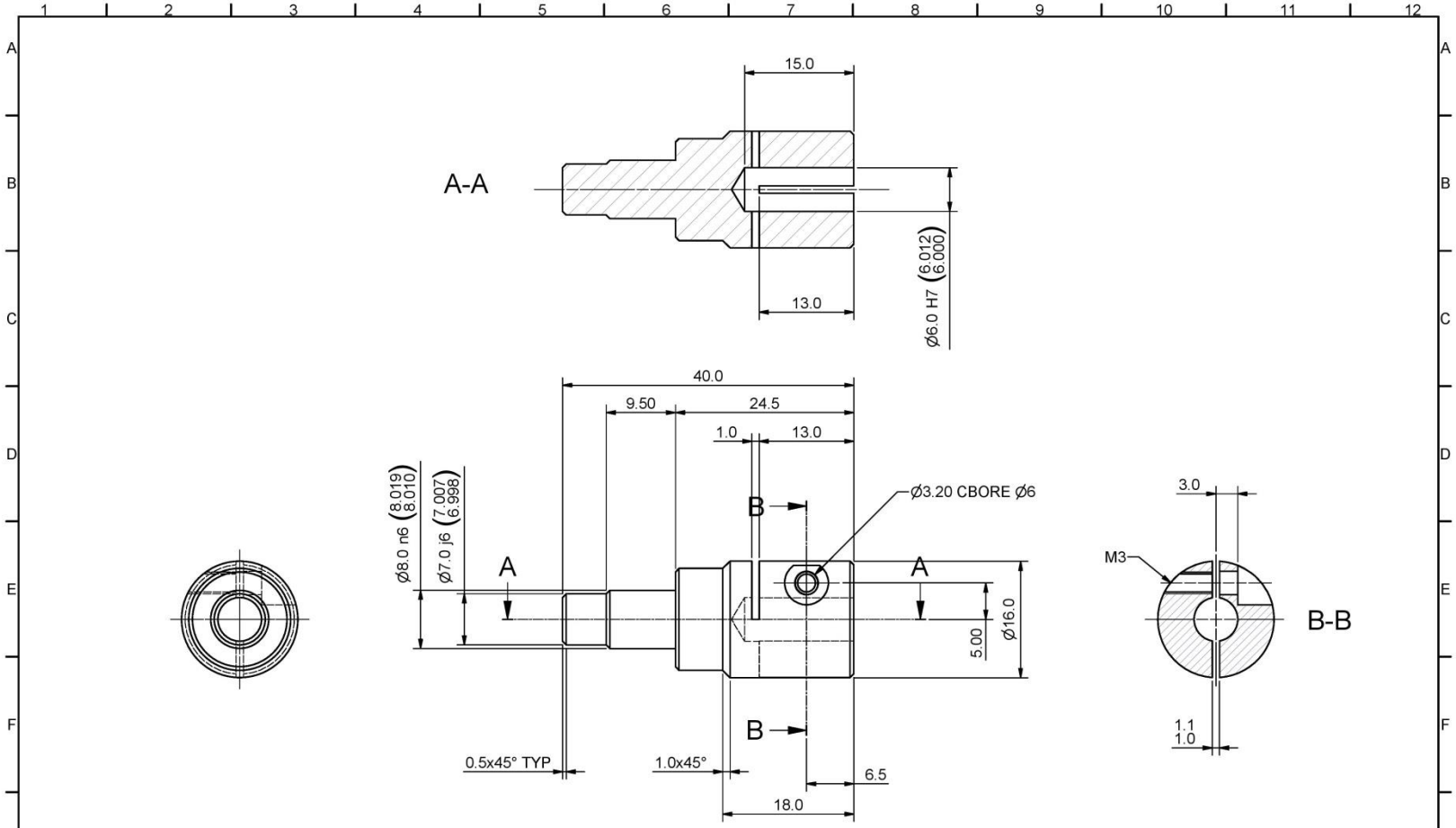

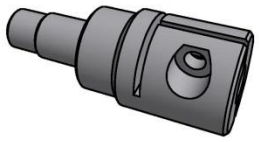

DO NOT SCALE		DRAWN BY: Mike Street		TOLERANCES UNLESS OTHERWISE STATED	UNIVERSITY OF Southampton
MASS: N/A	COST	DESIGNED BY: Mike Street		DIMS TO 1 DEC PLACE +/- 0.5mm; DIMS TO 2 DEC PLACES +/- 0.25mm; ANGULAR DIMS +/- 0.5mm	School of Engineering Sciences
A3		DATE: 21/03/2013	SCALE: 2:1	ALL DIMENSIONS IN mm UNLESS OTHERWISE STATED	TITLE: ONE WAY CLUTCH STUB SHAFT
PROJECT: INERTIA COUPLED GENERATOR	CUSTOMER: MEHDI HENDIJANIZADEH	MATERIAL: MILD STEEL	TEXTURE: OIL FINISH	SURFACE FINISH: ALL OVER UNLESS OTHERWISE STATED	
REMOVE ALL SHARP EDGES		THE INFORMATION CONTAINED IN THIS DOCUMENT IS THE PROPERTY OF THE UNIVERSITY OF SOUTHAMPTON DO NOT COPY WITHOUT WRITTEN PERMISSION.			
IF IN DOUBT PLEASE ASK					

SHEET	No OFF	ASSEMBLY NUMBER	DRAWING NUMBER	REVISION
1 of 1	1	0067-021	0067-023	A

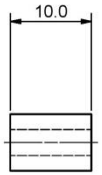

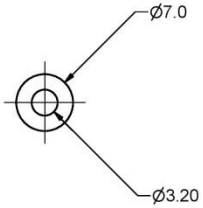

DO NOT SCALE		DRAWN BY: Mike Street		TOLERANCES UNLESS OTHERWISE STATED	UNIVERSITY OF Southampton
MASS: 0.003 kg	COST:	DESIGNED BY: Mike Street		DIMS TO 1 DEC PLACE +/- 0.5mm; DIMS TO 2 DEC PLACES +/- 0.25mm; ANGULAR DIMS +/- 0.5mm	School of Engineering Sciences
A3		DATE: 21/03/2013	SCALE: 2:1	ALL DIMENSIONS IN mm UNLESS OTHERWISE STATED	TITLE: SHAFT ENCODER POST
PROJECT: INERTIA COUPLED GENERATOR	CUSTOMER: MEHDI HENDIJANIZADEH	MATERIAL: BRASS	TEXTURE: CLEAN	SURFACE FINISH: ALL OVER UNLESS OTHERWISE STATED	
REMOVE ALL SHARP EDGES		THE INFORMATION CONTAINED IN THIS DOCUMENT IS THE PROPERTY OF THE UNIVERSITY OF SOUTHAMPTON DO NOT COPY WITHOUT WRITTEN PERMISSION.		SHEET: 1 of 1	No OFF: 2	ASSEMBLY NUMBER: 0067-001	DRAWING NUMBER: 0067-015	REVISION: A
IF IN DOUBT PLEASE ASK					

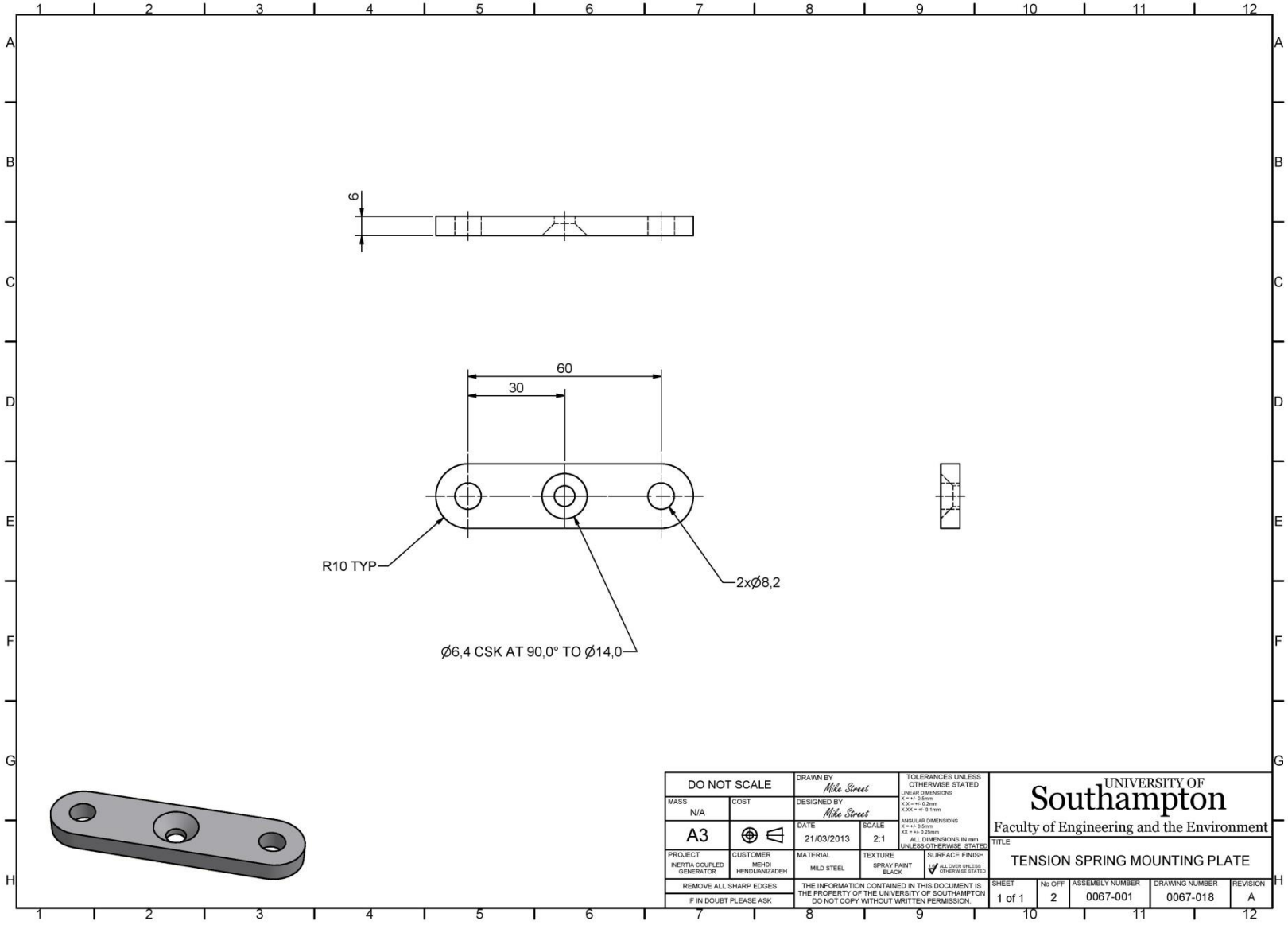

DO NOT SCALE		DRAWN BY: Mike Street	TOLERANCES UNLESS OTHERWISE STATED: LINEAR DIMENSIONS X = +/- 0.5mm, X.X = +/- 0.2mm, X.XX = +/- 0.1mm; ANGULAR DIMENSIONS X = +/- 0.5mm, XX = +/- 0.25mm; ALL DIMENSIONS IN mm UNLESS OTHERWISE STATED	UNIVERSITY OF Southampton, Faculty of Engineering and the Environment	
MASS: N/A	COST	DESIGNED BY: Mike Street			
A3		DATE: 21/03/2013	SCALE: 2:1	TITLE: TENSION SPRING MOUNTING PLATE	
PROJECT: INERTIA COUPLED GENERATOR	CUSTOMER: MEHDI HENDIJANIZADEH	MATERIAL: MILD STEEL	TEXTURE: SPRAY PAINT BLACK	SURFACE FINISH: ALL OVER UNLESS OTHERWISE STATED	
REMOVE ALL SHARP EDGES		THE INFORMATION CONTAINED IN THIS DOCUMENT IS THE PROPERTY OF THE UNIVERSITY OF SOUTHAMPTON DO NOT COPY WITHOUT WRITTEN PERMISSION.			
IF IN DOUBT PLEASE ASK					

SHEET	No OFF	ASSEMBLY NUMBER	DRAWING NUMBER	REVISION
1 of 1	2	0067-001	0067-018	A

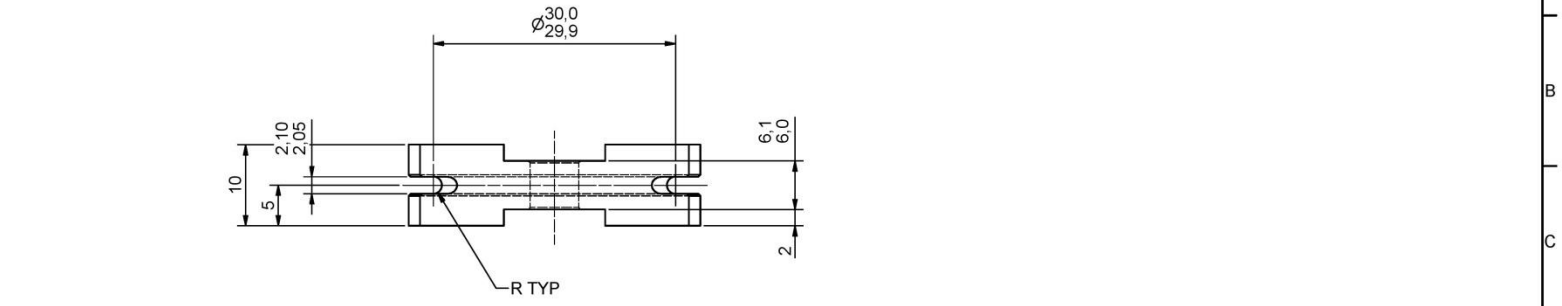

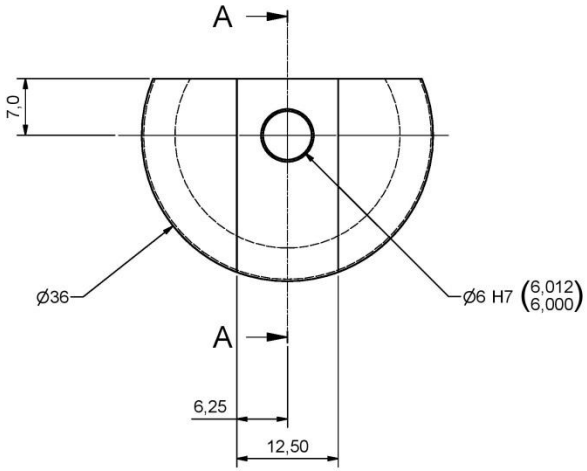

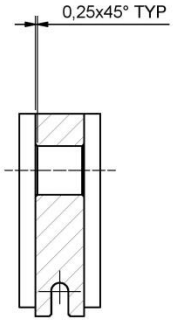

A-A

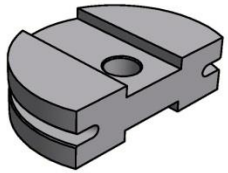

DO NOT SCALE		DRAWN BY Mike Street	TOLERANCES UNLESS OTHERWISE STATED	UNIVERSITY OF Southampton					
MASS N/A	COST	DESIGNED BY Mike Street	LINEAR DIMENSIONS X = +/- 0.5mm X.X = +/- 0.2mm X.XX = +/- 0.1mm	Faculty of Engineering and the Environment					
A3		DATE 21/03/2013	SCALE 2:1	ANGULAR DIMENSIONS X = +/- 0.5mm XX = +/- 0.25mm	TITLE TENSION SPRING PULLEY				
PROJECT INERTIA COUPLED GENERATOR	CUSTOMER MEHDI HENDIJANIZADEH	MATERIAL ALUMINIUM ALLOY 6082-T6	TEXTURE CLEAN	ALL DIMENSIONS IN mm UNLESS OTHERWISE STATED	SURFACE FINISH ALL OVER UNLESS OTHERWISE STATED				
REMOVE ALL SHARP EDGES		THE INFORMATION CONTAINED IN THIS DOCUMENT IS THE PROPERTY OF THE UNIVERSITY OF SOUTHAMPTON DO NOT COPY WITHOUT WRITTEN PERMISSION.		SHEET 1 of 1	No OFF 4	ASSEMBLY NUMBER 0067-001	DRAWING NUMBER 0067-013	REVISION A	
IF IN DOUBT PLEASE ASK									

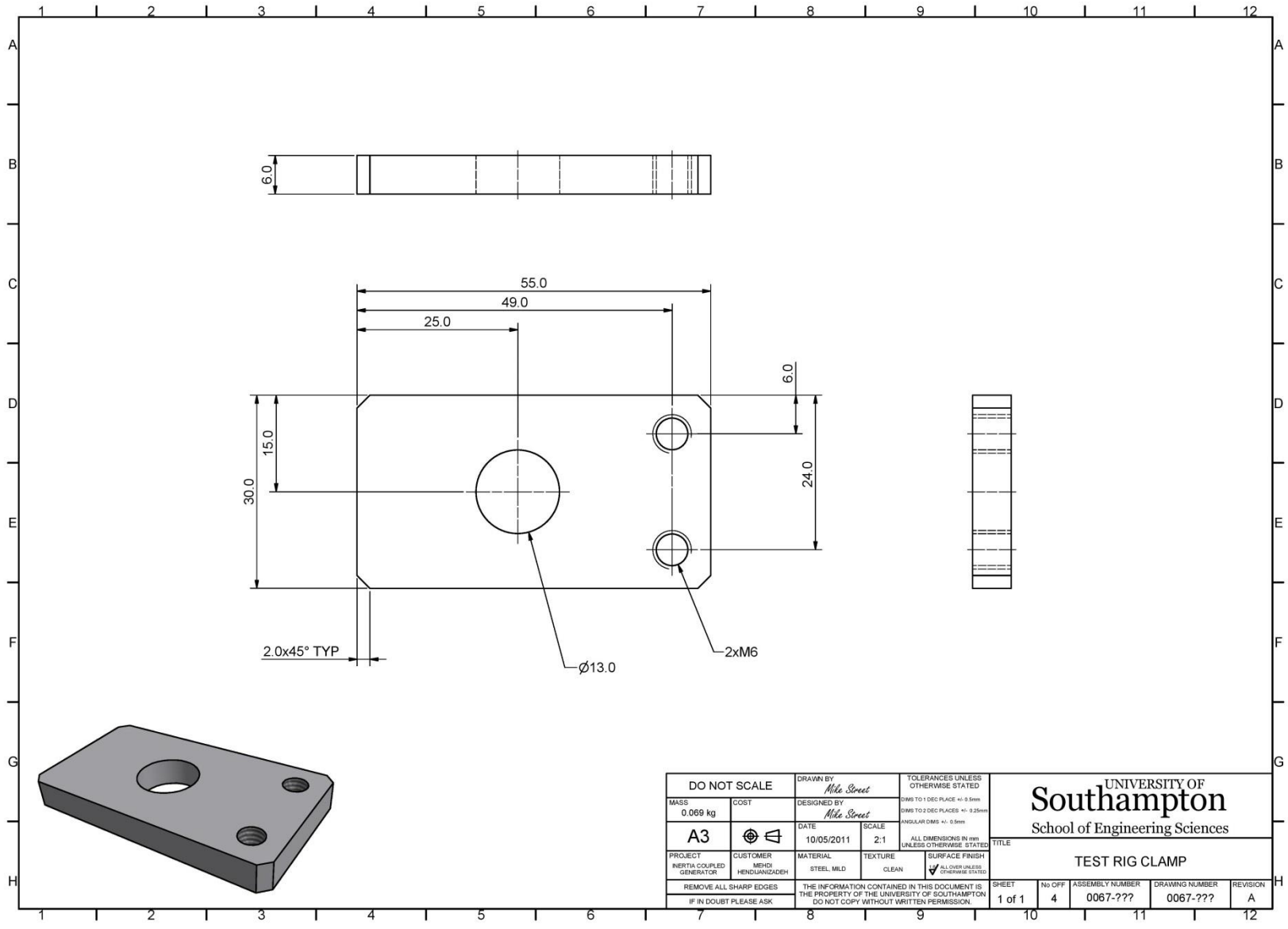

DO NOT SCALE		DRAWN BY: Mike Street		TOLERANCES UNLESS OTHERWISE STATED	UNIVERSITY OF Southampton
MASS: 0.069 kg	COST	DESIGNED BY: Mike Street		DIMS TO 1 DEC PLACE +/- 0.5mm; DIMS TO 2 DEC PLACES +/- 0.25mm; ANGULAR DIMS +/- 0.5mm	School of Engineering Sciences
A3		DATE: 10/05/2011	SCALE: 2:1	ALL DIMENSIONS IN mm UNLESS OTHERWISE STATED	TITLE: TEST RIG CLAMP
PROJECT: INERTIA COUPLED GENERATOR	CUSTOMER: MEHDI HENDIJANIZADEH	MATERIAL: STEEL, MILD	TEXTURE: CLEAN	SURFACE FINISH: ALL OVER UNLESS OTHERWISE STATED	
REMOVE ALL SHARP EDGES		THE INFORMATION CONTAINED IN THIS DOCUMENT IS THE PROPERTY OF THE UNIVERSITY OF SOUTHAMPTON DO NOT COPY WITHOUT WRITTEN PERMISSION.		SHEET: 1 of 1	No OFF: 4
IF IN DOUBT PLEASE ASK				ASSEMBLY NUMBER: 0067-???	DRAWING NUMBER: 0067-???
					REVISION: A

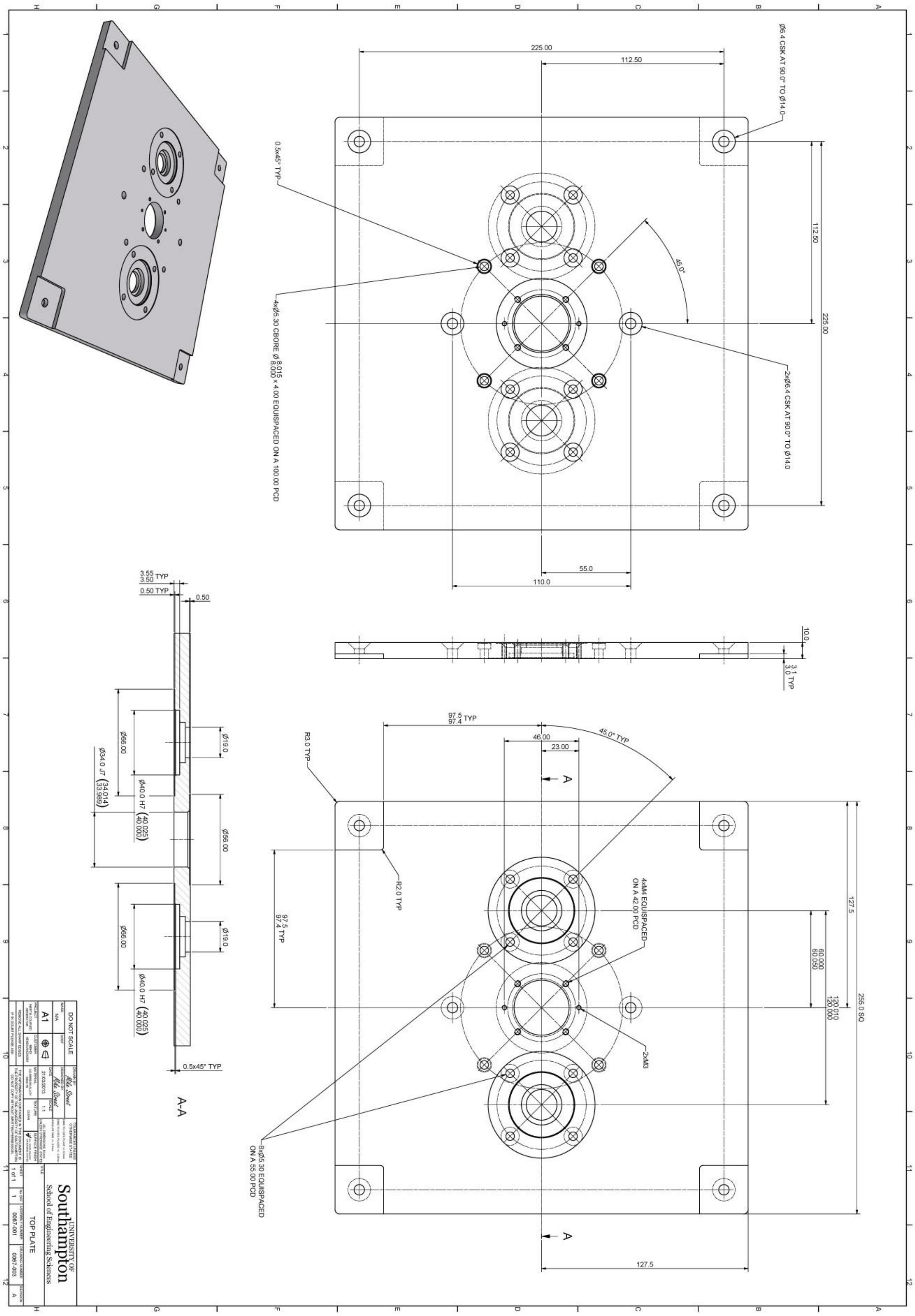
UNIVERSITY OF
Southampton
School of Engineering Sciences
TOP PLATE
0067-001
0067-003
DO NOT SCALE
A-A

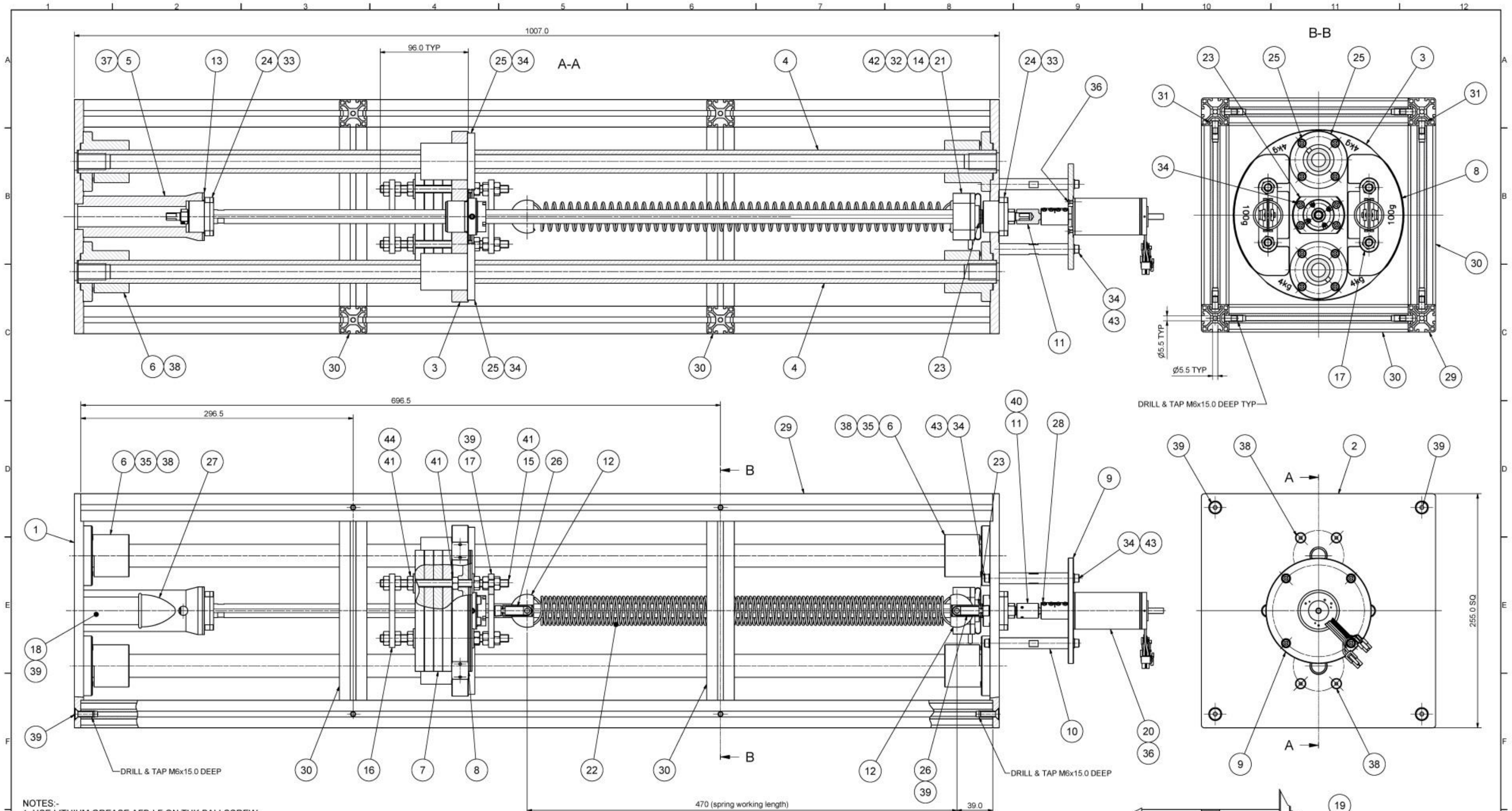

NOTES:-
1. USE LITHIUM GREASE AFB-LF ON THK BALLSCREW
2. PARTS 29 & 30 TO BE SUPPLIED PRE DRILLED BY "MACHINE BUILDING SYSTEMS Ltd"

PARTS LIST

ITEM	PART No	DESCRIPTION	QTY	MATERIAL
44	-	LARGE DIAMETER PLAIN WASHER - M8	8	MILD STEEL
43	-	PLAIN WASHER - M5	8	MILD STEEL
42	-	PLAIN WASHER - M3	2	MILD STEEL
41	-	HEX NUT - M8	28	MILD STEEL
40	-	HEX SOC SET SCREW - M3 x 4	2	MILD STEEL
39	-	HEX SOC COUNTERSUNK SCREW - M6 x 20	14	MILD STEEL
38	-	HEX SOC COUNTERSUNK SCREW - M5 x 20	16	MILD STEEL
37	-	HEX SOC COUNTERSUNK SCREW - M4 x 20	4	MILD STEEL
36	-	HEX SOC COUNTERSUNK SCREW - M3 x 10	4	MILD STEEL
35	-	HEX SOC CAP HD SCREW - M5 x 25	8	MILD STEEL
34	-	HEX SOC CAP HD SCREW - M5 x 20	20	MILD STEEL
33	-	HEX SOC CAP HD SCREW - M4 x 16	8	MILD STEEL
32	-	HEX SOC CAP HD SCREW - M3 x 16	2	MILD STEEL
31	-	STANDARD FASTENING SET 6 - ITEM 0.0.419.14	18	STEEL
30	-	CROSS BEAM - ITEM PROFILE 6 (0.0.419.06) 30x30 LIGHTx195mm LONG	8	ALUMINIUM
29	-	CORNER POST - ITEM PROFILE 6 (0.0.419.06) 30x30 LIGHTx993mm LONG	4	ALUMINIUM
28	-	COUPLING 6x6mm BORE - RADIO SPARES (435-1166)	1	ALUMINIUM
27	-	ANTI VIBRATION BUFFER - ONDRIVES (D-PAR-8-30-36)	2	RUBBER / STEEL
26	-	LONG SERIES CLEVIS - ONDRIVES (CLL-6)	4	STEEL
25	-	LINEAR BUSHING - THK (LMF 25)	2	STEEL
24	-	BALL SCREW FIXED SIDE SUPPORT - THK (FK10)	2	STEEL
23	-	BALLSCREW - THK (BLK1510-5.6_ZZ_+940L_T_H3H3)	1	STEEL
22	-	TENSION SPRING - THE ACTIVE SPRING Co (wire Dia=2.03mm, free length=160mm, No off coils=50)	2	DRAWN STEELto BS5216
21	-	HOLLOW SHAFT ENCODER - INDUSTRIAL ENCODERS (51HA-15-4A8D2DRUB-20)	1	VARIOUS
20	-	DC MOTOR - MAXON MOTOR (EC-max-40-393025)	1	VARIOUS
19	0067-020	SUB ASSEMBLY OF ONE WAY CLUTCH	1	VARIOUS
18	0067-019	BUFFER POST	2	ALUMINIUM ALLOY 6082-T6
17	0067-018	TENSION SPRING MOUNTING PLATE	2	MILD STEEL
16	0067-017	BUFFER PLATE	2	MILD STEEL
15	0067-016	VARIABLE MASS SCREW	4	MILD STEEL
14	0067-015	SHAFT ENCODER POST	2	BRASS
13	0067-014	SHIM	1	BRASS
12	0067-013	TENSION SPRING PULLEY	4	ALUMINIUM ALLOY 6082-T6
11	0067-012	BALL SCREW SHAFT ADAPTOR	1	MILD STEEL
10	0067-011	MOTOR POST	4	ALUMINIUM ALLOY 6082-T6
9	0067-010	MOTOR PLATE	1	ALUMINIUM ALLOY 6082-T6
8	0067-009	100g VARIABLE MASS	4	MILD STEEL
7	0067-008	500g VARIABLE MASS	8	MILD STEEL
6	0067-007	LINEAR SHAFT MOUNTING	4	ALUMINIUM ALLOY 6082-T6
5	0067-006	BALL SCREW LOWER SPACER	1	ALUMINIUM ALLOY 6082-T6
4	0067-005	LINEAR SHAFT THK Co Ltd - (SF25g6-1000LK)	2	SUJ2 BEARING STEEL
3	0067-004	4kg CONSTANT MASS PLATE	1	MILD STEEL
2	0067-003	TOP PLATE	1	ALUMINIUM ALLOY 6082-T6
1	0067-002	BASE PLATE	1	ALUMINIUM ALLOY 6082-T6

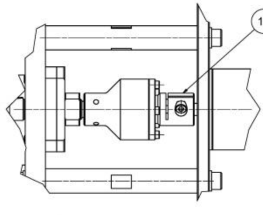

PARTIAL VIEW SHOWING ONE WAY CLUTCH COUPLING REPLACE ITEMS 11 & 28 WITH ITEM 19

DO NOT SCALE | A1 | DATE 21/03/2013 | SCALE 1:2

UNIVERSITY OF Southampton
School of Engineering Sciences

SUB ASSEMBLY OF INERTIA COUPLED GENERATOR

SHEET 1 of 2 | No OFF 1 | ASSEMBLY NUMBER 0067-000 | DRAWING NUMBER 0067-001 | REVISION A

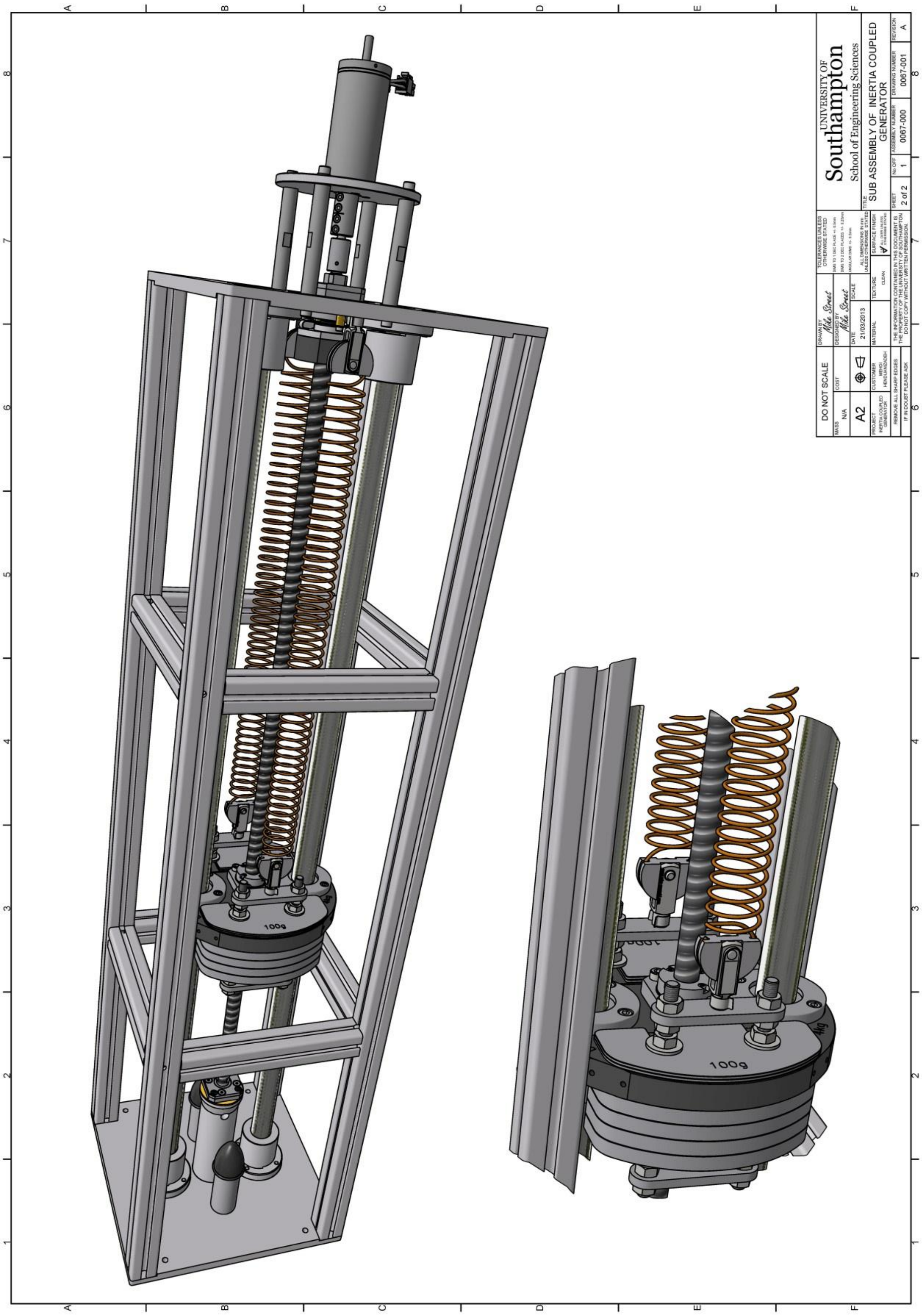
DO NOT SCALE
MASS
N/A
COST
A2
PROJECT
INERTIA COUPLED GENERATOR
CUSTOMER
MEHDI HENDIJANIZADEH
REMOVE ALL SHARP EDGES
IF IN DOUBT PLEASE ASK
DRAWN BY
Mike Street
DESIGNED BY
Mike Street
DATE
21/03/2013
SCALE
MATERIAL
TEXTURE
CLEAN
THE INFORMATION CONTAINED IN THIS DOCUMENT IS THE PROPERTY OF THE UNIVERSITY OF SOUTHAMPTON DO NOT COPY WITHOUT WRITTEN PERMISSION.
TOLERANCES UNLESS OTHERWISE STATED
ALL DIMENSIONS IN mm UNLESS OTHERWISE STATED
SURFACE FINISH
UNIVERSITY OF
Southampton
School of Engineering Sciences
TITLE
SUB ASSEMBLY OF INERTIA COUPLED GENERATOR
SHEET
2 of 2
No OFF
1
ASSEMBLY NUMBER
0067-000
DRAWING NUMBER
0067-001
REVISION
A
100g

ITEM	PART No	DESCRIPTION	QTY	MATERIAL
8	-	HEX SOC CAP HD SCREW - M3 x 8	1	MILD STEEL
7	-	HEX SOC SET SCREW - M2.5 x 4	2	MILD STEEL
6	-	HEX SOC CAP HD SCREW - M2 x 8	5	MILD STEEL
5	-	DEEP GROOVE BALL BEARING - SKF 628/7-2Z	1	STEEL
4	-	SPRAG CLUTCH - CROSS + MORSE (CKK8)	1	STEEL
3	0067-023	ONE WAY CLUTCH STUB SHAFT	1	MILD STEEL
2	0067-022	ONE WAY CLUTCH RETAINING PLATE	1	ALUMINIUM ALLOY 6082-T6
1	0067-021	ONE WAY CLUTCH HOUSING	1	ALUMINIUM ALLOY 6082-T6

PARTS LIST

NOTE:-

1. THE COUPLING ASSEMBLY MUST DRIVE IN AN ANTI CLOCKWISE DIRECTION, ITEM 4 MUST BE PRESSED ONTO ITEM 2 RESPECTIVELY.

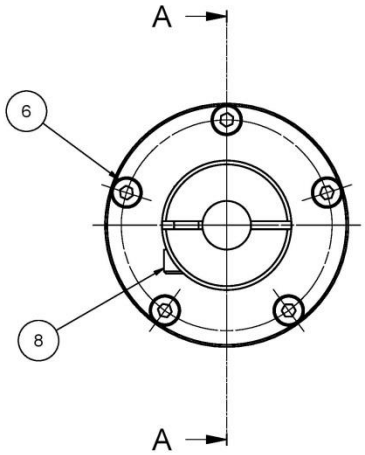

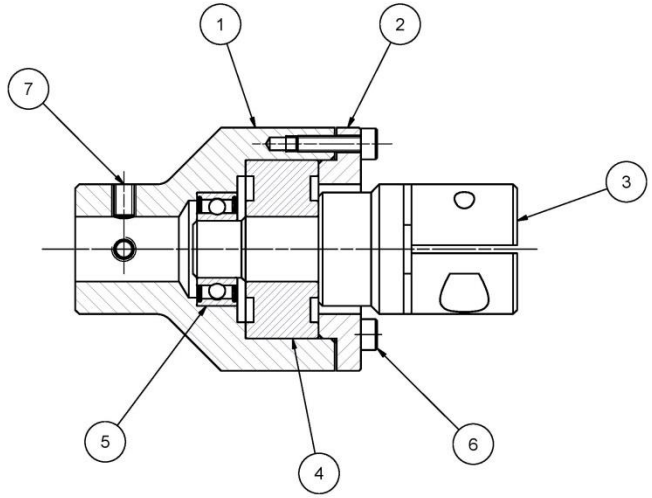

A-A

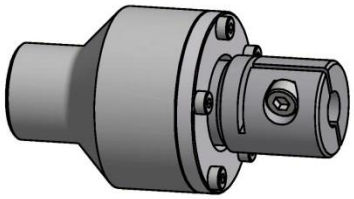

DO NOT SCALE		DRAWN BY: Mike Street	TOLERANCES UNLESS OTHERWISE STATED	UNIVERSITY OF Southampton
MASS: N/A	COST	DESIGNED BY: Mike Street	DIMS TO 1 DEC PLACE +/- 0.5mm; DIMS TO 2 DEC PLACES +/- 0.25mm; ANGULAR DIMS +/- 0.5mm	School of Engineering Sciences
A3		DATE: 21/03/2013	SCALE: 2:1	ALL DIMENSIONS IN mm UNLESS OTHERWISE STATED
PROJECT: INERTIA COUPLED GENERATOR	CUSTOMER: MEHDI HENDIANIZADEH	MATERIAL	TEXTURE: CLEAN	SURFACE FINISH: ALL OVER UNLESS OTHERWISE STATED
REMOVE ALL SHARP EDGES		THE INFORMATION CONTAINED IN THIS DOCUMENT IS THE PROPERTY OF THE UNIVERSITY OF SOUTHAMPTON. DO NOT COPY WITHOUT WRITTEN PERMISSION.		TITLE: SUB ASSEMBLY OF ONE WAY CLUTCH
IF IN DOUBT PLEASE ASK				

SHEET	No OFF	ASSEMBLY NUMBER	DRAWING NUMBER	REVISION
1 of 1	1	0067-001	0067-020	A

References

[1] Mahdi Rasouli and Louis Soo Jay Phee, “Energy sources and their development for application in medical devices,” *Expert Review of Medical Devices,* vol. 7, no. 5, pp. 693-709, 2010.

[2] Martin Deterre, Bertrand Boutaud, Renzo Dalmolin, Sébastien Boisseau and Jean-Jacques Chaillout, “Energy harvesting system for cardiac implant applications,” in *Symposium on Design, Test, Integration and Packaging of MEMS/MOEMS* , Aix-en-Provence, France, 2011.

[3] Winston K.G. Seah, Zhi Ang Eu and Hwee-Pink Tan, “Wireless sensor networks powered by ambient energy harvesting (WSN-HEAP) - Survey and challenges,” in *Wireless Communication, Vehicular Technology, Information Theory and Aerospace & Electronic Systems Technology*, Aalborg, 2009.

[4] John Paul M. Torregoza, In-Yeup Kong and Won-Joo Hwang, “Wireless Sensor Network Renewable Energy Source Life Estimation,” in *Communications and Electronics, First International Conference on*, Hanoi, 2006.

[5] A.B. Kanase-Patil, R.P. Saini and M.P. Sharma, “Integrated renewable energy systems for off grid rural electrification of remote area,” *Renewable Energy,* vol. 35, no. 6, p. 1342–1349, 2010.

[6] Bert J.M. de Vriesa, Detlef P. van Vuurenb and Monique M. Hoogwijka, “Renewable energy sources: Their global potential for the first-half of the 21st century at a global level: An integrated approach,” *Energy Policy,* vol. 35, no. 4, p. 2590–2610, 2007.

[7] Simon Perrya,Jin Klemes and Igor Bulatova, “Integrating waste and renewable energy to reduce the carbon footprint,” *Energy,* vol. 33, no. 10, p. 1489–1497, 2008.

[8] J. Krikke, “Sunrise for energy harvesting products,” *IEEE Pervasive Computing,* vol. 4, no. 1, pp. 4-5, 2005.

[9] Junji Hirokane, Tatsuo Saga, Tetsuroh Muramatsu and Isao Shirakawa, “History of contribution of photovoltaic cells to telecommunications,” in *Conference on the History of Telecommunications*, Madrid, 2010.

[10] H. Jabbar, Y.S. Song and T.T. Jeong, “RF energy harvesting system and circuits for charging of mobile devices,” *IEEE Transactions on Consumer Electronics*, vol. 56, no. 1, pp. 247-253, 2010.

[11] Enrico Barbier, “Geothermal energy technology and current status: an overview,” *Renewable and Sustainable Energy Reviews*, vol. 6, no. 1, pp. 3-65, 2002.

[12] D. C. Hoang, Y. K. Tan, H. B. Cheng and S.K. Panda, “Thermal energy harvesting from human warmth for wireless body area network in medical healthcare system,” in *International Conference on Power Electronics and Drive Systems*, Taipei, 2009.

[13] Raul Morais, Samuel G. Matos, Miguel A. Fernandes, Antonio L.G. Valente, Salviano F.S.P. Soares, P.J.S.G. Ferreira and M.J.C.S. Reis, “Sun, wind and water flow as energy supply for small,” *Computers and Electronics in Agriculture*, vol. 64, no. 2, p. 120–132, 2008.

[14] G.M. Joselin Herberta, S. Iniyanb, E. Sreevalsanc and S. Rajapandiand, “A review of wind energy technologies,” *Renewable and Sustainable Energy Reviews*, vol. 11, no. 6, p. 1117–1145, 2007.

[15] Dibin Zhu and Steve Beeby, “Kinetic energy harvesting,” in *Energy Harvesting Systems*, New York, Springer, 2011, pp. 1-77.

[16] Lei Zuo and Xiudong Tang, “Large-scale vibration energy harvesting,” *Journal of Intelligent Material Systems and Structures*, vol. 24, no. 11, pp. 1405-1430, 2013.

[17] Alireza Khaligh, Peng Zeng and Cong Zheng, “Kinetic Energy harvesting using piezoelectric and electromagnetic technologies—State of the art,” *IEEE Transaction on Industrial Electronics*, vol. 57, no. 3, pp. 850-859, 2010.

[18] Paul D. Mitcheson, Eric M. Yeatman, G. Kondala Rao, Andrew S. Holmes and Tim C. Green, "Energy Harvesting From Human and Machine Motion for Wireless Electronic Devices," *Proceedings of the IEEE,* vol. 96, no. 9, pp. 1457-1486, 2008.

[19] Ian L. Cassidy, Jeffrey T. Scruggs, Sam Behrens and Henri P. Gavin, "Design and Experimental Characterization of an Electromagnetic Transducer for Large-Scale Vibratory Energy Harvesting Applications," *Journal of Intelligent Material Systems and Structures,* vol. 22, no. 17, pp. 2009-2024, 2011.

[20] S-B Choi, M-S Seong and K-S Kim, "Vibration control of an electrorheological fluid-based suspension system with an energy regenerative mechanism," *Proceedings of the Institution of Mechanical Engineers, Part D: Journal of Automobile Engineering,* vol. 223, no. D, pp. 459-469, 2009.

[21] R. Sabzehgar and M. Moallem, "A review of ocean wave energy conversion systems," Montreal, QC, 2009.

[22] Abhijit Gupta, J. A. Jendrzejczyk, T. M. Mulcahy and J. R. Hull, "Design of electromagnetic shock absorbers," *International Journal of Mechanics and Materials in Design,* vol. 3, no. 2, pp. 285-291, 2006.

[23] Chengkuo Lee, Ye Mei Lim, Bin Yang, Rama Krishna Kotlanka, Chun-Huat Heng, Johnny Han He and Jin Min Tang, "Theoretical comparison of the energy harvesting capability among various electrostatic mechanisms from structure aspect," *Sensors and Actuators A,* vol. 156, p. 208–216, 2009.

[24] S. Meninger, J. Q. Mur-Miranda, R Amirtharajah, A. P. Chandrakasan and J. H. Lang , "Vibration-to-electric energy conversion," *Very Large Scale Integration ,* vol. 9, no. 1, pp. 64-76, 2001.

[25] Daniel Hoffmann, Bernd Folkmer and Yiannos Manoli, "Fabrication, characterization and modelling of electrostatic micro-generators," *Journal of Micromechanics and MicroengineeringEmail alert RSS feed,* vol. 19, no. 9, p. 094001 (11pp), 2009.

[26] Shad Roundy, Paul K. Wright and Jan Rabaey , “A study of low level vibrations as a power source for wireless sensor nodes,” *Computer Communications,* vol. 26, no. 11, p. 1131–1144, 2003.

[27] Dennis L. Polla, Lorraine F. Francis, “Processing and characterization of piezoelectric materials into microElectromechanical systems,” *Annual review of materials science,* vol. 28, pp. 563-597, 1998.

[28] Alper Erturk and Daniel J. Inman , “On mechanical modeling of cantilevered piezoelectric vibration energy harvesters,” *ournal of Intelligent Material Systems and Structures,* vol. 19, no. 11, pp. 311-1325, 2008.

[29] Hwan-Sik Yoon, Gregory Washington and Amita Danak, “Modeling, optimization, and design of efficient initially curved piezoceramic unimorphs for energy harvesting applications,” *Journal of Intelligent Material Systems and Structures,* vol. 16, no. 10, pp. 877-888, 2005.

[30] Jyoti Ajitsaria, Song-Yul Choe, D. Shen and D. J. Kim., “Modeling and analysis of a bimorph piezoelectric cantilever beam for voltage generation,” *Smart Materials and Structures* , vol. 16, no. 2, p. 447, 2007.

[31] Marco Ferrari, Vittorio Ferrari, Michele Guizzetti, Daniele Marioli and Andrea Taroni, “Piezoelectric multifrequency energy converter for power harvesting in autonomous microsystems,” *Sensors and Actuators A: Physical,* vol. 142, no. 1, p. 329–335, 2008.

[32] M. Renauda, K. Karakayac, T. Sterkena, P. Fiorinia, C. Van Hoofa, R. Puers, “Fabrication, modelling and characterization of MEMS piezoelectric vibration harvesters,” *Sensors and Actuators A: Physical,* vol. 145, pp. 380-386, 2008.

[33] Chih-Ta Chen, Rashed Adnan Islam and Shashank Priya, “Electric energy generator,” *IEEE Transactions on Ultrasonics, Ferroelectrics and Frequency Control,,* vol. 56, no. 3, pp. 656-661, 2006.

[34] Xiudong Tang and Lei Zuo, “Simulation and experiment validation of simultaneous vibration control and energy harvesting from buildings using Tuned Mass Dampers,” in *American Control Conference (ACC)*, San Francisco, 2011.

[35] Johannes Falnes, “A review of wave-energy extraction,” *Marine Structures*, vol. 20, no. 4, p. 185–201, 2007.

[36] P. Del Vecchio and A. Timidei, “Portable Photovoltaic Stand-alone System, Operating at Very Low Power Conditions,” Capri, 2007.

[37] Nicole C. Annis and Stuart W. Baur, “Performance Comparison of Modular Photovoltaic-Thermal Solar Panels,” in *Green Technologies Conference (IEEE-Green)*, 2011.

[38] A.T. Jones and W. Finley, “Recent development in salinity gradient power,” San Diego, USA., 2003.

[39] L. Meegahapola, L. Udawatta and S. Witharana, “The Ocean Thermal Energy Conversion strategies and analysis of current challenges,” Peradeniya, Srilanka, 2007.

[40] Liwei Li and Jianxing Ren, “Offshore Wind Turbines and Their Installation,” 2010.

[41] K. Yagi, T Tarutani, S Dohata and Y. Shiobara, “Construction of the first offshore wind turbines in Setana Port in Japan,” Kobe, Japan, 2004.

[42] H. Polinder and M. Scuotto, “Wave energy converters and their impact on power systems,” Amsterdam, Netherland, 2005.

[43] M. Leijon, O. Danielsson, M. Eriksson, K. Thorburn, H. Bernhoff, J. IsbergCorresponding author contact information, E-mail the corresponding author, J. Sundberg, I. Ivanova, E. Sjöstedt, O. Ågren, K.E. Karlsson and A. Wolfbrandt, “An electrical approach to wave energy conversion,” *Renewable Energy*, vol. 31, no. 9, p. 1309–1319, 2006.

[44] Marie Ruellan, Hamid BenAhmed, Bernard Multon, Christophe Josset, Aurelien Babarit and Alain Clemen, “Design Methodology for a SEAREV Wave Energy Converter,” *IEEE Transactions on Energy Conversion,* vol. 25, no. 3, pp. 760-767, 2010.

[45] Willie D. Jones, “A high schooler's invention turns water motion into "juice",” *IEEE Spectrum,* vol. 42, no. 4, p. 14, 2005.

[46] Lawrence C. Rome, Louis Flynn, Evan M. Goldman, Taeseung D. Yoo, “Generating Electricity While Walking with Loads,” *Science,* vol. 309, no. 5741, pp. 1725-1728 , 2005.

[47] Zhongjie Li, Lei Zuo, George Luhrs, Liangjun Lin and Yi-xian Qin, “Electromagnetic Energy-Harvesting Shock Absorbers: Design, Modeling, and Road Tests,” *IEEE Transaction on Vehicular Technology,* vol. 62, no. 3, pp. 1065 - 1074, 2013.

[48] Taichi Matsuoka, Kenichiro Omata, Hiroyuki Kanda and Kenichiro Tachi, “A study of wave energy conversion systems using ball screws – comparison of output characteristics of the fixed type and the floating type,” in *Conference of International Offshore and Polar Engineering* , Kitakyushu, Japan, 2002.

[49] Emmanuel B. Agamloh, Alan K. Wallace and Annette von Jouanne, “A novel direct-drive ocean wave energy extraction concept with contact-less force transmission system,” *Renewable Energy,* vol. 33, no. 3, pp. 520-529, 2008.

[50] Phill Brown, Dave Hardisty and T.C.A Molteno, “Wave-powered small-scale generation systems for ocean exploration,” Singapore, 2007.

[51] L. D.A. Thorner, P. D. Mitcheson, A. S. Holmes and E. M. Yeatman, “Scaling Laws for Energy Harvesters in a Marine Environment,” Washington DC, USA, 2009.

[52] P. Manganelli, Experimental investigation of dynamic loads offshore racing

yachts, PhD Thesis: University of Southampton, 2006.

[53] R. M. a. K. R. Henri P. Gavin, "Drift-free integrators," *Review of Scientific Instruments,* vol. 69, no. 5, pp. 2171 - 2175, 1998.

[54] S. Han, "Retrieving the time history of displacement from measured acceleration signal," *Journal of Mechanical Science and Technology* , vol. 17, no. 2, pp. 197-206, 2003.

[55] Keisuke Taira, Atsushi Takeda and Koji Ishikawa, "A shipborne wave-recording system with digital data processing," *Journal of Oceanography,* vol. 27, no. 4, pp. 175-186, 1971.

[56] B. C. Faulkner, F W Barton, T T Baber and W T McKeel Jr, "Determination of bridge response using acceleration data," Virginia Transportation Research Council, Virginia, 1996.

[57] Ki-Tae Park, Sang-Hyo Kim, Heung-Suk Park and Kyu-Wan Lee, "The determination of bridge displacement using measured acceleration," *Engineering Structures,* vol. 27, no. 3, p. 371–378, 2005.

[58] Y. Zhou, W. Zhang and H. Yu, " Analysis of long-period error for accelerograms recorded by digital seismographs," *Earthquake Engineering and Engineering Vibration* , vol. 17, pp. 1-9, 1997.

[59] J. Yanga, J.B. Lib and G. Linb, "A simple approach to integration of acceleration data for dynamic soil-structure interaction analysis," *Soil Dynamics and Earthquake Engineering,* vol. 26, no. 8, p. 725–734, 2006.

[60] Yun Hwa Hong, Ho-Kyung Kim and Hae Sung Lee, "Reconstruction of dynamic displacement and velocity from measured accelerations using the variational statement of an inverse problem," *Journal of Sound and Vibration,* vol. 329, no. 23, pp. 4980-5003, 2010.

[61] Andrew Smyth and Meiliang Wu, "Multi-rate Kalman filtering for the data fusion of displacement and acceleration response measurements in dynamic system

monitoring," *Mechanical Systems and Signal Processing*, vol. 21, no. 2, p. 706–723, 2007.

[62] R. G. Brown and P. Y. C. Hwang, Introduction to random signals and applied Kalman Filtering,, New York: John Wiley & Sons, 1997.

[63] Mohinder S. Grewal and Angus P. Andrews , Kalman Filtering: Theory and Practice Using MATLAB, 3rd ed., Wiley-Blackwell, 2008.

[64] M. D. Miles, "Measurement of Six Degrees of Freedom Model Motions using Strapdown Accelerometers," in *Proceedings of the 21st American Towing Tank Conference*, Washington, D.C., 1986.

[65] Alan Oppenheim, Discrete Time Signal Processing, Upper Saddle River: Pearson Higher Education, 2010.

[66] S.M. Sharkh, M. Hendijanizadeh, M. Moshrefi-Torbati and M. Russell, "An inertial coupled marine power generator for small boats," Ischia, Italy, 2011.

[67] Y C Shu and I C Lien, "Efficiency of energy conversion for a piezoelectric power harvesting system," *Journal of Micromechanics and Microengineering*, vol. 16, no. 11, p. 2429–2438, 2006.

[68] M Renaud, R Elfrink, M Jambunathan, C de Nooijer, Z Wang, M Rovers, R Vullers and R van Schaijk, "Optimum power and efficiency of piezoelectric vibration energy harvesters with sinusoidal and random vibrations," *Journal of Micromechanics and Microengineering*, vol. 22, no. 10, p. 105030 (13pp), 2012.

[69] P. Glynne-Jones, M.J. Tudor, S.P. Beeby and N.M. White, "An electromagnetic, vibration-powered generator for intelligent sensor systems," *Sensors and Actuators A: Physical*, vol. 110, no. 1-3, p. 344–349, 2004.

[70] Mohamed O. Mansoura, Mustafa H. Arafab and Said M. Megaheda, "Resonator with magnetically adjustable natural frequency for vibration energy harvesting," *Sensors and Actuators A: Physical*, vol. 163, no. 1, p. 297–303, 2010.

[71] C. B. Williams and R. B. Yates, “Analysis of a micro-electric generator for microsystems,” *Sensors and Actuators A: Physical,* vol. 52, no. (1-3), pp. 8-11, 1995.

[72] N. G. Stephen, “On energy harvesting from ambient vibration,” *Journal of Sound and Vibration,* vol. 293, no. 1-2, pp. 409-425, 2006.

[73] A Cammarano, S G Burrow, D A W Barton, A Carrella and L R Clare, “Tuning a resonant energy harvester using a generalized electrical load,” *Smart Materials and Structures,* vol. 19, no. 5, p. 055003 (7pp), 2010.

[74] Chitta Ranjan Saha, Terence O’Donnell, Heiko Loder, Steve Beeby and John Tudor, “Optimization of an Electromagnetic Energy Harvesting Devic,” *IEEE Transactions on Magnetics,* vol. 42, no. 10, pp. 3509-3511, 2006.

[75] Kimihiko Nakanoa, Yoshihiro Sudab and Shigeyuki Nakadaic, “Self-powered active vibration control using a single electric actuator,” *Journal of Sound and Vibration,* vol. 260, no. 2, p. 213–235, 2003.

[76] A. F. Z. a. G. A. T. N. P. Gargov, “Direct drive linear machine technologies for marine wave power generation,” in *Universities Power Engineering Conference (UPEC),* London, UK, 2012.

[77] R. Waters, M. Stålberg, O. Danielsson, O. Svensson, S. Gustafsson, E. Strömstedt, M. Eriksson, J. Sundberg and M. Leijon, “Experimental results from sea trials of an offshore wave energy system,” *Applied Physics Letters,* vol. 90, no. 3, p. 034105 (3pp), 2007.

[78] S. J. Elliott and M. Zilletti, “Scaling of electromagnetic transducers for shunt damping and power harvesting,” Leuven, Belgium, 2012.

[79] Shad Roundy, “On the Effectiveness of Vibration-based Energy Harvesting,” *Journal of Intelligent Material Systems and Structures,* vol. 16, no. 10, pp. 809-823, 2005.

[80] J. Peirs, Design of micromechateronic systems: scales laws, technologies and medical applications, Phd Thesis, Katholike Universiteit Lueven, 2001.

[81] Faulhaber , “Brushless DC-Servomotors,” catalog, 2012 .

[82] L. Auboin, “Measurement and analysis of vertical displacement of a sailing yacht,” Master of Science, University of Southampton., 2010.

[83] THK, 2012. [Online]. Available: www.thk.com. [Accessed 1 10 2012].

[84] H. Carlson, Spring Designer's Handbook, Marcel Dekker Inc, 1978.

[85] B.P. Mann, N.D. Sims, “On the performance and resonant frequency of electromagnetic induction energy harvesters,” *Journal of Sound and Vibration* , vol. 329, p. 1348–1361, 2010.

[86] J.M. Renno, M.F. Daqaq, D.J. Inman, “ On the optimal energy harvesting from a vibration source,” *Journal of Sound and Vibration,* vol. 320, p. 386–405, 2009.

[87] Yabin Liao and Henry A Sodano, “Optimal parameters and power characteristics of piezoelectric energy harvesters with an RC circuit,” *Smart Materials and Structures,* vol. 18, no. 4, p. 045011 (11pp), 2009.

[88] Christian Lalanne, Random Vibration, Hoboken: ISTE Ltd and John Wiley&Sons., 2009.

[89] Andre Preumont, Random Vibration and Spectral Analysis, Netherlands: Kluwer Academic Publisher Group, 1994.

[90] Giora Maymon, Some Engineering Applications in Random Vibrations and Random Structures, Israel: American Institute of Aeronautics and Astronautics, 1994.

[91] D E Newland, Mechanical Vibration Analysis and Computation, USA: Dover Publications, 2006.

[92] Paul H. Wirsching, Thomas L. Paez, Keith Ortiz, Random Vibrations: Theory and Practice, USA: Dover Publications, 2006.

[93] E. Halvorsen, "Energy Harvesters Driven by Broadband Random Vibrations," *Journal of Microelectromechanical Systems,* vol. 17, no. 5, pp. 1061 - 1071, 2008.

[94] S Adhikari, M I Friswell and D J Inman, "Piezoelectric energy harvesting from broadband random vibrations," *Smart Materials and Structures,* vol. 18, no. 11, p. 115005 (7pp), 2009.

[95] Xiudong Tang and Lei Zuo, "Vibration energy harvesting from random force and motion excitations," *Smart Materials and Structures,* vol. 21, no. 7, p. 075025 (9pp), 2012.

[96] C. Chatfield, The Analysis of Time Series—An Introduction, London: Chapman and Hall, 1989.

[97] J. B. Roberts and P. D. Spanos, Random Vibration and Statistical Linearization, Courier Dover, 2003.

[98] John A. Rice, Mathematical Statistics and Data Analysis, 3nd ed., Belmont: Duxbury Press, 2007.

[99] James E. Gentle, Random Number Generation and Monte Carlo Methods, 2nd ed., Iowa: Springer, 2003.

[100] N. L. Johnson, S. Kotz, and N. Balakrishnan, Continuous Univariate Distributions, New York: Wiley , 1994.

[101] Gabriela V. Cohen Freue, "The Pitman estimator of the Cauchy location parameter," *Journal of Statistical Planning and Inference,* vol. 137, p. 1900 – 1913, 2007.

[102] Jin Zhang, "A Highly Efficient L-estimator for the Location Parameter of the Cauchy Distribution," *Computational Statistics* , vol. 25, no. 1, p. 97–105, 2010.

[103] Dibin Zhu, Michael J Tudor and Stephen P Beeb, “Strategies for increasing the operating frequency range of vibration energy harvesters: a review,” *Measurement Science and TechnologyEmail alert RSS feed,* vol. 21, no. 2, p. 022001 (29pp), 2010.

[104] Lihua Tang, Yaowen Yang, and Chee Kiong Soh, “Toward Broadband Vibration-based Energy Harvesting,” *Journal of Intelligent Material Systems ad Structures,* vol. 18, pp. 1867-1897, 2010.

[105] Xiaoming Wu, Jianhui Lin, Seiki Kato, Kai Zhang, Tianling Ren and Litian Liu, “A frequency adjustable vibration energy harvester,” in *Proceedings of PowerMEMS 2008+ microEMS2008,* Sendai, Japan, November 9-12, 2008.

[106] J.-H. O. M. H. a. H. S. S. Jacek F. Gieras, “Electromechanical energy harvesting system”. USA Patent US8030807 B2, 4 October 2011.

[107] Christoph Eichhorn, Frank Goldschmidtboeing, and Peter Woias. , “A frequency tunable piezoelectric energy converter based on a cantilever beam,” *Proceedings of PowerMEMS,* vol. 9, no. 12, pp. 309-312, 2008.

[108] Vinod R Challa, M G Prasad, Yong Shi and Frank T Fisher, “A vibration energy harvesting device with bidirectional resonance frequency tunability,” *Smart Materials and Structures,* vol. 17, no. 1, p. 015035 (10pp), 2008.

[109] Wen-Jong Wu, Yu-Yin Chen, Bor-Shun Lee, Jyun-Jhang He, and Yen-Tun Peng, “Tunable resonant frequency power harvesting devices,” *Proc. SPIE ,* vol. 6169, p. 55–62, 2006.

[110] B.P. Mann and N.D. Sims, “Energy harvesting from the nonlinear oscillations of magnetic levitation,” *Journal of Sound and Vibration,* vol. 319, no. 1-2, pp. 515-530, 2009.

[111] T. Petropoulos, E. M. Yeatman, and P. D. Mitcheson, “MEMS coupled resonators for power generation and sensing,” in *Micromechanics Europe,* Leuven, Belgium,

, 2004.

[112] S.M. Shahruz, “Design of mechanical band-pass filters for energy scavenging,” *Journal of Sound and Vibration,* vol. 292, no. 3-5, p. 987–998, 2006.

[113] A. Erturk, J. Hoffmann, and D. J. Inman, “A piezomagnetoelastic structure for broadband vibration energy harvesting,” *Applied Physics Letters,* vol. 94, p. 254102, 2009.

[114] R. Ramlan, M. J. Brennan, B. R. Mace, and I. Kovacic, “Potential benefits of a non-linear stiffness in an energy harvesting device,” *Nonlinear Dynamics,* vol. 59, no. 4, pp. 545-558, 2010.

[115] Shad Roundy and Yang Zhang, “Toward self-tuning adaptive vibration-based microgenerators,” *Smart Structures, Devices and Systems,* vol. 5649, pp. 373-84, 2005.

[116] Fylde Electronic Laboratories Ltd., [Online]. Available: http://www.fylde.com/. [Accessed 30 November 2013].

[117] National Instruments, [Online]. Available: www.http://uk.ni.com/. [Accessed 2013 11 15].

[118] Maryam Ghandchi Tehrani, Stephen J. Elliott, “Extending the dynamics range of an energy harvester using nonlinear damping,” *Journal of Sound and Vibration,* vol. 333, no. 3, p. 623–629, 2014.